Keele
UNIVERSITY

This work is protected by copyright and other intellectual property rights and duplication or sale of all or part is not permitted, except that material may be duplicated by you for research, private study, criticism/review or educational purposes. Electronic or print copies are for your own personal, non-commercial use and shall not be passed to any other individual. No quotation may be published without proper acknowledgement. For any other use, or to quote extensively from the work, permission must be obtained from the copyright holder/s.

Characterising the molecular consequences of *LMNA* mutations in congenital muscular dystrophy

Emily Carolyn Storey

School of Pharmacy and Bioengineering

Submitted for the degree of Doctorate of Philosophy

December 2023

Keele University

Table of contents

Abstract

LMNA-related congenital muscular dystrophy (L-CMD) is a rare disorder predominantly causing muscle weakness and wasting, over time, leading to development of dysphagia and life-threating respiratory insufficiency, and sometimes cardiac arrhythmias. There are no pharmacological therapies for L-CMD, and treatment focuses on managing symptoms of the condition. L-CMD is caused by mutations in *LMNA*, a gene encoding nuclear lamina component lamin A/C. Many mechanisms downstream of *LMNA* mutations in L-CMD remain elusive, making the identification of non-genetic therapeutic targets difficult. Here, research focused on identifying conserved cellular and molecular defects across three myoblast cell lines derived from L-CMD patients, each harbouring different mutations in *LMNA* (R249W, del.K32, L380S). Throughout this thesis, a combination of molecular biology and biochemistry techniques and systematic reviewing were used. In the first results chapter, co-immunoprecipitation and mass spectrometry revealed new putative lamin A binding partners that were lost or gained across the three L-CMD myoblast cell lines, and new putative lamin A interactors that were present across all myoblast lines, as well as lamin A interactors that have been previously identified in other cells/tissues. In the second results chapter, a targeted approach uncovered nuclear defects, including abnormal nuclear morphology, in L-CMD myoblasts and myotubes compared to controls. Lamin A/C, emerin and SUN2 were all significantly decreased in expression in L-CMD myotubes compared to controls. In the third results chapter, quantitative proteomics revealed hundreds of differentially expressed proteins in L-CMD myoblasts and myotubes compared to healthy controls. Ingenuity pathway analysis identified downregulation of the necroptosis signalling pathway, and upregulation of the

synaptogenesis signalling pathway in L-CMD myoblasts, and upregulation of the insulin secretion signalling pathway and Huntington's disease signalling in L-CMD myotubes. In the final results chapter, genotype-phenotype correlations were determined in the genes encoding nuclear envelope (NE) proteins using a systematic review. Clusters of *LMNA* mutations causing striated muscle diseases were found to be located on exon 6 of *LMNA*, whilst metabolic-disease associated *LMNA* mutations were common in the region encoding the tail domain of lamin A/C. *LMNA* was the only NE protein to cause many distinct diseases. Identification and comparison of lamin A interactors in L-CMD and control myoblasts offers insight into the debated theory of whether *LMNA* mutations result in loss- or gain-of function. Cells derived from other laminopathy patients have previously exhibited nuclear defects, whilst reduced lamin A/C expression has been found in myoblasts and myotubes from the $Lmna^{\Delta K32/\Delta K32}$ mouse model of L-CMD. Confirmation of decreased lamin A/C expression in L-CMD myotubes suggests this may be a key feature of the disease that should be targeted for upregulation in future therapy development. Dysregulated pathways identified in L-CMD myoblasts and myotubes including the necroptosis pathway have previously been implicated in other neuromuscular disorders, so may contribute to L-CMD pathophysiology and should be considered for further study. Taken together, these results have identified numerous defects that are common to each of the three L-CMD myoblast cell lines harbouring different *LMNA* mutations. This thesis has offered insight into mechanisms which may underlie the pathophysiology of L-CMD, which may be targeted in future studies for the development of therapies, or alternatively for biomarker purposes, to track disease or treatment progression.

List of figures

List of tables

Abbreviations

2D Two-dimensional

3D Three-dimensional

AAV Adeno-associated virus

ACh Acetylcholine

AChRs Acetylcholine receptors

ACTB β-actin

AD Autosomal dominant

ADLD Adult onset autosomal dominant leukodystrophy

AF Atrial fibrillation

ALS Amyotrophic lateral sclerosis

AMC Arthrogryposis multiplex congenita

Apaf-1 Apoptotic protease-activating factor 1

AR Autosomal recessive

AVB Atrioventricular block

AVRD Arrhythmogenic right ventricular dysplasia

BAF Barrier-to-autointegration factor

BAX Bcl-2-associated X protein

BBS Bardet-Biedl syndrome

BCA Bicinchoninic acid

BCL7B B-cell CLL/lymphoma 7 protein family member B

BLAST Basic local alignment search tool

bp Base pairs

BP Biological processes

BSA Bovine serum albumin

Casp-7 Caspase-7

CC Cellular component

CCD Cardiac conduction disease

Cdk4 Cyclin-dependent kinase-4

cDNA Complementary deoxyribonucleic acid

CF Cystic fibrosis

CFTR Cystic fibrosis transmembrane conductance regulator

CH Calponin homology

ChIP-seq Chromatin immunoprecipitation-DNA sequencing

CMDs Congenital muscular dystrophies

CMT Charcot-Marie-Tooth

CMT2B1 Autosomal recessive axonal Charcot-Marie-Tooth type 2B1

Co-IP Co-immunoprecipitation

cpd27 Compound 27 (furo[2,3-d]pyrimidines)

CRISPR Clustered regularly interspaced short palindromic repeats

Cryo-ET Cryo-electron tomography

DAVID The Database for Annotation, Visualization and Integrated Discovery

DCM Dilated cardiomyopathy

DCM-CD Dilated cardiomyopathy associated with cardiac conduction disease

DDA Data dependent acquisition

DIA Data independent acquisition

DKD Double knock-down

DMD Duchenne muscular dystrophy

DMEM Dulbecco's Modified Eagle Serum

DMSO Dimethyl sulfoxide

DNA Deoxyribonucleic acid

dNTPs Deoxyribonucleoside triphosphates

DPP7 Dipeptidyl peptidase 2

dsDNA Double-stranded deoxyribonucleic acid

EDMD Emery-Dreifuss muscular dystrophy

EDTA Ethylenediaminetetracetic acid

ENU *N*-ethyl-*N*-nitrosourea

ER Endoplasmic reticulum

FBS Fetal bovine serum

FKBP1A Peptidyl-prolyl cis-trans isomerase FKBP1A

FoxO TFs Forkhead box O transcription factors

FPLD Familial partial lipodystrophy

FSHD Facioscapulohumeral muscular dystrophy

FTI Farnesyltransferase inhibitor

GAPDH Glyceraldehyde-3-phosphate dehydrogenase

GO Gene ontology

GRMD Golden retriever muscular dystrophy

H327me3 H3 trimethylated at lysine 27

HGPS Hutchinson Giford Progeria Syndrome

HMGA1 High-mobility group A1

HS Horse serum

hTERT Human telomerase reverse transcriptase

IAA Iodoacetamide

ICD Implantable cardioverter-defibrillator

IDH1 Isocitrate dehydrogenase 1

Igf1r Insulin-like growth factor I receptor

Igfbp5 Insulin-like growth factor binding protein 5

IgG Immunoglobulin G

IMS Industrial methylated spirits

INM Inner nuclear membrane

Insr Insulin receptor

IPA Ingenuity pathway analysis

iPSCs Induced pluripotent stem cells

Irs1 Insulin receptor substrate 1

ITS-X Insulin-transferrin-selenium-ethanolamine

KASH Klarsicht/Anc-1/Syne Homology

Ku70 X-ray repair cross complementing protein 6

LADs Lamina-associated domains

LAP2α Thymopoietin

LBR Lamin B receptor

L-CMD *LMNA*-related congenital muscular dystrophy

LCMS/MS Liquid chromatography mass spectrometry

LGMD Limb-girdle muscular dystrophy

LINC Linker of nucleoskeleton and cytoskeleton complex

MAD-A/B Mandibuloacral dysplasia type A and B

MB Myoblast

MD Molecular dynamics

MDC1A Congenital muscular dystrophy type 1A

MEFs Mouse embryonic fibroblast cells

MF Molecular function

MHC Myosin heavy chain

miRNA Micro ribonucleic acid

MKS Meckel syndrome type 1

MLKL RIPK1-RIPK3-mixed lineage kinase domain-like protein

MRM Multiple reaction monitoring

mRNA Messenger ribonucleic acid

MS Mass spectrometry

MSCs Mesenchymal stem cells

MT Myotube

MuSCs Muscle stem cells

MW Molecular weight

MyoD Myoblast determination protein

NCBI The National Centre for Biotechnology Information

NE Nuclear envelope

Nec-1 Necrostatin-1

Nec-1s Necrostatin 2 racemate

NHEJ Non-homologous DNA end joining

NL Nuclear lamina

NMJ Neuromuscular junction

Notch3 Notch receptor 3

NPC Nuclear pore complex

NPM Nucleophosmin

NTDs Neural tube defects

OneSTrEP Streptavidin/biotin system

ONM Outer nuclear membrane

OPMD Oculo-pharyngeal muscular dystrophy

OST OneSTrEP

PBS Phosphate buffered saline

PCA Principal component analysis

PCNA Proliferating cell nuclear antigen

PCR Polymerase chain reaction

Pik3r1 Phosphoinositide-3-kinase regulatory subunit 1

PNS Perinuclear space

PRISMA Preferred Reporting Items for Systematic Reviews and Meta-Analyses

qPCR Quantitative polymerase chain reaction

Rb Rabbit

RBL1 Retinoblastoma-like protein 1

RD Restrictive dermopathy

RFUS Relative fluorescence units

RIPA Radioimmunoprecipitation assay

RIPK1 Receptor-interacting protein kinase 1

RNA Ribonucleic acid

R-Smads Receptor-regulated Smads

RSS Rigid spine syndrome

RT-qPCR Real time quantitative polymerase chain reaction

SCAR8 Autosomal recessive cerebellar ataxia

SDS Sodium dodecyl sulfate

SDS-PAGE Sodium dodecylsulfate-polyacrylamide

sgRNAs Single guide ribonucleic acids

siRNA Silencing ribonucleic acid

SMA Spinal muscular atrophy

SMARCD2 SWI/SNF-related matrix-associated actin-dependent regulator of chromatin subfamily D member 2

SMaRT Spliceosome-mediated RNA trans-splicing

STAT1 Signal transducer and activator of transcription 1-alpha/beta

STRING Search Tool for the Retrieval of Interacting Genes/Proteins

SUN Sad1 and UNC-84

SWATH™-MS Sequential window acquisition of all theoretical mass spectra

TAN Transmembrane-associated nuclear

TAX1 Tax-1 binding protein 1

TCEP Tris(2-carboxyethyl)phosphine

TGF-β Transforming growth factor-β

TKO Total knock out

TKT Transketolase

TMPO Thymopoietin

TNF Tumor necrosis factor

TOMM34 Mitochondrial import receptor subunit TOM34

TOP1 DNA topoisomerase 1

WB Western blot

WT Wild-type

XXRC6 X-ray repair cross complementing protein 6

Y2H Yeast two-hybrid

YAP Yes-associated protein

γH2AX Phosphor-H2A.X Variant Histone

Dissemination
Publications:

Storey, E. C. and Fuller, H. R. (2022) 'Genotype-Phenotype Correlations in Human Diseases Caused by Mutations of LINC Complex-Associated Genes: A Systematic Review and Meta-Summary', Cells. MDPI, 11(24), p. 4065. doi: 10.3390/CELLS11244065/S1.

Storey, E., Holt I., Owen S., Synowsy S., Shirran S., Morris, G., Fuller, H. (2022) 'P.146 Characterising the molecular consequences of LMNA-related congenital muscular dystrophy in patient myoblasts', Neuromuscular Disorders. Elsevier, 32, p. S108. doi: 10.1016/J.NMD.2022.07.274.

Storey, E. and Fuller, H. (2022) 'P.148 Genotype-phenotype correlations in human diseases caused by mutations of LINC complex-associated genes: a systematic review and meta-summary', Neuromuscular Disorders. Elsevier, 32, p. S108. doi: 10.1016/J.NMD.2022.07.276.

Storey E.C., Holt I., Morris G.E. and Fuller H.R. (2021) OTHER NMDs: EP.350 A study of LINC complex proteins reveals temporal emerin and SUN2 expression changes during myoblast differentiation. *Neuromuscular Disorders;* 31: S156-S157. doi: 10.1016/j.nmd.2021.07.375

Storey E.C., Khilar S., Holt I., Shirran S., Morris G.E. and Fuller H.R. (2021) CONGENITAL MUSCULAR DYSTROPHIES: EP.66 Identification of lamin A interactors in healthy and congenital muscular dystrophy immortalized myoblasts. *Neuromuscular Disorders;* 31: S69. doi: 10.1016/j.nmd.2021.07.091

Storey E.C., Holt I., Morris G.E. and Fuller H.R. (2020) Muscle cell differentiation and development pathway defects in Emery-Dreifuss muscular dystrophy. *Neuromuscular Disorders;* 30 (6): 443-456. doi: 10.1016/j.nmd.2020.04.002

Oral presentations:

Faculty of Medicine & Health Sciences PGR Symposium (Keele University, UK 2021): A study of LINC complex proteins reveals temporal emerin and SUN2 expression changes during myoblast differentiation.

Poster presentations:

The World Muscle Society (WMS) 2022 Congress (Halifax, NS, Canada 2022): Characterising the molecular consequences of LMNA-related congenital muscular dystrophy in human muscle cells

The World Muscle Society (WMS) 2022 Congress (Halifax, NS, Canada 2022): Genotype phenotype correlations in human diseases caused by mutations of LINC complex associated genes: a systematic review and meta summary

Cure CMD 2022 SciFam (Nashville, TN, USA 2022): Characterising the molecular consequences of LMNA-related congenital muscular dystrophy in human muscle cells

Joint TCES / EPSRC CDT 2022 Conference (University of Birmingham, UK 2022): Characterising the molecular consequences of LMNA-related congenital muscular dystrophy in human muscle cells

The World Muscle Society (WMS) 2021 Virtual Congress (Virtual, 2021): Identification of lamin A interactors in healthy and congenital muscular dystrophy immortalized myoblasts.

The World Muscle Society (WMS) 2021 Virtual Congress (Virtual, 2021): A study of LINC complex proteins reveals temporal emerin and SUN2 expression changes during myoblast differentiation.

Future Leaders in Regenerative Medicine: Joint CDT and UKSB Conference (Virtual, 2021): Characterising the expression of muscular dystrophy-associated nuclear envelope proteins during myoblast differentiation.

Future Leaders in Regenerative Medicine: Joint CDT and UKSB Conference (Virtual, 2020): The expression of inherited muscular dystrophy associated nuclear envelope proteins during muscle cell differentiation.

Regenerative Medicine Theme Day (Keele University, UK 2019): The effect of age on congenital muscular dystrophy associated nuclear envelope proteins during myogenesis.

Acknowledgments

I would like to express my deepest appreciation to my primary supervisor, Dr. Heidi Fuller, for her mentoring and encouragement over the three years of my PhD. Without her guidance and feedback, this PhD would not have been possible. I am also extremely grateful for the support of my co-supervisor, Dr. Ian Holt, for teaching me numerous laboratory skills and for offering insight into my project with his wealth of knowledge. Special thanks to Dr. Sharon Owen for always being on hand for help and motivation, as well as the whole neuromuscular group at the Robert Jones and Agnes Hunt Orthopaedic Hospital. Additionally, many thanks to Keele University and The Orthopaedic Institute for funding this research.

I am also grateful to my other colleagues at the Robert Jones and Agnes Hunt Orthopaedic Hospital, in particular a special thanks to Dr. Jade Perry for her moral support and friendship throughout this entire process.

Lastly, I would like to thank my family and friends, especially my parents, for their continuous love and support, as well as continuous belief in me throughout this journey. I am also forever thankful to Joshua Davey, for all the encouragement, emotional support, and constantly picking me up during the toughest times.

Chapter 1: Introduction

1.1. *LMNA*-related congenital muscular dystrophy (L-CMD)

The congenital muscular dystrophies (CMDs) are a group of muscle disorders with significant clinical and genetic heterogeneity (Mercuri *et al.*, 2002), that typically present as hypotonia, muscle weakness and contractures, and histological evidence of a dystrophic myopathy, at birth or during the first year of life (Voit, 1998; Mercuri *et al.*, 2002). CMDs may be classified by the mutated gene, the respective protein's localization, and the protein's predicted function (Collins and Bönnemann, 2010). Possible pathophysiologic classes include: abnormalities of α-dystroglycan (α-DG) glycosylation (fukutin, *POMGnT1*, *POMT1*, *POMT2*, *FKRP*, and *LARGE*) and defects in another membrane receptor (*ITGA7*), abnormalities of extracellular matrix proteins (*LAMA2*, *COL6A1*, *COL6A3*), abnormalities of nuclear envelope proteins (*LMNA* and *SYNE1*), and abnormalities at the level of the endoplasmic reticulum (*SEPN1*) (Collins and Bönnemann, 2010). *LMNA*-related CMD (L-CMD) is a relatively newly discovered form of muscle laminopathy, first described in 2005 by D'Amico et al. (D'Amico *et al.*, 2005) (**Fig 1.1**) and caused by mutations in *LMNA*. L-CMD, the focus of this thesis, is an extremely rare condition, and there are only around 100 cases described in the literature (Avila *et al.*, 2021). Transmission of L-CMD can either be autosomal recessive or dominant (Bonati *et al.*, 2014). So far, two L-CMD subtypes have been distinguished: (a) an early-onset severe phenotype with poor spontaneous movements and limited motor achievements, (b) an initially milder phenotype with the ability to stand and walk, but inability to obtain free head control, typically described as a "dropped head" due to weakness in the neck muscles (Quijano-Roy *et al.*, 2008). Children with L-CMD also often develop multiple joint contractures, and talipes feet and a rigid spine with thoracic lordosis are also frequently observed characteristics of the condition

(Quijano-Roy *et al.*, 2008). Over time, progressive muscle weakness may cause infants and children with L-CMD to have difficulty eating (dysphagia) and breathing. These breathing problems result from restrictive respiratory insufficiency, which occurs when muscles in the chest are weakened and the ribcage becomes increasingly rigid (Quijano-Roy *et al.*, 2008). This complication can be life-threatening and may affected patients require mechanical ventilation to assist their breathing (Quijano-Roy *et al.*, 2008). As a result, the average life-expectancy for a child diagnosed with L-CMD is 18 years old. Cardiac arrhythmias have additionally been observed in some patients with L-CMD (Quijano-Roy *et al.*, 2008). As well as L-CMD, an extremely rare *SYNE-1* mutation (encoding nesprin-1) has been identified in a consanguineous family with a peculiar phenotype characterized by CMD with adducted thumbs, mental retardation and cerebellar hypoplasia (Voit *et al.*, 2007). Currently there are no pharmacological therapies available for L-CMD, and treatment plans focus on physiotherapy and managing the symptoms of the disease (Macquart *et al.*, 2016). Therefore, there is a desperate need for the development of new, innovative therapies for this condition. At the moment, the mechanisms downstream of *LMNA* mutations in L-CMD, and molecular pathways behind the development of the disease are uncertain, consequently hindering therapy development.

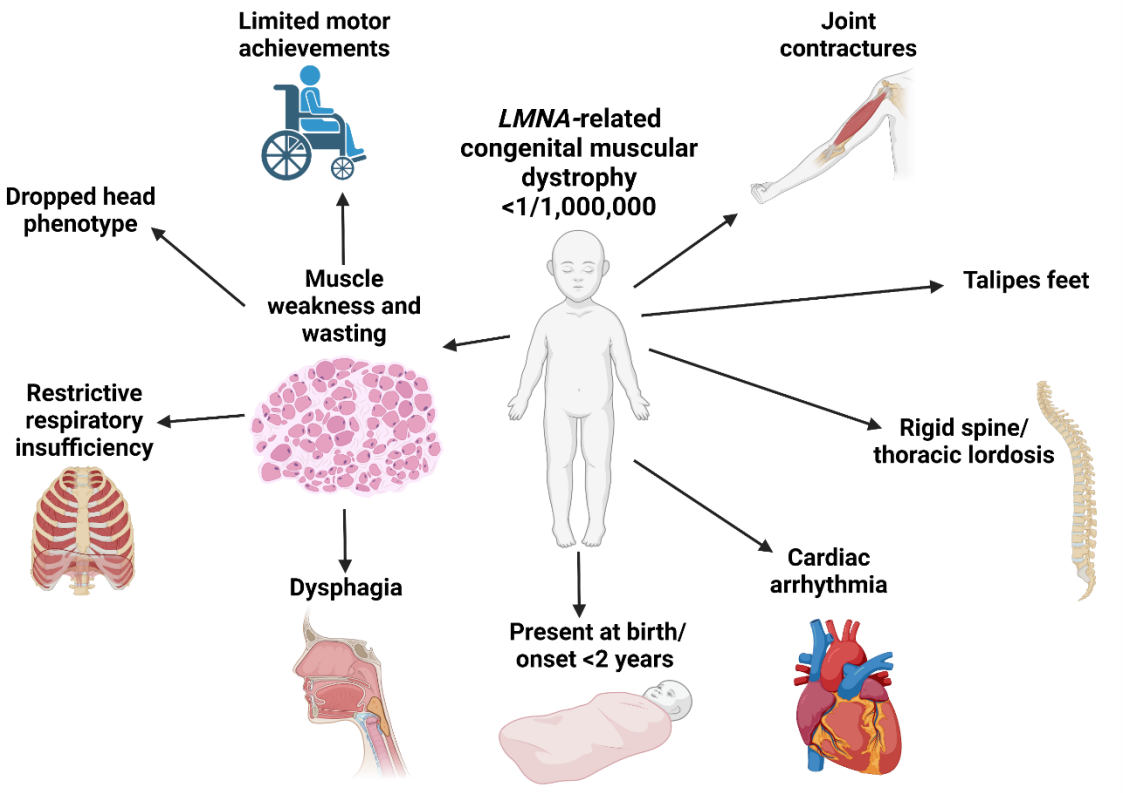

Figure 1.1- Summary of characteristics of LMNA-related congenital muscular dystrophy. *L-CMD has an estimated prevalence of around <1/1,000,000 and is a condition that is present at birth or has an onset within the first two years of life. Created with BioRender.com.*

1.2. L-CMD is a striated muscle laminopathy, with some features similar to Emery-Dreifuss Muscular Dystrophy (EDMD)

Similarly, to L-CMD, mutations in *LMNA* also cause other striated muscle diseases or "laminopathies", including limb-girdle muscular dystrophy type 1b (LGMD), Emery-Dreifuss muscular dystrophy (EDMD) and dilated cardiomyopathy associated with cardiac conduction system disease (DCM-CD). In this section, the focus will be on EDMD, as some aspects of this disease are similar to L-CMD. Unlike L-CMD, EDMD was first characterized over thirty years ago, in 1989 (Emery, 1989b). *EMD*, encoding emerin, was the first gene found to be responsible for causing the X-linked form of EDMD (Bione *et al.*, 1994), and shortly after, *LMNA* was identified as a causative gene

for the autosomal dominant and recessive forms of EDMD in 1999 (Bonne *et al.*, 1999). Since then, a number of other genes encoding NE proteins have been implicated in EDMD development (Q. Zhang *et al.*, 2007b; Gueneau *et al.*, 2009; Liang *et al.*, 2011; Meinke *et al.*, 2014). The prevalence of EDMD caused by *LMNA* mutations specifically is unknown, however the X-linked form is estimated to affect roughly 1 in 100,000 people, and autosomal dominant EDMD is believed to be more common (Nelson, 2000). Therefore, EDMD is predicted to be a more prevalent disease compared to L-CMD.

Whilst L-CMD is present at birth or emerges during infancy, EDMD has an onset of between five and ten years of age and is characterized by the triad of (1) early development of contractures of the elbows, Achilles tendons, and postcervical muscles, which usually become noticeable during adolescence, (2) slowly progressive muscle weakness and wasting with a humeroperoneal distribution early in the course of the disease, and (3) a cardiomyopathy usually presenting as heart block (Emery, 1989a; Bonne, Leturcq and Yaou, 2019) (**Fig 1.2**). EDMD is phenotypically different to other muscular dystrophies in that contractures develop before there is any significant muscle weakness. Elbow contractures result in the arms being carried in a semiflexed position, and contractures of the Achilles tendon cause the patient to walk on their toes (Emery, 1989b). Contractures of the postcervical muscles affect neck flexion, and later in the disease forward flexion of the entire spine becomes limited (Emery, 1989b). Muscle wasting and weakness mostly presents as proximal in the upper limbs (affecting the biceps and triceps) and distal in the lower limbs (such as the anterior tibial and peroneal muscles) (Emery, 1989b). This is described as a humeroperoneal distribution of muscle weakness. Later, EDMD patients develop weakness of the

pectoral girdle musculature and the knee and hip extensor muscles, and the distribution of muscle weakness shifts to what is described as scapula-humeropelvoperoneal (Emery, 1989b). As EDMD is a slowly progressive disease, patients usually survive into at least middle age with varying degrees of incapacity (Emery, 1989b).

Like L-CMD, very few treatment options exist for EDMD, which aim to treat the symptoms of the disease. Surgery is often used to release contractures, and the implantation of a cardiac pacemaker when symptomatic bradycardia or conduction defects are identified can decrease the risk of potentially life-threatening arrhythmias (Russo and Nigro, 2015; Storey *et al.*, 2020). In more severe cases of EDMD, pacemakers are often not sufficient to eliminate the cardiac risks of EDMD, and so implantation of an ICD (implantable cardioverter-defibrillator) is recommended (Storey *et al.*, 2020). Heart transplants are also often needed in patients with autosomal dominant EDMD with cardiomyopathy (Dell'Amore *et al.*, 2007).

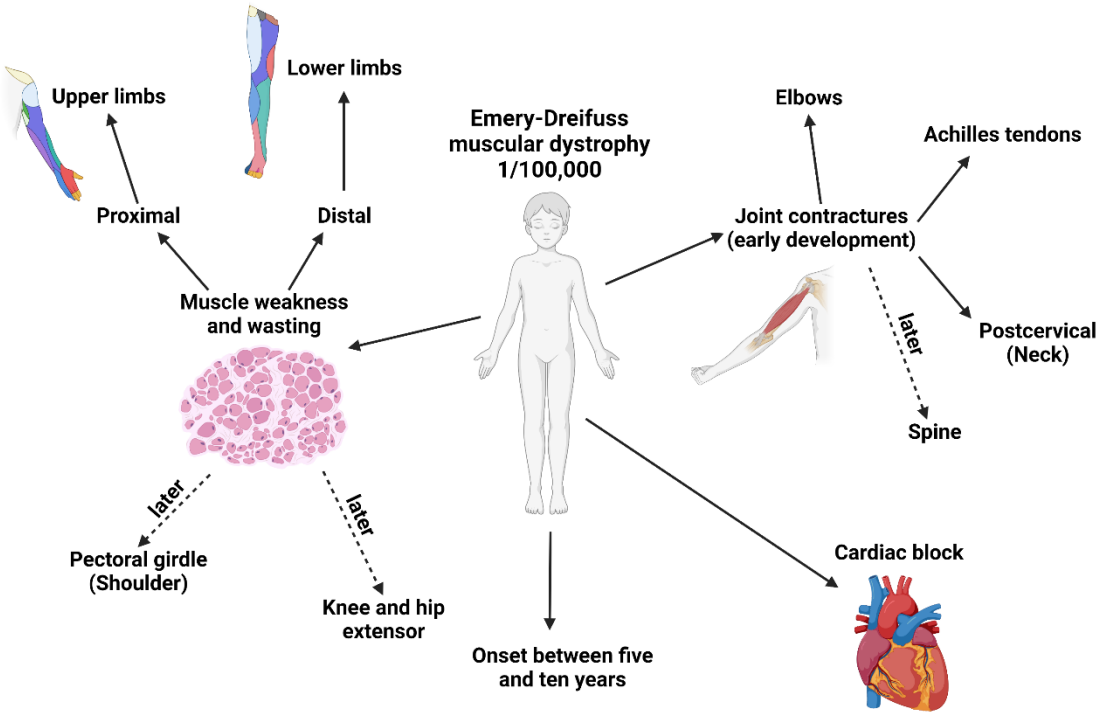

Figure 1.2 - Summary of characteristics of Emery-Dreifuss muscular dystrophy (EDMD). *X-linked EDMD has an estimated incidence of around 1/100,000, whilst the prevalence of the autosomal dominant form is unknown, it is thought to be more common. EDMD has an onset of between five to ten years and is characterised by a triad of symptoms (1) early onset of joint contractures, (2) muscle weakness and wasting, and (3) cardiac block. Characteristics of the disease which develop later in life are represented by arrows with dotted lines. Created with BioRender.com.*

L-CMD and EDMD are seen as two separate classes of skeletal muscle disorders, although they share genetic similarities and some clinical resemblances. As they are both muscular dystrophies, muscle weakness and wasting are a primary characteristic of the conditions. In EDMD, muscle weakness and wasting after the development of muscle contractures, but in L-CMD muscle weakness can be present at birth, or one of the first symptoms of the disease. For both conditions though, muscle weakness and wasting seems to occur in the arms and the lower legs (Quijano-Roy *et al.*, 2008; Madej-Pilarczyk, 2018). Both L-CMD and EDMD patients also develop contractures,

albeit these develop later in L-CMD. Contractures seen in EDMD patients can also affect the neck muscles (Emery, 1989b), whilst this does not occur in L-CMD patients, weakness in this muscle group is a hallmark of the condition (Quijano-Roy *et al.*, 2008). Rigidity of the spine can also be observed in both diseases (Quijano-Roy *et al.*, 2008; Madej-Pilarczyk, 2018). Finally, cardiac abnormalities are also features of both L-CMD and EDMD (Emery, 1989b; Quijano-Roy *et al.*, 2008).

The major difference between clinical aspects of L-CMD and EDMD are the age of onset of the conditions. Whilst the first symptoms of EDMD occur during childhood, L-CMD is a congenital condition which is present at birth. L-CMD has also been described as the most severe of the striated muscle laminopathies, this is mostly owing to the condition affecting a broader range of muscle groups compared to EDMD, notably muscles in the chest, which usually cause fatal complications in L-CMD patients at a young age (Quijano-Roy *et al.*, 2008). As a result, the prognosis for the L-CMD is worse than for EDMD.

Considering the similarities between L-CMD and EDMD, it is questionable whether they are entirely separate diseases, or perhaps these diseases are part of a spectrum of differing severity. To clarify this, further study and comparison between the pathophysiology of the two conditions is needed. This could be done by assessing whether cellular and molecular pathway defects that have been found downstream of mutations that cause EDMD also occur downstream of L-CMD *LMNA* mutations. Proteomics is also an approach that could be used to quantitatively compare the proteome of cells derived from EDMD patients to cells from L-CMD patients. This could be used to identify conserved dysregulated proteins and pathways across samples

from the two diseases. Until this is confirmed, given the resemblance between the two conditions, the findings from 20+ years of research into EDMD may be considered when studying L-CMD, especially seeing as there is little research on L-CMD. Research in EDMD has allowed us to further understand some consequences of loss-of or mutant lamin A/C in a number of cells and tissues, including skeletal muscle, myoblasts and myotubes. These findings in EDMD may help to direct research in L-CMD, to determine whether similar defects are seen in L-CMD models. However, it should be noted that as different *LMNA* mutations often cause EDMD and L-CMD, there may be different mechanisms involved in the pathophysiology of L-CMD. In the following sections, research in EDMD will be discussed as well as L-CMD.

1.3. The nuclear envelope and the linker of nucleoskeleton and cytoskeleton complex

The nuclear envelope (NE) is a specialized structure that functions to separate the cytoplasm from the nucleoplasm. It consists of two lipid bilayer membranes; the inner nuclear membrane (INM), and the outer nuclear membrane (ONM), divided by a gap known as the perinuclear space (PNS). The ONM is a continuation of the rough endoplasmic reticulum, whilst the INM interacts with chromatin and the nuclear lamina (NL), a protein meshwork that composes the nuclear skeleton (Güttinger, Laurell and Kutay, 2009; Linde and Stick, 2010). The major components of the NL are type V intermediate filaments, A- and B-type lamins (Taddei *et al.*, 2004). A-type lamins, lamins A and C are encoded by a single gene, *LMNA*, whereas B-type lamins, B1 and B2, are encoded by two separate genes, *LMNB1* and *LMNB2*. Mutations in the *LMNA* gene have been linked to a wide range of different diseases, including L-CMD

and EDMD, that are often known as “laminopathies” (Bonne *et al.*, 1999). Laminopathies tend to be tissue-specific degenerative diseases and can be broadly classified into two groups: neuromuscular disorders affecting skeletal muscle, cardiac muscle and the peripheral nervous system (e.g. EDMD, L-CMD, DCM, LGMD); and secondly, partial lipodystrophy syndromes with or without developmental abnormalities and premature ageing (e.g. familial partial lipodystrophy (FPLD), mandibuloacral dysplasia and Hutchinson-Gilford progeria sydrome) (Worman and Courvalin, 2004; Chi, Chen and Jeang, 2009).

The NL is connected to the cytoskeleton through a network called the Linker of Nucleoskeleton and Cytoskeleton (LINC) complex (**Fig.1.3**). The central components of the LINC complex are SUN (*SUN1/SUN2)* and giant nesprin proteins (*SYNE1/SYNE2)* that are situated in the INM and ONM, respectively. The Sad1 and UNC-84 (SUN) and Klarsicht/Anc-1/Syne Homology (KASH) domains of the respective proteins interact in the perinuclear space to form a bridge that spans the INM, perinuclear space and ONM (Cain *et al.*, 2018). The N-termini of SUN proteins, SUN1 and SUN2, interact with the NL, anchoring the LINC complex at the NE, whilst the cytoplasmic domains of the nesprins connect to the cytoskeleton (Tapley and Starr, 2013). Giant isoforms of nesprin-1/2 contain an N-terminal calponin homology domain that is responsible for actin binding and linkage to the centrosome through microtubules and their motor proteins (Rajgor and Shanahan, 2013). Nesprin-3 connects to the cytoplasmic intermediate filament network through interaction with plectin, whilst nesprin-4 is specific to epithelial cells and connects the NE to microtubules via the kinesin-1 motor protein (Rajgor and Shanahan, 2013). Other NE proteins are also associated with the LINC complex. These include INM proteins emerin (*EMD)* and TMEM43 (*TMEM43)*

(Manilal, Nguyen and Morris, 1998; Liang *et al.*, 2011), also known as LUMA, and four-and-a-half-lim domains protein 1 (*FHL1*) isoform FHL1B, which has been found to shuttle between the nucleus and the cytoplasm (Ziat *et al.*, 2016).

Besides mutations in *LMNA*, mutations in other NE proteins and constituents of the LINC complex have additionally been identified in various diseases. These diseases are sometimes referred to as "nuclear envelopathies" and affect a range of different tissues. For example, mutations in *EMD*, encoding emerin, also cause EDMD and some heart conditions (Bione *et al.*, 1994). EDMD is also caused by mutations in *SYNE1* (nesprin-1) (Q. Zhang *et al.*, 2007b), and *SYNE1* mutations are also implicated in autosomal recessive cerebellar ataxia type 8 (SCAR8) (Synofzik *et al.*, 2016), arthrogryposis (Baumann *et al.*, 2017), and dilated cardiomyopathy (DCM) (Zhou *et al.*, 2017). Genomic duplication of *LMNB1* is known to cause autosomal dominant leukodystrophy (ADLD) (Brussino *et al.*, 2010), and variants of *LMNB1* have been linked to the development of neural tube defects (Robinson *et al.*, 2013), whilst *LMNB2* mutations are known to cause acquired partial lipodystrophy (Gao *et al.*, 2012).

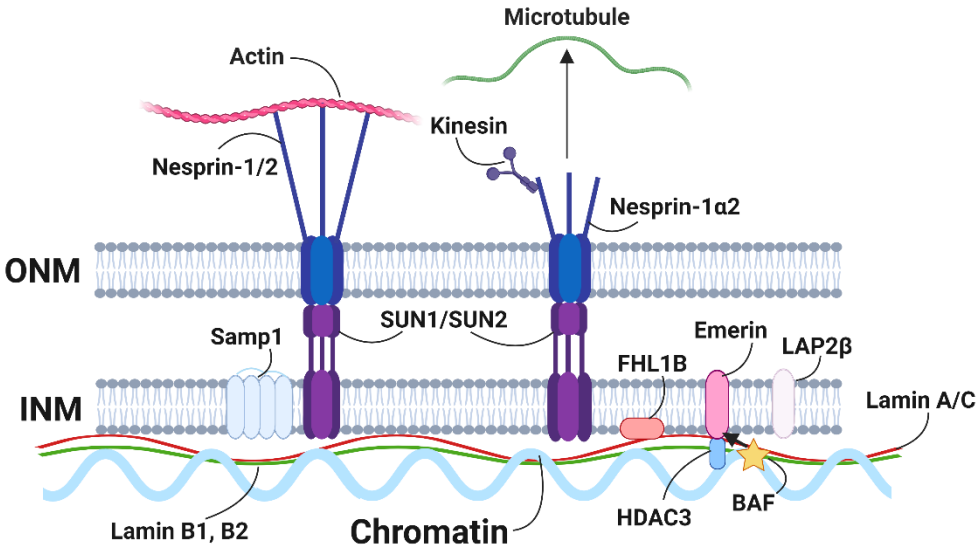

Figure 1.3- The linker of nucleoskeleton and cytoskeleton complex. *The Klarsicht/Anc-1/Syne (KASH) domain of nesprin-1 giant, found at the outer nuclear membrane (ONM), interacts with the Sad1 and UNC-84 (SUN) domain of inner nuclear membrane (INM) SUN1/SUN2 proteins in the perinuclear space, forming a bridge that spans the INM, perinuclear space and ONM (Cain et al., 2018). Nesprin-1 binds the actin cytoskeleton, whilst nesprin-1α2, a smaller nesprin-1 isoform, directly interacts with kinesin and microtubules (Zhou et al., 2012; Tapley and Starr, 2013; Holt et al., 2019). Lamin A/C composes the NL that underlies the INM. Emerin is an INM protein that interacts with BAF and HDAC3, which also interacts with LAP2β (Haraguchi et al., 2001; Somech et al., 2005; Collins, Ellis and Holaska, 2017). FHL1B is an isoform of FHL1 that interacts with emerin and lamin A/C (Ziat et al., 2016). Created with BioRender.com.*

1.4. Modelling EDMD/L-CMD

To further understand the pathogenesis of muscular dystrophies, many different disease models have been developed and used in research. Most often in studies, animal or cell culture models are used. However, the emergence and development of 3-dimensional tissue-engineered constructs has offered a new and exciting disease model. Here, the different EDMD/L-CMD models described in the literature are explored.

1.4.1. Cells and tissues

1.4.1.1. Human cells and tissues

A range of different cells and tissues have been used to examine the effects of EDMD/L-CMD associated mutations. Primary cells are cells that are isolated directly from live tissue (e.g., a patient biopsy) and established for growth *in-vitro*, they have normal cell morphology and maintain many of the important markers and functions seen *in-vivo* (Pan *et al.*, 2009). Primary cells, however, have a finite lifespan, limited expansion capacity, and with subsequent passages, the characteristics of primary cells may change. They are also extremely sensitive cells and may be more difficult to culture and sensitive to fluctuations in culture conditions. Primary cells from patients are also difficult to acquire. As described previously, L-CMD is an incredibly rare disease, thus there are less patients to acquire samples from. As well as this, it is difficult to isolate primary cells from tissue and obtain a pure population of the cell type of interest. As EDMD/L-CMD are striated muscle diseases, the most relevant cells to use for studies are myoblasts. Often primary myoblast cultures can become overrun by fibroblast cells, even cultures with a high (>90%) starting population of myoblasts (Alsharidah *et al.*, 2013). Using muscle tissue from patients may also be used for research and may arguably be more representative of *in-vivo* muscle compared to myoblast and myotube cell cultures, due to its composition of other different cell types besides muscle fibres including endothelial cells, fibro-apidogenic precursor cells, and immune cells (Pette and Staron, 1990). However, this heterogeneity may also be a disadvantage, as in the case of muscle diseases, it may primarily be muscle cells that are affected by disease and therefore the cell type of interest for experiments.

Immortal cell lines are often used in research as an alternative to primary cells. They are cost effective, provide an unlimited supply of material and they provide a pure population of cells. This is valuable as it provides a consistent sample and reproducible results (Kaur and Dufour, 2012). Mamchaoui *et al.* created a large collection of immortalized human myoblasts isolated from a wide range of neuromuscular disorders (Duchenne muscular dystrophy (DMD), facioscapulohumeral muscular dystrophy (FSHD), oculo-pharyngeal muscular dystrophy (OPMD), LGMD and L-CMD), to be used as experimental tools to study these diseases (Mamchaoui *et al.*, 2011). Replicative cellular senescence that is seen in human myoblasts is caused by two major mechanisms; (i) activation of the p16-mediated cellular stress pathway, and (ii) the progressive erosion of telomeres at each cell division until they reach a critical length that will trigger p53 activation and cell cycle exit (Renault *et al.*, 2002; Wright and Shay, 2002). Introducing the telomerase catalytic subunit (*human telomerase reverse transcriptase hERT*) cDNA alone allows an extension of the lifespan and even immortalization in a many cell types (Bodnar *et al.*, 1998; Vaziri and Benchimol, 1998). It has been shown, however, that the expression of both *hERT* and *cyclin-dependent kinase (CDK)-4* is required to successfully overcome cellular senescence in human myoblasts (Zhu *et al.*, 2007; Mamchaoui *et al.*, 2011). While hTERT elongates the telomere, CDK-4 blocks the $p16^{INK4a}$-dependent stress pathway (Mamchaoui *et al.*, 2011). As the cell cycle is related to other cellular processes including integrin regulation, the PI_3K/Akt pathway and microtubule stability, a study was conducted to determine whether genetic modification in the immortalized myoblasts relating to the cell cycle results in any secondary effects which may affect the validity of these cell models (Thorley *et al.*, 2016). Five healthy and disease muscle cell isolates were

subjected to transcriptomic analysis, comparing immortalized cell lines to their parent primary populations in both differentiated and undifferentiated states (Thorley *et al.*, 2016). Their myogenic character was also assessed by comparison with non-myogenic cells (Thorley *et al.*, 2016). From this, principal component analysis of global gene expression showed tight clustering of the immortalized myoblasts to their parent populations of primary cells, with clear differences shown from the non-myogenic reference (Thorley *et al.*, 2016). In conclusion, it was determined that the immortalization of these cells had no effect on the myogenic cascade or any other cellular processes (Thorley *et al.*, 2016). These human myoblast lines represent a powerful tool to assess signalling and/or functional dysregulations in neuromuscular diseases, in particular L-CMD and EDMD.

1.4.1.2. Use of other cell lines

Another approach to EDMD or L-CMD research is to genetically modify other cell lines so that they reflect the phenotype of patient cells and can be used for further studies. For these purposes, C2C12 is a frequently used cell line. C2C12s are an immortalized mouse myoblast cell line that is a subclone established from normal adult C3H mouse leg muscle treated with carcinogen 20, originally obtained by Yaffe and Saxel at the Weizmann Institute of Science in Isreal in 1977 (Yaffe and Saxel, 1977). These cells rapidly differentiate, forming multi-nucleated contractile myotubes and producing characteristic muscle proteins. As C2C12 cells are easy-to-grow, relatively hardy, and easily available, they are often used in a variety of experiments to model various muscle-related conditions. C2C12 cells are also relatively easy to transfect. This technique has been used to generate C2C12s harbouring *Lmna* exon 4 mutations

(Gómez-Domínguez *et al.*, 2020). In this study, CRISPR/Cas9 technology was used. Single guide RNAs (sgRNAs) were made to target exon 4 of *Lmna* (Gómez-Domínguez *et al.*, 2020). The sgRNAs were then cloned into a pX495 vector and transfected into C2C12s (Gómez-Domínguez *et al.*, 2020). The resulting cell models included different types of exon 4 deletions, as well as the R249W mutation, which is associated with L-CMD. The molecular, cellular, and functional features of these cells were studied, and the defects observed including lack of nuclear membrane integrity, defective myogenic differentiation, and protein mislocalization, were found to be consistent with previously reported cells harbouring *LMNA* mutations (Gómez-Domínguez *et al.*, 2020).

Using small interfering RNA (siRNA), cell lines may also be "knocked-out" for proteins of interest that are associated with the development of EDMD/L-CMD. This has previously been done in myoblasts derived from L-CMD patients. L-CMD human myoblasts have previously been shown to have enhanced activation of the yes-associated protein (YAP) signalling pathway (Bertrand *et al.*, 2014). siRNA was used in these cells to downregulate YAP, and the effects of this were studied, which included reduced adhesion and actin stress fibres in the *LMNA* myoblasts (Bertrand *et al.*, 2014). Similarly, knock-out cells have been produced by breeding *Emd*-null/*Lmna*-null mice with the H2K^{b}-*ts*A58 immortomouse, producing *Emd*-null/*Lmna*-null immortalized myogenic progenitor H2K cells (Koch and Holaska, 2012; Janin *et al.*, 2018). Emerin is a known binding partner of lamin A/C (Clements *et al.*, 2000), so the effects of ablation of emerin may be relevant to EDMD/L-CMD disease pathophysiology. *EMD*-null H2K cells have previously used to study the effects of emerin loss on signalling pathways in myogenic progenitors using whole genome

mRNA microarray analysis (Koch and Holaska, 2012). These cells have also been subjected to chromatin immunoprecipitation-DNA sequencing (ChIP-seq) to determine whether findings that have been observed in cells harbouring *LMNA* mutations, including disruption of epigenomic development programs and cell fate, also occur in the absence of emerin (Perovanovic *et al.*, 2016). *Lmna*-null H2K myoblasts have been used to model complete loss of lamin A/C expression in cells. Through comparing gene expression profiles in wild-type and *Lmna*-null H2K myoblasts, alterations of the bone morphogenetic protein (BMP) pathway have been revealed including Bmp4 downregulation and Smad6 overexpression (Janin *et al.*, 2018) (this is discussed in more detail in Section 1.6.). Knock-out of lamin A/C in cells is useful for elucidating the cellular roles of lamin A/C and processes that it is involved in, however, it is not an accurate representation of diseases-causing mutations in laminopathies. In cases where disease-causing mutations have loss-of-function effects, these models are a good approach, but mutations associated with L-CMD and EDMD do not cause complete ablation of the protein. Therefore, for modelling L-CMD/EDMD, a better approach is to transfect cells with disease-causing mutant constructs, as discussed above.

It is however important to mention, whilst C2C12 and H2K cells have been used to reveal insight into laminopathy pathophysiology, due to their immortal properties, these cell lines may have altered phenotype, native functions and responsiveness to stimuli (Kaur and Dufour, 2012). Serial passage of immortalized cell lines can further cause genotypic and phenotypic variation over time and genetic drift can also cause heterogeneity in cultures (Kaur and Dufour, 2012). Cell lines may therefore not adequately represent primary cells and may provide different results. As well as this,

C2C12 and H2K are derived from mice, therefore the effects of *Lmna* mutations, or ablation of protein expression, remains in a murine context, and there are often major biological differences between humans and mice (Mamchaoui *et al.*, 2011). Furthermore disease mechanisms may be different between the two species (Mamchaoui *et al.*, 2011). Consequently, human primary myoblasts that are isolated from patient biopsies provide the most pertinent experimental models to assess a variety of human genetic mutations in their natural genomic environment, but as mentioned previously, there are drawbacks to using primary cultures of human cells.

1.4.2. Tissue engineered models

The development of laboratory-grown tissues for many different scientific applications is rapidly expanding. For disease modelling, tissue-engineered constructs are an attractive option as they may be cheaper and more easily accessible than animal models and are superior to two dimensional (2D) cell culture models as they can mimic the *in-vivo* environment. In tissue engineering, cells are used with natural or synthetic scaffolds to create *in-vitro* bio-artificial tissue that can replace *in vivo* tissue in various applications (Gholobova *et al.*, 2018). Three-dimensional tissue can also be created by differentiation from stem cells (Gholobova *et al.*, 2018).

Maffioletti *et al* generated three-dimensional (3D) artificial skeletal muscle tissue from human pluripotent stem cells, including induced pluripotent stem cells (iPSCs) from patients with DMD, LGMD and L-CMD (Maffioletti *et al.*, 2018). The 3D skeletal myogenic differentiation of pluripotent cells was induced within hydrogels under unidirectional tension to provide myofiber alignment (Maffioletti *et al.*, 2018). In

similar studies, often primary human cells from invasive muscle biopsies are used. Here, iPSCs were used to overcome previously discussed issues with primary cells including limited cell expansion potential and exhaustion of differentiation ability. This 3D platform modelled cellular hallmarks of *LMNA*-related muscular dystrophies, and cell types present in muscle tissue, such as vascular cells and motor neurons, were derived from the same human induced pluripotent stem cell (hiPSC) source to generate isogenic multilineage muscle constructs (Maffioletti *et al.*, 2018).

As mentioned in Section 1.4.1.3., Gómez-Domínguez *et al.* used CRISPR-Cas9 technology to produce a selection of C2C12 cell models harbouring *Lmna* exon 4 mutations (Gómez-Domínguez *et al.*, 2020). This group also created 3D muscle models using these cells and a photo-molding technique (Gómez-Domínguez *et al.*, 2020). This enabled the nuclear morphology, fibre formation, and myogenic differentiation of the cells to be studied in a physiological condition, recreating native skeletal muscle (Gómez-Domínguez *et al.*, 2020).

Other studies that are unrelated to muscular dystrophy using 3D skeletal muscle models may also be useful for progressing research into neuromuscular disorders. Aguilar-Agon *et al.* developed a 3D tissue-engineered skeletal muscle model using the C2C12 murine cell line in order to determine whether mechanical loading stimulated hypertrophy and the consequential molecular and phenotypic responses (Aguilar-Agon *et al.*, 2019). The 3D tissue-engineered skeletal muscle was mechanically loaded using a bespoke bioreactor (Aguilar-Agon *et al.*, 2019). It has been speculated that the muscle wasting, weakness, and contractures that are observed in muscular dystrophies may be due to impaired skeletal muscle regeneration pathways. In this

case, it would be interesting to develop a 3D skeletal muscle model using human cells from patients with EDMD/L-CMD, and then similarly mechanically load the 3D skeletal muscle model and observe the effects.

1.4.3. Mouse models

Historically, mouse models have been used most frequently to model L-CMD and EDMD (**Table 1.1**). Mouse models provide a means to reproduce the human disease phenotype in a more closely phylogenetically related species, as there are numerous similarities between aspects of anatomy and physiology (Nicolas, Akimenko and Tesson, 2019). However, there are also differences between mice and humans in ontogeny, immunology, and the biomechanics of the musculoskeletal system (Hu *et al.*, 2017). In 1999, the first EDMD mouse model was created by Sullivan et al. A region of the mouse *Lmna* gene was deleted, extending from exon 8 to the middle of exon 11 (Sullivan *et al.*, 1999). This removed 114 codons as well as the 3'untranslated sequence, including the polyadenylation signal of lamin C, and 152 codons from the lamin A coding region, producing *Lmna*-null ($Lmna^{-/-}$) mice (Sullivan *et al.*, 1999). $Lmna^{-/-}$ mice have been used in various studies as a model of AD-EDMD. *Lmna*-null mice exhibit a severe muscular dystrophy phenotype, therefore there are advantages to using them in studies, however they are not necessarily an accurate representation of AD-EDMD. This is because *LMNA* mutations that are associated with AD-EDMD do not cause deletion or loss of function of the gene in humans. *Lmna* knock-in mice carrying a H222P mutation that was identified in the human *LMNA* gene in a family with AD-EDMD have also been produced and used to model AD-EDMD (Bonne *et al.*, 2000; Arimura *et al.*, 2005). $Lmna^{H222P/H222P}$ mice were created by reproducing the human

H222P mutation in the mouse genome. The same single nucleotide base change (C **A** T>C **C** T) in exon 4 of the murine *Lmna* gene and of the human *LMNA* gene directs the same amino acid replacement from histidine to proline at codon 222 in the murine lamins A/C as in the human proteins (c.665A>C, H222P) (Bonne *et al.*, 2000; Arimura *et al.*, 2005). These mice have been demonstrated to develop muscular dystrophy and dilated cardiomyopathy similar to that of human disease, suggesting they may be a better model of AD-EDMD (Arimura *et al.*, 2005). Prior to the creation of $Lmna^{H222P/H222P}$ mice, Mounkes *et al.* also attempted to create a mouse model for AD-EDMD using a similar strategy, by introducing a nucleotide base change into the *Lmna* gene, directing a substitution of proline for leucine at the residue 530 (L530P), a mutation that also causes AD-EDMD in humans (Mounkes *et al.*, 2003). Interestingly, it was found that mice homozygous for the mutation ($Lmna^{L530P/L530P}$) showed phenotypes markedly similar to symptoms observed in Hutchinson-Gilford progeria syndrome (HGPS), a disease which is also caused by mutations in *LMNA* (Mounkes *et al.*, 2003). It is not unusual for mouse models to exhibit a milder phenotype than the corresponding human disease, however it is curious that the L530P mutation, which causes AD-EDMD in humans, appears to have caused symptoms of a different laminopathy in mice. The disparity that can be seen between phenotypes in mice models and human disease raises questions about the reliability of these models.

In 2012, Bertrand *et al.* described the first mouse model of L-CMD, the knock-in $Lmna^{\Delta K32/\Delta K32}$ mouse harbouring the L-CMD K32del *LMNA* mutation (Bertrand *et al.*, 2012). Homozygous $Lmna^{\Delta K32/\Delta K32}$ mice exhibit generalized growth retardation and develop striated muscle and adipose tissue maturation defects, causing premature death in their third week of life (Azibani *et al.*, 2018). Standard systematic phenotyping

revealed a marked reduction or even an absence of white adipose tissue (WAT) in *Lmna*$^{\Delta K32/\Delta K32}$ mice, but brown adipose tissue was normal (Bertrand *et al.*, 2012). Histological analysis of WAT showed smaller adipocytes with reduced lipid accumulation compared to *Lmna*$^{+/+}$ and *Lmna*$^{+/\Delta K32}$ mice (Bertrand *et al.*, 2012). Whilst the development of the *Lmna*$^{\Delta K32/\Delta K32}$ mouse is a useful tool for investigating L-CMD, there are limitations to this model. Firstly, whilst the *Lmna*$^{\Delta K32/\Delta K32}$ mice develop striated muscle defects and exhibited a reduction in muscle fibre size compared with WT mice (Bertrand *et al.*, 2012), the metabolic defects including abnormal adipose tissue maturation and glucose homeostasis observed in these mice have not yet been observed in L-CMD patients. L-CMD patients should, however, be investigated for metabolic disorders, as fatty acid metabolism defects have previously been observed in patients with other neuromuscular disorders, such as SMA. Skeletal muscle is a tissue that is heavily involved in fatty acid metabolism, therefore impaired function of skeletal muscle could cause and/or amplify fatty acid metabolism (Morales, Bucarey and Espinosa, 2017). Unlike individuals with L-CMD, the mice eventually succumb to the metabolic abnormalities, not the muscle defects (Bertrand *et al.*, 2012). Another observation is that the K32del *LMNA* variant does not only cause L-CMD, but it has been reported that it also causes LGMD (Özyilmaz *et al.*, 2019), as well as EDMD (Muchir *et al.*, 2004).

Table 1.1- A summary of mouse models of skeletal muscle laminopathies.

Mouse model	Phenotypic features	Reference(s)
Lmna$^{-/-}$ (or *Lmna*$^{\Delta 8\text{-}11}$)	EDMD and DCM-CD	(Sullivan *et al.*, 1999; Jahn *et al.*, 2012)
Lmna$^{GT\text{-}/\text{-}}$	Impaired post-natal cardiomyocyte hypertrophy, skeletal muscle hypertrophy and metabolic defects.	(Kubben *et al.*, 2011)
Lmna$^{\Delta/\Delta}$	Similar to *Lmna*$^{GT\text{-}/\text{-}}$ mice, several growth defects and postnatal lethality.	(Kim and Zheng, 2013)
Lmna-Zp3	Reduced transcriptional activation of muscle related genes in muscle progenitor cells.	(Solovei *et al.*, 2013)
Lmna$^{H222P/H222P}$	EDMD and DCM-CD	(Arimura *et al.*, 2005)
Lmna$^{N195K/N195K}$	DCM-CD	(Mounkes *et al.*, 2005)
Lmna$^{M371K/M371K}$	EDMD and DCM	(Wang, Herron and Worman, 2006)
Lmna$^{\Delta K32/\Delta K32}$	L-CMD, defective skeletal and cardiac muscle maturation as well as metabolic defects.	(Bertrand *et al.*, 2012)
Lmna$^{\Delta K32/+}$	DCM	(Cattin *et al.*, 2013)
Lmna^{PLAO}	No defects	(Coffinier, Jung, *et al.*, 2010)
Lmna^{LAO}	No defects	(Coffinier, Jung, *et al.*, 2010)
Lmna^{LCO}	No defects	(Fong *et al.*, 2006)

Table lists all mouse models of skeletal muscle laminopathies including L-CMD and EDMD alongside phenotypical features associated with each mouse model and relevant references. Adapted from Brull *et al.* (Brull *et al.*, 2018)

1.4.4. Other Animal Models

Whilst other animals have not been used to develop models of laminopathies per se, they have proved useful for studying the roles of nuclear lamins and NE proteins in development, as well as other muscle diseases.

The nematode *Caenorhabditis elegans (C. elegans)* is a popular model organism that is used in a range of biological research. In 1998, *C. elegans* was the first multicellular organism to have its entire genome sequenced, and an extensive body of knowledge is now available on the molecular, cellular, developmental and behavioral biology of this organism (The C. elegans sequencing consortium, 1998). It is significantly anatomically simpler than a human, for example, it doesn't have a skeletal or circulatory system, however it shares many similarities such as genes and molecular pathways. There are many advantages to using *C. elegans*: the species can be grown cheaply and in large numbers, and they have a short, two-week lifespan. The anatomy and development of *C. elegans* can also be examined easily under a microscope as they are transparent throughout their lives. *C. elegans* is a particularly good model for studying laminopathies or NE-protein associated diseases as the organism has nuclear envelope proteins and dynamics that parallel the human nucleus, as well as differentiated cells and tissues including muscle (Wood, 1988; Culetto and Sattelle, 2000). *C. elegans* lamin (Ce-lamin) is encoded by a single gene *(lmn-1)* and shows many functional similarities to both human lamin A and lamin C proteins (Riemer, Dodemont and Weber, 1993; Liu *et al.*, 2000; Melcer, Gruenbaum and Krohne, 2007). Because of this conservation, it has been possible to mutate residues in Ce-lamin homologous to *LMNA* residues mutated in laminopathies to study their effects on a molecular level (Wiesel *et al.*, 2008; Ben-Harush *et al.*, 2009; Bank *et al.*, 2011). The LEM family of

nuclear proteins, to which emerin belongs, is also found in *C. elegans* (Gruenbaum *et al.*, 2002). Additionally, BAF, an interactor of emerin, is present in *C. elegans* (Gruenbaum *et al.*, 2002). Ce-emerin is encoded by *emr-1*, and other LEM-domain proteins, Ce-MAN1 and Ce-Lem3, are encoded by *lem-2* and *lem-3* (Lee *et al.*, 2000). Despite these similarities, humans do, however, have additional proteins at the INM that are unique to vertebrates (e.g. LAP2). Ce-emerin has been shown to be widely expressed, like human emerin, and is similarly dispensable during embryonic development, suggesting *C. elegans* is also an appropriate genetic model for emerin function (Gruenbaum *et al.*, 2002).

The fruit fly, *Drosophila melanogaster (D. melanogaster)*, is universally recognized as the main invertebrate model used to study developmental genetics and has now been used for over a century (Kohler, 1994). Similarly to *C. elegans,* one of the main advantages of using *Drosophila* is its short life cycle and minimal culturing requirements. Comparisons between the fully sequenced *Drosophila* and human genomes have revealed that approximately 75% of known human disease genes have a recognizable match in the genome of fruit flies, establishing its legitimacy as a model organism for medical research (Reiter *et al.*, 2001). The *Drosophila* genome possesses two genes encoding lamins, *Lamin C* and *lamin* Dm_0*,* which have been designated A- and B-type, respectively (Schulze *et al.*, 2009). Hence, *Drosophila* has been used as a model system to identify the roles of lamins in development. The effects of expressing mutant forms of the A-type *Drosophila* lamin, along with the effects of complete absence of the protein have been studied to provide insight on the roles of lamins in nuclear biology (Schulze *et al.*, 2009).

Danio rerio (D. rerio), also known as the zebrafish, is an established model of cardiac diseases due to its cardiac system's relative comparability to its mammalian counterpart, its transparency during early development, allowing for organ observation, its high fecundity and its ability to tolerate severe cardiac dysfunction that would be lethal at the fetal level in mammals (Vogel *et al.*, 2009; Shi *et al.*, 2018; Nicolas, Akimenko and Tesson, 2019). The vertebrate model zebrafish conserves the majority (84%) of the genes known to be associated with human diseases, both rare and common (Howe *et al.*, 2013). To produce disease models, three main methods are used in zebrafish: morpholino-mediated knockdown (Bedell, Westcot and Ekker, 2011), *N*-ethyl-*N*-nitrosourea (ENU) mutagenesis (Granato *et al.*, 1996), which has been widely used to identify new genes involved in muscle diseases (Plantié *et al.*, 2015), and finally genome-editing technologies such as clustered regularly interspaced short palindromic repeats technique (CRISPR) (Irion, Krauss and Nüsslein-Volhard, 2014). Zebrafish models have been most often previously used to study cardiac symptoms associated with skeletal muscle diseases.

1.5. Muscle cell development and differentiation pathway defects associated with mutations in LMNA thus far.

In this section, muscle cell development and differentiation pathways defects that have been identified thus far that are downstream of *LMNA* mutations in various models of EDMD are examined, as well as the general theories around the development of laminopathies.

As previously mentioned, mutations in *LMNA* are not only responsibly for skeletal muscle laminopathies, but a broad spectrum of diseases affecting a number of

different tissues and organ systems. Lamin A/C is expressed in almost all differentiated cells and tissues, though most laminopathies appear to affect only one or a few tissue types (Maggi, Carboni and Bernasconi, 2016). Two hypotheses are used in an attempt to explain this: the “structural” hypothesis and the “gene expression” hypothesis. According to the structural hypothesis, lamin A/C mutations alter the integrity of the NL leading to structural weakness and resulting in the nucleus being unable to resist mechanical stress within cells (Dubinska-Magiera, Zaremba-Czogalla and Rzepecki, 2013; Davidson and Lammerding, 2014). This primarily affects tissues that are exposed to strong mechanical tension, particularly muscle (Dubinska-Magiera, Zaremba-Czogalla and Rzepecki, 2013; Davidson and Lammerding, 2014). The gene expression hypothesis is based on interactions between the NL and chromatin, and between transcription factors and chromatin modifiers (Andrés and González, 2009). This theory assumes that mutations in *LMNA* alter the regulation of gene expression. There is accumulating evidence that these hypotheses may not be mutually exclusive, therefore it is likely that the development of L-CMD and EDMD are attributed to both a lack of structural integrity of the nucleus, as well as dysregulation of gene expression (Storey *et al.*, 2020). In the context of EDMD research, a number of studies have elucidated downstream molecular consequences of *LMNA* mutations, or complete ablation of *LMNA* in a variety of different models. The consequences of these defects include perturbation of muscle cell development and differentiation pathways, as will be discussed below.

Evidence has demonstrated that lamin A/C may be important for correct nuclear positioning in skeletal muscle. Altered anchorage of myonuclei and myonuclear clustering has been shown to lead to ineffective muscle contraction and has been

previously linked to the pathogenesis of muscle disorders (Mattioli *et al.*, 2011; Chapman *et al.*, 2014). A number of NE proteins have well-established roles in nuclear positioning in skeletal muscle, and it has been speculated that a protein complex that is involved in centrosome interplay during nuclear movement exists at the nuclear poles of differentiating myoblasts, which may be disrupted in skeletal muscle laminopathies (Mattioli *et al.*, 2018). Spindle associated membrane protein 1 (Samp1) is a binding partner of lamin A/C that is believed to be involved in nuclear movement and is necessary for muscle cell differentiation (Mattioli *et al.*, 2018). Prelamin A farnesylation (a precursor step to the formation of mature lamin A) impairment causes loss of Samp1 from the nuclear poles in myotubes from healthy donors, suggesting farnesylated prelamin A is needed to anchor Samp1 to the nuclear poles of differentiated muscle cells (Mattioli *et al.*, 2018). Samp1 has also been found to be absent from the nuclear poles in the nuclei of myoblasts and myotubes derived from an AD-EDMD patient harbouring a H506P *LMNA* mutation (Mattioli *et al.*, 2018). This suggests that mutations in *LMNA* cause mislocalization of Samp1, resulting in impairment of nuclear movement during myoblast differentiation. Another study, however, found that Samp1 was correctly localized in AD-EDMD patient myoblasts (Cadot, Gache and Gomes, 2015), suggesting Samp1 mislocalization is only affected by specific *LMNA* mutations.

Myogenic differentiation defects have also been associated with *LMNA* mutations. In *Lmna*$^{-/-}$ H-2K myoblasts, two major alterations in the bone morphogenetic protein (BMP) pathway have been identified: Bmp4 downregulation and Smad6 overexpression, leading to premature differentiation. These defects have also been identified and AD-EDMD patient myoblasts (Janin *et al.*, 2018; Storey *et al.*, 2020).

Receptor-regulated Smads (R-Smads), Smad1, Smad5 and Smad8 (pSmad1/5/8), are phosphorylated when Bmp4 binds to type 1 and type 2 transmembrane receptors, this then allows R-Smads to form a complex with Smad4 (Co- Smad), allowing their translocation into the nucleus to induce the transcription of target genes including Id1 and Id2 (Feng and Derynck, 2005). Id protein expression prevents the premature activation of differentiation factors, hence preventing premature muscle differentiation (Feng and Derynck, 2005). Alternatively, phosphorylated R-Smads can interact with Smad6, leading to an inhibitory effect on the BMP pathway and avoiding the expression of target genes (Feng and Derynck, 2005). Therefore, downregulation of Bmp4 prevents R-Smad phosphorylation and consequently the transcription of genes involved in preventing premature muscle differentiation, whilst Smad6 overexpression also leads to inhibition of transcription of these genes. The way by which lamins A/C may regulate Bmp4 and Smad6 expression is currently unclear.

Myogenic differentiation also involves three key cellular processes: the inactivation of pluripotency programs, exit from the cell cycle, and induction of myogenesis (by master transcriptional regulators, myoblast determination protein 1 (MyoD) and myogenin) (Perovanovic *et al.*, 2016). *LMNA* has a well-recognised role in the cell cycle and is transcriptionally induced at the point of exit from the cell cycle, as well as during the onset of terminal differentiation of myoblasts into myotubes (Furukawa *et al.*, 2009; Perovanovic *et al.*, 2016). Expression of EDMD-associated *LMNA* variant R453W in C2C12 cells impaired activation of the myogenin gene (*Myog)* and maintained a repressive chromatin state on the *Myog* promotor when differentiation was induced (Håkelien *et al.*, 2008). Furthermore, expression of the R453W variant in C2C12s redistributed H3K9me3 from pericentric heterochromatin (i.e., heterochromatin that

is located adjacent to the CENP-A rich centromere “central core” and is characterized by H3K9me3, a modified histone) (Probst and Almouzni, 2008). H3K9me3 contributes to gene regulation by forming repressive domains on chromosomes, preventing transcription factor binding (Probst and Almouzni, 2008). Conversely, the aggregation of pericentric heterochromatin into chromocenters is a hallmark of myogenic differentiation (Brero *et al.*, 2005; Håkelien *et al.*, 2008). These observations were all thought to contribute to impaired differentiation in the C2C12 cells that were transfected with *LMNA* R453W.

LMNA has also been implicated in the regulation of chromatin structure and function. The distribution of histone H3 trimethylated at lysine 27 (H327me3) and phosphorylated RNA polymerase II (markers of inactive and active chromatin domains, respectively), were found to be altered in myoblasts derived from a patient with EDMD caused by a R545C *LMNA* mutation (Kandert *et al.*, 2009). These findings support the theory that *LMNA* mutations affect transcription regulation in cells by changing the structure of chromatin and by modifying the function or distribution of factors that regulate gene expression. In addition, there is accumulating evidence that lamin A is involved in the epigenetic regulation of chromatin via an interaction with lamina-associated domains (LADs). LADS are heterochromatic (transcriptionally repressed domains) genomic regions that interact with the NL (Perovanovic *et al.*, 2016). Through mapping the euchromatin (transcriptionally active) transitions during muscle cell differentiation, it has been observed that *LMNA* mutation disrupt the normal euchromatic-heterochromatic (epigenomic) transitions at the NE during the differentiation of murine H2K cells and EDMD patient fibroblasts harbouring a H222P *LMNA* mutation (Perovanovic *et al.*, 2016). Perturbations of the epigenomic transitions

that were observed included exit from pluripotency and cell cycle programs, as well as the induction of myogenic loci (Perovanovic *et al.*, 2016).

The nuclear lamina interacts with chromatin at genomic regions called lamina-associated domains (LADs), which are transcriptionally repressed domains (Perovanovic *et al.*, 2016). The NL interacts with the INM and DNA, providing structural support and regulating DNA replication, transcription and cell division (Perovanovic *et al.*, 2016). There is accumulating evidence that lamin A is involved in the epigenomic regulation of chromatin via an interaction with LADs.

1.6. Approaches to therapy development in skeletal muscle laminopathies

One approach to L-CMD/EDMD therapy would be to correct the genetic defect, but by the time severe symptoms have developed, and a diagnosis is made, it may be too late for this to be fully effective (Storey *et al.*, 2020). This issue is further complicated by the fact that although EDMD disease onset is typically during childhood or early adolescence, this, along with the severity and phenotype of the disease, is often variable between individuals with little obvious relationship to the causative mutation (Storey *et al.*, 2020)(Bonne *et al.*, 2000). This is also a problem in L-CMD, as some cases present as an initially milder form of the disease that may progressively increase in severity, whilst some individuals are born with severe symptoms (Quijano-Roy *et al.*, 2008). An alternative approach is to identify and personalize therapies towards conserved features of the disease that could, in combination with gene-targeted therapy, offer maximum therapeutic benefit to all patients (Storey *et al.*, 2020). This approach is gaining momentum for spinal muscular atrophy (SMA). SMA is caused by

homozygous loss of *SMN1* gene in approximately 95% of cases, resulting in reduced levels of the survival of motor neuron (SMN) protein (Lefebvre *et al.*, 1995). Nusinersen (Spinraza™), an antisense oligonucleotide drug, or Zolgensma™ (previously known as AVXS-101), an adeno-associated viral-based gene replacement therapy, have been used to try to increase SMN protein levels. This has been successful to a certain degree, but none of these strategies show complete efficiency in patients (Finkel *et al.*, 2017; Mendell *et al.*, 2017; Mercuri *et al.*, 2018; Sumner and Crawford, 2018). Work is now underway to find alternative therapeutic strategies to be used in combination with SMN-targeted therapy to maximise the therapeutic benefit for SMA patients (Ramdas and Servais, 2020). For example, a SMN replacement therapy may be used alongside a drug which works to increase muscle mass or contraction, such as SRK-105 or Reldesemitiv (previously known as CY 5021 and CK-2,127,107) (Ramdas and Servais, 2020). SRK-105 is a monoclonal antibody that specifically inhibits myostatin activation which may promote a clinically beneficial increase in muscle strength, and Reldesemitiv is a selective small-molecule fast skeletal muscle troponin activator which aims to increase muscle fibre reactivity (Ramdas and Servais, 2020). These therapies are both currently still in late-stage development.

The ability to identify alternative therapeutic targets, however, requires an understanding of the molecular pathways acting downstream from the defective gene(s) to modulated disease pathogenesis, which, as discussed are still largely unknown in L-CMD/EDMD. In the sections below, current therapeutic strategies that are in development to treat L-CMD and EDMD are discussed.

1.6.1. Current therapeutic strategies in development to treat L-CMD

1.6.1.1. Gene therapy

One research group is working on developing a gene therapy for treating L-CMD, however this is currently only at the stage of testing proof of concept in the *Lmna*$^{\Delta K32}$ mouse model. Azibani *et al*. assessed the potential of *Lmna*-mRNA repair by spliceosome-mediated RNA trans-splicing (SMaRT) as a potential gene therapy for L-CMD (Azibani *et al.*, 2018). The SMaRT approach targets RNA at the pre-mRNA level and converts the endogenous mutated sequences to wild-type (WT) ones. This is achieved by expressing pre-*trans*-spliced molecules (PTMs) containing the WT coding sequence, a strong splicing site, and a binding domain to enable the specific binding of the PTMs to the targeted pre-mRNA (Azibani *et al.*, 2018). As the natural alternative splicing of A-type lamins occurs in a distal exon (exon 10, whilst there are 12 exons in total), and there is a high incidence of L-CMD associated mutations in the first exons of *LMNA*, the intron 5 of *Lmna* pre-mRNA was targeted by a 5'-*trans*-splicing strategy (Azibani *et al.*, 2018).

The group developed 5'-RNA pre-*trans*-splicing molecules containing the first five exons of *Lmna* and targeting intron 5 of *Lmna* pre-mRNA (Azibani *et al.*, 2018). Among nine pre-*trans*-splicing molecules that were created, differing in the targeted sequence in intron 5 and tested in C2C12 myoblasts, three induced *trans*-splicing events on endogenous *Lmna* mRNA. *Trans*-spliced lamin A/C was not detected in the C2C12 myoblasts using western blotting, due to low *trans*-splicing efficacy, so PCR was used to amplify the *trans*-spliced molecules and confirm the *trans*-splicing events at the molecular level (Azibani *et al.*, 2018). Immunofluorescence microscopy was then used

to verify that the *trans*-spliced mRNAs were properly translated into proteins and located at the nuclear envelope (Azibani *et al.*, 2018).

Further analysis conducted in myotubes from the L-CMD mouse model (*Lmna*$^{\Delta K32}$) led to partial rescue of the mutant phenotype. Previously, tissue from the *Lmna*$^{\Delta K32}$ mouse has been found to have reduced levels of lamin A/C, and lamin A/C fails to assemble properly under the nuclear lamina and so is found in the nucleoplasm (Azibani *et al.*, 2018). The nuclei of myoblasts derived from the *Lmna*$^{\Delta K32}$ mouse are misshapen and have reduced emerin staining compared to controls (Azibani *et al.*, 2018). *Trans*-splicing in *Lmna*$^{\Delta K32}$ mouse myotubes produced an increased proportion of A-type lamins at the NE, and improved staining of emerin (Azibani *et al.*, 2018). Myotube nuclei were also seen to regain their shape, as less elongated nuclei were observed after *trans*-splicing (Azibani *et al.*, 2018).

This approach was then tested *in-vivo* in newborn mice using the adeno-associated virus (AAV) delivery system, showing that *trans*-splicing events occurred in WT mice 50 days after AAV delivery, although this was at a very low rate (Azibani *et al.*, 2018). It was deduced that the modest increase in lamin A/C mRNA expression was too low to lead to any obvious benefits for the *Lmna*$^{\Delta K32}$ mice and after treatment, the mice showed no benefits in terms of survival rate and their severe phenotype did not appear to be rescued (Azibani *et al.*, 2018). These results are promising and provide the first evidence for reprogramming *LMNA* mRNA *in vitro*, although strategies to improve the rate of *trans*-splicing events still need to be developed for efficient application of this therapeutic approach.

1.6.1.2. Drug repurposing

A published abstract from the World Muscle Society (WMS) 2022 Congress also described a cohort pilot study to evaluate the effect of treatment with deflazacort in a cohort of 20 L-CMD or EDMD patients with infantile onset (Ricci *et al.*, 2022). Deflazacort is a glucocorticoid that is derived from prednisolone and is used to treat a range of inflammatory disorders. Chronic use of glucocorticoids cause extensive side effects including insulin resistance and muscle weakness through inducing skeletal muscle atrophy by stimulating atrogene expression (Bodine *et al.*, 2001; Strehl *et al.*, 2016), however glucocorticoids have also been used to enhance muscle performance and/or improve recovery from injury in short dosing regimens (Collomp *et al.*, 2016). Weekly and daily dosing of glucocorticoid steroids in mouse models of LGMD 2B (*Dysf-null*) and LGMD 2C (*Sgcg-null*) have been found to correlate with enhanced myofiber membrane repair after microinjury *in vitro,* which was accompanied by reduced immune and fibrotic muscle infiltrates *in vivo* (Quattrocelli, Salamone, *et al.*, 2017). Furthermore, weekly dosing of steroids correlated with enhanced muscle performance and regeneration (Quattrocelli, Salamone, *et al.*, 2017). Similarly, in the *mdx* model of Duchenne muscular dystrophy (DMD), weekly dosing of glucocorticoids improved muscle function and improved sarcolemma repair (Quattrocelli, Barefield, *et al.*, 2017). Deflazacort treatment of DMD has been shown to improve muscle strength and delay the loss of ambulation in these patients (Biggar *et al.*, 2001). The study of deflazacort treatment in L-CMD patients aims to analyse the secretome profile at basal condition and during steroid treatment, to evaluate variations and establish whether there is a correlation between steroid use and clinical outcomes (Ricci *et al.*, 2022). Even if this treatment proves to be efficacious, however, it will only alleviate symptoms to some

extent. Furthermore, it would only be an option for a certain subset of L-CMD patients with less severe symptoms for a benefit to be observed, as DMD patients are given deflazacort whilst their motor function is in the "plateau phase", where they still have good muscle strength.

1.6.2. Current therapeutic strategies in development to treat EDMD

Since the *LMNA* gene was identified as a causative mutation in EDMD, numerous potential treatment options have emerged. The efficacy of these therapies have mostly only been evaluated in mouse models, although some have reached the clinical trial stage. The treatment strategies have mostly been developed to target the MAPK signalling pathway in order to induce autophagy or inhibit apoptosis, and they all aim to ameliorate the cardiac phenotype observed in EDMD patients, this being the life-threatening aspect of the disease.

1.6.2.1. Targeting of the MAPK signalling pathway

Previously, activation of ERK, JNK and p38α cascades were observed in hearts from *Lmna*$^{H222P/H222P}$ mice, connecting the activation of MAPK pathways to *LMNA* mutations causing cardiomyopathy (Muchir *et al.*, 2007; Muchir, Wu, *et al.*, 2012). Therefore, inhibitors of MAPK have been explored as a therapeutic option in *LMNA* cardiomyopathy, which is also a feature of EDMD. MAPK signalling pathways are crucial transduction cascades that are initiated by cytokines, mitogens, and growth factors on the cell surface, which are finalized in the nucleus to control gene expression (Davis, 1993). They are involved in the regulation of a number of differentent cellular processes including cell proliferation and differentiation, survival, and apoptosis. The MAPK pathway consists of four key signalling cascades:

MAPK/ERK1/2 (the classical MAPK pathway), JNK, p38, and ERK5 signalling cascades (Keshet and Seger, 2010). Pharmaological inhibitiors of ERK1/2 have been shown to have some efficacy in *Lmna*$^{H222P/H222P}$ mice. An inhibitor of MEK1/2 (PD098059) was one of the first MEK (a phosphorylator of ERK1/2) inhibitors to be tested in these mice and was found to delay the development of left ventricular dilation, as well as improving function (Muchir *et al.*, 2009). Selumetinib, a more potent and selective inhibitor has also shown to improve left ventricular dilation, increase cardiac fraction shortening, decrease cardiac fibrosis, and prolong survival compared to placebo-treated mice (Muchir, Reilly, *et al.*, 2012). Inhibitors of both JNK and p38α have also been assessed in *Lmna*$^{H222P/H222P}$ mice. Treatment with ARRY-371797, a specific p38α inhibitor delayed left ventricular dilation, as observed with the ERK1/2 inhibitors, as well as a reduction in the decrease of fractional shortening compared to placebo-treated mice. ARRY-371797 was then tested in patients in the first clinical trial for individuals with cardiomyopathy caused by *LMNA* mutations (Muchir, Wu, *et al.*, 2012). ARRY-371797 was assessed in clinical trials and was shown to be generally well tolerated and efficacious (Judge *et al.*, 2022), however in August 2022 Pfizer announced that the Phase 3 trial to evaluate the efficacy and safety of ARRY-371797 was to be discontinued due to the trial being unlikely to meet its primary endpoint upon completion (Pfizer, 2022).

1.6.2.2. Autophagy induction

Activation of AKT (a mTORC1 activator), as well as mTORC1 and defective autophagy have been observed in the hearts of *Lmna*$^{H222P/H222P}$ mice prior to the onset of cardiomyopathy (Choi *et al.*, 2012). mTOR signalling is involved in a range of

fundamental cellular processes, including autophagy, and is a serine/theonine kinase that forms the core of two protein complexes, mTORC1 and mTORC2. mTORC1 plays a key role in controlling protein, lipid and nucleotide production, and also downregulated autophagy (Saxton and Sabatini, 2017). mTORC2, on the other hand, increases cellular proliferation and survival (Saxton and Sabatini, 2017). Rapamycin is a drug that is widely used in cancer treatment and is known to inhibit mTORC1, prolonged rapamycin treatment abolished mTORC2 signalling (Sarbassov *et al.*, 2006). Tesirolimus, an FDA approved semi-synthetic rapamycin analogue, was used to treat 14-week old *Lmna*$^{H222P/H222P}$ mice, and this was found to reactivate autophagy and decrease left ventricular end-systolic dilation, increased fractional shortening but did not stop cardiac fibrosis (Choi *et al.*, 2012). In addition to this, everolimus, another analogue of rapamycin, has been shown to improve the phenotype in laminopathy fibroblast cells (DuBose *et al.*, 2018). These studies suggest that a mTORC1 inhibitor may be a potential treatment option for laminopathy patients.

1.6.2.3. Apoptosis suppression

In the hearts of *Lmna*$^{\Delta 8-11}$ mice and cardiac myocytes, it was found that there was an activation of forkhead box O transcription factors (FoxO TFs) 1 and 3, and deleterious consequences of overactivation of FoxO TFs (Auguste *et al.*, 2018). FoxO TFs are downstream targets of AKT, which phosphorylates FoxO TFs, inhibiting their function, and contributing to cell growth, proliferation and survival (Zhang *et al.*, 2011). It was demonstrated that subcutaneous injection of AAV9 encoding short hairpin RNA (shRNA) specific to FoxO1 and 3 in *Lmna*$^{\Delta 8-11}$ newborn mice efficiently reduced cardiac FoxO1 and 3 transcript levels similar to wild-type, also reducing FoxO target genes that

are involved in apoptosis (Auguste *et al.*, 2018). Furthermore, knockdown of FoxO TFs within the heart of these mice resulted in prolonged survival compared to untreated *Lmna*$^{\Delta 8-11}$ mice (Auguste *et al.*, 2018). These findings therefore, also present a potential target to treat the cardiac phenotype in laminopathies.

1.7. Future approaches to research in L-CMD and striated muscle laminopathies

One approach to research in EDMD and L-CMD is to identify mutant genes, produce a model harbouring the mutations that are found in patients, then analyse the effects of the mutation within the cell. A range of different research techniques and technologies have been used to determine downstream consequences of *LMNA* mutations in models of L-CMD and EDMD. This approach has allowed some progress in understanding the underlying mechanisms behind the pathophysiology of the diseases; however, many aspects still remain elusive, as is discussed in further detail in Chapter 4, Section 4.1. Traditional biochemical methods for studying proteins, as have been often used in EDMD/L-CMD research, are biased towards a relatively small number of proteins for which high-quality, mainly antibody-based assays have been available (Schubert *et al.*, 2017). Over the past two decades, proteomics methods have emerged as the method of choice for the near-exhaustive identification and quantification of the proteins contained in a biological sample, and have significantly contributed to the unravelling of cellular signalling networks, elucidation of the dynamics of protein-protein interactions in different cellular states, and improved diagnosis and molecular understanding of disease mechanisms (Schubert *et al.*, 2017). Proteomics methods are described in more detail in Chapter 5, Section 5.1.

Proteomics can be used to further clarify the molecular perturbations downstream of disease-causing mutations, and this approach would be insightful in EDMD/L-CMD research. The identification of dysregulated pathways and protein interactions is required to fully understand the fundamental biological role(s) of EDMD/L-CMD related genes in cells and tissues of the body, as well as to develop a range of therapeutic targets for developing novel treatments for these diseases. This is an approach that is gaining popularity in many neuromuscular diseases including SMA research. Developments in proteomic screening technologies have facilitated proteome-wide investigations of a range of SMA models and tissues, generating novel insights into disease mechanisms by highlighting conserved changes in a range of molecular pathways (Fuller, Gillingwater and Wishart, 2016).

1.8. Conclusions

L-CMD is a relatively newly characterised, extremely rare skeletal muscle laminopathy, caused by mutations in *LMNA*. As a result, there is less known about the defective molecular mechanisms behind the pathophysiology of the disease. L-CMD, does, however, bare some clinical resemblance to AD-EDMD, and the similarities between the two conditions call into question whether these are two distinct conditions, or whether L-CMD is simply a more severe version of EDMD. As the two diseases are both caused by mutations in *LMNA,* and considering they share some phenotypical characteristics, the two decades of research into EDMD provides a starting point for further research into L-CMD. This research into EDMD has clarified key roles of lamin A/C in muscle cell differentiation and development, as well as elucidating some downstream consequences of *LMNA* mutations in numerous laminopathy models. This

has consequently identified various targets for the development of therapies that are at various stages of pre-clinical or clinical development. The therapies for EDMD, however, aim to ameliorate cardiac abnormalities in these patients. Whilst this is a key feature of EDMD that contributes to premature death in these patients, in L-CMD, the primary life-threatening symptom is weakening of the muscles in the chest leading to respiratory insufficiency. Cardiac arrhythmias are more frequently observed in L-CMD patients, rather than cardiomyopathy, which these therapies intend to treat in EDMD. Although L-CMD and EDMD may share some dysregulated pathways as a result of *LMNA* mutations, therapies for treating L-CMD may need a different direction.

Currently there are few models of L-CMD, and in past studies, the $Lmna^{\Delta K32}$ mouse has mostly been used for research purposes. Whilst this has been insightful, findings in the $Lmna^{\Delta K32}$ mouse should be confirmed in L-CMD derived patient cells. In this thesis, L-CMD patient myoblasts and myotubes harbouring different mutations in *LMNA* will be analysed to determine their cellular characteristics including cellular morphology and proliferation rate. Interaction partners of lamin A in L-CMD myoblasts will also be determined and compared to lamin A interactors in control myoblasts. A targeted approach will then be used to characterize protein expression and localization of specific LINC complex components and lamin A interactors in L-CMD myoblasts and myotubes compared to controls. Then using an unbiased, large-scale approach, proteomics will be used to quantitatively compare the proteome of L-CMD myoblasts and myotubes to control myoblasts and myotubes.

The aim of this thesis was to identify conserved molecular and cellular defects, as well as molecular pathways downstream of R249W, del.K32 and L380S *LMNA* mutations in myoblasts derived from L-CMD patients that may be targeted for therapy development or used for biomarker purposes in future studies.

Specific objectives were:

- To identify putative lamin A interactors in healthy control and L-CMD myoblasts using co-immunoprecipitation and liquid chromatography-mass spectrometry (LC-MS), and determine whether any lamin A interactors are lost or gained in myoblasts from L-CMD patients. To determine whether previously identified lamin A interactors in healthy cells and tissues are present in human myoblasts.
- To characterize the cellular morphology and growth rate, in addition to characterising the expression levels and distribution of key components of the LINC complex and lamin A interactors in myoblasts and myotubes derived from L-CMD patients compared to healthy controls.
- To use quantitative proteomics to compare the proteome of L-CMD myoblasts and myotubes to control myoblasts and myotubes to elucidate downstream molecular consequences of *LMNA* mutations in L-CMD cells, and to determine whether there is a core molecular signature of L-CMD that is shared across the three different *LMNA* mutations.
- To conduct a systematic review following PRISMA guidelines into published mutations of genes encoding NE proteins associated with the LINC complex. These include: *LMNA* (lamin A/C), *LMNB1/LMNB2* (lamin B1/B2), *EMD*

(emerin), *TMEM43* (LUMA), *SYNE1/SYNE2* (nesprin-1/2). To determine whether any genotype-phenotype correlations exist between the location of mutations on the NE protein gene, and different disease phenotypes

Chapter 2: Materials and Methods

2.1. Cell culture methods

2.1.1. Cell lines

Immortalized myoblast cell lines (**Table 2.1**.) were from six human control donors without neuromuscular disease (aged 5 days, 25 years, 41 years, 53 years, 79 years and 83 years), from three congenital muscular dystrophy patients with mutations in the lamin A/C gene (L380S, del.K32 and R249W) (Mamchaoui *et al.*, 2011). They were immortalized by transduction with human telomerase reverse transcriptase (*hTERT*) and cyclin-dependent kinase-4 (*Cdk4*) containing retroviral vectors, at the Institut de Myologie, Paris, as described previously (Mamchaoui *et al.*, 2011). Cellular senescence is thought to be triggered by telomere shortening, which occurs because of repeated cell division (Bernadotte, Mikhelson and Spivak, 2016). Introduction of hTERT elongates the telomere, which extends the life span of cells, and in some cell types may result in immortalization (Bodnar *et al.*, 1998). Cdk4, on the other hand, blocks the $p16^{INK4a}$-dependent stress pathway which triggers growth arrest (Ramirez *et al.*, 2003). The expression of hTERT in combination with Cdk4 have been found to successfully overcome cellular senescence in human myoblast (Mamchaoui *et al.*, 2011)

Table 2.1- Immortalized myoblast cell lines from control donors and congenital muscular dystrophy patients

Cell Line	Donor	Donor Muscle
C5d	Newborn (5.5 day old), female	Quadriceps
C25yr	25 years, male	Semitendinosus
C41yr	41 years, male	Pectoralis major
C53yr	53 years, male	Quadriceps
C79yr	79 years, female	Quadriceps
C83yr	83 years, male	Quadriceps
LMNA L380S	12 years, male. *LMNA* c.1139T > C, p.Leu380Ser Heterozygous	Paravertebral
LMNA del.K32	5 years, female. *LMNA* c.94_69delAAG, p.Lys32del Heterozygous	Gastrocnemius
LMNA R249W	3 years, male*. *LMNA* c.745C > T, p.Arg249Trp Heterozygous	Deltoid

Table listing each immortalized myoblast cell line, both from healthy control donors and L-CMD patients, along with the donor age, gender, and donor muscle. For the L-CMD cell lines the *LMNA* mutation is also listed. *For the *LMNA* R249W cell line, there was some discrepancy about the age of the donor. When the cell line was supplied, the gender was listed as male, however a publication using the same cells has the gender listed as female (Bertrand *et al.*, 2014).

2.1.2. Thawing of cell lines

Immortalized myoblasts were removed from storage in liquid nitrogen (N_2; -196°C) and placed in a -80°C freezer for at least one hour before being thawed in a 37°C water bath. The thawed cell suspension was transferred to a universal tube along with 4mL of skeletal muscle cell growth medium (Cat No: C-23060; PromoCell) containing supplement mix (Cat No: C-39365; PromoCell) with 20% fetal bovine serum (Cat No: 10270; Gibco; ThermoFisher Scientific) and 1% penicillin-streptomycin (Cat No: 15140122; Gibco; ThermoFisher Scientific) and centrifuged for 6 minutes at 1300 RPM (4K15; Sigma Laboratory Centrifuges). Following centrifugation, supernatant was removed, and the cell pellet was resuspended in complete growth medium.

2.1.3. Cell viability and cell count

Cell viability was determined using the trypan blue exclusion test. The dye exclusion test is based on the principle that live cells possess intact cell membranes that exclude certain dyes such as trypan blue, eosin, or propidium, whereas dead cells do not (Strober, 2015). Dead cells, therefore, are stained blue, whilst live cells remain colourless. For this test, 20-30µL of cell suspension was mixed with an equal volume of 0.4% trypan blue (Cat no: T6146; Sigma Aldrich), placed in the incubator at 37°C for three minutes, then pipetted onto a haemocytometer. Cells in the four squares of the haemocytometer were counted to assess the percentage of viable cells in the suspension, and cell concentration (number of viable cells per mL of medium) using the following calculations:

Cell viability (%) = (number of live cells/ total number of cells) x 100

Cell concentration (cells/mL) = [(N/4) x d] x 10000

"*N/4*" represents the average number of viable cells across the four corner squares of the haemocytometer, and "*d*" represents the trypan blue dilution factor.

2.1.4. Cell culture and harvest

After thawing cell lines, as described in Section 2.1.2., immortalized myoblast cells were seeded at a density of around $2.2x10^4$ cells/cm. Cell pellets were resuspended in skeletal muscle cell growth medium supplemented with 20% fetal bovine serum and 1% penicillin-streptomycin, and cell suspension was added into three T25 flasks (Starstedt) and maintained in a humidified incubator (Leec) at 37°C, 5% carbon dioxide (CO_2) concentration. Cells were grown to approximately 60-80% confluency before passaging into larger T75 flasks. For the time-course experiment, cells were expanded in T75 flasks before being re-seeded into seven individual T25 flasks, each representing seven different time-points.

This method was also adapted for the study where Necrostatin-1 (Nec-1) was used to treat L-CMD myoblasts. L-CMD myoblasts (L380S, del.K32, R249W) were thawed and culture as mentioned above. For the drug study, after expansion into T75 flasks, when the cells reached approximately 70-80% confluency, cells were tripsinized and re-seeded in T25 culture flasks containing complete medium. Each cell line was grown in seven T25 flasks; three flasks were treated with drug, three were untreated, and three were vehicle treated; this provided three technical replicates for each group. The

remaining T25 flasks were used to assess cell viability after drug treatment. The cells were maintained as outlined above. The L-CMD myoblasts were treated with Nec-1, to investigate whether the expression of proteins associated with the necroptosis pathway were altered in the cells after treatment. Once the cells reached 70-80% confluency, they were treated with Nec-1 at a concentration of 30µM. This concentration was determined as Nec-1 EC50=490nM for blocking necroptosis, and previous studies have determined 30µM is the optimal concentration for this purpose (Feyen et al., 2013). Nec-1 was dissolved in DMSO according to instructions provided with the datasheet to make a stock solution. This stock solution was then diluted 1:1000 with complete media, and sterile filtered to prevent microbial contamination. Cell culture medium was removed from the cells, and the medium prepared with Nec-1 was applied to the cells for four hours. After 4 hours of Nec-1 treatment the cells were harvested as described in Section 2.1.4. Media containing a 1:1000 dilution of DMSO was also applied to vehicle treated cells. This dilution was chosen to ensure all drug and vehicle treated flasks contained the same final concentration of the vehicle (i.e., 0.1%). Untreated control cells were only grown in complete media.

To harvest cells, the culture medium was removed from the flasks and the cells were incubated 37°C with trypsin-EDTA (0.25%) (Cat no: 25200056; Gibco; Thermofisher Scientific) for 2 minutes. Trypsin is a proteolytic enzyme that cleaves peptides on the C-terminal side of lysine and arginine residues of adhesion in cell-cell or cell-matrix, allowing cells to detach from their culture vessel. EDTA is a chelating agent that neutralises calcium and magnesium ions that integrins require to maintain cell adhesion. By removing these ions, enzyme activity is increased. Cells were aided in their detachment by gently tapping the flask. Dulbecco's Modified Eagle Serum

(DMEM) (Cat no: 31966-021; Gibco; ThermoFisher Scientific) with 10% Fetal Bovine Serum was added to neutralize trypsin activity before centrifuging the cell solution for 6 minutes at 1300 RPM. The supernatant was discarded, and cell pellets were resuspended in either complete growth medium, to be seeded into T75 or T25 cell culture flasks, or serum free DMEM and washed by centrifuging at 1300 RPM for 6 minutes to harvest the cell pellets. Cell pellets were generally harvested at 80-90% confluency, although an exception to this was during the time-course experiment when cells were harvested based on their respective time-point (**Table 2.2**). The DMEM was then removed and the universal tube containing the cell pellet was wrapped in parafilm and stored in a -80°C freezer until needed for further processing.

Table 2.2- Time-points used in time course experiment

Time-point	Time at which cells were harvested
Time-point 1	24 hours after myoblasts were seeded
Time-point 2	Once myoblasts had reached 80-90% confluency (72-144 hours depending on the cell line)
Time-point 3	24 hours after differentiation media was added to myoblast cultures
Time-point 4	48 hours after differentiation media was added to myoblast cultures
Time-point 5	72 hours after differentiation media was added to myoblast cultures
Time-point 6	96 hours after differentiation media was added to myoblast cultures (point at which 80% of myoblasts should have formed myotubes)
Time-point 7	120 hours after differentiation media was added to myoblast cultures (point at which majority of myoblasts should have formed myotubes)

Table listing each time-point used in time course experiment, along with a description of time at which cells were harvested.

Differentiation was induced in myoblasts once they had reached 80-90% confluency by washing adherent myoblasts in serum free medium and then culturing in DMEM supplemented with Insulin-Transferrin-Selenium-Ethanolamine (ITS-X) (Cat No: 51500-056; Gibco; ThermoFisher Scientific) and 1% Penicillin-Streptomycin. ITS-X reduces the levels of serum in the culture, enhancing the formation of myotubes (Lawson and Purslow, 2000). After a further four days of cell culture, approximately 80% of the cells had fused into myotubes.

For immunohistochemistry analysis, cell pellets were resuspended in skeletal muscle cell growth medium supplemented with 20% fetal bovine serum and 1% penicillin-streptomycin and seeded onto glass coverslips (22mm x 22mm) at a density of between 2.5 x 10^4 and 5 x 10^4 per coverslip. Coverslips were placed in petri dishes and maintained in an incubator under the conditions previously described. After reaching 80% confluency or the desired timepoint for the time-course experiment, as outlined in **Table 2.2.** medium was removed and coverslips were washed twice in phosphate buffered saline (PBS) (0.02M Sodium Phosphate Dibasic Dodecahydrate; (Cat no: 71649; Sigma Aldrich) and 0.15M Sodium Chloride (Cat no: BP359; ThermoFisher Scientific); pH 7.2 adjusted with phosphoric acid (Cat no: 52P-6560; Sigma Aldrich)). Cells were then fixed in acetone (Cat no: 67641; ThermoFisher Scientific): methanol (Cat no: 67561; ThermoFisher Scientific) (50:50 solution ratio) for 5-10 minutes. The solution was then removed, and the coverslips were left to dry for 15-20 minutes before being stored in a -80°C freezer until needed.

2.1.5. Cryopreservation

As previously outlined, myoblasts were trypsinised and centrifuged at 1300 RPM for 6 minutes. After discarding the supernatant, cells were resuspended in fetal bovine serum and 10% dimethyl sulfoxide (DMSO) (Cat no: BP231-100; ThermoFisher Scientific) and placed in cryovials in a -80°C freezer for at least one hour before being transferred to liquid nitrogen for storage. The addition of DMSO prevents the formation of ice crystals which may lyse cells during the thawing process.

2.2. Analysis of protein expression and localization

2.2.1. Quantitative western blotting

Quantitative western blotting is an established technique which allows the identification and separation of specific proteins from cell lysates. Here, western blotting was used to quantify protein expression levels in immortalized control (n=6) and L-CMD (n=3) myoblasts and myotubes as described in section 2.1.1.

2.2.1.1. Protein extraction

Myoblast and myotube pellets were resuspended in 2 x modified radioimmunoprecipitation assay (RIPA) buffer (0.25% deoxycholic acid (Cat no: D6750; Sigma Aldrich), 1mM ethylenediaminetetracetic acid (EDTA) (Cat no: 104245S, BDH), 150mM sodium chloride (Cat no: BP358; ThermoFisher Scientific) and 50mM TRIS-HCl buffer, pH 7.4 (Cat no: T1503; Sigma Aldrich)). Deoxycholic acid is an ionic surfactant which aids in the solubilization of proteins, whilst EDTA protects against oxidative damage and acts as a protease inhibitor, preventing the degradation of proteins. Tris-HCl buffer maintains pH within a physiological range to prevent proteins from precipitating or becoming unstable, and the addition of a salt, such as sodium chloride,

also prevents protein precipitation. Samples were left on ice for 5 minutes, then sonicated briefly at 5 microns for 10 seconds (Sonicrep 150; MSE). Samples were centrifuged for 5 minutes at 13,000 RPM (Harrier 18/80R; MSE) at 4°C to pellet any insoluble material.

2.2.1.2. Protein quantification using bicinchoninic acid (BCA) protein assay

The protein concentration of cell extracts was determined using the Pierce™ BCA Protein Assay Kit (Cat no: 23227; ThermoFisher Scientific). The principle of the bicinchoninic acid (BCA) assay method is that proteins reduce Cu^{+2} to Cu^{+1} in an alkaline solution (the biuret reaction) which results in a purple colour formation in bicinchoninic acid (Smith *et al.*, 1985). Colour intensity, therefore, is directly proportionate to protein concentration. Bovine serum albumin standards were prepared at a working range from 0.125-2mg/mL in extraction buffer. Working reagent was produced by combining BCA reagent A with reagent B in a ratio of 50:1. Samples were produced in triplicate and prepared in a 96-well plate by pipetting 10µL of diluted cell extract into each well followed by 200µL of working reagent. The plate was placed on a plate shaker for 30 seconds to ensure the reaction components were combined before being incubated at 37°C for 30 minutes. Absorbance was then measured at 526nm using a FLUOstar Omega (BMG Labtech) microplate reader. A standard curve was prepared by plotting the average blank-corrected absorbance of the standards against their corresponding concentrations. From this, a quadratic equation could be derived so that unknown concentrations of samples could be determined.

2.2.1.3. Sodium dodecylsulfate -polyacrylamide (SDS-PAGE) gel electrophoresis

Based on the calculated measurements obtained from the BCA protein assay, protein extracts were diluted with the appropriate volume of 2x Laemmli sample buffer (4% sodium dodecyl sulfate (SDS) (Cat no: AM9823; Invitrogen), 10% 2-mercaptoethanol (Cat no: M3148; Sigma Aldrich), 20% glycerol (Cat no: G9012; Sigma Aldrich), 0.125 M TRIS-HCl ph 6.8 (Cat no: T1503; Sigma Aldrich)) (Laemmli, 1970) . This ensured the protein concentration in the samples were correctly balanced. The prepared samples were then briefly heated to 95°C for 3 minutes. SDS is a detergent that disrupts non-covalent bonds within proteins to destabilize the secondary, tertiary, and quaternary structural assemblies, also imparting a uniform negative charge and linearizing proteins. 2-mercaptoethanol breaks covalent cysteine-cysteine disulphide bridges, therefore both of these components work to denature the proteins within the samples. By applying an electric current through the system, negatively charged proteins migrate to the positively charged cathode and are separated by their mass on the polyacrylamide gel. Samples along with PageRuler™ Protein Ladder (Cat no: 26619; Thermo Scientific) were then loaded into Bolt™ 4-12% Bis-Tris 15-well precast gels (Cat No: NW04125BOX; Life Technologies) which was submerged in 1 x SDS running buffers. Either NuPAGE™ MOPS (Cat no: B0001; Invitrogen) or MES (Cat no: B000202; Invitrogen) SDS Running Buffer (20X) was used for the separation of large to medium, or small sized proteins, respectively. MES has a lower pKa than MOPS, which allows the MES buffer to run faster than MOPS. The difference in ion migration affects stacking and results in a difference in protein separation range between these buffers. Proteins were subjected to gel electrophoresis at 140 V using PowerPac BASIC™ (Biorad).

2.2.1.4. Protein transfer to nitrocellulose membrane and immunoblotting

A small section of the gel which did not contain any proteins of interest was excised and stained with Coomassie blue (0.2% Coomassie Brilliant Blue R (Cat no: B-0149; Sigma Aldrich), 10% acetic acid (Cat no: 64197; Thermofisher Scientific), 20% industrial methylated spirits (IMS) (Genta Medical) and 70% dH_2O) overnight, as an internal loading control for total protein. Coomassie dye binds to proteins (primarily arginine, lysine and histidine) through ionic interactions between sulfonic acid groups and positive protein amine groups through Van der Waals attractions. After leaving the gel in Coomassie blue, it was left in de-stain solution (10% acetic acid, 20% IMS, 70% dH_2O) until the background staining was removed and stained protein bands could be clearly seen. A nitrocellulose membrane was placed on top of the remaining gel, this was then positioned between two pieces of filter paper to create a "sandwich" and submerged in transfer buffer (Towbin buffer) (192 mM glycine (Cat no: G7126; Sigma Aldrich), 25 mM Trizma base (Cat no: T1503; Sigma Aldrich)). Proteins were transferred onto the nitrocellulose membrane by electroblotting at 100 mA using PowerPac BASIC™ overnight (Towbin, Staehelin and Gordon, 1979). To keep the system from overheating, cold water was constantly running through a cooler that was placed in the transfer tank.

After protein transfer was finished, the membrane was removed from the system and placed in blocking buffer (4% powdered milk in PBS) for one hour. This prevents non-specific antibody binding. The membranes were washed three times for 5 minutes in PBS before incubating with primary antibody (**Table 2.3.**) in western blot buffer (1% FBS, 1% Horse Serum (Cat no: 16050130; Gibco), 0.1% BSA (Cat no: A7906, Sigma Aldrich) and 0.05% Triton X-100 (Cat no: X100, Sigma Aldrich) in PBS) at room

temperature for two hours. After washing the membranes again three times in PBS for 5 minutes, they were incubated with secondary antibody, either HRP-labelled goat anti-rabbit Ig (Cat no: P0448; DAKO) or HRP-labelled rabbit anti-mouse Ig (Cat no: P0260; DAKO) in western blot buffer at a dilution of 1:1000 for one hour at room temperature. Membranes were then washed four times, once in 0.001% triton in PBS, then three times in PBS for 5 minutes. SuperSignal™ West Pico (Cat no: 34580; ThermoFisher Scientific) or SuperSignal™ West Femto (Cat no: 34904; Thermofisher Scientific) chemiluminescence substrate was then applied to the membranes and left for 7 minutes at room temperature and visualised using a Gel Image Documentation system (Biorad).

Table 2.3- Primary antibodies used in western blotting

Antibody	Supplier	Dilution	Predicted molecular weight (kDa)
Rabbit monoclonal anti-Ku70	ab92450; Abcam	1:200	70kDa
Rabbit monoclonal anti-topoisomerase I	ab109374; Abcam	1:100	70-100kDa
Mouse monoclonal anti-lamin A/C	MANLAC1 4A7; Wolfson Centre for Inherited Neuromuscular Disease (Manilal *et al.*, 2004)	1:100	74 & 65kDa
Rabbit monoclonal anti-lamin A/C	ab169532; Abcam	1:1000	74 & 65kDa
Mouse monoclonal anti-emerin	MANNEM1 5D10; Wolfson Centre for Inherited Neuromuscular Disease (Manilal *et al.*, 1996, 1999)	1:100	34kDa

Rabbit monoclonal anti-SUN2	ab124916; Abcam	1:200	80kDa
Rabbit polyclonal anti-SUN2	HPA001209; Sigma Aldrich	1:500	80kDa
Rabbit polyclonal anti-TOMM34	PA5-98448; ThermoFisher Scientific	1:100	35kDa
Rabbit polyclonal anti-STAT1	10144-2-AP; Proteintech	1:500-1:1000	91kDa

Catalogue number and supplier are listed for each primary antibody, along with the dilution used and molecular weight of the target protein.

2.2.1.5. Densitometry measurements of antibody reactive bands

Densitometry measurements of antibody reactive bands were obtained using ImageJ software (version 1.8.0_112) (Sheffield, 2007). Before the analysis, images were converted to 8-bit and contrast and brightness were adjusted to better define the bands and enhance signal detection. The rotation tool was also used to ensure the image was straight. Once this fine-tuning was done, selections could be defined as a region of interest. The rectangle tool was selected, and a box was drawn around the first band in lane 1 and marked as selection one. The same frame could then be moved, placed around the second band in lane 2, and marked as selection two. This was repeated for all of the bands and then "analyse → plot lanes" was used to draw a profile plot of each lane. Profile plots represent the relative density within the selection box, peaks correspond to the antibody reactive bands. The straight-line tool was used to draw a line at the base of the peak to separate the background, then using the wand tool, the peak was measured. This method was also used to measure Coomassie stained gel. To do this, the rectangular tool was selected, and a box was drawn around all lanes. The same steps were then used to derive a densitometry

measurement for each lane. The densitometry measurements of antibody reactive bands were then normalized to measurements of the Coomassie stained gel.

2.2.2. Immunocytochemistry

Myoblasts and myotubes grown on coverslips were washed once in PBS and incubated with primary antibody (**Table 2.4**) in immunofluorescence buffer (1% FBS, 1% HS and 0.1% BSA in PBS) for at least one hour at room temperature. The coverslips were then washed 4 times in PBS before adding secondary antibody, either goat-anti rabbit IgG Alexa Fluor 488 or 546 (Cat no: A11034 or A11010; Life Technologies), or goat anti-mouse IgG Alexa Fluor 488 or 546 (Cat no: A11029 or A11030; Life Technologies) in immunofluorescence buffer in darkness at room temperature for one hour. Cells were then washed once in PBS and mounted with ProLong™ Gold Antifade Mountant with DAPI (Cat No: P36941; Thermofisher Scientific).

Table 2.4- Primary antibodies used for immunocytochemistry analysis

Antibody	Supplier	Dilution
Rabbit monoclonal anti-Ku70	ab92450; Abcam	1:100
Mouse monoclonal anti-lamin A/C	MANLAC1 4A7; Wolfson Centre for Inherited Neuromuscular Disease	1:4
Mouse monoclonal anti-emerin	MANNEM1 5D10; Wolfson Centre for Inherited Neuromuscular Disease	1:4
Rabbit polyclonal anti-SUN2	HPA001209; Sigma Aldrich	1:100

Catalogue number and supplier are listed for each primary antibody used in immunocytochemistry analysis, with the dilution.

2.2.2.1. Imaging and quantitative analysis

Myoblasts and myotubes were imaged using a Leica SP5 confocal microscope with 63x oil immersion objective and LAS AF software. Argon laser power was set to and fixed at 10% and was used to detected DAPI staining of the nucleus. HeNe 543 and Diode 405 laser power was set to around 10% and slightly adjusted to improve detection of Alexa Fluor fluorophore 488 and 546, respectively. When quantifying protein expression between different cell samples, laser power intensity and gain were not adjusted, and settings were kept consistent.

To quantify fluorescence staining intensity on IMF images, optical density measurements were performed using ImageJ software (version 1.8.0_112) (Sheffield, 2007). In ImageJ, for each image, colour threshold was adjusted so that the stained sections of the image were highlighted and reflected the brightness of the staining in the IMF image. The "Analyse" tool was then used to determine a numerical value of area for the staining. This was done for both DAPI and antibody stained channels. The value obtained for the area stained by the antibody of interest was then divided by the area stained by DAPI to determine optical density.

2.2.2.2. Quantifying nuclear morphology defects

L-CMD (L380S, del.K32, R249W) and control (C5d, C25, C41) myoblasts and myotubes were examined for nuclear morphology defects (van Tienen *et al.*, 2018). The nuclei were categorized based on their nuclear deformity: donut, honeycomb-like structure, nuclear blebs/blebbing, and nuclear shape abnormalities, as described in Tienen et al., 2018. Only cells that were completely within the field of view were analysed. A total of

100 cells were counted per cell line and analysed for nuclear morphology defects, thus 300 cells were analysed in both the L-CMD and control groups.

2.3. Functional studies

2.3.1. Cell proliferation

Control (C5d, C25, C41) and L-CMD (L380S, del.K32, R249W) myoblasts were thawed and grown in complete medium, as described in Section 2.1.1. After reaching approximately 70-80% confluency, the cells were trypsinized and re-seeded in T25 cell culture flasks at a density of 30,000 cells per flask. The cells were maintained in a humidified incubator (Leec) at 37°C and 5% CO_2 concentration for three days. After this point, the media was removed from the flask and cells were trypsinized and counted as described in Section 2.1.3. Each cell line was grown in three T25 flasks (to provide technical replicates), and each flack was counted four times. A total of 12 measurements were performed for each cell line. Doubling time (DT) for each cell was calculated using the following equation:

$$DT = ln(2) \times t/(ln(C_2) - (ln(C_1))$$

Here, t represents the culture duration in hours, C_2 is the number of cells at the end of the culture, and C_1 is the number of seeded cells at the beginning of the experiment.

2.4. Quantitative real time reverse transcription polymerase chain reaction (RT-qPCR)

2.4.1. Extraction and quantification of total RNA

Total RNA was extracted using the RNeasy Plus Mini Kit (Cat No: 74314; Qiagen) following the protocol outlined in the handbook supplied with the kit. Immortalised myoblasts and myotubes were lysed and homogenized in 600µL of Buffer RLT Plus containing 1% 2-mercaptoethanol (Cat No: M6250, Sigma-Aldrich) by repeated pipetting. The homogenized lysate was transferred to a gDNA Eliminator spin column placed in a 2mL collection tube and centrifuged for 30 seconds at 10000 RPM (Harrier 18/80R, MSE) to remove double stranded chromosomal DNA. The column was discarded, 600µL of 70% ethanol was added to the flow through and mixed thoroughly by pipetting. This precipitates the RNA from the aqueous solution. The sample was transferred to a RNeasy Spin column placed in a 2mL collection tube and centrifuged for 15 seconds at 10000 RPM. The RNA binds to the column, whilst contaminants are removed and discarded in the flow-through. The spin column was washed with 700µL of Buffer RW1 by centrifugation for 15 seconds at 10000 RPM, then 500µL of Buffer RPE was added twice and centrifuged for 15 seconds and then 2 minutes at the same speed. The RNeasy Spin column was placed in a new 2mL collection tube and centrifuged at full speed for 1 minute to eliminate any remaining Buffer RPE. This collection tube was discarded, and the spin column was placed in a new 1.5mL collection tube before adding 50µL of RNase-free water to the spin column membrane to elute the total RNA by centrifugation for 1 minute at 10000 RPM. Total RNA was quantified using RNA Screentape Analysis on the TapeStation 4150 System (Aligent) following manufacture protocol.

2.4.2. Synthesis of complementary DNA (cDNA)

Total RNA was reversed transcribed to generate first-strand cDNA using SuperScript™ VILO™ cDNA Synthesis Kit (Cat no: 11754-050, Invitrogen), according to instructions outlined in the product handbook. Total RNA from immortalized myoblasts and myotubes was prepared in 20µL reactions and subjected to cDNA synthesis using Prime Thermo Cycler (Bibby Scientific) (**Table 2.5**). The cycle was set to 25°C for 10 minutes (primer annealing), 42°C for 60 minutes (reverse transcription), and the reaction was terminated at 85°C at 5 minutes (enzyme inactivation). The 10X SuperScript™ Enzyme Mix contains SuperScript™ III RT (reverse transcriptase), a recombinant DNA polymerase that synthesizes a complementary DNA strand from single-stranded RNA, RNaseOUT™ Recombinant Ribonuclease Inhibitor, which prevents the degradation of target RNA due to ribonuclease contamination, and a proprietary helper protein. The 5X VILO™ Reaction Mix includes random primers, magnesium chloride, and deoxyribonucleoside triphosphates (dNTPs).

Table 2.5- cDNA reaction components and quantities

cDNA reaction component	Quantity
5X VILO Reaction Mix	4µL
10X SuperScript™ Enzyme Mix	2µL
RNA (up to 2.5µg)	XµL
RNase-free water	To 20µL

2.4.3. Quantitative PCR (qPCR)

Quantitative PCR (qPCR) for predicted *SUN2* isoforms was performed using the SYBR Green detection system (Ririe, Rasmussen and Wittwer, 1997). SYBR™ Select

Mastermix (Cat no: 4472908, Applied Biosystems) was used, and the protocol was followed from the product handbook. In this method, fluorescent SYBR Green dye binds to double-stranded DNA (dsDNA) by intercalating between the DNA bases. Once intercalated to DNA, SYBR Green becomes less mobile, causing energy to be omitted as fluorescence. Therefore, fluorescence intensity is directly related to the concentration of dsDNA, which can be measured at the end of each amplification cycle of qPCR (Ponchel *et al.*, 2003). cDNA (myoblasts and myotubes) was diluted to give the equivalent of 6.7ng/µL RNA in 20µL reactions (**Table 2.6**).

Table 2.6- qPCR reaction components and quantities

qPCR reaction component	96-well plate (20µL per well)
SYBR Select Master Mix (2x)	10µL
Forward and Reverse Primers	300nM of each
cDNA	X µL
RNase-free water	Make up to final volume of 20µL

All qPCR reactions were performed in duplicate. Glyceraldehyde-3-phosphate dehydrogenase (*GAPDH*) and β-actin (*ACTB*) were used as reference genes, although it should be considered that the validity of these two genes as housekeeping genes has been questioned as they have been found to change in expression in different tissues and under different circumstances (Glare *et al.*, 2002; Dheda *et al.*, 2005). QuantStudio

3 Real Time PCR System (Applied Biosystems) was used to perform qPCR and was set to the following parameters: 50°C for 2 minutes (UDG activation), 95°C for 90 minutes (DNA polymerase activation), and 40 cycles of 95°C for 15 seconds (denaturation) and 60°C for 1 minute (annealing/extension phase). The amplification plots were generated from plotting cycles against ΔRn, which is defined as the normalised reporter value (Rn) of the experimental reaction minus the Rn value of the baseline signal generated from the instrument. Both baseline and threshold values were automatically defined by the instrument software. The baseline value is equated to the background of the experiment that is deduced during calculations. The threshold cycle value or Ct value is the cycle number at which the fluorescence generated within a reaction crosses the fluorescence threshold, a fluorescence signal considerably above the background fluorescence. The Phaffl method was used to quantify relative gene expression (Pfaffl, 2001). First, the mean of the reference genes (*GAPDH* and *ACTB*) was subtracted from the Ct value, giving the ΔCt value. Relative gene expression (R) was then calculated using 2^-(ΔCt), and a mean R value was deduced from the replicates.

2.4.4. Primer design

Primer sequences were designed for *SUN2*, *GAPDH*, and *ACTB* using Primer3Plus (Untergasser *et al.*, 2007). Nucleotide and protein sequences for *SUN2* isoforms were identified and obtained in FASTA format from The National Centre for Biotechnology Information (NCBI). Primers were each designed to recognise different predicted isoforms of *SUN*. Differences in the nucleotide sequences of the *SUN2* variants were identified by using multiple sequence alignment software Multalin (Corpet, 1988), and

primers were designed across the regions where there were variations in the sequence. In cases where SUN2 variants only differed by small, deleted regions of the sequences, primers were designed across the deletion so that they were unique. Primers also had the following properties: a length of 18-24 bases, 40-60% G/C content, start and end with a G or C and a melting temperature (Tm) of 50-60°C. Primer sequences are listed in **Table 2.7.** The efficiency of each of the primers was determined by making serial dilutions of cDNA and performing qPCR as previously described. The log values of cDNA were then plotted against Ct values. The primer efficiency was then calculated from the slope value using the following equation: efficiency (%) = $(10^{(-1/Slope)}-1) \times 100$ (Pfaffl, 2001). A theoretical maximum efficiency of 100% indicates that for every PCR cycle, the number of copies of the PCR product will double in size during the logarithmic phase of the PCR reaction. Primers with an efficiency of between 90-110% are considered optimal and were used for qPCR.

Table 2.7- Primer sequences used for qPCR.

Target gene	Sequence	Size of the PCR product
***SUN2* isoform 1 (Variant 1)**		
Primer pair 1:	F: GAGACTGAGCCAGTGTCCTC R: CCAGCCCACCAGTAGAGAAG	161bp
Primer pair 2:	F: GAGACTGAGCCAGTGTCCTC R: AACGTCTTCAGGGACGAGAA	245bp
Primer pair 3:	F: GAGACTGAGCCAGTGTCCTC R: GCCTGGTTAAAACGAAGACG	223bp
Primer pair 4:	F: GAGACTGAGCCAGTGTCCTC R: GAACGTCTTCAGGGACGAGA	246bp
Primer pair 5:	F: GAGACTGAGCCAGTGTCCTC R: AGAAGCGCCTGGTTAAAACG	229bp
***SUN2* isoform 3 (Variant 4)**		
Primer pair 1:	F: CCAGTCTGGTCTCAAACTCC R: GGAAATGTGGCGATGAGTCT	197bp
Primer pair 2:	F: CCAGTCTGGTCTCAAACTCC R: TGGAAATGTGGCGATGAGT	198bp
Primer pair 3:	F: CCAGTCTGGTCTCAAACTCC R: CTGGAAATGTGGCGATGAGT	199bp
Primer pair 4:	F: CCAGTCTGGTCTCAAACTCC R: AATGTGGCGATGAGTCTCTG	194bp
Primer pair 5:	F: CCAGTCTGGTCTCAAACTCC R: CTGGAAATGTGGCGATGAG	199bp
***SUN2* isoform 4 (Variant 6)**		
Primer pair 1:	F: CAACTGGGAAGCTCTTGGAG R: AGAGGAGTAGCCCGAGGAAG	175bp
Primer pair 2:	F: CAACTGGGAAGCTCTTGGAG R: AGGAGTAGCCCGAGGAAGAG	173bp
Primer pair 3:	F: CAACTGGGAAGCTCTTGGAG R: AACTCTGCTGGTCCACATCC	218bp
Primer pair 4:	F: CAACTGGGAAGCTCTTGGAG R: GGAACTCTGCTGGTCCACAT	220bp
Primer pair 5:	F: CAACTGGGAAGCTCTTGGAG R: GAGCTGGAACTCTGCTGGTC	225bp
***SUN2* isoform 5 (Variant 8)**		
Primer pair 1:	F: CTCCTTTCCCACAGCTCAAG R: CCCAACCCCTCTTGTGTAAA	156bp
Primer pair 2:	F: CTCCTTTCCCACAGCTCAAG R: ACCCAACCCCTCTTGTGTAA	157bp
Primer pair 3:	F: CTCCTTTCCCACAGCTCAAG R: CACCCAACCCCTCTTGTGTA	158bp
Primer pair 4:	F: CTCCTTTCCCACAGCTCAAG	157bp

	R: ACCCAACCCCTCTTGTGTAAA	
Primer pair 5:	F: CTCCTTTCCCACAGCTCAAG R: CCCAACCCCTCTTGTGTAAAG	156bp
***SUN2* isoform 6 (Variant 14)**		
Primer pair 1:	F: TTGGAGTGACAGAGGAGGTG R: ACATCTGGCTGGAGGATGAC	223bp
Primer pair 2:	F: TTGGAGTGACAGAGGAGGTG R: CATCTGGCTGGAGGATGACT	222bp
Primer pair 3:	F: TTGGAGTGACAGAGGAGGTG R: CCGTCTTGGTCTCGTAGGTC	150bp
Primer pair 4:	F: TTGGAGTGACAGAGGAGGTG R: ATCTGGCTGGAGGATGACTC	221bp
Primer pair 5:	F: TTGGAGTGACAGAGGAGGTG R: CACATCTGGCTGGAGGATG	224bp
***SUN2* isoform 7 (Variant 15)**		
Primer pair 1:	F: CTCTCAGTGAGTCGCTGGTC R: AGAGGAGTAGCCCGAGGAAG	203bp
Primer pair 2:	F: CTCTCAGTGAGTCGCTGGTC R: AGGAGTAGCCCGAGGAAGAG	201bp
Primer pair 3:	F: CTCTCAGTGAGTCGCTGGTC R: AACTCTGCTGGTCCACATCC	246bp
Primer pair 4:	F: CTCTCAGTGAGTCGCTGGTC R: GGAACTCTGCTGGTCCACAT	248bp
Primer pair 5:	F: CTCTCAGTGAGTCGCTGGTC R: TAGCCCACGTAGTCGTCCTC	223bp
***SUN2* isoform 8 (Variant 16)**		
Primer pair 1:	F: CTGGGGCTACTCGGATGTG R: AACGTCTTCAGGGACGAGAA	219bp
Primer pair 2:	F: CTGGGGCTACTCGGATGTG R: GCCTGGTTAAAACGAAGACG	197bp
Primer pair 3:	F: CTGGGGCTACTCGGATGTG R: CGCCTGGTTAAAACGAAGAC	198bp
Primer pair 4:	F: CTGGGGCTACTCGGATGTG R: GAACGTCTTCAGGGACGAGA	220bp
Primer pair 5:	F: CTGGGGCTACTCGGATGTG R: AGCAGGAACCAGAGGAACG	234bp
***SUN2* isoform 10 (Variant 20)**		
Primer pair 1:	F: ACAGTCCTCTCAGGCGCTTC R: GGAAATGTGGCGATGAGTCT	210bp
Primer pair 2:	F: ACAGTCCTCTCAGGCGCTTC R: TGGAAATGTGGCGATGAGT	211bp
Primer pair 3:	F: ACAGTCCTCTCAGGCGCTTC R: CTGGAAATGTGGCGATGAGT	212bp
Primer pair 4:	F: ACAGTCCTCTCAGGCGCTTC R: AATGTGGCGATGAGTCTCTG	207bp
Primer pair 5:	F: ACAGTCCTCTCAGGCGCTTC	212bp

	R: CTGGAAATGTGGCGATGAG	
***SUN2* isoform 11 (Variant 21)**		
Primer pair 1:	F: TCGTTTTAACCAGCATGACC R: GGGAACTGAGATTCCACGTC	196bp
Primer pair 2:	F: TCGTTTTAACCAGCATGACC R: GCAAGGAACTGACTGATCCA	220bp
Primer pair 3:	F: TCGTTTTAACCAGCATGACC R: GAACTGAGATTCCACGTCGTC	194bp
Primer pair 4:	F: TCGTTTTAACCAGCATGACC R: CTCGGGCAAGGAACTGACT	225bp
Primer pair 5:	F: TCGTTTTAACCAGCATGACC R: AACTGAGATTCCACGTCGTC	193bp

Forward and reverse primers for *SUN2* isoforms are listed in the table, as well as the size of the PCR product.

2.5. Polymerase chain reaction (PCR)

RNA was extracted from a healthy control myoblast cell line (C25) and quantified, as described in Section 2.4.1., then reversed transcribed into cDNA, as outlined in Section 2.4.2. Polymerase chain reaction (PCR) reactions were setup using PCR SuperMix,(Cat no: 10572-014; ThermoFisher Scientific), control myoblast cDNA and SUN2 Variant 16 and SUN2 Variant 16.1 primers (**Table 2.7)** as outlined in the product handbook. Samples were made up in 50µL reactions and subjected to PCR using the Prime Thermo Cycler (**Table 2.8**). The Thermo Cycler was programmed to the following parameters: 94°C for 2 minutes (initial denaturation), 35 PCR cycles of 94°C for 15 seconds (denaturation), 55°C for 30 seconds (annealing stage based on primer T_m), then 72°C for 4 minutes (extending stage).

Table 2.8- PCR reaction components and quantities

PCR reaction component	Quantity
Autoclaved, distilled water	To 50 µL
PCR SuperMix	45µL
10 µM forward primer	1µL
10 µM reverse primer	1µL
cDNA	<500ng

2.5.1. PCR product clean-up

The PCR products were subjected to ExoSAP-IT™ PCR Product Cleanup Reagent for the enzymatic clean-up of amplified PCR produce. ExoSAP-IT hydrolyzes excess primers and nucleotides so that they do not interfere with downstream applications including DNA sequencing. Instructions were followed as per the ExoSap-IT product brochure. In this procedure, 5µL of PCR product was combined with 2µL of ExoSap-IT reagent, for a combined 7µL reaction volume. To scale the reaction up with increased volumes of PCR product, the quantity of ExoSap-IT was increased proportionately. Once the PCR product and ExoSap-IT reagent were combined, samples were incubated at 37°C for 15 minutes to degrade the remaining primers and nucleotides, and then incubated at 80°C for 15 minutes to inactivate ExoSap-IT reagent. Treated PCR products were then stored at -20°C until required for further analysis.

2.5.2. Quantitating PCR products using agarose gel electrophoresis

Once the PCR products had been removed of excess primers and nucleotides, they were quantified using agarose gel electrophoresis. The agarose gel was made by dissolving 1.5% agarose (Cat no: 30-10, Severn Biotech Ltd) in 1 x tris/borate/EDTA

(TBE) buffer by gently heating and mixing the solution. Once the agarose powder was fully dissolved in 1 x TBE buffer, approximately 3µL of SYBR® Safe DNA Gel Stain (Cat no: S33102; Invitrogen, Life Technologies) was added to the solution, which gave it a slight orange colour. The inside plates of the gel electrophoresis system were then assembled, along with the electrophoresis comb used to create wells in the gel, and the agarose gel solution was poured into the middle of the system and allowed to set (for around 15 minutes until firm).

PCR product samples were then prepared using a 100bp DNA Ladder kit (Cat no: 15628019; ThermoFisher Scientific), as per the product handbook. Within the DNA Ladder kit was 10X BlueJuice™ Gel Loading Buffer, and 3µL of this buffer was combined with 6µL PCR product and 1µL nuclease free water. The DNA ladder was prepared by mixing 1µL DNA ladder with 3µL of BlueJuice buffer and 6µL nuclease free water.

Once the agarose gel had set, the electrophoresis comb and plates either side of the gel were gently removed so as not to break the gel. 1 x TBE buffer was then poured into the system so that the gel was submerged in buffer. The prepared PCR product samples and DNA ladder were then carefully loaded into each well. Once the samples had been loaded, the system lid was closed, the wires were connected, and an electric current was applied to the system at 100V. Similarly, to as described in Section 2.2.1.3., the negatively charged DNA migrates through the gel from the negative anode towards the positive cathode. Once the dye front had migrated approximately half-way through the gel, the electric current was stopped, and the gel was removed from the system and imaged using a Gel Image Documentation system.

An estimation of PCR product quantity was then performed by comparing the PCR product bands to a marker band that is close in intensity and size to the PCR band. As there is approximately 0.5µg/µL of DNA in the DNA ladder, an estimation of PCR product quantity can be made.

2.5.3. PCR product sequencing

Once the PCR products had been quantified, each product was diluted to give 6-20ng of PCR product in 30µL samples. In addition to this, forward and reverse SUN2 Variant 16 and Variant 16.1 primers were diluted to 3.2µM. The PCR products were then sequenced by MRC PPU DNA Sequencing and Services at the University of Dundee.

2.6. Identification of lamin A/C interactors

2.6.1. Immunoprecipitation

Immunoprecipitation (IP) is the small-scale affinity purification of antigens using a specific antibody that is immobilized to a solid support such as magnetic particles, as described previously (Bonifacino, Dell'Angelica and Springer, 1999). Dynabeads™ Pan mouse IgG (Cat no: 11041; Invitrogen) were washed 4 times using 200µL of 4% BSA in PBS to block non-specific binding, 50µL of magnetic beads were used per sample. A DynaMag™ Spin Magnet (Cat no: 12320D, Invitrogen) was used at each step to remove the beads from the solution. The beads were then incubated with 100µL of neat, undiluted antibody for one hour at room temperature on a roller. A negative control was also included containing beads with PBS to determine any non-specific binding of proteins to the beads. The antibodies used were mouse monoclonal anti-lamin A/C (MANLAC1 4A7; Wolfson Centre for Inherited Neuromuscular Disorders), rabbit

monoclonal anti-KU70 (ab924590; abcam), rabbit monoclonal anti-TOP1 (ab109374; abcam). The supernatant was then removed and discarded, and the beads were washed twice in 200µL 4% BSA in PBS and twice in plain PBS before being incubated with 60µL of myoblast lysate extracted using standard RIPA buffer (150mM Sodium Chloride, 1% NP-40 (Cat no: 155942; ICN Biomedicals Inc.), 0.5% Sodium Deoxycholate, 0.1% SDS, 50mM Tris pH 7.5 in dH_2O with protease inhibitor cocktail (Cat no: P8340; Sigma Aldrich) to prevent protein degradation) for one hour at room temperature with gentle rolling. Some of this input was stored as a control for use in immunoblotting. Following incubation, the supernatant containing unbound material was removed and stored in a -80°C freezer until needed for further analysis. The beads were then washed once in 200µL standard RIPA buffer, four times in 200µL PBS and then the proteins that were bound to the beads were eluted by boiling in 80µL of 2 x Laemmli sample buffer at 96°C for 3-5 minutes. Samples were then subjected to western blotting as described in Section 2.2.1 to determine potential binding partners.

2.6.2. Identification of published interactors of lamin A

To identify interactors of lamin A that had previously been identified in other studies, a literature search was conducted. A search strategy was outlined to find suitable articles which identified potential lamin A interactors.

2.6.2.1. Inclusion criteria

Articles included must have investigated interactors of lamin A in healthy cells or tissues. Quantitative, qualitative, or commentary articles on the topic of these proteins were accepted. Interactions were not limited to *Homo sapiens* cells or tissues, but

articles investigating interactions in cells or tissues from other species were also considered.

2.6.2.2. Exclusion criteria

Articles were not included if they investigated proteins that are interactors of B-type lamins, lamin B1 or B2. B-type lamins are functionally different proteins that are generated by the *LMNB1* and *LMNB2* genes, whereas lamin A/C are produced by the *LMNA* gene. Articles were excluded if they studied lamin A interactions in models of Hutchinson Giford Progeria Syndrome (HGPS). It is known that HGPS is caused by the expression of aberrant forms of pre-lamin A that remain farnesylated within cells due to mutations that are known to result in the deletion of the ZMPSTE24 protease site (Pendás *et al.*, 2002; Mutesa *et al.*, 2007; Galant *et al.*, 2016). Articles were also excluded if they investigated protein interactions with prelamin A, as a post-translational modification is required to form mature lamin A from prelamin A.

2.6.2.3. Literature search strategy

Only bibliographic databases that were relevant to the study were searched, these included: MEDLINE, EMBASE and Cochrane Reviews. Medical Subject Headings (MeSH) database was used to find alternative terms for lamin A/C, as well as “interact”, which were main terms within the research question. Alternative terms for lamin A included “Type A lamins”, “Lamins, Type A”, “Lamins A-C”, “Lamin A C”, and “Lamin A”. Alternative terms for interact included “Interactome”, “Partner”, “Bind”, “Link” and “Associate” (**Table 2.9**). The articles were then screened, and data was extracted and tabulated from articles that satisfied the inclusion criteria.

Table 2.9- Search terms used in the literature search

Search Term
Type A Lamins (Interact* OR Interactome OR Bind* OR Link* OR Partner* OR Associate*) Protein
(Type A Lamins OR Lamins, Type A OR Lamin A-C OR Lamin A C OR Lamin A) AND (Interact* OR Interactome OR Bind* OR Link*OR Partner*) AND Protein
Type A Lamins AND (Interact* OR Interactome OR Bind* OR Link* OR Partner* OR Associate*) AND Protein
Lamins, Type A AND (Interact* OR Interactome OR Bind* OR Link* OR Partner* OR Associate*) AND Protein
Lamin A-C AND (Interact* OR Interactome OR Bind* OR Link* OR Partner* OR Associate*) AND Protein
Lamin A C AND (Interact* OR Interactome OR Bind* OR Link* OR Partner* OR Associate*) AND Protein
Lamin A AND (Interact* OR Interactome OR Bind* OR Link* OR Partner* OR Associate*) AND Protein

Asterisk (*) was used to account for variations in the truncated terms, "AND" was used to further refine the search and ensured the inclusion of all terms, "OR" was used to fit more search terms into one search.

2.6.3. Liquid chromatography-mass spectrometry analysis

The immunoprecipitation protocol was followed as outlined in Section 2.5.2., but the volumes were scaled up. Per sample, 75µL of beads were used, 150µL of antibody was used, and 300µL of cell extract (either healthy control or L-CMD myoblasts) was used. Instead of eluting the proteins from the beads by boiling in 2 x Laemmli sample buffer, the beads were washed once with standard RIPA buffer and four times with PBS before being digested overnight at 36°C with 1µg sequencing grade trypsin (Cat no: V5111; Promega) in 25µL 50mM ammonium hydrogen carbonate buffer.

Liquid chromatography mass spectrometry (LCMS/MS) analysis was performed by Dr Sally Shirran at the BSRC Mass Spectrometry & Proteomics Facility at the University of

St Andrews, who also supplied the methods described in this section. Centrifugal evaporation was used to dry the peptide samples (SpeedVac; Thermofisher Scientific) before they were resuspended in 40µL of loading buffer (2% acetonitrile and 0.05% trifluoroacetic acid). One quarter of the sample was then injected onto an Aclaim pepmap 100µm x 2cm trap (Thermofisher Scientific) and washed for 10 minutes with loading buffer to waste after which the trap was turned in-line with the analytical column (Aclaim pepmap RSLC 75µm × 15cm; Thermofisher Scientific). The analytical solvent system consisted of buffer A (2% acetonitrile and 0.1% formic acid in water) and buffer B (2% water with 0.1% formic acid in acetonitrile) at a flow rate of 300 nL/min with the following gradient: linear 1–20% of buffer B over 60 minutes, linear 20–40% of buffer B for 15 minutes, linear 40–99% of buffer B for 5 minutes, isocratic 99% of buffer B for 5 minutes, linear 99–1% of buffer B for 2.5 minutes, and isocratic 1% solvent buffer B for 12.5 minutes.

The eluate was sprayed into a TripleTOF 5600+ electrospray tandem mass spectrometer (Sciex) and analysed in Information Dependent Acquisition (IDA) mode, performing 120 ms of MS followed by 80 ms MS/MS analyses on the 20 most intense peaks seen by MS.

The raw data files were analysed using the Mascot search algorithm (Matrix Science), against the SwissProt all species database, using trypsin as the cleavage enzyme and methionine oxidation as a variable modification. The peptide mass tolerance was set to 20 ppm and the MS/MS mass tolerance to ± 0.1 Da. For visualisation purposes, the data files from mascot were extracted and loaded into Scaffold (ProteomeSoftware).

2.6.3.1. Filtering data obtained from liquid chromatography-mass spectrometry analysis

Once the Scaffold report had been generated from the LCMS/MS analysis, the data was filtered. It was noticed that the data contained keratin proteins, which are likely contamination from hair or skin when preparing the samples in the laboratory, therefore these were removed. There were also mouse immunoglobulins (IgG) present, which were attached to the DynaBeads® that were used to bind the lamin A/C antibody to precipitate lamin A/C and bound proteins out of cell extracts, so these were also removed from the data. Some protein entries were also listed as "HUMAN-R", these indicate reverse peptide sequences that are used during the LCMS/MS analysis to rule out false hits. Any proteins with "HUMAN-R" in their UniProt ID were therefore deleted.

Usually the next stage of data filtering would involve removing proteins if they were only identified with a single peptide, however it was noticed that barrier-to-autointegration factor 1 (BAF1), a known interactor of lamin A, was only identified with one peptide. This is likely to due BAF1 having a small molecular weight (10kDa). Therefore, it was decided that all proteins identified with only a single peptide would be included to avoid cutting out valuable data. Next, an enrichment factor was calculated for the proteins identified in each cell line. In the experiment, a "beads only" control was included to account for any non-specific protein binding to the beads (i.e., not specifically binding to the antibody). The enrichment factor was calculated by dividing the peptide count for a sample by the peptide count for the beads only control, then multiplying this number by 100. If a protein was not detected in the beads only control, the peptide count in the samples were simply multiplied by

100. Proteins that had an enrichment of <200% were then excluded if they were also detected in the beads only sample.

2.6.4. Bioinformatics analysis

2.6.4.1. Search Tool for the Retrieval of Interacting Genes/Proteins (STRING)

Search Tool for the Retrieval of Interacting Genes/Proteins (STRING) (Szklarczyk *et al.*, 2021) was used to identify statistically significant interactions between proteins identified as lamin A interactors in previous studies in the literature. STRING extracts data from multiple sources including KEGG Pathway Database, Reactome Pathway Database, The Biomolecular Interaction Network Database amongst others. Therefore, STRING integrates information about protein interactions from more than 2000 organisms (Szklarczyk *et al.*, 2021).

A list of proteins was uploaded under the "multiple proteins" tab, and the background was set to auto detect, since the interactors identified from the literature search encompassed a number of different species. The protein association network that STRING generates consists of nodes (which represent the input proteins), and edges which indicate predicted functional associations (Szklarczyk *et al.*, 2021). Data was filtered to include protein interactions with high confidence (0.700) interaction score to exclude any false positive results. The confidence score is determined from seven types of evidence, each of which is scored separately (Szklarczyk *et al.*, 2021). Each of these evidence scores are then combined to determine a final interaction score. The different types of evidence are shown using different coloured edges in the associated network. Red edges represent fusion evidence, where an interaction score for proteins is generated if their orthologs have fused into a single, protein-coding gene in at least

one organism. Green edges indicate neighbourhood evidence, where genes are given an association score is they are consistently observed in one another's genome neighbourhood. A blue edge is indicative of co-occurence evidence, assessing the phylogenetic distribution of orthologs of all proteins in a given organism. In this case, proteins are given an interaction score if their orthologs show a high similarity in their distribution. Purple edges represent experimental evidence, where proteins are assigned an interaction score if it has been demonstrated that they interact experimentally. A light blue edge indicates database evidence, where an interaction score is assigned to proteins if there is evidence for their interaction in curated databases. Yellow edges represent text-mining evidence, where proteins are given an interaction score if in text collections they are mentioned together. Finally, black edges indicate co-expression evidence, where a high association score is determined for proteins if their expression patterns are consistently similar under a variety of conditions (Szklarczyk *et al.*, 2021).

2.6.4.2. Database for annotation, visualization and integrated discovery (DAVID)

The gene ontology (GO) analysis tool of the database for annotation, visualization and integrated discovery (DAVID) platform (Huang, Sherman and Lempicki, 2008; Sherman *et al.*, 2022) was used to investigate the likely functions of proteins identified as lamin A interactors in previous studies in the literature, as well as proteins identified as lamin A interactors in L-CMD (L380S, del.K32, R249W) and control (C5d, C25, C41) myoblasts using co-immunoprecipitation and LCMS/MS analysis. In the GO analysis, genes and/or proteins are systematically mapped to biological annotations (GO terms), including biological processes (BP), molecular function (MF), and cellular

component (CC) terms (Huang, Sherman and Lempicki, 2008). This allows the identification of biological processes associated with gene/protein lists imputed into DAVID. A Fisher exact test is used to calculate the *p*-value, through measuring the gene/protein-enrichment in annotated terms (Huang, Sherman and Lempicki, 2008). Firstly, the number of genes/proteins associated with a specific GO term are determined from the reference dataset. The reference dataset is referred to in DAVID as the "background". For a default background, usually the entire genome of the species that the data was derived from is used (Huang, Sherman and Lempicki, 2008). In this comparison, the background was selected as *Homo sapiens.* The number of genes/proteins that are associated with a GO term is then determined from the input dataset. The number of genes/proteins that are associated with the same GO term is then determined from the input dataset. If more genes/proteins are identified in the input dataset compared to the reference dataset, a specified term is significantly enriched in the input dataset (i.e., the association is not due to chance). GO terms were included that had a significant *p*-value of ≤0.05 and that had a minimum of three proteins assigned to them.

2.7. Quantitative SWATH™-MS proteomics analysis

Quantitative sequential window acquisition of all theoretical mass spectra (SWATH™-MS) is a specific method of data independent acquisition (DIA) (Gillet *et al.*, 2012). It allows the quantitative analysis of peptides covering 1000s of proteins with a high quantitative consistency and accuracy. For a SWATH-MS measurement, non-labelled protein samples are digested with trypsin and the resulting peptides are analysed by liquid chromatography coupled to a tandem mass spectrometer operating in DIA

mode. In this mode, all ionized compounds of a given sample that fall into a specified mass range are fragmented in a systematic and unbiased manner (Ludwig *et al.*, 2018b).

2.7.1. Protein extraction and quantification

Protein was extracted from myoblast and myotube samples from healthy control donors (n=3) and CMD patients harbouring mutations in *LMNA* (n=3) using 250µL of extraction buffer (8M urea (Cat no: U0631; Sigma Aldrich), 100mM ammonium bicarbonate, 2% sodium deoxycholate in sterile dH_2O) as described in section 2.2.1.1. Samples were sonicated at 5 microns for 10 seconds and centrifuged at 13000 RPM for 5 minutes at 4°C to pellet insoluble material.

A small aliquot of cell extract from each sample was used to determine protein concentration, whilst the remaining samples were stored at -80°C for downstream analysis. The protein concentration of each sample was determined using the Pierce™ BCA Protein Assay Kit and method described in section 2.2.1.2. A minimum of 30µg of protein is needed to perform SWATH™-MS analysis therefore we ensured each sample contained more than the minimum protein concentration.

2.7.2. Sample preparation

Sample preparation was performed by Dr Silvia A. Synowsky and Dr Sally L. Shirran at the BSRC Mass Spectrometry & Proteomics Facility at the University of St Andrews, who also supplied the methods described in this section. Each sample (50µg) was diluted with extraction buffer to obtain equal concentrations and then reduced with

5mM tris(2-carboxyethyl)phosphine (TCEP) at 30°C for one hour followed by alkylation with 10mM iodoacetamide (IAA) in darkness at room temperature for 30 minutes. Reduction and alkylation are used to facilitate the identification of proteins. Disulfide bonds between sulfhydryl groups of cysteine side chains often regulate protein folding and the final functional structures of proteins (Bulaj, 2005). Phosphorous-containing TCEP cleaves disulfide bonds resulting in the formation of phosphine oxide (Burns *et al.*, 2002), whilst IAA converts cysteine thiols to thioethers, also preventing unwanted side reactions (Paulech, Solis and Cordwell, 2013). Without reducing and alkylating samples, the peptides involved in disulfide bonds would be difficult to identify during database searching (Sechi and Chait, 1998). The reaction was quenched with 20mM DTT, this deactivates any unreacted reagents. Then the samples were digested overnight with trypsin in a ratio of 1µg of protease to 50µg protein.

The peptides were subjected to cleanup using C18 columns. This purifies and concentrates the peptides, whilst removing buffers and compounds that may interfere with MS (Naldrett *et al.*, 2005). The peptides bind to porous reverse-phase C18 columns, salts and buffers are washed off, and then peptides are eluted using a high-organic mobile phase. The cleaned, digested sample was then dried and resuspended to 1µg/µl in loading buffer (100% water, 0.1% formic acid). Data independent acquisition was performed on individual samples (DIA-MS). In addition, a pool of all the samples was prepared, and a portion subjected to nanoLC MS/MS analysis using data dependent acquisition (DDA-MS). The remnant of the pooled sample was then fractionated on high pH C18 Reverse Phase into 12 fractions before analysing the fractions individually in DDA mode.

2.7.3. Data acquisition and processing

Data acquisition and processing was performed by Dr Silvia A. Synowsky and Dr Sally L. Shirran at the BSRC Mass Spectrometry & Proteomics Facility at the University of St Andrews, who also supplied the methods for this section.

2.7.3.1. Data dependent acquisition (DDA)

Peptides (5 µg) were subjected to LCMS/MS using an Ultimate 3000 RSLC (Thermo Fisher Scientific) coupled to an Orbitrap Fusion Lumos mass spectrometer (Thermo Fisher Scientific). The peptides were injected onto a Pepmap100 C18 5µm 0.3 × 5 mm reverse-phase trap for pre-concentration and desalted with loading buffer, at 5 µL/min for 10 minutes. The trap was then switched in-line with the analytical column (Easy-spray Pepmap RSLC C18 2µm, 50cm x75um ID). Peptides were eluted from the column using a linear solvent gradient using the following gradient: linear 4–40% of buffer B over 120 minute, linear 40–60% of buffer B for 30 minutes, sharp increase to 95% buffer B within 0.1 minute, isocratic 95% of buffer B for 15 minutes, sharp decrease to 2% buffer B within 0.1 minute and isocratic 2% buffer B for 15 minutes. The mass spectrometer was operated in DDA positive ion mode with a cycle time of 1.5 seconds. The Orbitrap was selected as the MS1 detector at a resolution of 120000 with a scan range of from m/z 375 to 1500. Peptides with charge states 2 to 5 were selected for fragmentation in the ion trap using HCD as collision energy.

The raw data files were converted into mgf using MSconvert (ProteoWizard) and searched using Mascot with trypsin as the cleavage enzyme and carbamidomethylation as a fixed modification of cysteines, against the Swissprot database, restricted only to proteins from humans. Note that the iRT peptides were

added to this database. The mass accuracy for the MS scan was set to 20 ppm and for the fragment ion mass to 0.6 Da.

2.7.3.2. Data independent acquisition (DIA) mode

Sample (5 µg) was injected onto the same LCMS set up as above with the same gradient, however data acquisition was done in DIA mode. The DIA MS method alternates between a MS scan and a tMS2 scan containing 24 scan windows. The MS scan has the following parameters: the Orbitrap at 120000 resolution is selected as detector with a m/z range from 400 to 1000. The tMS2 scan uses HCD as activation energy with fragments detected in the Orbitrap at 30000 resolution. The first 20 m/z windows are 20 mass units wide from 410 to 790 followed by a 30m/z window from 790-820, a 40m/z window from 820-860, a 50m/z window from 860-910 and a 60m/z window from 910-970.

2.7.4. Filtering the raw data to identify upregulated and downregulated proteins in L-CMD cells compared to controls

The SWATH™-MS proteomics data was exported from Skyline and formatted in a Microsoft Excel spreadsheet containing a list of identified proteins along with their corresponding accession number, the number of peptides identified for each protein, sum total average and sum total area. Firstly, each of the proteins where only one peptide was identified were removed. The sum total area value for each of the proteins identified in the L-CMD (n=3) and control samples (n=3) was then averaged, and fold change was calculated by dividing the average from the three L-CMD samples by the average value calculated across the controls. Any proteins that had a fold

change of between 0.8 and 1.25 were removed. This is a standard procedure used in proteomics data processing used previously (Brown *et al.*, 2022). A two-tailed unequal variance T-test was then performed, and the proteins were removed which were found to not be statistically significantly ($p > 0.05$) upregulated or downregulated in the L-CMD cells compared to controls.

2.7.5. QUIAGEN Ingenuity Pathway Analysis (IPA)

Dysregulated pathways were identified downstream of *LMNA* mutations in L-CMD patient myoblasts and myotubes (compared to controls) using QIAGEN Ingenuity Pathway Analysis (IPA) software (QIAGEN; https://digitalinsights.qiagen.com/products-overview/discovery-insights-portfolio/analysis-and-visualization/qiagen-ipa/). The fold change value for each protein (as calculated in Section 2.8.4.) along with the assigned *p*-value was inputted into IPA in the form of an Excel spreadsheet.

IPA uses right-tailed Fisher's Exact Test to calculate the *p*-value determining the probability that each cellular and molecular function or canonical pathway assigned to that dataset is due to chance alone, and the final lists of functions and pathways were ranked accordingly to the resulting *p*-value. IPA also produces a Z-score for enriched canonical pathways. The Z-score is a prediction of whether a pathway is activated or inhibited based on the direction of expression change in the input dataset. This is done by comparing the IPA database, which predicts what the expect when an upstream regulator interacts with its downstream target, to the direction of differential gene/protein expression that was observed in the input dataset. Z-score of ≥2

represents the prediction of activation, while Z-score ≤ -2 represents the prediction of inhibition.

2.8. Systematic review and meta-summary

Preferred Reporting Items for Systematic Reviews and Meta-Analyses (PRISMA) guidelines were followed when conducting a systematic review and meta-summary into LINC complex-associated genes known to cause human disease (Liberati *et al.*, 2009). The PRISMA statement consists of a 27-item checklist and a four-phase flow diagram. The checklist includes items deemed essential for transparent and complete reporting of a systematic review.

2.8.1. Eligibility criteria

2.8.1.1. Inclusion criteria

Articles were selected if they clearly described a human mutation in a gene encoding a NE protein associated with the LINC complex (*LMNA, LMNB1, LMNB2, EMD, TMEM43, FHL1, SYNE1/SYNE2*) using the standard nomenclature for describing genetic sequence variants (i.e., describing the nucleotide base pair change and/or amino acid change). Cases where there were multiple mutations in the same gene were included. As identical mutations in certain genes, notably *LMNA*, are known to cause entirely different diseases, multiple reports of the same mutation were included so that the disease phenotype in different cases could be recorded and compared. Both single and multiple case reports were included. Articles were only included if they were reported in English.

2.8.1.2. Exclusion criteria

Articles were excluded if they did not report a mutation in a gene encoding a NE protein associated with the LINC complex, along with articles that mentioned relevant NE proteins in the title or abstract but failed to describe a mutation in the main body of the article. It is known that the accumulation of pre-lamin A induces premature senescence within cells, and this is attributed to the development of the following premature aging disorders (Bonello-Palot *et al.*, 2014): Hutchinson-Guilford progeria syndrome (HGPS), atypical Werner syndrome/ atypical progeria, mandibuloacral dysplasia and restrictive dermopathy. These diseases were excluded as they are caused by the expression of truncated forms of pre-lamin A that remain farnesylated within cells due to specific mutations that are known to result in the deletion of the ZMPSTE24 protease site (Pendás *et al.*, 2002; Mutesa *et al.*, 2007; Galant *et al.*, 2016). Additionally, for the same reasons, articles were also excluded if they only mentioned mutations in pre-lamin A. Adult onset autosomal dominant leukodystrophy (ADLD) was excluded as this disease is caused by a genomic deletion upstream of the lamin B1 gene causing overexpression of *LMNB1*. Therefore, the causation of this disease is entirely different to other nuclear envelopathies. Cases where more than one mutation was reported in different genes were not included, as it is unclear which is the causative mutation. Silent mutations were excluded as it is uncertain whether they cause disease, and asymptomatic carriers were excluded as they do not reflect the patient population that are affected by disease. Non-human or man-made mutations that were created in a laboratory setting were also excluded. Articles were not included if they were not published in English.

2.8.2. Information sources

Only bibliographic databases that were deemed relevant to the systematic review topic were searched. These were Medline (EBSCO) (12th January 2021), CINAHPlus (EBSCO) (12th January 2021) and AMED (EBSCO) (12th January 2021). UniProt, neXtProt and The Human Protein Atlas were accessed as knowledge sources to aid with the analysis of the results yielded from the review.

2.8.3. Search strategy

No limits or restrictions on date or time-period were applied to the search strategy, however searches were restricted to only include articles that were published in English. No published search filters were used. The database searching yielded a total of 2128 results. There were 875 duplications that were removed using both Mendeley Reference Manager and manual searching, leaving a total of 1253 articles to be screened. The search strategy, including search terms and a full breakdown of search results, can be viewed in detail in the **Supplementary File (1).**

2.8.4. Selection process

Two reviewers screened the articles gathered from the searches using the eligibility criteria outlined above. The web-based application Rayyan was used for this process (Ouzzani *et al.*, 2016). Rayyan allows the user to create a review within the programme and records can be imported using various text formats. The records from the searches were uploaded to Rayyan from Mendeley in RIS format. Rayyan then presents the title of each article in a selection box in the centre of the page. From here, articles can be selected, and the abstract of the article can be viewed along with other information including authors and the journal the report was published in. Blind screening was turned on, and reviewers could select whether an article should be

included, maybe included, or excluded. Articles that were excluded could be marked with a reason justifying the reason for exclusion and a record was made of this. Rayyan then automatically sorted articles which both reviewers deemed acceptable or unacceptable into relevant folders, leaving any conflicts or articles selected as maybe acceptable within the selection screen. Any conflicts were recorded and discussed further between the two reviewers until a consensus was reached.

2.8.5. Data collection process

One reviewer independently collected data from each report manually. Data was tabulated and recorded using Microsoft Excel. For each NE protein, mutations were recorded using the cDNA nomenclature and protein nomenclature. In some instances, if this information was not available (i.e., cDNA nomenclature was stated, but protein nomenclature was not or vice-versa), this was manually determined where possible. The type of mutation (i.e., missense, nonsense, insertion, deletion, frameshift) was also noted. The exon, codon and protein structure where the mutation is located were recorded or determined based on other information. The number of reports associated with each mutation were recorded if this information was stated in the article (this was therefore recorded as “minimum number of reports of mutation” as this was not always available). Diseases reported as being associated with each mutation were documented and if clinical details were available, disease severity was ranked (either mild, moderate or severe).

2.8.6. Risk of bias and certainty assessment

Articles were rejected in the screening process if the reviewers determined that the information on the mutation was questionable, recorded incorrectly or unclearly. Examples include those where the mutation was not reported using standard nomenclature, or if the position of the mutation on the codon did not align with the cDNA position. Due to the nature of this systematic review, it was possible to manually check whether mutations were correctly recorded by looking at the mutation (the nucleotide or protein change) on the FASTA genetic sequence available on The National Center for Biotechnology Information database.

2.8.7. Limitations of the study

Some mutations are reported directly to genetic databases and as a result are not published in journal articles. This may be a limitation to this study, as a number of variants may not have been recorded. There are, however, also limitations to database searching. Therefore, we believe that a systematic review was the most appropriate method to use to conduct this study.

Chapter 3: Identification of Lamin A Interactors in Healthy and *LMNA*-Congenital Muscular Dystrophy Immortalized Myoblasts

3.1. Introduction

As outlined in Chapter 1, mutations in *LMNA* cause *LMNA*-associated congenital muscular dystrophy (L-CMD), as well as a broad range of diseases that are collectively known as laminopathies. Encoded by the *LMNA* gene, proteins lamin A and C are the major structural constituents of the nuclear lamina (NL). They are A-type lamins that are ubiquitously expressed and assemble into higher-order filaments through lamin-lamin interactions (further details on lamin-lamin interactions and lamin assembly can be found in Chapter 6, Section 6.3.4.1.) (Fisher, Chaudhary and Blobel, 1986). As well as interacting with one-another, lamin A/C also interact with B-type lamins, lamin B1 and B2 to form the NL (Ye and Worman, 1995; Schirmer and Gerace, 2004). These lamin complexes contribute to nuclear structure and influence nuclear organisation (Dittmer and Misteli, 2011). The most-studied functional aspects of A-type lamins are the structural role that they play in ensuring the integrity of the nucleus, but they are increasingly being recognised as mediators, and maybe regulators, or different nuclear processes (Gonzalez *et al.*, 2011). Lamin A/C have been implicated in higher-order genome organisation, as they physically interact with chromatin, and may also play a role in DNA repair (Liu *et al.*, 2005; Manju, Muralikrishna and Parnaik, 2006). There is also evidence that A-type lamins are linked to signal transduction pathways involved in differentiation and homeostasis by regulating the activity of proteins within the mitogen-activated protein kinase- and RB-cell cycle pathways (Gonzalez *et al.*, 2011), and may be involved in transcription and DNA replication, perhaps by aiding assembly of the transcription and replication machineries (Spann *et al.*, 2002; Zastrow, Vlcek and Wilson, 2004).

These processes rely on lamin A/C- protein interactions, which could be disrupted in L-CMD. Since the field of molecular biology was established, it has been deduced that proteins do not function in isolation. Rather, interactions between proteins and other molecules (such as DNA and RNA) mediate metabolic and signalling pathways, cellular processes, and organismal systems (Gonzalez and Kann, 2012). “Protein interaction” is a term that is generally used to describe the physical contact between proteins and their interacting partners (Gonzalez and Kann, 2012). Together, proteins associate to produce macromolecular structures of varying complexities and heterogeneities. Proteins can interact in pairs to form dimers, multi-protein complexes, or long chains. The subunits creating the complexes can consist of multiples of the identical proteins (homodimers) or different proteins (heterodimers). Proteins can interact in a transient fashion (such as proteins involved in signal transduction), or permanently (for example, some ribosomal proteins) (Gonzalez and Kann, 2012).

As mentioned previously, lamin A/C are known to associate with B-type lamins and homopolymerize (Ye and Worman, 1995), and in addition to lamin-lamin interactions, at the NE, it has been demonstrated that lamin A/C bind to proteins anchored at the inner nuclear membrane (INM) including thymopoietin (TMPO/LAP2α) (Dechat *et al.*, 2000; Kubben *et al.*, 2010; Dittmer *et al.*, 2014), emerin (Clements *et al.*, 2000; Lee *et al.*, 2001; Sakaki *et al.*, 2001; Zastrow, Vlcek and Wilson, 2004; Kubben *et al.*, 2010), LEM2 (Brachner *et al.*, 2005; Kubben *et al.*, 2010), and MAN1 (Mansharamani and Wilson, 2005; Kubben *et al.*, 2010). Lamin A/C targets LEM2, a protein involved in nuclear structure organisation, to the INM (Brachner *et al.*, 2005). MAN1 binds Smad2 and Smad3 and antagonizes transforming growth factor-β signaling (Lin *et al.*, 2005), whilst emerin has been found to be involved in various signalling pathways including

muscle cell differentiation, as outlined in more detail in Chapter 1. It is believed that lamin A/C forms a complex with LAP2α that is involved in the regulation of the retinoblastoma protein-mediated pathway and other signaling pathways balancing proliferation and differentiation, and in the stabilization of higher-order chromatin organization throughout the nucleus (Markiewicz *et al.*, 2002; Dorner *et al.*, 2006). As well as this, lamin A/C has been found to directly interact with central component of the retinoblastoma pathway, retinoblastoma 1 (RB1) (Ozaki *et al.*, 1994). Lamin A/C also interact with SUN1/SUN2 at the INM, forming part of the linker of nuecloskeleton and cytoskeleton (LINC) complex, which physically couples the nucleus to the cytoskeleton (Crisp, Liu, Roux, J.B. Rattner, *et al.*, 2006). Evidence also suggests that lamin A/C can also interact with nucleoplasmic proteins such as barrier-to-autointegration factor (BAF), which is involved in mitosis, post-mitotic nuclear assembly, intrinsic immunity against foreign DNA, transcription regulation, and the DNA damage response (Montes de Oca *et al.*, 2009; Jamin and Wiebe, 2015), as well as the cytoskeletal protein actin (Simon, Zastrow and Wilson, 2010). Protein-protein interaction data, such as data yielded from experimental studies determining lamin A interactors, can be used on a large scale to determine networks of interactions. By studying these networks, we can understand more about the evolution proteins, and about the different systems that they are involved in. Protein interaction networks can also suggest new functions for proteins by revealing their role in different pathways or protein complexes.

Elucidation of specific lamin A-protein interactions has led to the discovery of disease-related mechanisms. From the association of lamin A and RB1, a further study suggested that the RB-MyoD pathways involved in muscle cell differentiation are

disrupted in Emery-Dreifuss muscular dystrophy (EDMD), and that key interactions between the NE and RB and MyoD fail in EDMD at the point of myoblast exit from the cell cycle, leading to uncoordinated phosphorylation and acetylation steps (Bakay *et al.*, 2006). Interactors of lamin A have also been found to be mislocalized in cells from laminopathy patients, or cells harbouring mutations in *LMNA,* suggesting interactions between lamin A and its binding partners may be lost, which may be related to disease pathology. C2C12 cells harbouring L-CMD *LMNA* mutations were observed to have mislocalization of emerin and some nucleoplasmic localization of lamin B1 (Gómez-Domínguez *et al.*, 2020). Lamin B localization has also been observed in C2C12s harbouring EDMD-related mutations (Scharner *et al.*, 2011). Emerin was also found to be mislocalized in fibroblasts harbouring the del.K32 L-CMD mutation, but lamin B1 and SUN2 localization were unaffected (Bertrand *et al.*, 2020). In del.K32 myotubes, however, a number of NE proteins were also found to be mislocalized including emerin, lamin B1, SUN2 and Nup153 (Bertrand *et al.*, 2020). L-CMD fibroblasts have also been observed to have nucleoplasmic aggregation of lamin A/C, indicating nuclear assembly defects which are likely a result of aberrant interactions between lamin filaments (Bertrand *et al.*, 2020). Together, this evidence suggests that lamin A interactions may be compromised in striated muscle laminopathies and L-CMD.

Whilst the identification of interactors of lamin A has allowed us to further understand lamin A function, and consequently some mechanisms behind L-CMD and laminopathy pathology through the loss of interactions, studies on lamin A interactions have used a variety of different techniques in different healthy cells and tissues which have both advantages and limitations. Firstly, most of these interactions have been identified in non-human cells and tissues including murine cardiomyocytes (Kubben *et al.*, 2010),

C2C12 myoblasts (immortalized myoblasts derived from mouse skeletal muscle) (Simon, Zastrow and Wilson, 2010), rat skeletal muscle and rat liver (Sakaki *et al.*, 2001), or mouse embryonic fibroblast cells (MEFs) (Brachner *et al.*, 2005; Crisp, Liu, Roux, J. B. Rattner, *et al.*, 2006). Whilst using models such as C2C12s and rat skeletal muscle, which lamin A binding partners actin and emerin have been identified in (Sakaki *et al.*, 2001; Simon, Zastrow and Wilson, 2010), offers insight into lamin A interactions that may occur in human skeletal muscle, which is relevant to skeletal muscle laminopathies, these interactions need to be verified in human skeletal muscle cells. In some instances, interactions have been examined in human cells including cancer cell lines (HeLa, A549, U2OS) (Sasseville and Langelier, 1998; Dreuillet *et al.*, 2002; Harper *et al.*, 2009; Kubben *et al.*, 2010; Dittmer *et al.*, 2014), which are favoured for their infinite expansion capabilities, HEK293 cells (immortalized embryonic kidney cells)(Markiewicz *et al.*, 2002), or fibroblasts (Crisp, Liu, Roux, J. B. Rattner, *et al.*, 2006). Whilst these cell lines have also been useful at elucidating lamin A interactions, they may not be entirely relevant to laminopathy pathology. It would offer further insight if these interactions could be verified in tissues affected by *LMNA* diseases. In terms of techniques and methods used to identify lamin A interactors, most studies have used a targeted approach, whereby a protein that is likely to associate with lamin A due to its proximity with lamin A, for example, is selected for investigation or verification of lamin A interaction. A number of methods have used for this approach including Co-immunoprecipitation, where antibodies specific to the target protein (in this case, lamin A) are used to immunoprecipitated intact lamin A complexes out of cell extracts. Following this, western blotting can be used to identify whether specific proteins were immunoprecipitated out of a sample along with lamin

A. The blot overlay assay method can also be used, where a radiolabelled protein probe is used to overlay protein samples immobilized on nitrocellulose.

In a couple of studies where interactions between lamin A with actin and lamin B1 were ascertained (Sasseville and Langelier, 1998; Schirmer and Gerace, 2004), recombinant or purified proteins have been used to analyse the interaction. Whilst it is useful to use recombinant proteins to establish binding partners and binding domains on proteins, they do not necessarily reflect protein interactions that occur *in-vivo.* Similarly, biomolecular interactional analysis, as has previously been used to evaluate the interaction between lamin A and emerin interaction (Clements *et al.*, 2000), can help to determine how molecules interact with each other using surface plasmon resonance, isothermal titration calorimetry, or fluorescence energy transfer, for example, but this also may not represent interactions under physiological conditions. As these methods have their limitations, a good approach is to use a combination of techniques to verify protein-protein interactions. For the lamin A interactors that are most well-established, including actin, B-type lamins, and emerin, multiple studies have been published using different procedures, which helps to prove these interactions.

For the identification of protein interactions on a larger scale, high-throughput methods have been developed, which a couple of studies on lamin A interactors have also used. Yest two-hybrid (Y2H) is one of the most commonly used direct methods of this kind, although it can also be used to assess specific interactions on a smaller scale. This system tests the interaction of two proteins by fusing each of them to a transcription binding domain. If the proteins successfully interact, the transcription

complex is activated, which transcribes a reporter gene whose product can be detected. As it is an *in vivo* technique, the Y2H system is effective at detecting transient interactions and can also be applied to screen large genome-wide libraries (to map an organism's whole interactome). There are some drawbacks to this approach, though, as Y2H is limited by its biases toward non-specific interactions, cannot identify protein complexes, or interactions of proteins initiating transcription by themselves. Other high-throughput methods include mass spectrometry (MS) and affinity purification. These have similar advantages to the Y2H system in that they are able to detect interactions on a large scale, however they are *in vitro* detection methods, therefore interactions occurring *in vitro* do not necessarily encapsulate what is happening *in vivo* (for example, when proteins are compartmentalized in different locations of the cell). Whilst studies have used high-throughput methods to successfully identify a large number lamin A interactors using an unbiased, large scale approach (Kubben *et al.*, 2010; Dittmer *et al.*, 2014), it is necessary to use other techniques to verify these interactions and due to the volume of data that these approaches produce, it is not possible to verify all identified interactions. Therefore, many lamin A interactions may have been overlooked.

As they have a central role in biological function, protein interactions control the underlying mechanisms leading to healthy and diseased states in organisms. Diseases may be caused by mutations interfering with the binding interface or leading to biochemically dysfunctional allosteric changes in proteins. Thus, protein interaction networks can also elucidate the molecular basis of disease, which can therefore inform methods for prevention, diagnosis, and treatment. As mentioned above, modified interactions between lamin A and some of its known binding partners have already

been reported in cells harbouring *LMNA* mutations. Some studies have also elucidated interactors of progerin, the lamin A isoform that is responsible for the premature aging disorder Hutchinson-Gilford progeria syndrome on a larger, unbiased scale using quantitative proteomics (Kubben *et al.*, 2010; Dittmer *et al.*, 2014). This has allowed the identification of putative progerin interactors that may be lost of gained in progeria compared to interactors of functional lamin A (Kubben *et al.*, 2010; Dittmer *et al.*, 2014). Further studies, however, are required to identify interactors of mutant lamin A associated with other laminopathies, including L-CMD. Mutations in *LMNA* additionally cause a wide range of diseases that affect different tissues and organ systems, and currently it remains unknown how mutations in one protein can cause many different diseases (Song, Zhang and Zhong, 2005). Perhaps an explanation for this is that there are tissue-specific differences in lamin A interactors. Different tissues have different compositions of cells, different functions and therefore have different requirements for protein interactions so that they can effectively carry out their roles within the human body. Whilst proteins like lamin A can be ubiquitously expressed in almost all tissues, often universally expressed proteins have tissue-specific interactors (Bossi and Lehner, 2009). It has been also documented that the NE proteome differs notably between tissues (Korfali *et al.*, 2010, 2012; Wilkie *et al.*, 2011). Comparison of the proteome of blood leukocyte, muscle and liver tissue NEs using proteomics, antibody staining of cryosections, tissue western blot and tissue RT-qPCR found that there were few proteins common to all three tissues (Korfali *et al.*, 2010, 2012; Wilkie *et al.*, 2011). These differences in NE proteomes is perhaps unsurprising considering that different tissues are made up of many different cell types that have differences in nuclear size, shape, and the amount of dense chromatin at the NE (Korfali *et al.*, 2012).

GO functional assignments also suggested that the observed tissue differences in NE composition contribute to signalling and gene regulation (Korfali *et al.*, 2012). Thus, this suggests that the differences in proteins identified at the NE in different tissues may have tissue-specific contributions. This evidence may suggest that lamin A has different interactors in different tissues, and loss of tissue-specific interactors could cause different disease pathologies. For example, a muscle-specific NE interactor that binds to lamin A could be lost from the NE as a result of *LMNA* mutations that is linked to a striated muscle laminopathy. Differences in NE signalling pathways or chromatin organization/gene regulation in tissues could also result in particular tissues having increased susceptibility to disruption of specific functions with particular *LMNA* mutations (Korfali *et al.*, 2012).

Particularly relevant to L-CMD and other striated muscle laminopathies, many muscle specific proteins have been identified in rat skeletal muscle NEs that have not been observed in NEs in other tissues (Wilkie *et al.*, 2011). These muscle-specific NE proteins have been shown to be upregulated during myogenesis, and have been found to be associated with the microtubule cytoskeleton (Wilkie *et al.*, 2011). These associations between these proteins and microtubules appeared to occur during interphase and mitosis, suggesting potential mechanisms towards mechanical instability and cell cycle regulation (Wilkie *et al.*, 2011). Skeletal muscle is also able to modify its mass and phenotype in response to trauma or activity overload and it has been observed that genes are differentially expressed during these processes (Carson, Nettleton and Reecy, 2002; Goldspink, 2002; Paoni *et al.*, 2003), as well as during muscle development, muscle cell differentiation and regeneration (Massenet *et al.*, 2021).

Therefore, different protein interactions will be required in myoblasts, which will also differ to those in other different tissues.

Taking the above into consideration, further research is required to assess interactors of lamin A in human skeletal muscle. Due to muscle specific NE proteins previously being found to be upregulated during myogenesis, it is of particular interest to determine lamin A interactors in healthy human myoblasts, the precursor cells to skeletal muscle tissue, as well as interactors of mutant forms of lamin A in L-CMD patient myoblasts. As well as this, future studies should aim to identify lamin A interactors in other tissues associated with other laminopathies and determine whether these differ from interactors of lamin A in L-CMD This may help to explain the diversity of diseases caused by *LMNA* mutations.

The aim of this chapter was to first conduct a literature search to identify known interactors of lamin A in different cells and tissues, including lamin A interactors which may have been identified in multiple studies but have been overlooked and have not been further investigated or verified. Then, using co-immunoprecipitation, to use a targeted approach to characterise lamin A interactors in both healthy control and L-CMD myoblasts harbouring mutations in *LMNA*.

Specific objectives include:

- To identify lamin A interactors common to 2 or more previous published studies, which may identify lamin A interactors that have been overlooked in high-throughput studies when considered in isolation.
- To use co-immunoprecipitation and liquid chromatography-mass spectrometry (LC-MS) to identify putative lamin A interactors in L-CMD and healthy control myoblasts.
- To identify interactors of "healthy" lamin A, and compare experimental results to published findings to determine whether healthy lamin A interactors identified in control myoblasts have been previously described.
- To determine whether any lamin A interactors are lost or gained in myoblasts from L-CMD patients.
- To use the database for annotation, visualization and integrated discovery (DAVID) to identify functions associated with lamin A interactors in healthy and L-CMD cells

3.2. Results

3.2.1. Identification of previously described lamin A interactors in healthy cells and tissues

3.2.1.1. A literature search identified a total of 243 proteins that were interactors of lamin A in healthy cells and tissues, fifteen of which were identified in ≥2 studies.

Prior to experimental work, a literature search was first conducted as described in Chapter 2, Section 2.5.2. to collate proteins that had previously been identified as potential lamin A interactors in healthy tissue or cell lines, including those which may have been overlooked when results of high through-put studies were considered in isolation. From this point forward these proteins will be termed “healthy” lamin A interactors. This was done to provide a baseline for comparing the experimentally derived results to. By comparing experimentally determined healthy lamin A interactors to previously described healthy lamin A interactors, new putative healthy lamin A interactors could be deduced. As well as this, the identification of previously identified healthy lamin A interactors can verify the efficacy of the experiment.

The literature search yielded a total of 243 proteins, fifteen of which were identified in ≥2 studies (**Table 3.1**). These studies spanned the following species: *Homo sapiens*, *Mus musculus*, *Rattus norvegicus*, *Cercopithecus aethiops*, and used a variety of different techniques to identify interactors. Eight studies used immunoprecipitation to identify lamin A binding partners, most often this technique was used in combination with either western blotting or blot overlay assay, but a few studies used immunoprecipitation as well as the GST-fusion protein system or yeast-two hybrid screening (Y2H). In two studies, the Streptavidin/biotin system (OneSTrEP) method was used to identify protein-protein interactions. One study used OneSTrEP with mass spectrometry, which was also the only study to utilise mass spectrometry. Four studies

used recombinant proteins for their model to identify lamin A interactors, whilst the other studies used cell or tissue extracts. No studies were found to use derived human skeletal muscle.

Table 3.1- Lamin A interactors that were identified in ≥2 studies.

	Identified protein	Gene name	No. of studies	Species	Tissue or cell line	Methodology	Reference(s)
1	**F-Actin**	*ACTB*	3	*Homo sapien*[1,3], *Mus musculus*[2]	A549[1], C2C12[2], Human recombinant lamin A tails[3]	GST-fusion protein system[1], Immunoprecipitation[2], Western blotting[1,2], High speed pelleting assay	(Sasseville and Langelier, 1998[1]; Lattanzi *et al.*, 2003[2]; Simon, Zastrow and Wilson, 2010[3])
2	**Lamin B1**	*LMNB1*	4	*Homo sapien*[5,7], *Mus musculus*[4], *Escherichia coli*[6]	Murine cardiac myocyte NklTAg cells[4], Human recombinant proteins[5], BL21(DE3)[6], U2OS[7]	Streptavidin/biotin system (OneSTrEP)[4,7], Mass spectrometry[4], Y2H system[5,7], Binding assay[6], Western blotting[6]	(Ye and Worman, 1995[5]; Schirmer and Gerace, 2004[6]; Kubben *et al.*, 2010[4]; Dittmer *et al.*, 2014[7])
3	**Lamin B2**	*LMNB2*	3	*Homo sapien*[7], *Mus musculus*[4], *Escherichia coli*[6]	Murine cardiac myocyte NklTAg cells[4], BL21(DE3)[6], U2OS[7]	Streptavidin/biotin system (OneSTrEP)[4,7], Mass spectrometry[4], Binding assay[6], Western blotting[6], Y2H system[7]	(Schirmer and Gerace, 2004[6]; Kubben *et al.*, 2010[4]; Dittmer *et al.*, 2014[7])
4	**Emerin**	*EMD*	4	*Homo sapien*[4], *Mus musculus*[4], *Escherichia coli*[8,9,10], *Rattus norvegicus*[9]	Murine cardiac myocyte NklTAg cells[4], U2OS[4], BL21(DE3)[8,9,10], Rat skeletal muscle[9], Rat liver[9]	Streptavidin/biotin system (OneSTrEP)[4], Mass spectrometry[4], Blot overlay assay[8], Immunoprecipitation[8,9], Y2H system[9], Biomolecular Interaction Analysis, Biacore[10]	(Clements *et al.*, 2000[10]; Lee *et al.*, 2001[8]; Sakaki *et al.*, 2001[9]; Kubben *et al.*, 2010[4])
5	**LAP2α**	*TMPO/LAP2*	3	*Homo sapien*[4,7,11], *Mus musculus*[4] *Rattus norvegicus*[11]	Murine cardiac myocyte NklTAg cells[4], U2OS[4,7], HeLa[11], Rat liver[11]	Streptavidin/biotin system (OneSTrEP)[4,7], Mass spectrometry[4], Y2H system[7], Immunoprecipitation[11], Blot overlay assay[11], Western blotting[11]	(Dechat *et al.*, 2000[11]; Kubben *et al.*, 2010[4]; Dittmer *et al.*, 2014[7])
6	**LEM2**	*LEMD2*	2	*Homo sapien*[12], *Mus musculus*[4,12]	Murine cardiac myocyte NklTAg cells[4], MEFs[12], Human recombinant proteins[12]	Streptavidin/biotin system (OneSTrEP)[4], Mass spectrometry[4], Immunofluorescence[12], Blot overlay assay[12], GST-fusion protein system[12]	(Brachner *et al.*, 2005[12]; Kubben *et al.*, 2010[4])
7	**Zinc finger protein 239**	*ZNF239/MOK2*	2	*Homo sapien*[13,14]	HeLa[13,14]	Y2H system[13], GST-fusion protein system[13,14], Immunoprecipitation[13], Western blotting[13]	(Dreuillet *et al.*, 2002[13]; Harper *et al.*, 2009[14])
9	**Retinoblastoma-associated protein**	*RB1*	2	*Homo sapien*[15]	HEK293 cells[15], HDF[15]	GST-fusion protein system[15], Blot overlay assay[15], Immunoprecipitation[15]	(Ozaki *et al.*, 1994[16]; Markiewicz *et al.*, 2002[15])
10	**SUN domain-containing protein 2**	*SUN2*	2	*Homo sapien*[17], *Mus musculus*[4]	Murine cardiac myocyte NklTAg cells[4], Fibroblasts[17], MEFs[17]	Streptavidin/biotin system (OneSTrEP)[4], Mass spectrometry[4], GST-fusion protein system[17], Immunofluorescence[17], Immunoprecipitation[17]	(Crisp, Liu, Roux, J. B. Rattner, *et al.*, 2006[17]; Kubben *et al.*, 2010[4])
11	**SUN domain-containing protein 1**	*SUN1*	2	*Homo sapien*[17,18], *Mus musculus*[4]	Murine cardiac myocyte NklTAg cells[4], Fibroblasts[17], MEFs[17], U2OS[18]	Streptavidin/biotin system (OneSTrEP)[4], Mass spectrometry[4], GST-fusion protein system[17,18], Immunofluorescence[17], Immunoprecipitation[17,18], Y2H system[18]	(Crisp, Liu, Roux, J. B. Rattner, *et al.*, 2006[17]; Haque *et al.*, 2006[18]; Kubben *et al.*, 2010[4])

12	**MAN1**	*MAN1*	2	*Mus musculus*[4], *Escherichia coli*[19]	Murine cardiac myocyte NklTAg cells[4]	Streptavidin/biotin system (OneSTrEP)[4], Mass spectrometry[4], Blot overlay assay[19]	(Mansharamani and Wilson, 2005[19]; Kubben *et al.*, 2010[4])
13	**Nesprin 2**	*SYNE2*	2	*Mus musculus*[4], *Cercopithecus aethiops*[20], *Escherichia coli*[20]	Murine cardiac myocyte NklTAg cells[4], COS7[20]	Streptavidin/biotin system (OneSTrEP)[4], Mass spectrometry[4], Y2H system[20], GST-fusion protein system[20], Blot overlay assay[20]	(Libotte *et al.*, 2005[20]; Kubben *et al.*, 2010[4])
14	**Nucleoporin 155**	*NUP155*	2	*Homo sapiens*[21], *Mus musculus*[4]	Murine cardiac myocyte NklTAg cells[4], HeLa[21]	Streptavidin/biotin system (OneSTrEP)[4], Mass spectrometry[4], Immunoprecipitation[8], Western blotting[8], GST-fusion protein system[8]	(Kubben *et al.*, 2010[4]; Han *et al.*, 2019[21])
15	**Proliferating cell nuclear antigen**	*PCNA*	3	*Homo sapiens*[7,22], *Mus musculus*[4]	Murine cardiac myocyte NklTAg cells[4], U2OS[7], Human recombinant proteins[22]	Streptavidin/biotin system (OneSTrEP)[4,7], Mass spectrometry[4] Y2H system[7], Binding assay[22], Western blotting[22]	(Shumaker *et al.*, 2008[22]; Kubben *et al.*, 2010[4]; Dittmer *et al.*, 2014[7])

This table contains the 15 healthy lamin A interactors that were identified in ≥2 studies including the cell line or tissue that the interactor was identified in, the species, the method used and references.

3.2.1.2. Bioinformatics tools were used to identify functions for previously described healthy lamin A interactors

Once a list of previously identified lamin A interactors had been established, using bioinformatics tools, the functions of these proteins were deduced in order to provide insight into the processes that lamin A may be involved in through its interactors in healthy cells and tissues.

The list of healthy lamin A interactors that were identified in the literature search in one or more studies (n=243) were first inputted into STRING to identify significant interactions between the proteins that have been previously reported in the literature (**Fig. 3.1**) (Szklarczyk *et al.*, 2021), as described in Chapter 2, Section 2.5.4.1. It was decided that lamin A interactors identified in one or more studies in the literature would be used, as only 15 proteins were identified in two or more studies. It was thought that more conclusions could be drawn from the larger number of proteins identified as potential lamin A interactors in one or more study. Association network analysis was performed with high confidence (0.700) interaction to exclude false positive results. Each node in the network are individual proteins, the "edges" (or lines connecting the nodes) represent predicted functional associations between proteins. Edges are drawn with different coloured lines to represent the existence of different types of evidence used in predicting associations. Disconnected nodes were hidden, and one protein (lamin companion 1, *LCO1*) was not identified by STRING's databases and therefore was not included in the output.

STRING allows the identification of clusters of interacting proteins that have similar functions or that belong to similar protein families. Several clusters of proteins were identified from the healthy lamin A interactors literature search input list. A number of

proteins (n=7) that are constituents of the linker of nucleoskeleton and cytoskeleton (LINC) complex, that connects the nucleus to the cytoskeleton within mammalian cells, were identified in STRING analysis, these included lamins B1 and B2, nesprin-1 and -2, SUN1 and SUN2 and emerin. All of these proteins were lamin A interactors identified from healthy cells or tissues that were identified in ≥2 studies, except nesprin-1, which was only identified in a single study. Another cluster of nuclear envelope (NE) proteins were identified as nucleoporins which are involved in nuclear pore complex assembly (n=10). The nuclear pore complex (NPC) is a structure that mediates all macromolecular transport across the NE. Members of the rab family of proteins were also identified (n=9). Rab proteins are small guanosine triphosphatases which regulate protein transport along the endocytic and exocytic pathways in all cell types (Yap and Winckler, 2009). These proteins participate in vesicle budding, membrane fusion, and interactions with the cytoskeleton (Yap and Winckler, 2009). A small cluster of proteins were found to be involved in DNA repair processes (n=5), and a few proteins were part of the collagen family (n=4).

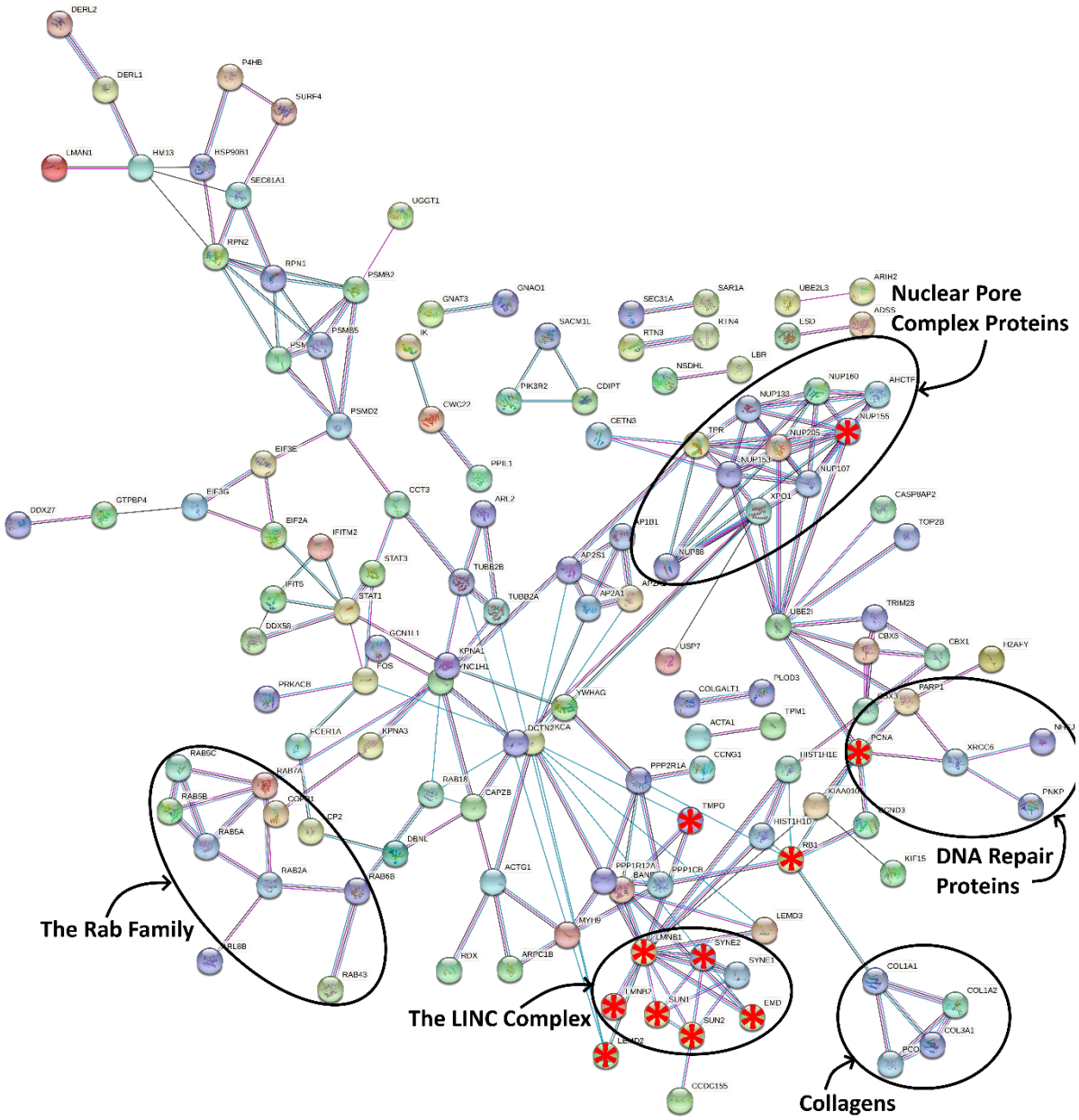

Figure 3.1- STRING analysis of healthy lamin A interactors identified in the literature. *The results of the literature search for lamin A interactors (n=234) were inputted into STRING. Purple lines represent experimental evidence, light blue lines indicate database evidence, and black lines symbolise co-expression evidence. Disconnected nodes were hidden, and one protein (lamin companion 1, LCO1) was not identified by STRING's databases and therefore was not included in the output. Several clusters of proteins were identified including constituents of the linker of nucleoskeleton and cytoskeleton (LINC) complex, proteins involved in nuclear pore complex assembly, proteins involved in DNA repair processes, collagens, and members of the rab protein family. Proteins that were identified in ≥2 studies are denoted using a red Asterix (*).*

As described in Chapter 2, Section 2.5.4.2., the same list of healthy lamin A interactors identified from the literature in one or more studies (n=243) were then inputted into DAVID (database for annotation, visualisation, and integrated discovery) (Sherman *et al.*, 2022). DAVID analysis highlighted enriched biological processes (BP), cellular components (CC), and molecular functions (MF) associated with the healthy lamin A interactors (*p*-value <0.05) (**Table 3.2**). Top BP terms included processes that occur at the nuclear envelope, with the largest proportion of proteins being involved in protein transport (n=21, 8.9%) and protein import into the nucleus (n=11, 4.7%). Other BP terms included nuclear envelope organisation (n=8, 3.4%), nucleocytoplasmic transport (n=9, 3.8%), and nuclear pore complex assembly (n=5, 2.1%). CC GO terms revealed most proteins are cytosolic (n=119, 50.4%), with membrane (n=77, 32.6%), nuclear membrane (n=24, 10.2%), and nuclear envelope (n=30, 12.7%) also appearing as top terms alongside endoplasmic reticulum membrane (n=52, 22.0%). The top MF GO term was protein binding, with 90.7% (n=214) of proteins associated with the phrase. Lamin binding also appeared as a MF, but only 3.8% (n=9) of proteins were linked to it. Other MF terms included GTP binding (n=23, 9.7%), GTPase activity (n=20, 8.5%) and GDP binding (n=10, 4.2%). KEGG pathways that were identified included nucleoplasmic transport (n=15, 6.4%), salmonella infection (n=16, 6.8%), chemical carcinogenesis- receptor activation (n=14, 5.9%), amoebiasis (n=10, 4.2%) and vasopressin-regulated water reabsorption (n=7, 3.0%).

Table 3.2- Top DAVID GO terms for healthy lamin A interactors that were identified in one or more study in the literature

GO Term- Biological Processes	No. of proteins	% of proteins	p-value
Nuclear envelope organisation	8	3.4	4.8E-9
Nucleocytoplasmic transport	9	3.8	1.8E-7
Protein transport	21	8.9	3.7E-7
Protein import into nucleus	11	4.7	4.5E-7
Nuclear pore complex assembly	5	2.1	2.4E-6
GO Term- Cellular Component	**No. of proteins**	**% of proteins**	**p-value**
Nuclear envelope	30	12.7	4.2E-24
Endoplasmic reticulum membrane	52	22.0	6.5E-19
Membrane	77	32.6	7.2E-16
Nuclear membrane	24	10.2	6.6E-15
Cytosol	119	50.4	8.3E-15
GO Term- Molecular Function	**No. of proteins**	**% of proteins**	**p-value**
Protein binding	214	90.7	5.9E-20
Lamin binding	9	3.8	1.0E-11
GTP binding	23	9.7	5.1E-9
GTPase activity	20	8.5	7.9E-8
GDP binding	10	4.2	4.4E-7

GO terms were determined for the following categories: biological processes, cellular components, molecular functions, and KEGG pathways. Number of proteins alongside the percentage of proteins out of the total input (n=243) are stated alongside *p*-value (<0.05).

3.2.2. Experimentally determining lamin A interactors in healthy and L-CMD myoblasts

Previous studies have identified a number of healthy lamin A interactors, as outlined in the preceding sections, and this has been insightful into lamin A functions. In consideration of the work that has already been done on lamin A interactors, a co-immunoprecipitation (Co-IP) protocol was established and optimised to immunoprecipitate protein interactors of lamin A/C from healthy and L-CMD myoblast cell extracts. LC-MS was then used to identify the proteins in the healthy and L-CMD myoblast immunoprecipitates. Together, these two techniques allowed the identification of potential undescribed healthy lamin A interactors in control myoblasts, and to identify whether lamin A interactions are lost and/or gained in L-CMD myoblasts.

3.2.2.1. Testing the co-immunoprecipitation protocol through the identification of known lamin A interactors

Control myoblasts (C5d) were subjected to Co-IP with a mouse monoclonal anti-lamin A/C antibody (MANLAC1 4A7; Wolfson Centre for Inherited Neuromuscular Disease (Manilal *et al.*, 2004)), as described in Chapter 2, Section 2.5.1. Firstly, the C5d control myoblast immunoprecipitate sample was probed for lamin A/C to determine if the antibody was successful at binding to lamin A/C. This is important to establish, to ensure the target protein, in this case, lamin A/C, is being immunoprecipitated out of the C5d control myoblast sample. Two anti-lamin A/C antibodies were used to identify lamin A/C by western blot, the mouse monoclonal anti-lamin A/C antibody that was used for the Co-IP, and a rabbit monoclonal anti-lamin A/C (ab169532; Abcam). The two antibodies were used to determine whether there would be any interference by

the mouse immunoglobulin G (IgG) that coat the Dynabeads® that are used for Co-IP when using the mouse monoclonal antibody. Mouse IgG has a molecular weight of around 150kDa and consists of two 50kDa heavy chains and two 25kDa light chains connected by disulphide bond. Considering lamin A has a molecular weight of 65kDa, the larger subunit of the mouse IgG could additionally be detected by the mouse monoclonal antibody and interfere with detection of lamin A by western blot.

Lamin A/C (70/65kDa) was successfully detected in the pulldown eluates using both of the antibodies (**Fig 3.2 A, B**), and the mouse IgG did not appear to interfere with the mouse monoclonal antibody result. There did, however, appear to be strong bands detected in the negative control eluate on the rabbit monoclonal antibody western blot at around 70kDa and 55kDa. As outlined mentioned above, the heavy mouse IgG chains are 50kDa, therefore the 55kDa band may represent this. It is uncertain what the 70kDa band could be as it does not align to the weight of mouse or human IgG. Instead, perhaps this band represents something that has stuck un-specifically to the beads and had been detected as a cross-reaction of the primary or secondary antibodies used. Once lamin A/C had been successfully detected in the Co-IP samples, providing evidence that lamin A/C is in fact being immunoprecipitated out of the C5d control myoblast sample, other known interactors of healthy lamin A/C could be investigated. Healthy lamin A/C interactors emerin and SUN2, that had been previously identified in ≥2 studies, were chosen as candidates for verification. Using a mouse monoclonal anti-emerin antibody (MANNEM1 5D10; Wolfson Centre for Inherited Neuromuscular Disease (Manilal *et al.*, 1996, 1999)), emerin (34kDa) was identified by the presence of a faint band in the pulldown eluate, but there was also a substantial amount of emerin in the negative control eluate, suggesting that the

pulldown may not have worked as well (**Fig 3.2, C**). Using a rabbit polyclonal anti-SUN2 antibody (HPA001209; Sigma Aldrich), SUN2 (80kDa) may have been detected in the pulldown eluate, as a very faint band was present around 80kDa (**Fig 3.2, D**). However, there appeared to be no SUN2 detected in the input sample, making it difficult to determine that SUN2 has been pulled down by lamin A. As the signal of the IgG bands in the emerin and SUN2 western blots were very strong, these may be reducing the signals from the emerin and SUN2 bands in the pulldown eluate samples. These experiments were conducted during the Covid-19 pandemic, and around this time there had been no access to the laboratory for 5 months. On return to the laboratory, other experiments took priority and therefore due to time constraints, these experiments were not re-run or optimised. It is also important to consider there are limitations to Co-immunoprecipitation. This method may not allow the identification of transient interactions which may occur *in-vivo*, the extraction method used may disrupt some interactions, and only a very small percentage of the pool of protein within a sample may interact.

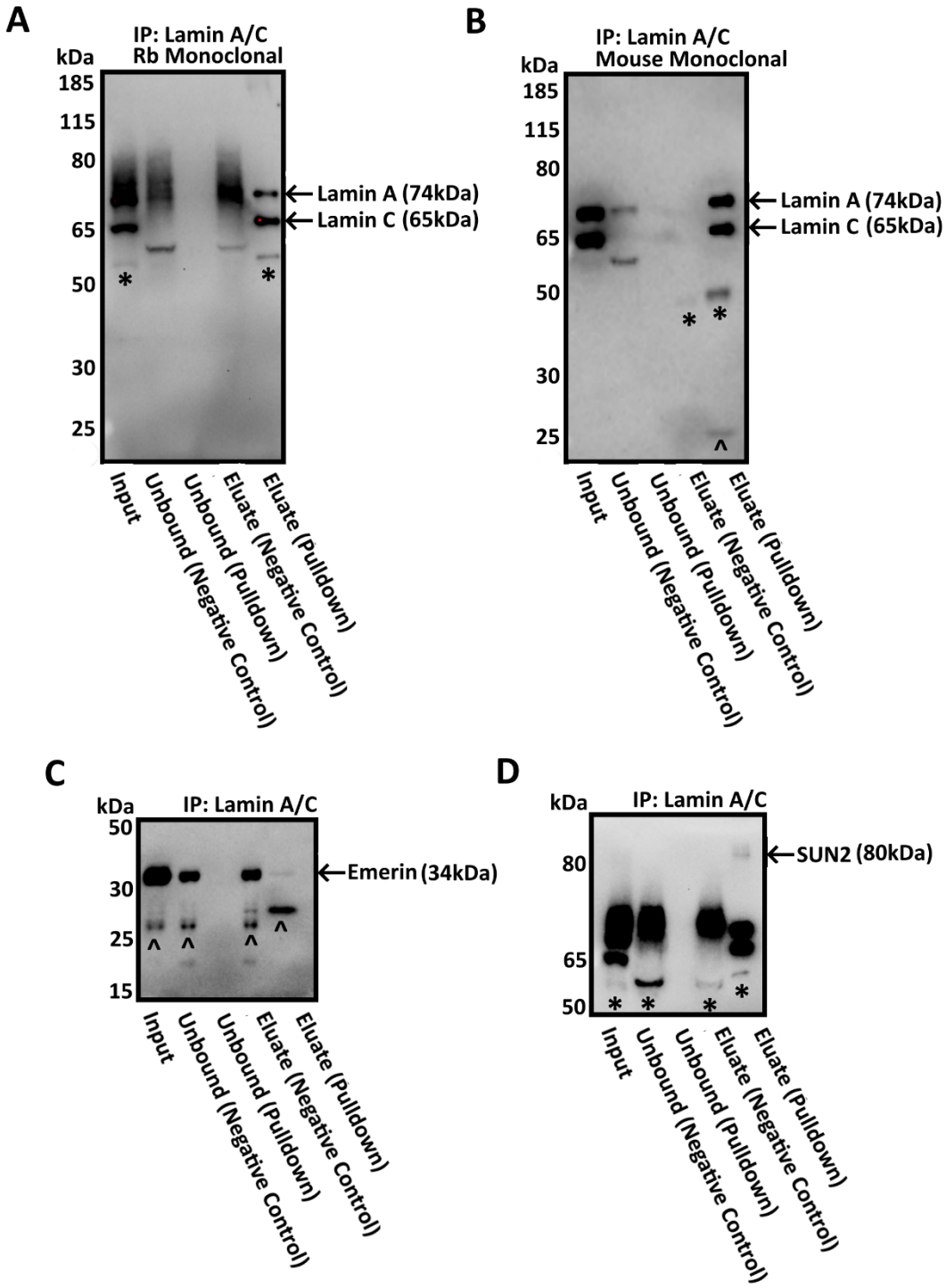

Figure 3.2- Western blots probing for lamin A/C, emerin and SUN2 in lamin A/C Co-IP control C25 myoblast extract. *Lamin A/C was successfully detected in pulldown eluate using (A) an ab169532 rabbit monoclonal anti-lamin A/C antibody (Abcam) and using (B) the MANLAC1 4A7 mouse monoclonal anti-lamin A/C antibody (Wolfson Centre for Inherited Neuromuscular Diseases). (C) Emerin was detected in lamin A/C pulldown eluate, as characterised by a faint band at 34kDa. (D) SUN2 was also detected in lamin A/C pulldown eluate, as demonstrated by a faint band at 80kDa. Bands indicated by an Asterisk (*) are likely indicative of the large mouse or rabbit IgG subunit, whilst the wedge (^) symbol indicates the small mouse IgG subunit.*

3.2.2.2. LCMS-MS analysis revealed putative lamin A interactors in healthy and L-CMD myoblast extracts

Once the Co-IP protocol had been tested by verifying that the mouse monoclonal anti-lamin A/C antibody was binding to lamin A and precipitating lamin A out of the healthy control (C5d) myoblast extract, L-CMD and healthy control myoblast samples were subjected to Co-IP and then LC-MS analysis to identify lamin A interactors.

As described above in Section 3.3.2.1., as well as in Chapter 2, Section 2.5.2., Co-IP with a mouse monoclonal anti-lamin A/C antibody was done on three myoblasts cell lines derived from L-CMD patients (L380S, del.K32, R249W), and three myoblast lines from healthy donors closest in age to the L-CMD patients (C5d, C25, C41). After this, the samples were prepared for LCMS/MS, and sent to the BSRC Mass Spectrometry & Proteomics Facility at the University of St Andrews for LCMS/MS analysis, performed by Dr Sally Shirran, as outlined in Chapter 2, Section 2.5.3. The LCMS/MS analysis produces a Scaffold report file containing a complete list of proteins that were identified in each of the L-CMD and healthy control samples. A unique peptide count value for each identified protein is assigned to each sample, and this indicates the number of peptide sequences identified that are unique to a protein group. The Scaffold data was filtered using specific criteria to remove background and account for non-specific binding, as described in Chapter 2, Section 2.5.4. To note, usually proteins that are identified with only one unique peptide are removed at the filtering stage (Fuller *et al.*, 2010; Holt *et al.*, 2020), however it was noticed that BAF, a known interactor of lamin A, was only identified with one peptide across all L-CMD and healthy control samples. This may be reflective of the small size of BAF (10kDa). For

this reason, proteins identified with only one peptide were still included in the data analysis.

Across the three healthy control myoblast samples, a total of 162 proteins were identified (**Fig 3.3, A**). Of these 162 potentially healthy lamin A interactors, 41 proteins were detected in all of the control cell lines (25.3% of total proteins detected in all control samples). Amongst these proteins, seven had been previously identified in the literature search as healthy lamin A interactors. In comparison, 378 proteins were found across the three L-CMD cell lines (**Fig 3.3, B**). Out of these 378 possible mutant lamin A interactors, 61 proteins (16.1% of total proteins detected in all three L-CMD cell lines) were detected across all three L-CMD samples. The 41 proteins that were identified across all healthy control myoblast samples were compared to the 61 proteins detected in all three of the L-CMD myoblast samples, and a total of 32 commonalities were found between the two groups (**Fig 3.3, C**).

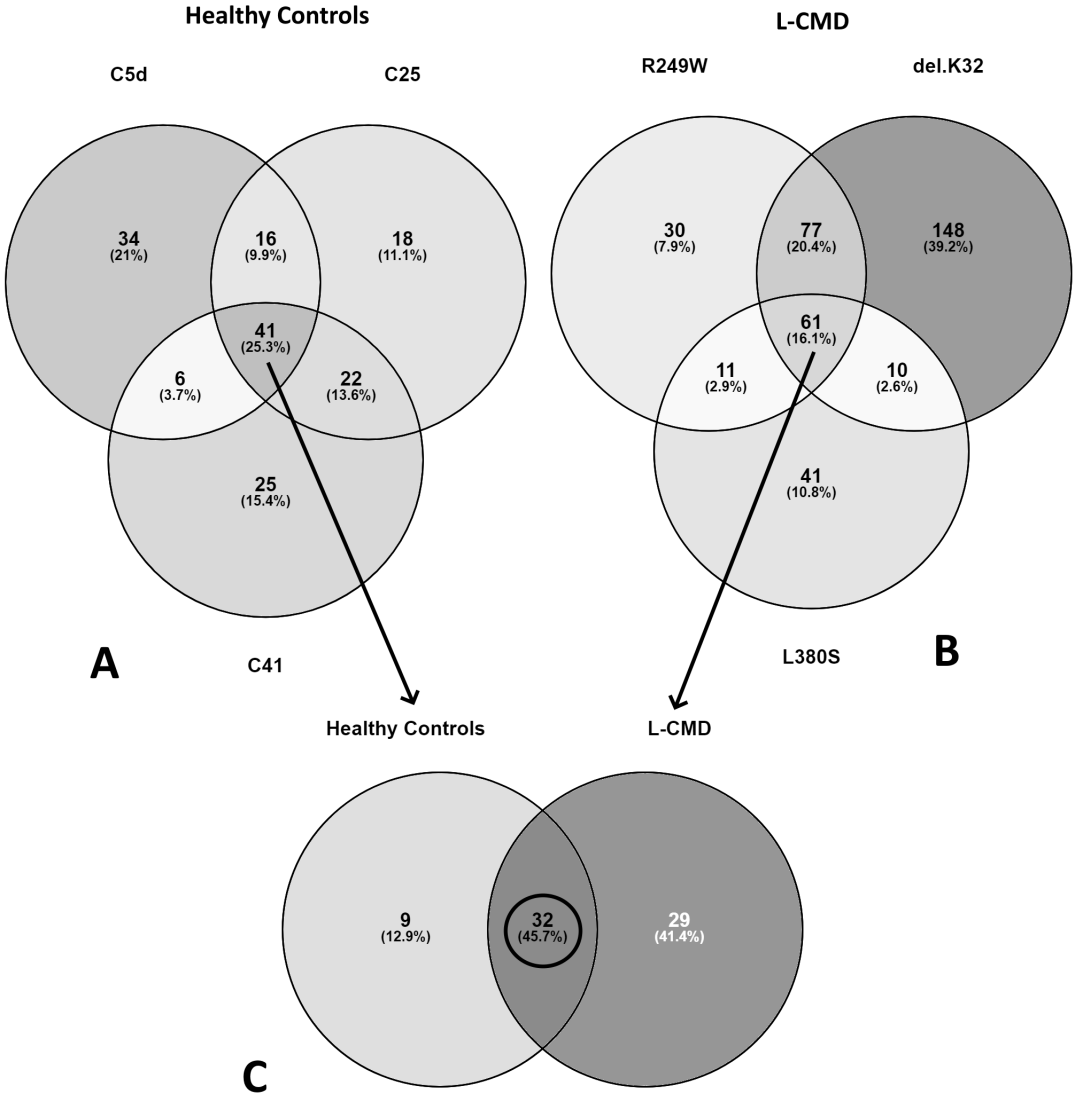

Figure 3.3- Venn diagrams illustrating the numbers of proteins identified in the LCMS/MS analysis. *Numbers of putative lamin A interactors found in the immunoprecipitates from (A) each of the healthy control cell lines, C5d, C25, and C 41, (B) the L-CMD cell lines, R249W, del.K32, and L380S. The proteins detected across all of the healthy controls and then all of the L-CMD cell lines are shown in (C). There were 33 commonalities found across both the healthy controls and L-CMD cell lines.*

The 32 proteins were found across all healthy control and L-CMD myoblasts samples could more likely be lamin A interactors, given that they were identified in all healthy and L-CMD samples (**Table 3.3**). This suggests that healthy and mutant lamin A interacts with these proteins, and that these interactions are also not lost as a result of

the *LMNA* mutations that the L-CMD cell lines harbour. Amongst these 32 proteins included seven proteins that were previously identified as healthy lamin A interactors; lamin B1, lamin B2, X-ray repair protein 6, core histone macro- H2A.1, SUN2, emerin and BAF. This substantiates previous findings that these proteins are lamin A interactors. The remaining 25 proteins have not previously been linked to lamin A and represent potential new healthy (and mutant) lamin A interactors.

Table 3.3- List of proteins identified across all healthy controls and L-CMD cell lines.

			Controls						L-CMD					
			C5d		C25		C41		R249W		del.K32		L380S	
	Identified protein	Gene name	Peptide count (n=X)	Enrichment (%)	Peptide count (n=X)	Enrichment (%)	Peptide count (n=X)	Enrichment (%)	Peptide count (n=X)	Enrichment (%)	Peptide count (n=X)	Enrichment (%)	Peptide count (n=X)	Enrichment (%)
1	**Lamin A/C**	LMNA	44	1467	37	1233	34	1133	45	1500	39	1300	43	1433
2	**Lamin B1***	LMNB1	30	3000	28	2800	26	2600	30	3000	25	2500	28	2800
3	**Lamin B2***	LMNB2	21	2100	15	1500	12	1200	21	2100	13	1300	21	2100
4	**X-Ray Repair Protein 6***	XRCC6	7	700	16	1600	12	1200	21	2100	8	800	4	400
5	**Core Histone Macro- H2A.1***	H2AY	7	700	7	700	6	600	10	1000	7	700	4	400
6	**SUN2***	SUN2												
7	**Emerin***	EMD	6	600	7	700	6	600	8	800	6	600	7	700
8	**TNFAIP3-Interacting Protein 1**	TNIP1	4	400	1	100	2	200	2	200	2	200	6	600
9	**ATP Synthase Subunit Alpha, Mitochondrial**	ATPA	4	400	2	200	1	100	6	600	8	800	3	300
10	**60S Ribosomal Protein L23a**	RL23	4	400	2	200	1	100	2	200	2	200	2	200
11	**X-Ray Repair Protein 5**	XRCC5	3	300	10	1000	7	700	22	2200	4	400	2	200
12	**Histone H3.1t**	H31T	3	150	3	150	3	150	4	200	3	150	4	200
13	**Histone H1.2**	H12	2	200	4	400	3	300	5	500	3	300	1	100
14	**Hornerin**	HORN	2	200	1	100	2	200	2	200	2	200	1	100
15	**Histone H2A.V**	H2AV	2	200	2	200	2	200	4	400	2	200	2	200
16	**Histone H2B Type 1-B**	H2B1B	2	200	1	100	1	100	2	200	2	200	1	100
17	**Histone H1.5**	H15	2	200	4	400	3	300	5	500	2	200	2	200
18	**High Mobility Group Protein HMG-I/HMG-Y**	HMGA1	2	200	2	200	2	200	4	400	2	200	1	100
19	**40S Ribosomal Protein S4, X Isoform**	RS4X	2	100	2	100	2	100	2	100	4	200	2	100
20	**BAF***	BAF	1	100	2	200	2	200	2	200	2	200	1	100
21	**Exportin 2**	XPO2	1	100	1	100	1	100	2	200	1	100	1	100

22	**Kelch-Like Protein 35**	KLH35	1	100	1	100	1	100	1	100	1	100	1	100
23	**Cytoplasmic FMR1-Interacting Protein 1**	CYFP1	1	100	1	100	1	100	1	100	1	100	1	100
24	**Proto-Oncogene Serine/Threonine-Protein Kinase Mos**	MOS	1	100	1	100	1	100	1	100	1	100	1	100
25	**Heterogeneous Nuclear Ribonucleoproteins C1/C2**	HNRPC	1	100	3	300	1	100	7	700	3	300	1	100
26	**Inter-Alpha-Trypsin Inhibitor Heavy Chain H3**	ITIH3	1	100	1	100	1	100	2	200	2	200	2	200
27	**60S Ribosomal Protein L23a**	RL23A	1	100	1	100	1	100	1	100	2	200	1	100
28	**60S Ribosomal Protein L34**	RL34	1	100	2	200	1	100	1	100	1	100	1	100
29	**Hemoglobin Subunit Zeta**	HBAZ	1	100	1	100	1	100	1	100	1	100	1	100
30	**Myosin Light Chain 6B**	MYL6B	1	100	1	100	1	100	1	100	8	800	1	100
31	**Histone H2A Type 1-C**	H2A1C	1	100	1	100	1	100	2	200	1	100	1	100
32	**60S Ribosomal Protein L24**	RL24	1	100	1	100	1	100	3	300	2	200	1	100
33	**60S Ribosomal Protein L15**	RL15	1	100	1	100	2	200	3	300	4	400	1	100

The complete list of proteins that were identified across all healthy control (C5d, C25, C41) samples, and all L-CMD (L380S, R249W, del.K32) samples. Each protein, along with its corresponding gene name are listed. The number of unique peptides (peptide count) for each protein in each sample is listed, along with the enrichment of each protein in each sample. Enrichment is a calculation of the fold increase of unique peptides identified in each sample compared to the number of peptides identified in the “beads only” control. This control is put in place to account for non-specific binding of proteins to the Dynabeads® used to pull lamin A protein complexes out of protein extract samples. Proteins identified previously as lamin A interactors are indicated with an Asterix by the protein name (*).

A total of nine proteins were identified in each of the healthy control myoblast samples, which were not detected in all of the L-CMD myoblast samples (**Table 3.4**). By cross checking this list of nine proteins to the lamin A interactors identified in the literature search, it appeared that none of these nine proteins had been previously identified as lamin A interactors. As these proteins were only identified in all of the healthy controls, this could suggest that these interactions are lost as a result of LMNA mutations in some of the L-CMD myoblast samples. Included among these nine proteins were FACT complex subunit SPT16, FACT complex subunit SSRP1, and DNA topoisomerase 1. Interestingly, these proteins are all involved in DNA replication or repair processes. In Section 3.1, where STRING analysis was conducted on the list of healthy lamin A interactors that were identified in the literature search, a cluster of DNA repair proteins were revealed.

Table 3.4- List of proteins identified across all healthy control cell lines.

			Controls					
			C5d		C25		C41	
	Identified protein	Gene name	Peptide count (n=X)	Enrichment (%)	Peptide count (n=X)	Enrichment (%)	Peptide count (n=X)	Enrichment (%)
1	**FACT complex subunit SPT16**	SP16H	4	400	7	700	6	600
2	**FACT complex subunit SSRP1**	SSRP1	3	300	4	400	3	300
3	**DNA topoisomerase I**	TOP1	2	200	5	500	11	1100
4	**Interferon alpha-14**	IFN14	1	100	1	100	1	100
5	**Serine/threonine-protein kinase Nek10**	NEK10	1	100	1	100	1	100
6	**Phosphoglucomutase-like protein 5**	PGM5	1	100	1	100	1	100
7	**High mobility group protein HMGI-C**	HMGA2	1	100	1	100	5	500
8	**Probable ATP-dependent RNA helicase DDX5**	DDX5	1	100	1	100	1	100
9	**Heterogeneous nuclear ribonucleoprotein H**	HNRH1	1	100	1	100	1	100

The complete list of proteins that were identified across all healthy control (C5d, C25, C41) samples, but not all L-CMD (L380S, R249W, del.K32) samples. Each protein, along with its corresponding gene name are listed. The number of unique peptides (peptide count) for each protein in each sample is listed, along with the enrichment of each protein in each sample. Enrichment is a calculation of the fold increase of unique peptides identified in each sample compared to the number of peptides identified in the "beads only" control. This control is put in place to account for non-specific binding of proteins to the Dynabeads® used to pull lamin A protein complexes out of protein extract samples. Proteins identified previously as lamin A interactors are indicated with an Asterix by the protein name (*).

There were also 29 proteins that were identified across all of the L-CMD myoblast samples, but not in all of the healthy control myoblast samples. Of these 29 proteins, three had been previously identified in the literature as healthy lamin A interactors; SUN1, DNA topoisomerase 2-beta, and endoplasmin, but here, none of these proteins were identified in any of the healthy myoblast samples. The proteins identified only in the L-CMD myoblast samples indicate lamin A interactions that might be gained or enriched as a result of the *LMNA* mutations in the L-CMD myoblasts, and that these are only interactors of "mutant" lamin A.

Table 3.5- List of proteins identified across all three L-CMD cell lines.

			L-CMD					
			R249W		L380S		del.K32	
	Identified protein	**Gene name**	**Peptide count (n=X)**	**Enrichment (%)**	**Peptide count (n=X)**	**Enrichment (%)**	**Peptide count (n=X)**	**Enrichment (%)**
1	**DNA topoisomerase 2-beta**	TOP2B	9	900	4	400	4	400
2	**Tubulin beta-6 chain**	TBB6	6	200	11	367	3	100
3	**Clathrin heavy chain 1**	CLH1	6	600	11	1100	2	200
4	**Thrombospondin-1**	TSP1	5	100	14	280	9	180
5	**Plectin**	PLEC1	4	400	24	2400	37	3700
6	**Heterogeneous nuclear ribonucleoprotein M**	HNRNPM	4	400	13	1300	1	100
7	**60S ribosomal protein L18**	RL18	3	150	4	200	2	100
8	**ADP/ATP translocase 3**	ADT3	3	300	5	500	2	200
9	**60S ribosomal protein L7**	RPL7	3	300	4	400	1	100
10	**60S ribosomal protein L11**	RL11	2	200	2	200	2	200
11	**Endoplasmin**	ENPL	2	200	8	800	1	100
12	**60S ribosomal protein L10**	RL10	2	200	2	200	2	200
13	**Serine/arginine-rich splicing factor 7**	SRSF1	2	200	1	100	2	200
14	**14-3-3 protein beta/alpha**	1433B	2	200	6	600	1	100
15	**Sequestosome-1**	SQSTM	2	200	4	400	3	300
16	**Phosphate carrier protein, mitochondrial**	MPCP	2	200	2	200	1	100
17	**SUN domain-containing protein 1**	SUN1	2	200	1	100	2	200

18	**Charged multivesicular body protein 4b**	CHM4B	2	200	1	100	1	100
19	**40S ribosomal protein S13**	RS13	1	100	3	300	3	300
20	**Nucleophosmin**	NPM	1	100	1	100	1	100
21	**Cyclin-dependent kinase 4**	CDK4	1	100	3	300	1	100
22	**40S ribosomal protein S23**	RS23	1	100	3	300	1	100
23	**60S ribosomal protein L26-like 1**	RPL26L1	1	100	2	200	1	100
24	**WD repeat-containing protein 1**	WDR1	1	100	10	1000	1	100
25	**Alpha-actinin-1**	ACTN1	1	100	9	900	1	100
26	**Guanine nucleotide-binding protein G(i) subunit alpha-2**	GNAI2	1	100	2	200	1	100
27	**Tax1-binding protein 1**	TAX1BP1	1	100	8	800	3	300
28	**Peroxiredoxin**	PRDX6	1	100	3	300	1	100
29	**Caveolae-associated protein 2**	CAVIN2	1	100	3	300	2	200

The complete list of proteins that were identified across all L-CMD (L380S, R249W, del.K32) cell lines, but not all control (C5d, C25, C41) cell lines. Each protein, along with its corresponding gene name are listed. The number of unique peptides (peptide count) for each protein in each sample is listed, along with the enrichment of each protein in each sample. Enrichment is a calculation of the fold increase of unique peptides identified in each sample compared to the number of peptides identified in the "beads only" control. This control is put in place to account for non-specific binding of proteins to the Dynabeads® used to pull lamin A protein complexes out of protein extract samples. Proteins identified previously as lamin A interactors are indicated with an Asterix by the protein name (*).

Overall, the results of the LCMS/MS analysis of healthy control and L-CMD pull-down extracts have revealed that there are differences in the interactome of the L-CMD myoblasts compared to the healthy controls, due to potential loss and gain of interactions in the L-CMD samples.

3.2.3. DAVID GO analysis of the lamin A interactors identified using LCMS/MS

DAVID GO analysis was used to gain insight into the functions associated with the potential interactors in each group. DAVID GO analysis was conducted on the proteins in each of the groups, healthy lamin A interactors (n=9), mutant lamin A interactors (n=29), and healthy and mutant lamin A interactors (n=32). In doing this, BP, CC and MF GO terms (*p*-value <0.05) associated with these protein lists were determined.

It was difficult to draw many conclusions from the DAVID analysis on the lamin A interactors that were identified only across all control cell lines, as only nine proteins were in this group. The outputs from DAVID for the healthy lamin A interactors were less than for the other categories, generally less proteins were assigned to each term, and fewer terms were assigned significant *p*-values. It was, however, found that most proteins were components of the nucleoplasm (n=6, *p*=8.8E-3), and the majority of BP or MF terms were related to processes that occur within the nucleus, including DNA replication (n=3, *p*=1.1E-3), nucleosome disassembly (n=2, *p*=7.8E-3), nucleic acid binding (n=3, *p*=1.2E-1), DNA binding (n=2, *p*=1.2E-1) and nucleosome binding (n=2, *p*=1.4E-1). These terms were mostly different to those previously identified in Section 3.2.1.2, that were assigned to healthy lamin A interactors previously identified from the literature. Although, the previously identified lamin A interactors were found to be

associated with CC terms nuclear envelope, nuclear membrane, membrane, and most BP and MF terms were related to processes that occur within the nucleus. Therefore, there were some similarities.

The list of mutant lamin A interactors (n=29) was then subjected to DAVID analysis (**Table 3.4**). These terms differed entirely from the terms identified for the previously identified lamin A interactors in, as well as from the terms identified above for the healthy lamin A interactors identified here. A major difference was that none of the top CC terms for the mutant interactors were related to the nucleus or nuclear envelope. As well as this, cytoplasmic translation (n=7, *p*=3.0E-9) and positive regulator of translation (n=3, *p*=6.6E-3), were found to be top BP terms. These processes occur in the cytoplasm.

Most of the BP terms for both the previously identified healthy lamin A interactors, and the healthy lamin A interactors identified in this study, were related to processes that happen in the nucleus. As well as this, other top BP terms for the mutant lamin A interactors included negative regulation of apoptotic processes (n=5, *p*=6.8E-3) and autophagy (n=3, *p*=2.0E-2). These terms were interesting considering dysregulation of apoptosis has been implicated in other diseases, and dysregulation of proteins involved in apoptosis was identified in the L-CMD cells and is discussed further in Chapter 6, Sections 5.3.1 and 5.3.6.

Table 3.6- DAVID GO terms generated for the mutant lamin A interactors.

GO Term- BP	**Number of proteins**	**% of total proteins**	***p*-value**	**Associated proteins**
Cytoplasmic translation	7	24.1	3.0E-9	RL10, RL11, RL18, RL26L, RL7, RS13, RS23
Translation	7	24.1	6.7E-7	RL10, RL11, RL18, RL26L, RL7, RS13, RS23
Ribsomal large subunit biogenesis	4	13.8	1.6E-5	NPM, RL11, RL26L, RL7
Positive regulator of translation	3	10.3	6.6E-3	CDK4, NPM, TSP1
Negative regulation of apoptotic processes	5	17.2	6.8E-3	TAXB1, ENPL, NPM, RL10, TSP1
Protein localization	3	10.3	1.4E-2	NPM, PLEC, SQSTM
Autophagy	3	10.3	2.0E-2	CHM4B, CLH1, SQSTM
GO Term- CC	**Number of proteins**	**% of total proteins**	***p*-value**	
Extracellular exosome	19	65.5	1.6E-11	GNAI2, TAXB1, WDR1, ACTN1, CHM4B, CLH1, ENPL, HNRPM, PRDX6, PLEC, RL11, RL26L, RS13, SQSTM, SRSF7, MPCP, TSP1, TBB6, 1433B
Cytosolic ribosome	6	20.7	5.9E-8	RL10, RL11, RL18, RL7, RS13, RS23
Focal adhesion	9	31.0	6.7E-8	ACTN1, CLH1, ENPL, NPM, PLEC, RL18, RL7, RS13, 1433B
Cytosol*	21	72.4	1.1E-6	TOP2B, GNAI2, TAXB1, WDR1, ACTN1, CAVN2, CHM4B, CLH1, CDK4, ENPL, NPM, PRDX6, PLEC, RL10, RL11, RL18, RL7, RS13, RS23, SQSTM, 1433B
Cytosolic large ribosomal subunit	5	17.2	1.3E-6	RL10, RL11, RL18, RL26L, RL7
Membrane	16	55.2	3.0E-5	GNAI2, CLH1, ENPL, HNRPM, NPM, PRDX6, PLEC, RL10, RL11, RL18, RL7, RS13, RS23, MPCP, ADT3, 1433B
Ribosome	5	17.2	9.0E-5	RL10, RL11, RL18, RS13, RS23
Cytoplasm	18	55.2	2.0E-4	GNAI2, SUN1, ACTN1, CAVN2, CHM4B, HNRPM, NPM, PRDX6, PLEC, RL11, RL18, RL7, RS13, RS23, SQSTM, SRSF7, TBB6, 1433B
Polysomal ribosome	3	17.2	9.2E-4	RL11, RL18, RS23
Ribonucleoprotein complex	4	62.1	1.9E-3	TOP2B, HNRPM, NPM, RL7
GO Term- MF	**Number of proteins**	**% of total proteins**	***p*-value**	
Structural constituents of ribsome	7	24.1	2.9E-7	RL10, RL11, RL18, RL26L, RL7, RS13, RS23
RNA binding	13	44.8	4.4E-7	CLH1, ENPL, HNRPM, NPM, PLEC, RL10, RL11, RL18, RL26L, RL7, RS13, RS23, SRSF7
Protein kinase C binding	3	10.3	3.2E-3	TOP2B, CAVN2, SQSTM

Protein binding*	26	89.7	6.2E-3	GNAI2, SUN1, TAXB1, ACTN1, CAVN2, CLH1, CDK4, ENPL, HNRPM, NPM, PRDX6, PLEC, RL10, RL11, RL18, RL26L, RL7, RS13, RS23, RQSTM, SRSF7, ADT3, TSP1, TBB6, 1433B
Protein domain specific binding	4	13.8	6.9E-3	ACTN1, HNRPM, RSSF7, 1433B
Cadherin binding	4	13.8	1.1E-2	CHM4B, PRDX6, PLEC, 1433B
Macromolecular complex binding	4	13.8	2.3E-2	CDK4, SQSTM, MPCP, 1433B
Identical protein binding	7	24.1	3.7E-2	CHM4B, NPM, PRDX6, RL7, SQSTM, TSP1, 1433B
Actin filament binding	3	10.3	4.4E-2	WDR1, ACTN1, PLEC

Biological process (BP), cellular component (CC) and molecular function (MF) GO terms were generated for the proteins that were exclusively identified across all L-CMD samples (termed mutant lamin A interactors). Included in the table are the number of proteins associated with each pathway, the percentage of the total protein input list, along with a *p*-value assigned to each term. In the final column, each of the associated proteins are listed.

Finally, the list of proteins that were identified as both healthy and mutant lamin A interactors was analysed using DAVID. There was some cross over between the terms assigned to these proteins, with the terms generated for the healthy lamin A interactors previously identified in the literature. Similarly to the nucleus-related CC terms generated for the previously identified healthy lamin A interactors, as well as the healthy lamin A interactors identified in this study, nucleosome (n=7, *p*=4.4E-8), nuclear envelope (n=7, *p*=3.2E-7), nucleoplasm (n=17, *p*=3.1E-5), and nuclear inner membrane (n=4, *p*=1.1E-4) were top CC terms for the healthy and mutant lamin A interactors. Nuclear envelope organization (n=4, *p*=5.1E-6) and nuclear pore localization (n=3, *p*=1.4E-5) were top BP terms, and similar terms were associated with the previously identified healthy lamin A interactors. As well as these, cytoplasmic translation (n=6, *p*=2.5E-7) and translation (n=7, *p*=1.0E-6) were also top BP terms for the healthy and mutant lamin A interactors, which were also identified as top BP terms for the mutant lamin A interactors. Although, mostly, the BP terms for the healthy and lamin A interactors were processes occurring within the nucleus, including negative regulation of chromatin silencing (n=3, *p*=2.1E-4), chromosome condensation (n=3, *p*=5.8E-4), and heterochromatin assembly (n=3, *p*=9.9E-4).

Table 3.7- DAVID GO terms generated for the healthy and mutant lamin A interactors.

GO Term- BP	Number of proteins	% of total proteins	*p*-value	Associated proteins
Cytoplasmic translation	6	18.8	2.5E-7	RL15, RL23, RL23A, RL24, RS4X
Translation	7	21.9	1.0E-6	TNIP1, RL15, RL23, RL23A, RL24, RL34, RS4X
Nuclear migration	4	12.5	2.3E-6	SUN2, LMNA, LMNB1, LMNB2
Nuclear envelope organization*	4	12.5	5.1E-6	SUN2, LMNA, LMNB1, LMNB2
Nuclear pore localization	3	9.4	1.4E-5	LMNA, LMNB1, LMNB2
Protein localization to nuclear envelope	3	9.4	6.5E-5	LMNA, LMNB1, LMNB2
Nucleosome assembly	5	15.6	8.8E-5	H12, H15, H2B1B, H31T, H2AY
Negative regulation of chromatin silencing	3	9.4	2.1E-4	H12, H15, HMGA1
Chromosome condensation	3	9.4	5.8E-4	BAF, H12, H15
Heterochromatin assembly	3	9.4	9.9E-4	LMNA, LMNB1, LMNB2
GO Term- CC	**Number of proteins**	**% of total proteins**	***p*-value**	**Associated proteins**
Nucleosome	7	21.9	4.4E-8	H12, H15, H2A1C, H2AV, H2B1B, H31T, H2AY
Cytosolic ribosome	6	18.8	8.5E-8	RL15, RL23, RL23A, RL24, RL34, RS4X
Extracellular exosome	16	50.0	9.4E-8	ATPA, H2A1C, H2AV, H31T, XPO2, HBAZ, HNRPC, HORN, ITIH3, H2AY, MYL6B, RL23, RL23A, RL24, RL34, RS4X
Nuclear envelope*	7	21.9	3.2E-7	BAF, SUN2, XPO2, EMD, LMNA, LMNB1, LMNB2
Cytosolic large ribosomal subunit	5	15.6	1.7E-6	RL15, RL23, RL23A, RL24, RL34
Chromosome, telomeric region	6	18.8	4.8E-6	H2B1B, H31T, SUN2, XRCC5, XRCC6, H2AY
Ribosome	6	18.8	5.2E-6	RL15, RL23, RL23A, RL24, RL34, RS4X

Nucleoplasm	17	53.1	3.1E-5	BAF, H15, H2A1C, H2B1B, H31T, TNIP1, XRCC5, XRCC6, XPO2, EMD, HNRPC, HMGA1, LMNA, LMNB1, H2AY, RL23, RS4X
Nuclear inner membrane	4	12.5	1.1E-4	SUN2, EMD, LMNB1, LMNB2
Cytosol*	19	59.4	1.3E-4	BAF, H2B1B, MOS, TNIP1, XRCC5, XRCC6, XPO2, EMD, HNRPC, HMGA1, LMNA, LMNB1, MYL6B, RL15, RL23, RL23A, RL24, RL34, RS4X
GO Term- MF	**Number of proteins**	**% of total proteins**	***p*-value**	**Associated proteins**
Structural constituent of chromatin	8	25.0	1.8E-10	H12, H15, H2A1C, H2AV, H2B1B, H31T, HMGA1, H2AY
RNA binding	13	40.6	1.6E-6	ATPA, H12, H15, XRCC5, XRCC6, HNRPC, HMGA1, RL15, RL23, RL23A, RL24, RL34, RS4X
Structural constituent of ribsome	6	18.8	1.3E-5	RL15, RL23, RL23A, RL24, RL34, RS4X
Nucleosomal DNA binding	4	12.5	3.8E-5	H12, H15, HNRPC, H2AY
Double-stranded DNA binding	5	15.6	3.9E-5	BAF, H12, H15, XRCC5, XRCC6
5’deoxyribose-5-phosphate lyase activity	3	9.4	3.9E-5	XRCC5, XRCC6, HMGA1
Protein binding*	31	96.9	5.9E-5	ATPA, BAF, H12, H15, H2A1C, H2B1B, H31T, MOS, SUN2, TNIP1, XRCC5, XRCC6, XPO2, EMD, HBAZ, HNRPC, HMGA1, HORN, ITIH3, KLH35, LMNA, LMNB1, LMNB2, H2AY, MYL6B, RL15, RL23, RL23A, RL24, RL34, RS4X
DNA binding	9	28.1	1.1E-3	BAF, H2A1C, H2AV, H2B1B, H31T, XRCC5, XRCC6, HMGA1, H2AY
Cadherin binding	5	15.6	1.7E-3	EMD, RL15, RL23A, RL24, RL34
Protein heterodimerization activity	5	15.6	3.1E-3	H2A1C, H2AV, H2B1B, H31T, H2AY

Biological process (BP), cellular component (CC) and molecular function (MF) GO terms were generated for the proteins that were identified across all L-CMD and control samples (termed healthy and mutant lamin A interactors). Included in the table are the number of proteins associated with each pathway, the percentage of the total protein input list, along with a p-value assigned to each term. In the final column, each of the associated proteins are listed

3.2.4. Verifying putative lamin A interactors

The lists of putative "healthy", "mutant" and "healthy and mutant" lamin A interactors were considered for further verification. It is important to verify the findings from the MS analysis as we cannot be certain that putative interactors are not due to non-specific binding, even though attempts were made to control for this. As well as this, verification is especially needed for proteins that have not previously been identified as lamin A interactors in other published studies (different methods, techniques and cells and tissues analysed in previous studies may account for differences in identified interactors). Of these proteins, it was decided that a couple of candidates were to be selected from the list of healthy, or healthy and mutant lamin A interactors, to verify novel interactions of proteins with healthy lamin A and/or interactions that are not lost in the presence of *LMNA* mutations in L-CMD cells. These putative interactors were verified with a view to using more targeted studies in future to understand the function of the interactions.

Proteins identified as potential healthy or healthy and mutant lamin A interactors that had a high peptide enrichment across samples were favoured for further verification. Peptide enrichment was calculated by determining the fold increase of peptide count compared to that of the "beads only" control, which is used to account for non-specific protein binding (as previously described in Chapter 2, 2.5.4.). Peptide count is not an exact measure of quantity but can be used to give a very rough sense of abundance. A high peptide enrichment indicates that there was a relatively higher number of peptides detected across the samples compared to the number of peptides that may have been non-specifically bound to the beads only control. Whilst a high peptide enrichment may suggest that a protein is more likely a lamin A interactor and

not an unspecific interaction, it is important to note that some genuine lamin A interactors may have been excluded if a large number of peptides also bound non-specifically to the beads only control. As well as peptide enrichment, proteins were considered for further verification If they were known to be involved in key processes as identified in the DAVID analysis (e.g., processes occurring in the nucleus that involve interactions with DNA or chromatin).

Taking the aforementioned into consideration, X-ray repair cross complementing protein 6 (XRCC6, also known as Ku70), and DNA topoisomerase 1 (TOP1) were selected for further study. XRCC6 was identified across all healthy control and L-CMD pull-down samples with an average peptide enrichment of 2700% and 1100% compared to the beads only control, respectively. TOP1 was identified across all healthy pull-down samples with an enrichment of 1066% compared to the beads only control. XRCC6 was previously identified as a healthy lamin A interactor in a high through-put study (Kubben *et al.*, 2010), whilst TOP1 had never previously been identified as an interactor of lamin A. These proteins are both involved in DNA repair, recombination, or transcription within the nucleus.

To verify whether XRCC6 and TOP1 were interactors of lamin A/C, Co-IP was performed on a healthy control (C25) myoblast extract, using the same lamin A/C mouse monoclonal antibody as described in the previous sections. Anti-XRCC6 and anti-TOP1 antibodies (as described in Chapter 2, Section 2.2.1.4) were used on western blots to probe for the respective proteins, and it was found that XRCC6 (70kDa) and TOP1 (100kDa) were both identified in the lamin A/C Co-IP eluate (**Fig 3.4, A, B**). There was, however, an artifact, seen as a small black dot, in the negative

control eluate on the XRCC6 western blot. This may just be attributed to background as it appeared to be a “blob” rather than a clear band.

Once it had been verified that lamin A/C appeared to bind both XRCC6 and TOP1, reverse Co-IP was done to determine whether XRCC6 and TOP1 antibodies could bind lamin A/C. As described in Chapter 2, Section 2.5.1., rabbit monoclonal anti-XRCC6(Ku70) (ab924590; Abcam) and rabbit monoclonal anti-TOP1 (ab109374; Abcam) were used to pull XRCC6 and TOP1 protein complexes out of healthy control C25 myoblast extract. Western blot using a mouse monoclonal anti-lamin A/C antibody was then used to detect lamin A/C in the XRCC6 and TOP1 Co-IP eluate samples (**Fig 3.4, C, D**). The results of the XRCC6 pull-down western blot probe for lamin A/C show a very faint band in the pull-down eluate at the predicted molecular weight of lamin A (around 70kDa), but a faint band can also be seen in the negative control eluate, suggesting a proportion of lamin A is also binding non-specifically to the Dynabeads®. Lamin A/C did not appear to be detected on the TOP1 Co-IP western blot. This does not necessarily suggest that TOP1 does not bind to lamin A/C, as the TOP1 antibody may not be efficient at immunoprecipitating TOP1 out of the cell extract.

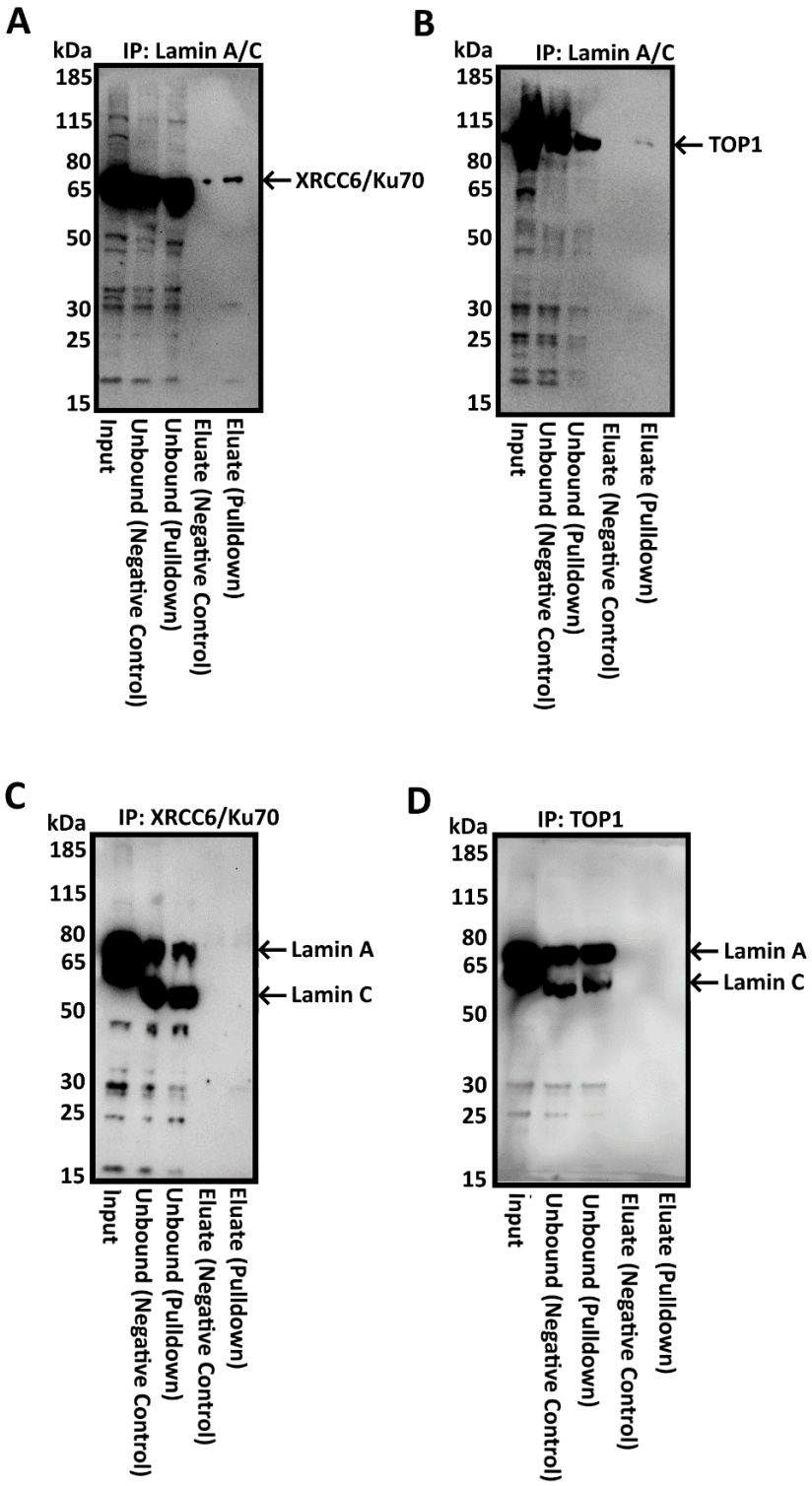

Figure 3.4- Western blots probing for Ku70 and TOP1 in lamin A/C Co-IP control C25 myoblast extract*. (A) X-ray repair protein (XRCC6/Ku70) was successfully detected in lamin A/C pulldown eluate at around 70kDa, however there was an artifact band in the negative control eluate. (B) DNA topoisomerase 1 (TOP1) was also detected in lamin A/C IP eluate at 100kDa. Reverse IPs were then performed using (C) XRCC6 and (D) TOP1 antibodies to pulldown lamin A/C. A very faint band in the XRCC6 pulldown eluate at 70kDa suggest the presence of lamin A, however lamin A did not appear to be present in the TOP1 pulldown eluate.*

Considering there appeared to be a very faint band appearing to be lamin A in the XRCC6 Co-IP eluate, the next step was to visualise XRCC6 and lamin A within cells using immunofluorescence microscopy (IMF) to determine whether the two proteins co-localise. Healthy control (C25) myoblasts were double-label immunostained with rabbit monoclonal anti-XRCC6 (red) and mouse monoclonal anti-lamin A/C (green), and also stained with DAPI (blue) (**Fig 3.5**). Zoomed in magnification of single cells showed that there was no apparent co-localization, as there appeared to be no areas of overlap of yellow lamin A/C staining and magenta Ku70 staining in the cell nuclei. It appeared that lamin A/C was located at the nuclear periphery, whilst Ku70 seemed to be within the nucleus and not at the NE. This may indicate that lamin A/C and Ku70 are localized in different compartments of the cell nucleus and do not interact, although it is difficult to determine this from these images as it would be difficult to visualise overlap of the two proteins at the NE, as this is a very small region around the perimeter of the nuclei, and especially considering the Ku70 (magenta) staining appeared not as strong as the lamin A/C (yellow) staining. The two proteins still appear to be in close proximity of one another, therefore it is still possible that they may interact despite this result.

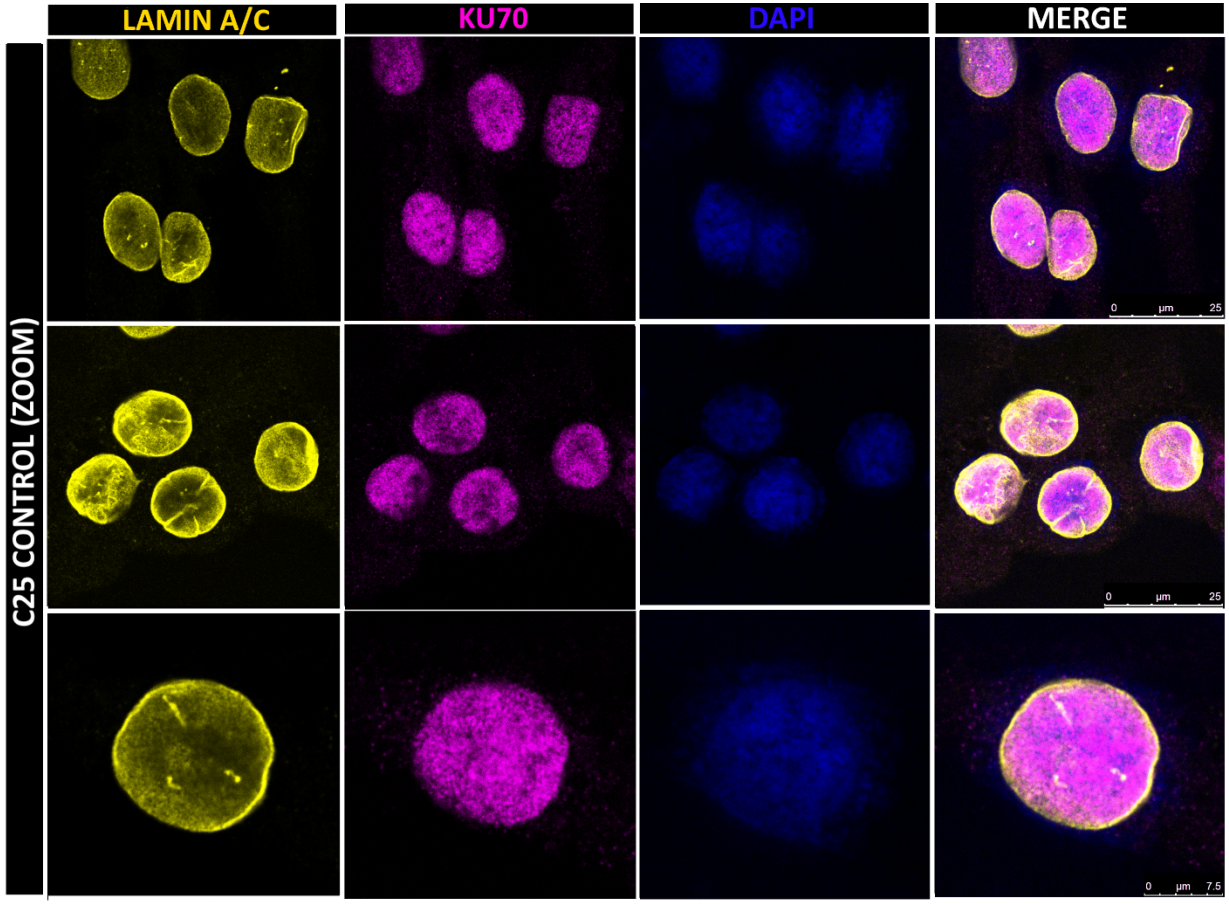

Figure 3.5- Immunofluorescence double-label staining of lamin A/C and Ku70 in C25 control myoblasts. *Healthy control myoblast cells were stained with DAPI (blue), lamin A/C (yellow) and Ku70 (magenta). The two proteins did not appear to co-localize as this would be indicated by overlay of yellow and magenta staining on the merged images.*

3.2.5. Summary of results

To summarise, firstly a literature search yielded a list of proteins that have previously identified as lamin A interactors in various healthy cells and tissues in one or more published studies. This demonstrated that studies of lamin A interactors in human myoblasts or skeletal muscle have not previously been published. Despite this, the literature provided a baseline for experimental comparison of lamin A interactors, and bioinformatics analysis revealed processes that lamin A interactors were most often involved in. Once the Co-IP method was tested by confirming that lamin A/C was being immunoprecipitated out of cell extract samples, healthy control and L-CMD myoblasts were subjected to Co-IP and LCMS/MS and criteria was used to identify lamin A interactors that were exclusively in the healthy myoblasts ("healthy" interactors), lamin A interactors that were only identified in L-CMD myoblasts ("mutant" interactors), and lamin A interactors that were present across all healthy and L-CMD myoblast samples ("healthy and mutant" interactors). GO analysis was then used to identify biological processes and molecular functions common to each of the lists of interactors. This revealed that healthy and mutant lamin A interactors were involved in a variety of processes that occur within the nucleus, whilst terms associated with interactors of only mutant lamin A were linked to activities that happen within other compartments of the cell. Of the healthy and mutant lamin A interactors, XRCC6/Ku70 and Top1 were chosen as candidates for further analysis. Western blot analysis of immunoprecipitates from a control cell lines (C25) indicated that Ku70 and Top1 may be healthy lamin A interactors, however further clarification is needed.

3.3. Discussion

Studying a protein's interactome allows us to gain understanding into a protein's functions, and in a disease context, may elucidate potential therapeutic targets. Lamin A has already been implicated in a number of different cellular processes, and some lamin A interactors are already well-established. First, previously identified lamin A interactors and the roles that these proteins have been associated with were determined in order to establish what is already known about lamin A interactors. Co-IP and LCMS/MS identified proteins that interact exclusively with lamin A in healthy myoblasts, and interactors of mutant lamin A in L-CMD myoblasts, as well as proteins that were potential interactors in both healthy and L-CMD myoblasts. A number of previously characterised healthy lamin A interactors were identified across these groups, as well as a number of novel putative lamin A interactors. To further ascertain the functional relevence of interactions, one approach could be to use siRNA to "knock-out" the protein of interest and observe the consequences in healthy myoblasts.

3.3.1. Previously identified and putative lamin A interactors were identified in healthy and L-CMD myoblasts.

The first aim of this chapter was to determine previously identified interactors of healthy lamin A in the literature. In doing this, a total of 243 proteins were identified as healthy lamin A interactors, however only 15 of these proteins had been identified in two or more studies. It was noticed that some studies used high through-put methods to identify healthy lamin A interactors, and consequently, although interactors had been identified using this approach, many had not been verified further. It was observed that none of these studies had examined healthy lamin A

interactors in human myoblasts or muscle tissue extract. This is relevant as lamin A may have different interactors in different cells and tissues. Whilst cells including the C2C12 immortalized murine muscle cell line, murine cardiomyocytes, and rat skeletal muscle were used in some studies, the lamin A interactors identified still remain in a murine context, and whilst this is insightful, there are many molecular and biological differences between humans and mice. The literature search also did not reveal any studies where lamin A interactors that have been identified in humans and mice were compared to establish whether there are any differences in lamin A/C interactors in the two species. Nevertheless, the identification of previous lamin A interactors provided a baseline for comparison to later experimental work. This would enable the determination of whether healthy lamin A interactors identified in different species or cells would differ in human myoblasts.

The interactors that were experimentally determined across all healthy and L-CMD samples are likely healthy lamin A interactors, and interactors that are not lost as a result of the mutations in *LMNA* in L-CMD cells. However, it is important to consider the possibility that these proteins may be non-specific binders, even though steps were taken to mitigate the likelihood that proteins may have bound non-specifically (as previously discussed in Section 3.2.5.). A number of healthy lamin A interactors previously identified in the literature were in this group: lamin B1 (Ye and Worman, 1995; Schirmer and Gerace, 2004; Kubben et al., 2010; Dittmer et al., 2014), lamin B2 (Schirmer and Gerace, 2004; Kubben et al., 2010; Dittmer et al., 2014), X-ray repair protein 6 (Kubben *et al.*, 2010), core histone macro- H2A.1 (Kubben *et al.*, 2010), SUN2 (Crisp, Liu, Roux, J. B. Rattner, et al., 20061; Kubben et al., 2010), emerin (Lee et al., 2001; Sakaki et al., 2001; Kubben et al., 2010), and BAF (Lee *et al.*, 2001). This

substantiates previous evidence that these are interactors of lamin A and provides new evidence that these interactions may also be present in human myoblasts and that these interactions are not completely lost in L-CMD myoblasts. The remaining proteins that were not previously identified in other studies represent new putative interactors of healthy and mutant lamin A.

Using DAVID, functional roles for the lamin A interactors in healthy control and L-CMD myoblasts were elucidated, which mostly differed from the terms that were generated for the lamin A interactors identified in previous studies. Biological processes for these interactors included processes that lamin A has previously been associated with. These included nuclear migration (Mattioli *et al.*, 2011; Bone *et al.*, 2014), protein localization (Vaughan *et al.*, 2001), heterochromatin assembly (Scaffidi and Misteli, 2005; Shumaker *et al.*, 2006), gene silencing (Shaklai *et al.*, 2007). Furthermore, defects in a number of these processes have previously been implicated in laminopathies, highlighting lamin A plays a crucial role in these activities. Nuclear migration is the directed movement of the nucleus, and proper nuclear positioning is important for muscle contraction (Roman and Gomes, 2018). In myotubes derived from EDMD patients carrying *LMNA* mutations, defective nuclear positioning has been observed (Mattioli *et al.*, 2011). Protein mislocalization, in particular, mislocalization of emerin has been observed in various different laminopathies, as discussed in more detail in Chapter 4, Section 3.3.2. Finally, somatic cells from patients with HGPS show a global loss of heterochromatin (Scaffidi and Misteli, 2005; Shumaker *et al.*, 2006), and cells from EDMD patients and lamin A knockout mice show altered organization of heterochromatin at the nuclear periphery (Sabatelli *et al.*, 2001). Other top BP processes for healthy and mutant lamin A interactors which lamin A does not appear

to have been previously explicitly linked to included nuclear pore localization, nucleosome assembly, and chromosome condensation, suggesting new roles for lamin A through its interactors. Nuclear pore complexes (NPCs) allow the transport of molecules across the NE and are composed of nucleoporins. Recent evidence has proven that NPCs closely associate with lamin fibers, and that lamin A/C filaments interact closely with the NPCs at the nucleoplasmic ring (Kittisopikul *et al.*, 2021). This has previously been demonstrated using datasets prepared from subpixel and segmentation analyses of 3D-structured illumination microscopy images of wild-type and lamin isoform knockout mouse embryonic fibroblasts (Kittisopikul *et al.*, 2021). In this study, cryo-electron tomography (cryo-ET) was used to reveal that the lamin filaments composing the fibres contact the nucleoplasmic ring of the NPCs (Kittisopikul *et al.*, 2021). Knockdown of the nucleoporin TPR or NUP153 has been found to alter the arrangement of lamin fibres and NPCs, and knockdown of the ring-associated nucleoporin ELYS induces NPC clusters that exclude lamin A/C fibers but include lamin B1 and B2 fibers (Kittisopikul *et al.*, 2021). Overall, the results from this study demonstrate that lamin isoforms and nucleoporins work together to maintain the normal organization of lamin meshworks and NPCs at the NE (Kittisopikul *et al.*, 2021). Studies on *Lmna*$^{-/-}$ mouse embryonic fibroblasts (MEFs) have also shown that lamin A/C loss caused major changes in nuclear morphology with some NPC clustering (Sullivan *et al.*, 1999). A number of healthy lamin A interactors that were identified in the literature search were nucleoporins, which were identified by Kubben *et al.* in U2OS cells (a cancer derived cell line) (Kubben *et al.*, 2010). However, no nucleoporins were identified across any of the healthy or mutant samples as lamin A interactors. This could be due to buffers used in the Co-IP disrupting interactions between lamin A

and nucleoporins, or perhaps lamin A does not associate as closely with nucleoporins in human myoblasts. Molecular function analysis revealed healthy and mutant lamin A interactors were associated with a number of DNA-related functions including nucleosomal DNA binding, double-stranded DNA binding, and DNA binding, as well as proteins being a structural constituent of chromatin. It has been demonstrated that lamin A itself binds to DNA and interacts with chromatin using recombinant proteins (Shoeman and Traub, 1990; Stierlé *et al.*, 2003; Maji *et al.*, 2020), and alterations in lamins function impact DNA transactions such as transcription, replication, and repair, as well as epigenetic modifications that change chromatin structure (Gonzalo, 2014). HeLa cells expressing mutant forms of lamin A associated with muscular dystrophy and progeria have also been found to exhibit a delay in recruitment of repair factors to sites of DNA damage and show increased numbers of double-strand breaks (Liu *et al.*, 2005; Manju, Muralikrishna and Parnaik, 2006). Therefore, it was expected that lamin A interactors would be also involved in these processes.

3.3.2. Some lamin A interactors may be lost as a consequence of *LMNA* mutations in L-CMD myoblasts.

Nine lamin A interactors were only identified across all healthy myoblast samples, and these may represent interactions that are lost in the L-CMD myoblasts. Although experimentally it is difficult to verify loss-of protein interactions, it is entirely plausible that lamin A protein-protein interactions could be lost due to *LMNA* mutations in L-CMD myoblasts. One way of gaining insight on this would be to use immunofluorescence microscopy to first determine whether two proteins normally co-localize in control cells. If an interaction is lost, the proteins may not be seen to co-localize, or may be mislocalized in L-CMD myoblasts.

Protein-protein interfaces (special regions on a protein's surface allowing interactions with other proteins) generally occur over a large surface area, involving numerous residues (Bogan and Thorn, 1998). Most of the resides only contribute a small amount to the interface, however residues that contribute a large amount to binding are known as "hot-spots" (Bogan and Thorn, 1998). As these "hot-spots" are so important, mutations within them can lead to loss or impairment of an interaction. These hot-spots are likely to include tryptophan, tyrosine or arginine resides (Bogan and Thorn, 1998; Betts and Russell, 2003). Certain mutations may be more damaging in these regions, for example a missense mutation that drastically changes an amino acid's properties (Yates and Sternberg, 2013). It is known that the R249W L-CMD mutation is located at the ERK1/2 binding domain, involving an arginine residue being substituted for a tryptophan (The Universal Mutations Database, http://www.umd.be/LMNA/). These two residues do have very different properties, and this is discussed further in Chapter 4, Section 4.3.2., so it is likely that this mutation affects lamin A protein-protein binding. There is little information available in the literature about lamin A's ERK1/2 binding domain, but it is suggested that this area interacts with mitogen-activated protein kinase (ERK1/2) (Gonzàlez *et al.*, 2008). This protein was not detected in any of the healthy of L-CMD pull-down samples, so it is uncertain whether lamin A and ERK1/2 interaction is disrupted in the R249W L-CMD myoblasts, but it is also plausible that lamin A interacts with other proteins via this domain and that the mutation within it consequently affects lamin A interactions. Some protein-protein interfaces also involve specific salt bridges, disulphide bonds, or hydrogen bonds, and mutations of residues involved in these could disrupt binding (Betts and Russell, 2003; Yates and Sternberg, 2013). The del.K32 L-CMD mutation causes an in-frame deletion

affecting a lysine residue. Lysine is involved in the formation of salt bridges (Betts and Russell, 2003), and thus is also frequently found at protein binding sites. Therefore, it is likely that the del.K32 *LMNA* variant could also cause loss of protein interactions in L-CMD myoblasts. The L380S L-CMD mutation causes a leucine residue to change to serine. Whilst these two amino acids are not frequently found at binding domains, they also have different properties, so this could also have deleterious effects on lamin A interactions with other proteins. The consequences of each of these *LMNA* mutations are discussed in further detail in Chapter 4, Section 4.3.2

Disease-causing mutations can frequently occur at the core of a protein (David *et al.*, 2012). A mutation changing a hydrophobic residue (as the core of a protein is generally hydrophobic) to a charged or polar residue within the proteins core can lead to complete destabilization of the protein (Yue, Li and Moult, 2005). Mutations changing a small residue to a larger one could also lead to steric clashes, whilst a change from a large residue to a smaller one could lead to gaps (Yue, Li and Moult, 2005). Either way, this could impair protein folding and function (Yue, Li and Moult, 2005). A mutation leading to severe protein mis-folding or instability could lead to loss of all the interactions of that protein. This is relevant to the R249W and L380S mutations, as discussed in Chapter 3, Section 4.3.2., however these mutations unlikely lead to complete destabilization of lamin A, as it would be expected in this case that these mutations would then lead to near-complete ablation of lamin A interactions. This was not observed, as only a relatively small number of proteins were identified that were only in the healthy control myoblasts. Instead, it is likely that these *LMNA* mutations lead to smaller changes that affect protein binding sites.

Whilst the proteins identified only in the healthy control myoblasts may be representative of loss-of interactions in L-CMD cells, it is important to note that interactions with other proteins may be also be compromised, but not completely ablated. For example, it was demonstrated in Chapter 4, Section 4.2.7. that emerin was found to be mislocalized in R249W myoblasts, but some emerin still remained at the NE, suggesting that not all emerin-lamin A interactions were compromised. This is further proven in this Chapter, where emerin was detected in R249W pull-down extracts. Emerin has also been seen to also be mislocalised to the cytoplasm, particularly the ER, previously in lamin A/C deficient mouse fibroblasts (Holt et al., 2006), lamin A/C -/- mouse embryonic fibroblasts (MEFs) (Sullivan et al., 1999), as well as in fibroblasts from LGMD patients (Muchir, van Engelen, et al., 2003). This is further examined in Chapter 4.

3.3.3. Interactors that are only detected in L-CMD myoblasts may represent interactions that are gained in the presence of *LMNA* mutations.

There were a number of interactors that were only present across all of the L-CMD myoblasts, termed "mutant" lamin A interactors. These may be interactions that are gained as a result of *LMNA* mutations in the L-CMD cells. In addition to mutations disrupting wild-type interactions, it is possible for new interactions to be introduced by the mutation. These are known as gain-of-function mutations and result from a change in the specificity of particular protein-substrate interactions or a change in the specificity of interactions with regulatory proteins (Yates and Sternberg, 2013). This has been observed in a number of different diseases. The L-CMD cells harbouring the R249W and L380S *LMNA* mutations involve amino acid residues being substituted for

other amino acids with very different properties, as mentioned above. The introduction of these new residues could cause lamin A to interact with proteins outside of its usual interactome. In sickle cell anaemia, the Glu6Val mutation of β-haemoglobin introduces a hydrophobic residue on the surface of the protein, which under low oxygen conditions can bind to a hydrophobic patch on another haemoglobin molecule, leading to polymerization and the characteristic sickling of the erythrocyte (Ingram, 1956; Wishner *et al.*, 1975).

In Section 3.3.2., it was discussed how mutations may lead to complete protein misfolding, and consequently this can disrupt lamin A interactions. Protein misfolding may also lead to gain-of-function interactions. It is not confirmed whether the R249W, L380S or del.K32 *LMNA* mutations in the L-CMD myoblast lead to protein misfolding, but it is still a possibility. In neurodegenerative diseases, amyloidosis is thought to be caused by incorrect interactions. The first stage of amyloidosis is believed to be protein misfolding, which exposes β-strands that then form β-sheets with other misfolded proteins (Yates and Sternberg, 2013). This leads to polymerization and fibril formation. Transthyretin is a throxine transporter that usually forms a homotetramer. However, the hydrogen bonding in a β-sheet is disrupted by the Leu75Pro mutation during protein folding of transthyretin, favouring the dissociation of the tetramer and leading to the formation of amyloid (Lashuel *et al.*, 1999). This mutation causes familial amyloid polyneuropathy (Lashuel *et al.*, 1999).

As well as gain-of-function, mutations can also result in a “switch-of-function”. This is an acquisition of new specific interaction partners compared to wild-type and, consequently leads to a new biological function for the protein (Yates and Sternberg,

2013). A mutation that is located in a protein-binding site, as is the case for the R249W L-CMD mutation, can lead to new specific interactions. This has been discovered in glioma, where a mutation in a binding site of isocitrate dehydrogenase 1 (IDH1) alter the activity of the enzyme so that isocitrate is no longer converted to alpha-ketoglutarate, but instead alpha-ketoglutarate is converted to R(-)-2-hydroxyglutarate, elevating the risk of brain tumours (Dang *et al.*, 2009).

3.3.4. Loss-of-function versus gain-of-function model for action of *LMNA* mutations in laminopathies

Further investigation is needed to determine whether L-CMD mutations cause gain-of or loss-of-function. However, it has been debated whether other diseases caused by lamin A mutations are underpinned by a gain-of-function of loss-of-function of lamin A mutants (Liu, Jin and Zhou, 2012), but some evidence is supporting the gain-of-function model for the action of lamin A in laminopathies. In particular, abnormal accumulation of SUN1 has been attributed to degenerative features of laminopathies (Liu, Jin and Zhou, 2012). Chen *et al.* observed that the level of Sun1 protein was up-regulated and mislocalized to golgi in $Lmna^{-/-}$ and $Lmna^{\Delta 9}$ cells. In HGPS cells, this irregular accumulation of SUN1 was not observed, but the levels of total and INM-localized SUN1 were significantly up-regulated and well correlated with the abnormally shaped nucleus, a hallmark of HGPS fibroblasts, as well as other laminopathies (Chen *et al.*, 2012). Further investigation showed that knocking-down or genetically depleting SUN1 from the mutant cells mostly rescued the misshapen nuclei and increased cell survival. It was also shown that farnesylated progerin/ prelamin A (an accumulation of farnesylated progerin/prelamin A is a consequence of HGPS-

causing lamin A mutations) increased the binding capacity of SUN1 (Chen *et al.*, 2012). These results suggest that whilst loss of function of lamin A in *Lmna*$^{-/-}$ and *Lmna*$^{\Delta 9}$ cells upregulates the level of SUN1, but loses the capacity to maintain its NE-anchorage; gain of function of progerin attracts more SUN1 to the NE (Liu, Jin and Zhou, 2012). Another study has also found that loss of SUN1 in mice with a cardiomyocyte-specific *Lmna* deletion ameliorates cardiac pathology induced by *Lmna* loss (Chai *et al.*, 2021), although SUN1-lamin A interaction was not assessed in this study. Interestingly, it was found that SUN1 was a putative mutant lamin A interactor, as it was only identified as an interactor across all of the L-CMD myoblast samples and was undetected in all of the healthy myoblast samples.

Further supporting the gain-of-function model for the action of *LMNA* mutations, the R482W lamin A mutation, which is known to cause familial partial lipodystrophy (FPLD) has also been shown to work as a gain-of-function mutation (Rajendran, Purohit and Sethumadhavan, 2012). Rajendran *et al.* used biomolecular interaction and molecular dynamics (MD) simulation analysis based on the crystalline structures of lamin A/C, SREBP1, and emerin, to understand the dynamic behaviour of wild-type and mutant lamin A/C structures at the atomic level. Analysis of the structural and functional consequences of the R482W mutation using computational modelling found that R482W mutant lamin A/C interacts with emerin and SREBP1 with more affinity that wild-type lamin A/C. Mutant lamin A/C was shown to have increased interaction with it's binding partners due to its expansion of interaction surface and flexible nature of binding residues than wild-type lamin A/C (Rajendran, Purohit and Sethumadhavan, 2012). MD simulation indicated that the flexibility of interacting residues of mutant

lamin A/C are mainly due to less involvement in formation of inter and intramolecular hydrogen bonds (Rajendran, Purohit and Sethumadhavan, 2012).

3.3.5. Revealing potential new roles for mutant lamin A through gained interactors in L-CMD myoblasts

The list of proteins that were identified as only putative mutant lamin A interactors was inputted into DAVID, and this revealed that the mutant lamin A interactors had roles that were different to the healthy and mutant interactors, as well as the healthy lamin A interactors identified in the literature. The most major difference was that none of the CC terms generated for interactors for only mutant lamin A were related to the nucleus or the NE, suggesting that mutant lamin A is interacting with proteins that primarily have roles in other compartments of the cell. Top BP terms for the mutant lamin A interactors included translation, cytoplasmic translation, positive regulator of translation, ribosomal large subunit biogenesis, and ribosomal large subunit assembly. Each of these processes were mostly attributed to numerous ribosomal proteins. Ribosomal proteins were also identified as interactors of both healthy and mutant lamin A, and translation and cytoplasmic translation were also identified as top terms for healthy and mutant lamin A interactors, however a higher percentage of the total mutant lamin A interactors were involved in ribsosome and translation-related processes. Most interestingly, negative regulation of apoptotic processes, as well as autophagy, were also top BP terms for the mutant lamin A interactors. Dysregulation of apoptosis has been previously attributed to neurological conditions including Huntington's disease and Alzheimer's disease (Sang et al., 2005; Yamazaki, Esumi and Nakano, 2005), and this is discussed in more detail in Chapter 5,

Section 5.3.6. This suggests that perhaps mutant lamin A interacts and consequently interferes with regulators of apoptosis, leading to the dysregulation of apoptotic processes. In particular, TAX1, or Tax-1 binding protein 1 was a putative mutant lamin A interactor that was associated with negative regulation of apoptotic processes. This protein interacts with TNFAIP3, and inhibits TNF-induced apoptosis by mediating the TNFAIP3 anti-apoptotic activity (Lindholm, Reid and Brady, 1992). As well as this, NPM, or nucleophosmin, was identified as a mutant lamin A interactor implicated in apoptosis, which is known to prevent apoptosis when located in the nucleolus (Ye, 2005). Aberrant interaction between mutant lamin A and either of these proteins could disrupt normal apoptosis. Some of the top MF terms related to the mutant lamin A interactors were similar to those for the healthy and mutant lamin A interactors such as cadherin binding and protein binding, however there were no top terms for the mutant lamin A interactors that were associated with DNA related functions.

3.3.6. XRCC6/Ku70 and TOP1 may be new putative interactors of healthy lamin A.

Of the lamin A interactors that were identified across all healthy and L-CMD myoblasts, it was decided that a couple of candidates would be selected for further verification as new putative interactors of healthy lamin A. As described in Section 3.2.5, X-ray repair cross complementing 6 (XRCC6 or Ku70) and DNA topoisomerase 1 (TOP1) were chosen due to their high enrichment, as well as their roles in DNA repair, replication and/or binding, which were common processes linked to healthy and mutant lamin A interactors, as well as previously identified lamin A interactors. Ku70 was identified as a lamin A interactor across all healthy and L-CMD myoblast samples. It was also identified as an interactor of healthy lamin A in a previous study on murine

cardiomyocytes (Kubben *et al.*, 2010). Conversely, Top1 was only identified across all healthy myoblast samples. Identification of new putative interactors of healthy and mutant lamin A, such as Ku70, may reveal new roles for lamin A, whilst identification of putative interactors of only healthy lamin A, such as TOP1, suggests this interaction may be lost in L-CMD. In future, experiments could be conducted to determine whether TOP1 protein expression and activity is compromised in L-CMD myoblasts. TOP1 protein expression in L-CMD myoblasts compared to controls could be determined using RT-qPCR, whilst an assay assessing the enzymatic activity of TOP1, such as a REEAD assay could be used to determine whether TOP1 activity is changed in L-CMD myoblasts (Stougaard *et al.*, 2009; Tesauro *et al.*, 2019). Although further studies would be needed to further explore lamin A-TOP1 interactions in L-CMD and determine whether this interaction is compromised in L-CMD, TOP1 may represent a target for future therapy development. To further elucidate the roles and functions of these proteins, siRNA could be used to knock-out the expression of TOP1 or Ku70 in healthy control myoblasts to determine cellular effects and downstream molecular consequences.

Co-IP with a lamin A antibody using healthy myoblast extract, and subsequent western blot analysis of Ku70 and Top1 in the pull-down eluate, suggested that they were both interactors of healthy lamin A, although the Ku70 band on western blot was clearer. A reverse Co-IP was then done using Ku70 and Top1 antibodies to determine whether lamin A was bound to either of the proteins. This result was less clear-cut. Although western blot analysis suggested that lamin A could be bound to Ku70, it did not appear that lamin A was bound to Top1. This could be due to the Top1 antibody being ineffective at precipitating Top1 out of the cell extract, rather than Top1 not being an

interactor of lamin A. Further experiments are needed to deduce whether the Top1 antibody effectively binds Top1. IMF labelling of Ku70 and lamin A/C showed that there could be some co-localisation of the two proteins, suggesting that Ku70 and lamin A/C could bind to the same spatial compartments, although further work is needed to clarify this.

Ku70 was previously identified as a lamin A interactor in mouse myocyte NkITAg cells using a OneSTrEP (OST) pull-down assay (Kubben *et al.*, 2010). In this study, A-type lamins were tagged with the OST tag (OST-A) and expressed at endogenous levels in mouse myocyte NkITAg cells (Kubben *et al.*, 2010). The co-purified proteins were then separated and retrieved from SDS-PAGE gels and analysed by MS. Amongst these identified proteins was Ku70. Ku70 was then selected for validation of the MS data by targeted co-precipitation, as it was a protein that was close to the lamin A interactors selection cut-off and was most likely to represent a false-positive (Kubben *et al.*, 2010). On western blot, it was demonstrated that OST-A did successfully co-precipitate Ku70 (Kubben *et al.*, 2010). Taking this study, as well as the above results into consideration, it is likely that Ku70 is an interactor of lamin A.

Ku70 is a crucial component of the NHEJ (non-homologous DNA end joining) pathway, the primary pathway for the repair of DNA double-strand breaks (DSBs) throughout the cell cycle (Chang *et al.*, 2017). In this pathway, the DSB is recognized by the Ku70-Ku80 heterodimer (referred to as Ku), which acts as a loading protein to which other NHEJ proteins can be recruited to promote the joining of DNA ends (Chang *et al.*, 2017). Ku70 also has diverse roles in other processes including chromosome maintenance, transcription regulation and V(D)J recombination (Koike, 2002). Ku70

appears to be generally abundant in the nucleus, although several studies have reported cytoplasmic or cell surface localization of Ku70 in various cell types (Prabhakar *et al.*, 1990; Dalziel, Mendelson and Quinn, 1992; Koike, 2002). In the cytoplasm, it has been demonstrated that Ku70 binds to Bax (Bcl-2-associated X protein). Bax is a member of the Bcl-2 gene family and is a regulator of apoptosis. Ku70 has been shown to interact with Bax, blocking its translocation from the cytosol to the mitochondria where cells receive apoptotic stimuli (Sawada *et al.*, 2003). This Ku70/Bax interaction has been implicated in congenital muscular dystrophy type 1A (MDC1A) caused by mutations in laminin-α2. Acetylation of Ku70, which inhibits binding to Bax and renders Ku70 unable to maintain an inactive state of Bax, was found to be more abundance in *Lama2*-null mouse muscle compared to wild-type (Vishnudas and Miller, 2009). Myotubes formed in culture from human laminin-α2-deficient patient myotubes also were found to have reduced cytoplasmic Ku70, as well as increased acetylation compared to control myotubes (Vishnudas and Miller, 2009). Together, these results suggest that laminin-α2-deficient myotubes have increased susceptibility to cell death. Perhaps if lamin A is an interactor of Ku70, similar mechanisms could be involved in L-CMD pathogenesis, as in Chapter 5, it was found that other proteins involved in apoptotic pathways were dysregulated in L-CMD myoblasts (refer to this Chapter for further details).

Top1, on the other hand, is an essential enzyme that is required for normal mammalian development (Morham *et al.*, 1996). Top1 unwinds supercoiled DNA to remove helical constraints that can hinder DNA replication and transcription, therefore preventing cell growth (Gilmour *et al.*, 1986; Wu *et al.*, 2010). In doing this, Top1 binds to supercoiled DNA, cleaves one strange of the duplex DNA creating an incision,

allowing the duplex DNA to untwist (Wang, 2002). In addition to its role in relaxing supercoiled DNA, accumulating evidence supports a direct role for Top1 in transcriptional regulation. During transcription, RNA polymerase II pauses at initiation and splice sites, whilst Top1 has been proposed to hold RNA polymerase II at the promoter-proximal pause site (Khobta *et al.*, 2006). The exact mechanism behind this is uncertain, however. There does not appear to be any evidence in the literature relating Top1 and lamin A to one another, therefore Top1 represents a possible new interactor of healthy lamin A. Additionally Top1 has not been implicated in any skeletal muscle conditions, although it is interesting that it was only identified as a lamin A interactor across the healthy myoblasts. Future work should aim to clarify whether Top1 is a lamin A interactor, perhaps by using different Top1 antibodies for Co-IP, and determine whether Top1 activity is compromised in L-CMD myoblasts.

3.4. Conclusions and future work

Overall, this work has allowed the identification of potential "mutant" lamin A interactors in L-CMD myoblasts, and "healthy" lamin A interactors in healthy control myoblasts, as well as interactors that were detected across all L-CMD and healthy control myoblast samples, known as "healthy and mutant" lamin A interactors. In addition to this, a number of previously identified interactors of healthy lamin A such as lamin B1, lamin B2, SUN2, emerin and BAF were successfully detected in L-CMD and healthy control myoblast samples, strengthening the evidence that they are in fact lamin A interactors and confirming these interactions also likely occur in human myoblasts. Interactors that were only detected in healthy control myoblasts represent interactions that may be lost in L-CMD myoblasts due to *LMNA* mutations, whilst

proteins that were only identified in the L-CMD myoblasts, and not in the healthy control myoblasts, may signify interactions that are gained as a result of mutations. Loss of interactors in L-CMD myoblasts may consequently disrupt cellular and molecular processes within the cells that lamin A is involved with, and gain of interactors may cause lamin to incorrectly associate with proteins outside of its usual interactome and gain new functions. Both of these factors could be part of L-CMD disease pathophysiology. Future work may aim to clarify whether the *LMNA* mutations that cause L-CMD lead to gain- or loss- of function of lamin A. This can be done using computational software that models the effect of mutations in protein structures. These findings could then be further verified in knock-in models of L-CMD mutations or models where *LMNA* is completely ablated. The identification of lamin A interactors in both healthy and L-CMD cells may represent potential therapeutic targets for further investigation. Interactions that are lost or gained between lamin A and other proteins could be further explored to determine whether the molecular pathways downstream of these interactions are dysregulated in L-CMD myoblasts, which may be targeted for therapy development.

Chapter 4: Targeted characterisation of *LMNA*-associated congenital muscular dystrophy myoblasts and myotubes

4.1. Introduction

4.1.1. *LMNA*-related congenital muscular dystrophy, what is known so far?

LMNA-related congenital muscular dystrophy (L-CMD) is an extremely rare genetic condition, and the incidence of the disease is estimated to be <1/1,000,000, with only around 100 cases reported in the literature (Avila *et al.*, 2021). L-CMD has been described as the most severe of the striated muscle laminopathies, and is characterized by an onset before the age of 2 years old (Quijano-Roy *et al.*, 2008). Distinct features of this disorder include major muscle atrophy and weakness, mainly affecting the axial muscles, which leads to complete absence of or limited motor achievements (Quijano-Roy *et al.*, 2008). A hallmark of L-CMD is a "dropped head" due to weakness of muscles in the neck, and other characteristics include the presence of multiple joint contractures, and life-threatening severe respiratory insufficiency, requiring mechanical ventilation (Quijano-Roy *et al.*, 2008). Cardiac arrhythmias have additionally been identified in L-CMD patients, suggesting there is some cardiac involvement in this disease (Quijano-Roy *et al.*, 2008). Currently, there are no therapeutic options available for the treatment of L-CMD, and affected individuals have an estimated life-span of up to 18 years old.

L-CMD is a relatively newly characterized laminopathy (D'Amico *et al.*, 2005), and compared to other diseases caused by *LMNA* mutations, there are few research groups working on this disorder and consequently less research being produced. In the last five years, however, some progress has been made to elucidate the pathophysiological mechanisms behind L-CMD. Barateau *et al.* identified a heterozygous *LMNA* R388P mutation in a patient with a severe L-CMD and lipodystrophy phenotype (Barateau *et al.*, 2017). This group studied fibroblasts derived

from this patient, as well as C2C12 myoblasts that were transfected with a construct carrying the patient's mutation. In culture, the patient's fibroblasts were difficult to expand due to their slow growth (Barateau *et al.*, 2017). This was attributed to the cells senescing prematurely, characterized by their altered morphology (flattened, enlarged cells with a greater nuclear area), as well as an increased percentage of the cells being positive for β-galactosidase activity (a known marker of senescence) (Barateau *et al.*, 2017). Some fibroblast nuclei were also found to have abnormal honeycomb patterns (described as multiple holes in the nucleus, likened to a honeycomb), although this only accounted for around 4% of total nuclei (Barateau *et al.*, 2017). These observations suggest the patient fibroblasts show defects in lamina organization, as well as cell proliferation capacity. In the transfected C2C12 cells, mutant lamin A mostly accumulated within the nucleoplasm, whilst less lamin A was correctly localized at the nuclear periphery (Barateau *et al.*, 2017). Additionally, the anchorage of inner nuclear membrane protein emerin and LAP2α, another NE protein, were altered (Barateau *et al.*, 2017).

Gómez-Domínguez *et al.* published a study where the consequences of *Lmna* exon 4 mutations in myoblast function were assessed (Gómez-Domínguez *et al.*, 2020). Amongst other variants, the R249W *LMNA* mutation, which is notorious for causing L-CMD was examined. Here, CRISPR/Cas9 technology was used to introduce *Lmna* mutations into C2C12 myoblasts (Gómez-Domínguez *et al.*, 2020). Components of the nuclear lamina were seen to be mislocalized in the R249W cells, with emerin being detected at the endoplasmic reticulum (Gómez-Domínguez *et al.*, 2020). Although other NE proteins, including SUN1 and SUN2, were correctly localized (Gómez-Domínguez *et al.*, 2020). The circularity index of the nuclei (i.e. the measurement of

how spherical the nuclei are) of these myoblasts was also established, and the R249W myoblasts showed a significant reduction in the circularity index of their nuclei (Gómez-Domínguez *et al.*, 2020). The R249W clones also exhibited impaired differentiation, as myogenic fiber and myosin heavy chain expression was undetectable (Gómez-Domínguez *et al.*, 2020). Another interesting finding was that high levels of DNA damage were attributed to the R249W mutation, as quantified by detection of γH2AX (phosphor-H2A.X Variant Histone) (Gómez-Domínguez *et al.*, 2020). The accumulation of DNA damage is a result of a weak nuclear envelope affecting DNA integrity, and possibly a lack of/inefficient DNA repair mechanisms.

Owens *et al.* have recently discovered that L-CMD mutations interfere with mechanosignalling pathways in skeletal muscle, subsequently affecting muscle growth (Owens *et al.*, 2020). Human muscle stem cells (MuSCs) carrying L-CMD mutations (del.K32, R249W and L380S) were found to have impaired myogenic fusion, due to disorganized cadherin/β catenin adhesion complexes, and stretched myotubes and overloaded muscle fibres with L-CMD mutations also display aberrant regulation of the yes-associated protein (YAP) (Owens *et al.*, 2020). Skeletal muscle from *Lmna*-CMD mice was also unable to hypertrophy in response to functional overload, due to defective accretion of activated satellite cells (Owens *et al.*, 2020).

Bertrand *et al.* conducted a study to determine whether any mechanisms could be identified that may be responsible for the increased severity of L-CMD compared to Emery-Drefiuss muscular dystrophy (EDMD) (Bertrand *et al.*, 2020). Skin fibroblasts were cultured from individuals with EDMD harbouring H222P and R453W mutations, and L-CMD patients carrying R249W and del.K32 variants in *LMNA.* Lamin A/C localized

mainly at the nuclear rim in the EDMD fibroblasts, whilst in L-CMD fibroblasts, lamin A/C was almost exclusively found in the nucleoplasm (Bertrand *et al.*, 2020). Based on these observations, it was suggested that L-CMD mutations are responsible for pronounced lamin A/C assembly defects, whilst EDMD mutations probably lead to weaker interactions between lamin A filaments and/or perturbed interactions with its partners (Bertrand *et al.*, 2020). Emerin was also found to be mislocalized in the del.K32 cells, but lamin B1 and SUN2 localization were unaffected (Bertrand *et al.*, 2020). There was also a strong reduction of lamin A/C in del.K32 myoblasts (Bertrand *et al.*, 2020). The del.K32 myoblasts were also found to have impaired differentiation, and del.K32 myonuclei were found to be highly misshapen, elongated, enlarged, and situated in the middle of myotubes (Bertrand *et al.*, 2020). This was not observed in EDMD or control myotubes. In del.K32 myotubes, a number of NE proteins were also found to be mislocalized including emerin, lamin B1, SUN2 and Nup153 (Bertrand *et al.*, 2020). Overall, it appeared that nuclear defects in these cells were exacerbated with differentiation.

4.1.2. The nuclear envelope during myogenic differentiation

Type V intermediate filament proteins, lamins A and C are A-type lamins, and along with B-type lamins are the major components of the nuclear lamina (NL) (Taddei *et al.*, 2004). Lamin A/C are connected to other NE proteins through their mutual associated with the Linker of Nucleoskeleton and Cytoskeleton (LINC) complex, which functions to connect the NL to the cytoskeleton in mammalian cells and are known to interact directly with some proteins including emerin, SUN1 and SUN2. The LINC complex proteins are involved in a wide variety of processes, but here, the focus will be on the

roles of these proteins in relation to myogenic differentiation. The specific roles of these proteins were also examined in more detail in Chapter 1, Sections 1 and 2.

Lamin A has been found to be decreased in expression in predifferentiated myoblasts from chicken embryonic muscle, before increasing in expression during differentiation (Lourim and Lin, 1989). Lamin A/C has been linked to the regulation of genes that are important for myogenic differentiation. Myoblasts lacking lamin A/C (*Lmna*$^{-/-}$*)* have a reduction of desmin and myoblast determination protein (MyoD) transcripts, suggesting A-type lamins directly or indirectly affect the transcription of these genes (Frock *et al.*, 2006). Expression of the R453W *LMNA* mutation in C2C12 cells also impaired activation of the myogenin gene (*Myog*) and maintained a repressive chromatin state on the Myog promoter upon induction of differentiation (Håkelien *et al.*, 2008).

There is also evidence that lamin A/C is involved in pathways involved in muscle cell differentiation. Major alterations in the bone morphogenetic pathway due to Bmp4 downregulation and Smad6 overexpression have been identified in *Lmna*$^{-/-}$ myoblasts, leading to premature differentiation (Janin *et al.*, 2018). Receptor-regulated Smads (R-Smads) are phosphorylated when Bmp4 binds to type 1 and 2 transmembrane receptors, allowing the formation of a complex with Co-Smad, and their translocation into the nucleus to induce the transcription *Id1* and *Id2* (Feng and Derynck, 2005). The expression of Id proteins prevents premature muscle differentiation by disallowing the induction of differentiation factors (Feng and Derynck, 2005). Phosphorylated R-Smads can also interact with Smad6, which inhibits the BMP pathway and therefore target genes are not activated (Feng and Derynck, 2005).

Emerin has been linked to the regulation of myogenic differentiation through regulating intracellular signaling cascades and the regulation of chromatin architecture (Collins, Ellis and Holaska, 2017). *Emd*-null mouse myogenic progenitors revealed disruptions to the Wnt, IGF-1, TGF-β, and Notch signalling pathways, which are involved in regulating myogenic differentiation and muscle regeneration (Massagué *et al.*, 1986; Ridgeway *et al.*, 2000; Polesskaya, Seale and Rudnicki, 2003; Koch and Holaska, 2012). These pathways have roles in maintaining satellite cell quiescence (periods of inactivation or dormancy of satellite cells), satellite cell activation and myogenic differentiation after injury (Iyer, Koch and Holaska, 2017). In emerin-knockdown C2C12 cells, the ERK pathway was also found to be upregulated (Muchir, Wu and Worman, 2009). Differentiation was impaired in these cells but was rescued using an ERK inhibitor (Huber, Guan and Gerace, 2009). ERK inhibition initiates myogenesis early during differentiation, and early and late ERK activity is crucial for proper myogenic differentiation (Koch and Holaska, 2012). A study of the expression of emerin in C2C12 myoblasts found that emerin was decreased in resting myoblasts but appeared to be highly expressed in developing myotubes during the early stages of cell fusion (Lattanzi *et al.*, 2000).

Aside from lamin A/C and emerin, the connection between the NL and the cytoskeleton that the LINC complex provides as a whole protein structure is also important for correct myogenic differentiation. SUN2, along with nesprin-2 giant assembles into transmembrane actin-associated nuclear (TAN) lines that couple actin cables to the nucleus via anchorage by A-type lamins and emerin. This allows the nucleus to move rearward and reorient the centrosome toward the leading edge in migrating NIH323 fibroblasts (Folker *et al.*, 2011). In C2C12 myoblasts, it was found

that depletion of nesprin-2 giant, SUN2 or lamin A/C prevented nuclear movement (Chang *et al.*, 2015). Furthermore, depleting nesprin-2 giant strongly interfered with directed cell migration and reduced the efficiency of myoblast fusion into multinucleated myotubes (Chang *et al.*, 2015). These results show that nuclear movement mediated by the LINC complex contributes to centrosome orientation and polarity for efficient migration and fusion of myoblasts.

4.1.3. Characterising nuclear envelope protein expression in *LMNA*-congenital muscular dystrophy and control cells

Aside from the studies described previously, most articles on L-CMD are case reports describing the clinical features that a patient has presented with alongside the identified *LMNA* variant. As a result, the molecular mechanisms downstream of *LMNA* mutations in L-CMD muscle remain unclear, and there is still a lack of understanding surrounding the pathways involved in L-CMD pathogenesis. This makes the development of non-genetic therapies for L-CMD challenging.

Whilst research is gaining momentum in the field of L-CMD, until now, most research has focused on characterising the function of L-CMD patient cells, or cells transfected with L-CMD mutations. Whilst these findings have been insightful, aside from muscle cell lines transfected with *LMNA* variant constructs, patient cells that have been studied are mostly not pathologically relevant (i.e., skin fibroblasts as opposed to myoblasts or muscle tissue). Therefore, using myoblasts and myotubes derived from L-CMD patients for characterization studies may be more reflective of the L-CMD phenotype.

In addition to this, some of the intrinsic role(s) and expression patterns of nuclear envelope proteins (NE), in particular members of the linker of nucleoskeleton and cytoskeleton (LINC) complex during muscle cell differentiation, are still not confirmed. Currently, little is known about the expression of NE proteins associated with lamin A/C and the LINC complex during myogenic differentiation in L-CMD cells. Moreover, the expression patterns of NE proteins during the period of muscle cell differentiation have not previously been deduced in a healthy control cell model. Findings in the literature suggest that LINC complex proteins including lamin A/C, emerin and SUN2 have important roles during myogenic differentiation. Therefore, it is plausible that these proteins are expressed at different points during muscle cell differentiation. These expression patterns then may be changed in L-CMD cells compared to controls and this could be related to L-CMD pathophysiology.

The aim of this chapter was to characterize the cellular morphology and growth rate, in addition to characterizing the expression levels and distribution of key components of the LINC complex in myoblast and myotubes derived from L-CMD patients compared to healthy controls. Through doing this, shared molecular and/or cellular differences between control and L-CMD cells, across all cell lines harbouring different mutations, may be identified. This may assist future therapy design and further understanding of molecular mechanisms involved in L-CMD pathophysiology.

Specific objectives include:

- To determine if the growth rate of L-CMD myoblasts differs compared to healthy controls using a cell proliferation assay.
- To assess whether nuclear morphology defects are detectable in the L-CMD myoblasts and myotubes, as previously reported in laminopathy patient cells.
- To verify the localization of LINC complex proteins, emerin and SUN2, that are known to be associated with lamin A/C, as well as lamin A/C itself, in control and L-CMD myoblasts and myotubes
- To characterize the protein expression levels of LINC complex proteins (lamin A/C, emerin and SUN2) in L-CMD and control cells during muscle cell differentiation to identify any differences in LINC complex protein expression in L-CMD cells.

4.2. Results

4.2.1. Characterising the cellular morphology of control and L-CMD myoblasts and myotubes in culture

The L-CMD myoblasts did not appear to be visually differ from the control myoblasts in culture. Similarly to descriptions of human myoblasts in the literature, all L-CMD and control myoblasts appeared small and triangular in shape (**Fig 4.1, b-c, 4.2, g-i**) (Cossu, Tajbakhsh and Buckingham, 1996; Swailes *et al.*, 2006), although the C5d control cell line looked slightly different in that the cells appeared slightly larger, less uniform in shape, with some myoblasts appearing elongated (**Fig 4.1, a**). After differentiation had been initiated in the myoblast cultures by addition of serum-free DMEM supplemented with insulin, -transferrin-selenium-ethanolamine (ITS-X) at day 3 of culture, once the cells had reached around 80% confluency, the cells were seen to align. After a further five days in culture, fully formed myotubes were observed across all L-CMD and control cell lines (**Fig 4.1, d-f, 4.2, j-l**). It was noticed that there appeared to be more cells in the C25 and C41 control cultures (**Fig 4.1, b-c, e-f**), which prompted an investigation into the doubling time of the L-CMD myoblasts compared to control myoblasts.

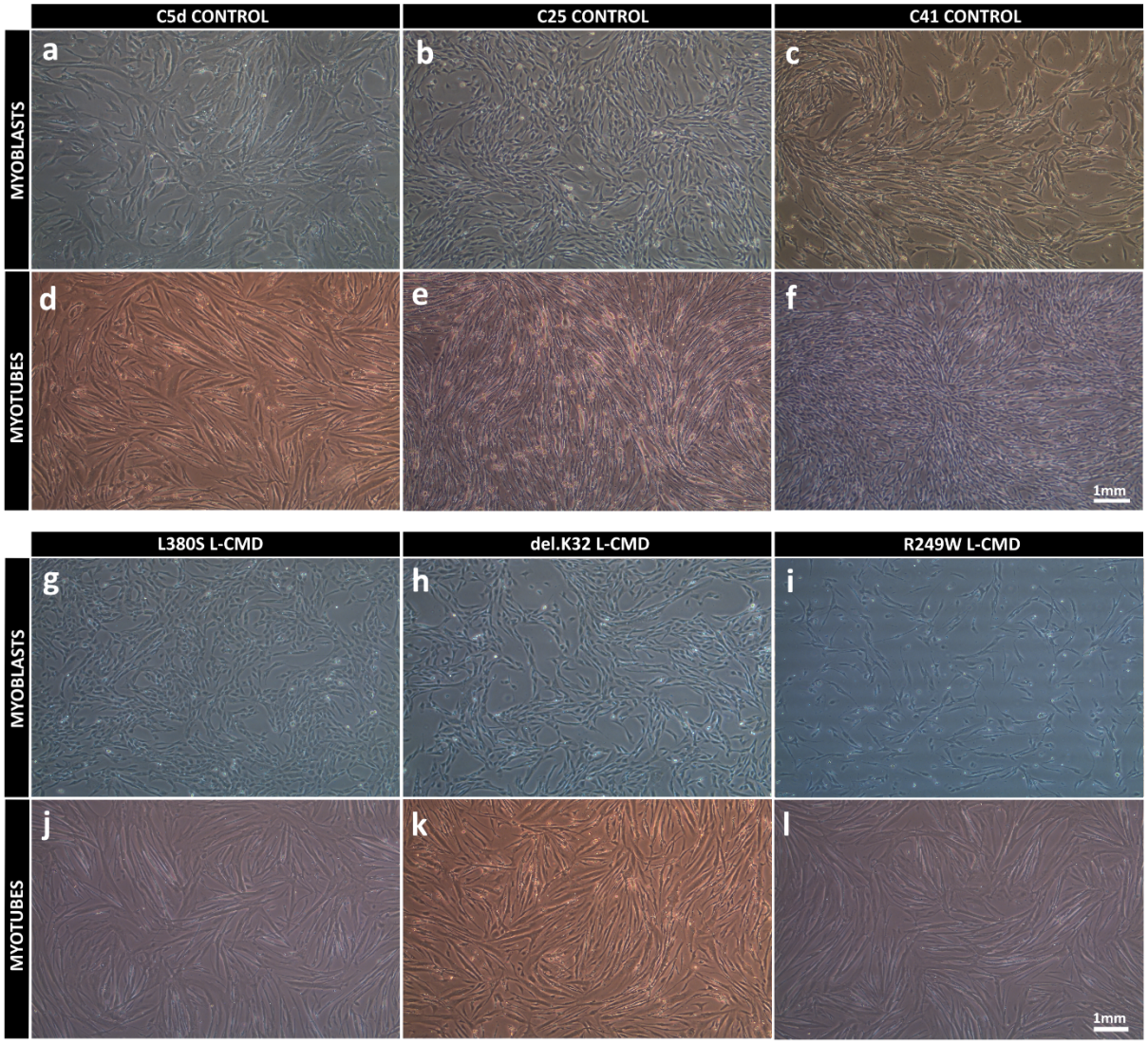
C5d CONTROL
C25 CONTROL
C41 CONTROL
MYOBLASTS
MYOTUBES
a
b
c
d
e
f
1mm
L380S L-CMD
del.K32 L-CMD
R249W L-CMD
MYOBLASTS
MYOTUBES
g
h
i
j
k
l
1mm

Figure 4.1- Healthy control and L-CMD myoblasts and myotubes photographed in culture. *(a-c) C5d, C25 and C41 healthy control myoblasts, (d-f) myotubes. The C5d myoblasts appeared morphologically different to the other control myoblasts. The C5d myoblasts appeared larger, slightly less uniform in shape, and more elongated in culture (a). In comparison, the C25 and C41 myoblasts were smaller and had a more consistent shape (b,c). The C5d myoblasts also formed thicker myotubes (d), whilst the C25 and C41 myotubes formed thinner myotubes where clusters of fused myoblasts made the myotubes thicker in some areas (e,f). (g-i) L380S, del.K32, R249W L-CMD myoblasts, (j-l) myotubes. The L-CMD myoblasts and myotubes did not visually appear morphologically different compared to the control cells. Each of the L-CMD myoblast cell lines appeared similar in appearance to the C25 and C41 myoblasts, and were small cells which were uniform in their size and shape (g-i). Similarly, to the C5d control myotubes, each of the L-CMD cell lines formed myotubes with a thicker appearance (j-l)*

4.2.2. Cell proliferation rate was decreased in L-CMD myoblasts compared to controls.

Cell proliferation was determined by measuring myoblast doubling time in three control (C5d, C25 and C41) and three L-CMD (R249W, L380S, del.K32) cell lines (as described in Chapter 2, Section 2.3.1.). Before the final cell count, each of the cell lines were less than 50% confluent, indicating that the myoblasts were still growing exponentially. On average, the L-CMD myoblasts had a longer doubling time (36.24h (hours) ± 1.74h) compared to the control cells (26.72h ± 3.39h), indicating that the L-CMD cells had a significantly decreased proliferation rate (p=0.023) (**Fig 4.2**). Despite harboring different *LMNA* mutations, the L-CMD myoblasts all had very similar doubling times of 37.69h, 36.72h, and 34.31h, for the L380S, R249W, and del.K32 myoblast lines, respectively.

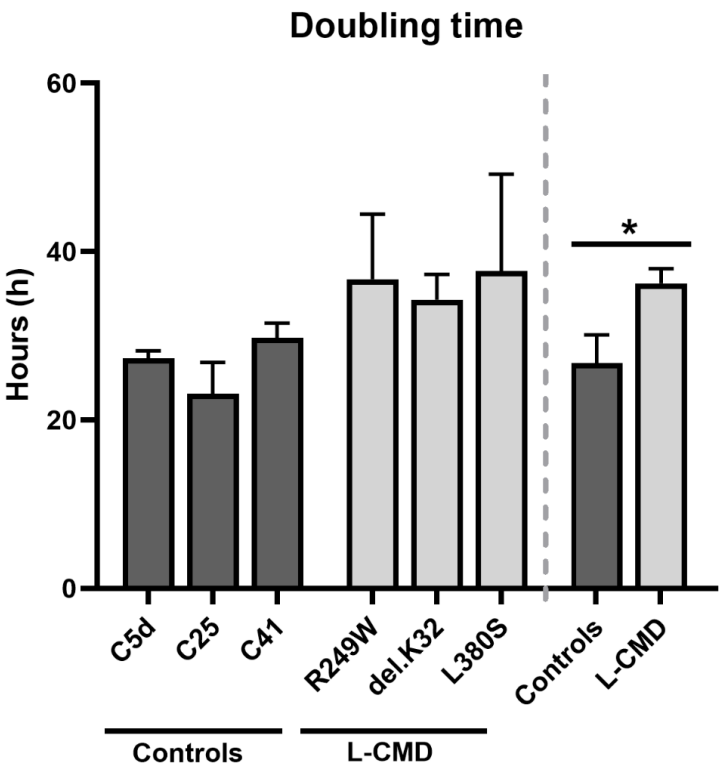

Figure 4.2- Cell proliferation rate is increased in L-CMD myoblasts. *Cell proliferation expressed as doubling time in myoblasts from L-CMD patients (L380S, R249W, del.K32) compared to controls (C5d, C25, C41). Individual values for each cell line are presented, as well as the average for each group, with error bars indicating standard deviation from the mean. On average, the L-CMD myoblasts had a longer doubling time (36.24h (hours) ± 1.74h) compared to the control cells (26.72h ± 3.39h), indicating that the L-CMD cells had a significantly decreased proliferation rate (p=0.023). Two-tailed Student's t-test with unequal variance was used to determine significance, Asterisk (*) indicates significance.*

4.2.3. Congenital muscular dystrophy cells harbouring different *LMNA* mutations exhibit abnormal nuclear shape.

In cells derived from patients with *LMNA*-related diseases, abnormalities in nuclear morphology are often observed. A recent study characterized nuclear shape defects in fibroblast derived from laminopathy patients with a range of different conditions (van Tienen *et al.*, 2018). This study classified types of nuclear abnormalities, which included protrusions from nuclei, known as nuclear blebbing, honeycomb shaped nuclei, nuclei with apparent holes termed “donuts”, and general nuclear shape abnormalities such as elongated or severely misshaped nuclei (van Tienen *et al.*, 2018).

Here, the morphology of the L-CMD patient cells was assessed, alongside DAPI staining, immunostaining for lamin A/C was done on the L-CMD derived cells, and using immunofluorescent confocal microscopy, nuclear shape was characterized following the same method as described by van Tienen *et al*. Lamin A/C immunostaining in combination with DAPI allowed the nuclear envelope and nuclear defects to be visualized more clearly.

As predicted, L-CMD cells exhibited abnormal nuclear morphology (**Fig 4.3**). The myoblast and myoblast cultures of the L-CMD L380S and del.K32 cell lines had a similar number of abnormal nuclei. Approximately 49% and 50% of myoblast nuclei were abnormal in the L380S and del.K32 myoblasts, whilst 47% and 54% of the nuclei in the myotubes for the respective cell lines were abnormally shaped (**Table 4.1**). The R249W cell line, on the other hand, exhibited an increased amount of abnormally shaped nuclei in myotubes (95%) compared to myoblasts (54%), suggesting that nuclear defects in this L-CMD cell line are exacerbated during differentiation (**Table 4.1**). This resulted in the L-CMD myoblast and myotube cultures having 51% and 65% abnormal

nuclei on average. In comparison, only 4% of control myoblasts had nuclear abnormalities, which is comparable to the previous study by van Tienen *et al*., where 4.8% of healthy cell nuclei were abnormal. Additionally, only 2% of control myotube nuclei appeared to have abnormalities (**Table 4.1**).

Nuclear shape abnormalities were the most frequent abnormalities seen across L-CMD myoblasts and myotubes, followed by blebs. L-CMD L380S myoblasts also exhibited a large number of nuclei with donut shapes, whereas this morphology was not observed in the other L-CMD cell lines. In comparison to the L-CMD nuclei, the control cell nuclei were spherical or slightly oval in shape (**Fig 4.3, e**).

The nuclei within myotubes were counted to determine whether the L-CMD myotubes contained fewer nuclei, which may suggest that they had not formed as efficiently as the control myotubes. On average, control myotubes had 16 nuclei per myotube, whilst L-CMD myotubes had a similar amount of nuclei, an average of 14 nuclei per myotube (ten myotubes were counted per cell line). Compared to the other L-CMD and control myotubes, however, the del.K32 L-CMD myotubes had a reduced number of nuclei per myotube. On average, the L-CMD myotubes contained 9 nuclei (**Fig 4.4**).

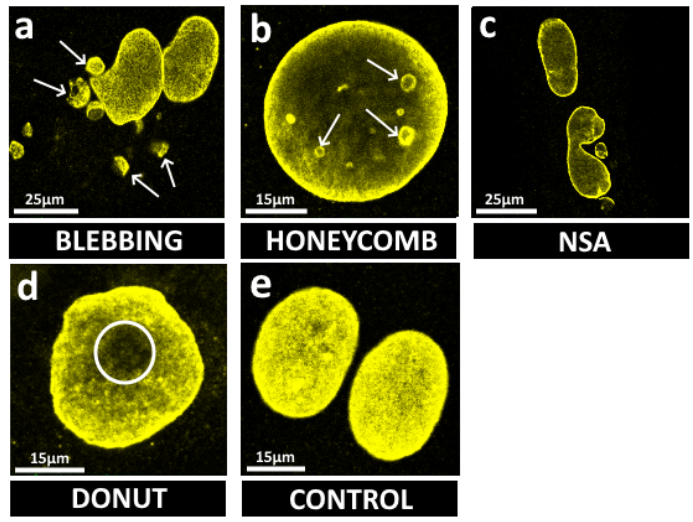

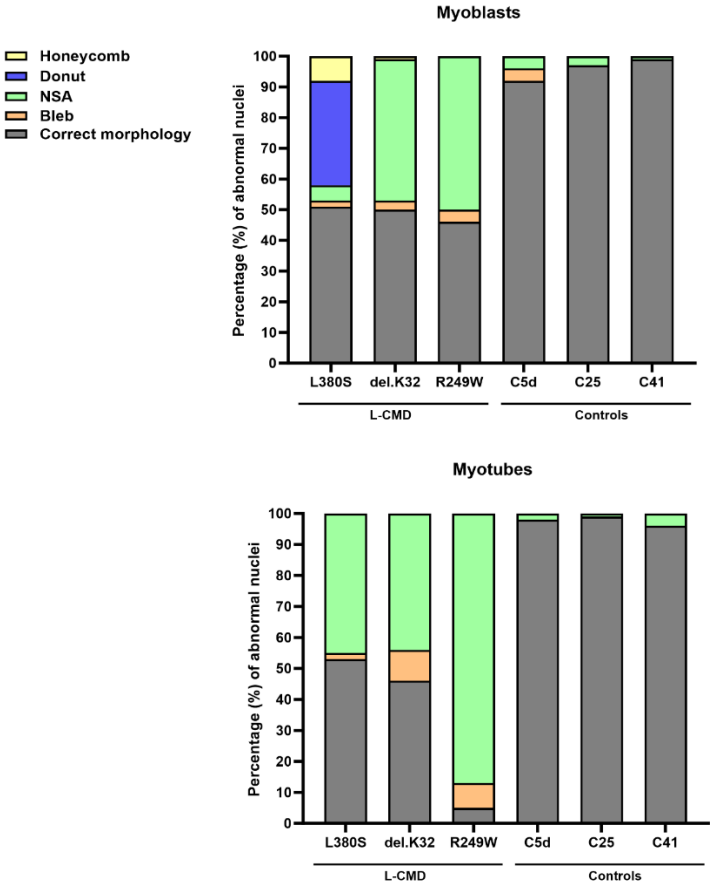

Figure 4.3- Nuclear abnormalities seen in L-CMD myoblasts and myotubes. *Abnormal L-CMD (L380S, del.K32, R249W) myoblast and myotube nuclei were characterised based on the defect type using lamin A/C immunostaining (yellow). (a) Nuclear blebbing is defined as protrusions from the nucleus, sometimes these are seen to become detached from the nucleus itself, (b) honeycomb nuclei have multiple distinct holes that sometimes resemble a honeycomb, (c) nuclear shape abnormalities are nuclei that are shaped differently to control nuclei, elongated nuclei are an example of this, (d) donut shaped nuclei have a single hole through the centre, (e) correctly shaped control nuclei for comparison. Graph depicts percentage (%) of abnormal nuclei identified in each L-CMD and control cell lines.*

Table 4.1- Nuclear morphology defects in control and L-CMD myoblasts and myotubes.

Myoblast cell line	% Abnormal nuclei	Correct morphology (%)	Bleb (%)	Nuclear shape abnormality (NSA) (%)	Donut (%)	Honeycomb (%)
L380S	49	51	2	5	34	8
del.K32	50	50	3	46	0	1
R249W	54	46	4	50	0	0
C5d	8	92	4	4	0	0
C25	3	97	0	3	0	0
C41	1	99	0	1	0	0
Myotube cell line	**% Abnormal nuclei**	**Correct morphology (%)**	**Bleb (%)**	**Nuclear shape abnormality (NSA) (%)**	**Donut (%)**	**Honeycomb (%)**
L380S	47	53	2	45	0	0
del.K32	54	46	10	44	0	0
R249W	95	5	8	87	0	0
C5d	2	98	0	2	0	0
C25	1	99	0	1	0	0
C41	4	96	0	4	0	0

Nuclear morphology defects were assessed in three L-CMD cell lines (L380S, del.K32, R249W) and three control cell lines (C5d, C25, C41). The number of cells with correct nuclear morphology were counted and listed in the table, along with the number of abnormal nuclei. Types of abnormalities were recorded including blebs, nuclear shape abnormalities (NSA), donuts and honeycombs. The percentage of abnormal nuclei were then calculated. A total of 100 cells were counted for each cell line.

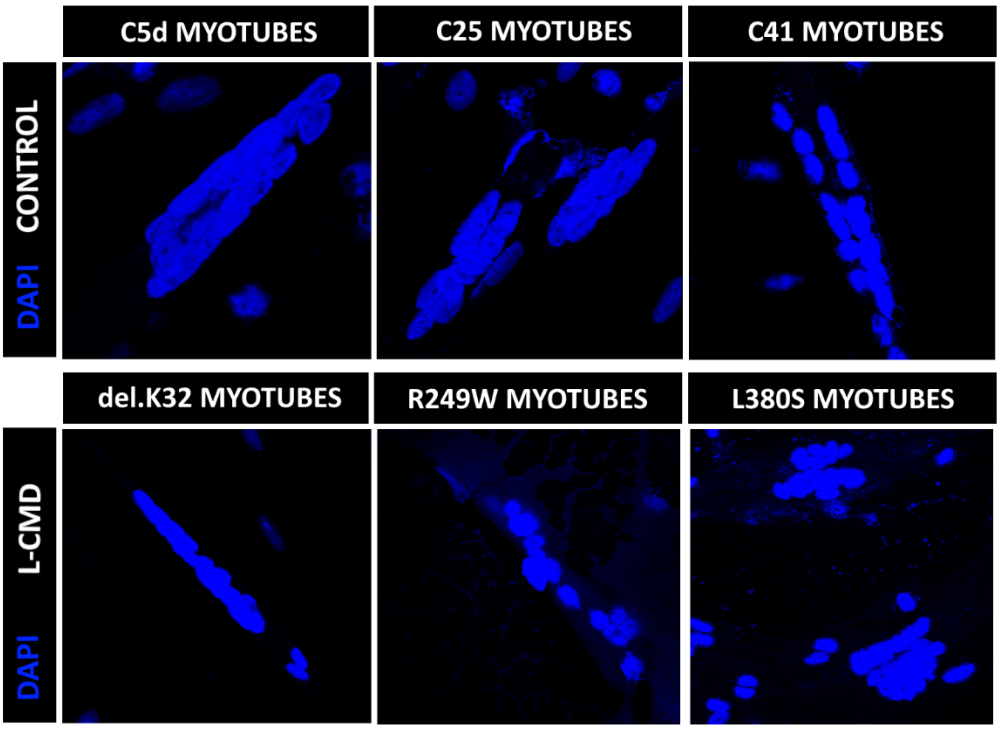

Figure 4.4- L-CMD myotubes had fewer nuclei compared to controls. *Representative images of control (C5d, C25, C41) and L-CMD (del.K32, R249W, L380S) myotubes stained with DAPI. On average, control myotubes had 16 nuclei per myotube, whilst L-CMD myotubes had a similar amount of nuclei, an average of 14 nuclei per myotube (ten myotubes were counted per cell line). Compared to the other L-CMD and control myotubes, however, the del.K32 L-CMD myotubes had a reduced number of nuclei per myotube. On average, the L-CMD myotubes contained 9 nuclei.*

4.2.4. Lamin A/C was present in nuclear aggregates in the nucleoplasm of del.K32 L-CMD myoblasts

Using lamin A/C immunostaining, lamin A/C localization was determined in three (L380S, R249W, del.K32) L-CMD cell lines (**Fig 4.5**), as well as in three control cell lines (C5d, C25, C41) (**Fig 4.6**). Lamin A/C appeared to be correctly localized at the nuclear periphery in the control myoblasts and myotubes (**Fig 4.6, a-i**), as well as in the L-CMD L380S and R249W myoblasts and myotubes (**Fig 4.5, a-c, g-i**). In the L-CMD del.K32 myoblasts, some lamin A/C appeared to be present in nuclear aggregates in the nucleoplasm, with 100% of cells (of 100 cells counted) exhibiting this defect (**Fig 4.5,**

e), there also appeared to be more nucleoplasmic staining in L-CMD del.K32 myotubes (**Fig 4.5, f**).

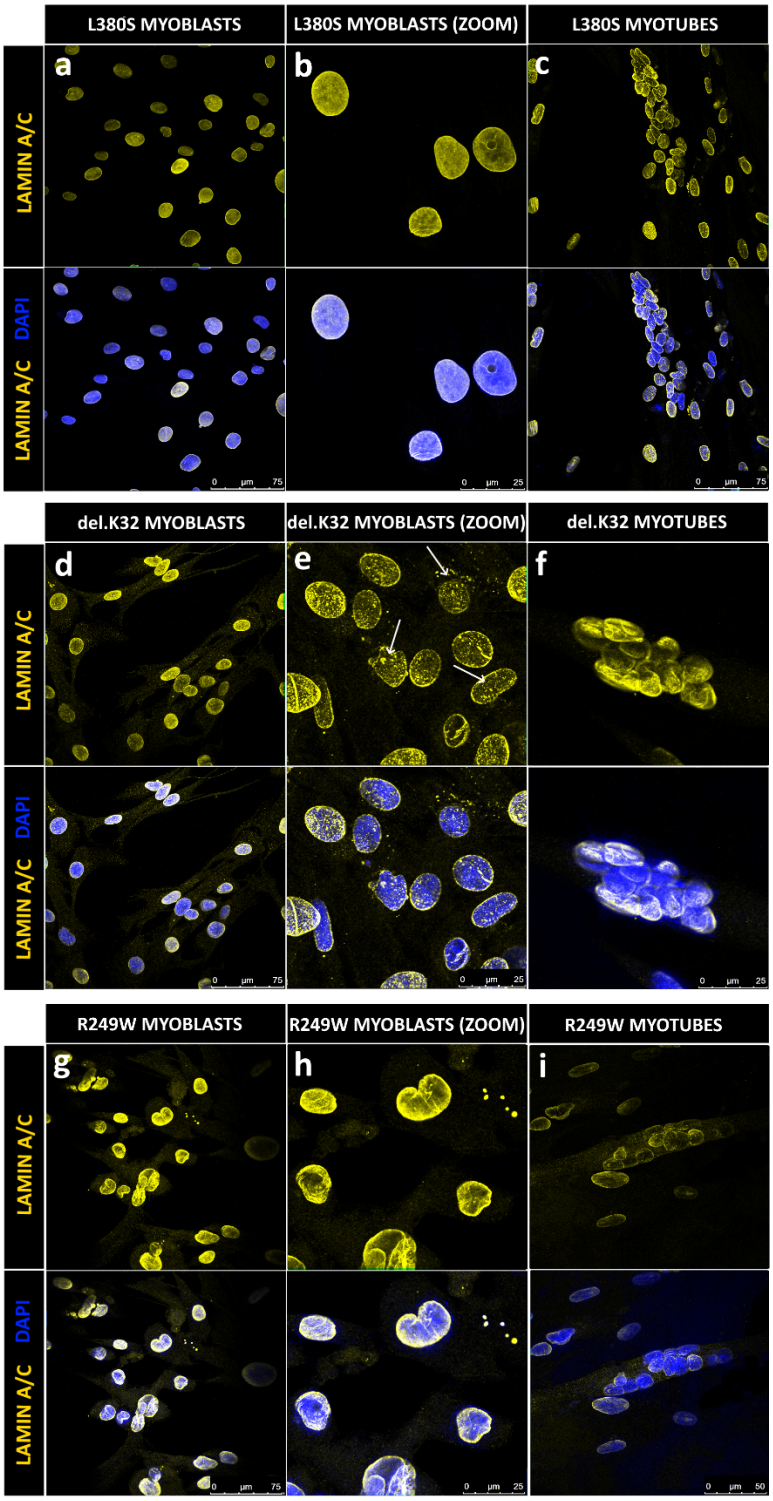

Figure 4.5- Immunofluorescent labelling of lamin A/C in L-CMD myoblasts and myotubes.
Representative immunocytochemistry images showing lamin A/C (yellow) and DAPI (blue) staining in L-CMD myoblasts and myotubes (L380S, del.K32, R249W). Lamin A/C was found in nucleoplasmic aggregates in del.K32 myoblasts, as indicated by white arrows, with 100% of cells (of 100 cells counted) exhibiting this defect.

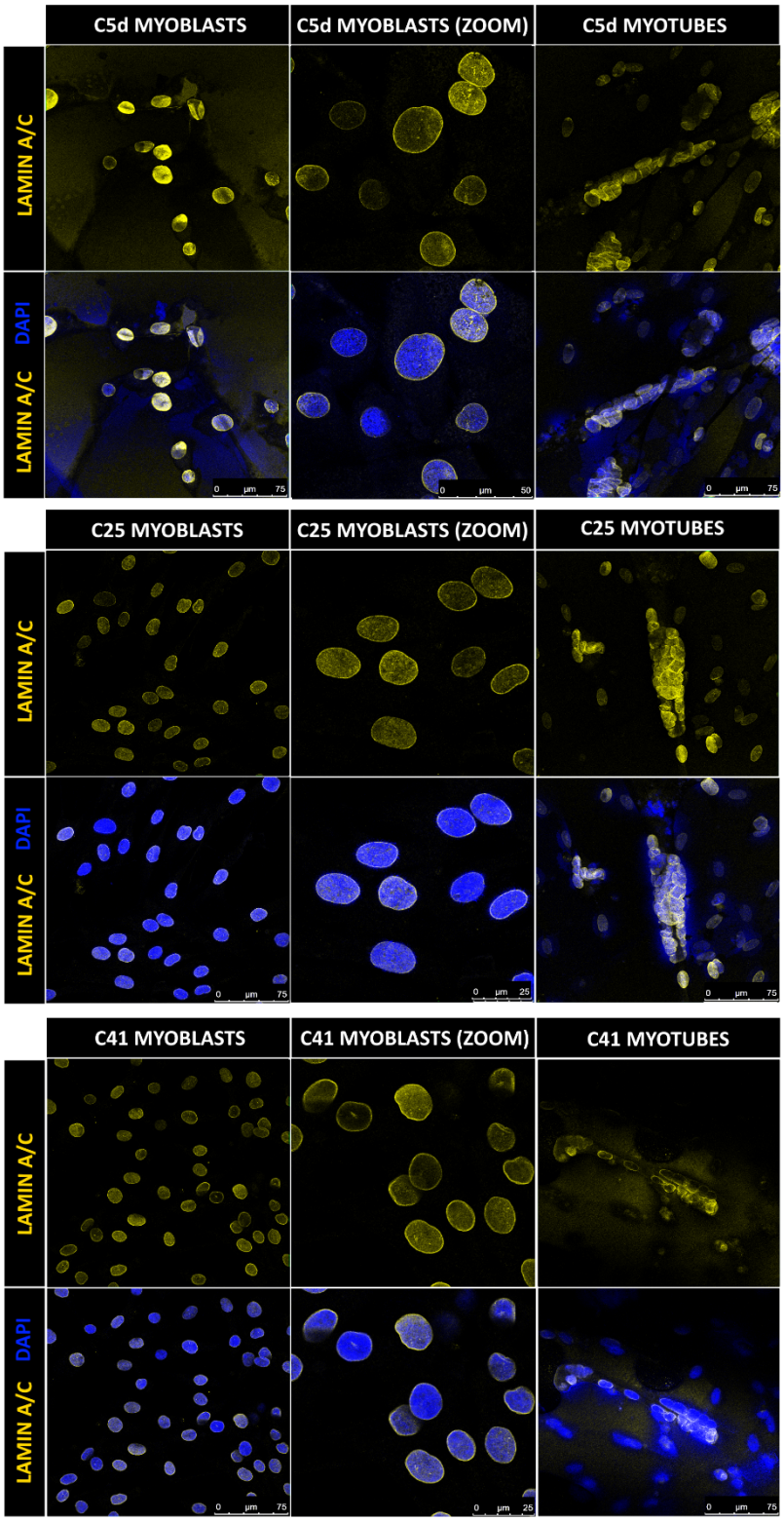

Figure 4.6- Immunofluorescent labelling of lamin A/C in control myoblasts and myotubes.
Representative immunocytochemistry images showing lamin A/C (yellow) and DAPI (blue) staining in control myoblasts and myotubes (C5d, C25, C41). Lamin A/C was found to be correctly localized at the nuclear envelope across all control myoblasts and myotubes.

4.2.5. Lamin A/C expression patterns during differentiation are variable across all control and L-CMD cell lines

Considering that the L-CMD cells are derived from patients carrying lamin A/C mutations, along with the observations that L-CMD have abnormal nuclei and in some cases, abnormal localization of lamin A/C, it is plausible that the expression of lamin A/C might be altered in the cells.

Lamin A/C expression was first examined during healthy muscle cell differentiation in control cell lines. This was done to identify whether lamin A/C expression is altered under normal circumstances during differentiation. Once this was established, the expression patterns of lamin A/C in L-CMD cells could be compared to the findings in control cells to identify any differences.

Lamin A/C expression was determined across seven time-points during differentiation. The first time-point was 24h after seeding the myoblasts, time-point two reflected confluent myoblasts, time-point three was 24h after differentiation was induced, whilst time-points four to seven represent 24h increments from time-point three until the time-point seven where the myoblast cultures had formed myotubes.

Lamin A/C expression appeared to be incredibly variable across all control cell lines (C5d, C25, C41, C53, C79, C83) during myoblast differentiation, with no common patterns observed between controls from donors of different ages (**Fig 4.7, A-F**). Additionally, it was found at some time-points, lamin C was detected, but lamin A was not. It was observed, however, that lamin A/C expression does appear to be reduced in the two control cell lines from the oldest donors (C79 and C83, **Fig 4.7, E-F**). Lamin A/C appeared to only be detected at time-point 4 in the C79 cells, and only detected at

time-point 1 in the C83 cells. This result suggests that lamin A/C expression is decreased with age, although it is difficult to draw conclusions from only two cell lines.

Although it was determined that there were no consistent lamin A/C expression patterns across the control cell lines, lamin A/C expression during differentiation was still assessed in the L-CMD myoblasts (L380S, del.K32, R249W) for comparison (**Fig 4.7, G-I**). There were no similarities in lamin A/C expression during differentiation across the three L-CMD cell lines, nor did lamin A/C expression follow a similar pattern to any of the controls in any of the L-CMD cell lines (**Fig 4.7, J-K**). Although, in the L-CMD L380S cell line, it was difficult to detect lamin A/C during at any of the time-points during differentiation (**Fig 4.7, I**).

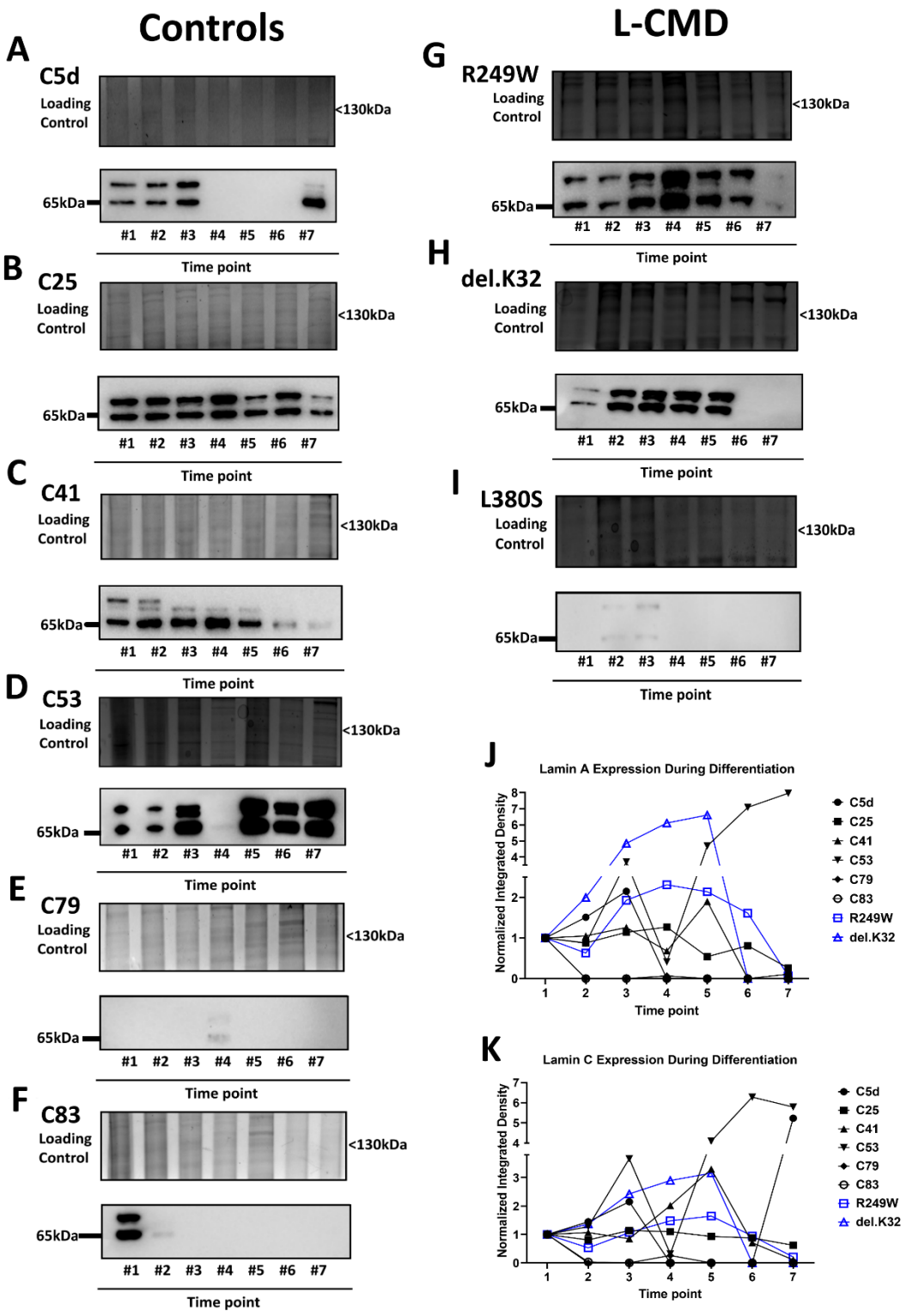

Figure 4.7- Lamin A/C expression appears variable across both control and L-CMD cell lines during differentiation but seems reduced in older cell lines. *Lamin A/C expression did not follow a clear pattern during muscle cell differentiation in control (A-F) (C5d, C25, C41, C53, C79 and C83) and L-CMD (G-I) (R249W, del.K32, L380S) cells and was highly variable between cell lines. It was found, however, that lamin A/C appeared to be reduced in the two oldest cell lines, C79 and C83. (J) Lamin A and (K) Lamin C expression during differentiation in all cell lines. The L-CMD L380S cell line is absent from graph J and K as it was difficult to measure bands due to low signal.*

4.2.6. Lamin A and C were significantly reduced in L-CMD myotubes compared to controls, and mutant lamin A was reduced in size in L-CMD myoblasts

Previously, it has been shown that *Lmna*$^{\Delta K32/\Delta K32}$ mouse muscle had reduced levels of lamin A/C protein, but not reduced mRNA, suggesting a reduced translation efficiency or higher rate of degradation of mutant lamin A/C (Bertrand *et al.*, 2012). Due to this finding, using western blotting, lamin A/C protein expression levels were directly compared in L-CMD (L380S, del.K32, R249W) and the closest age-matched healthy control (C5d, C25, C41) myoblasts and myotubes.

Expression levels of lamin C appeared relatively consistent across all myoblast samples, with no obvious change in expression observed in L-CMD myoblasts compared to controls (p=0.805) (**Fig 4.8, A, C**). Lamin A, on the other hand, did appear reduced in L-CMD myoblasts compared to controls, however this finding was not statistically significant (54.55%, p=0.244) (**Fig 4.8, A, C**). Lamin A and C both were found to be significantly reduced in L-CMD myotubes compared to controls (98.68%, p=0.044, 63.29%, p=0.043, respectively) (**Fig 4.8, D, E**).

It was also observed that the molecular weight of the lamin A band appeared to be slightly smaller in the L-CMD myoblasts compared to control myoblasts (**Fig. 4.8, B**). However, in L-CMD myotubes, lamin A appeared to be approximately the same molecular weight as in the control myotubes (**Fig. 4.8, D**). The lower molecular weight lamin A band in L-CMD myoblasts may indicate the presence of truncated lamin A in each of the L-CMD cell lines. Another possibility, however, could be that the lower MW lamin A in the L-CMD myoblasts is a degraded form of mature lamin A, due to lamin A being more unstable in the L-CMD myoblasts.

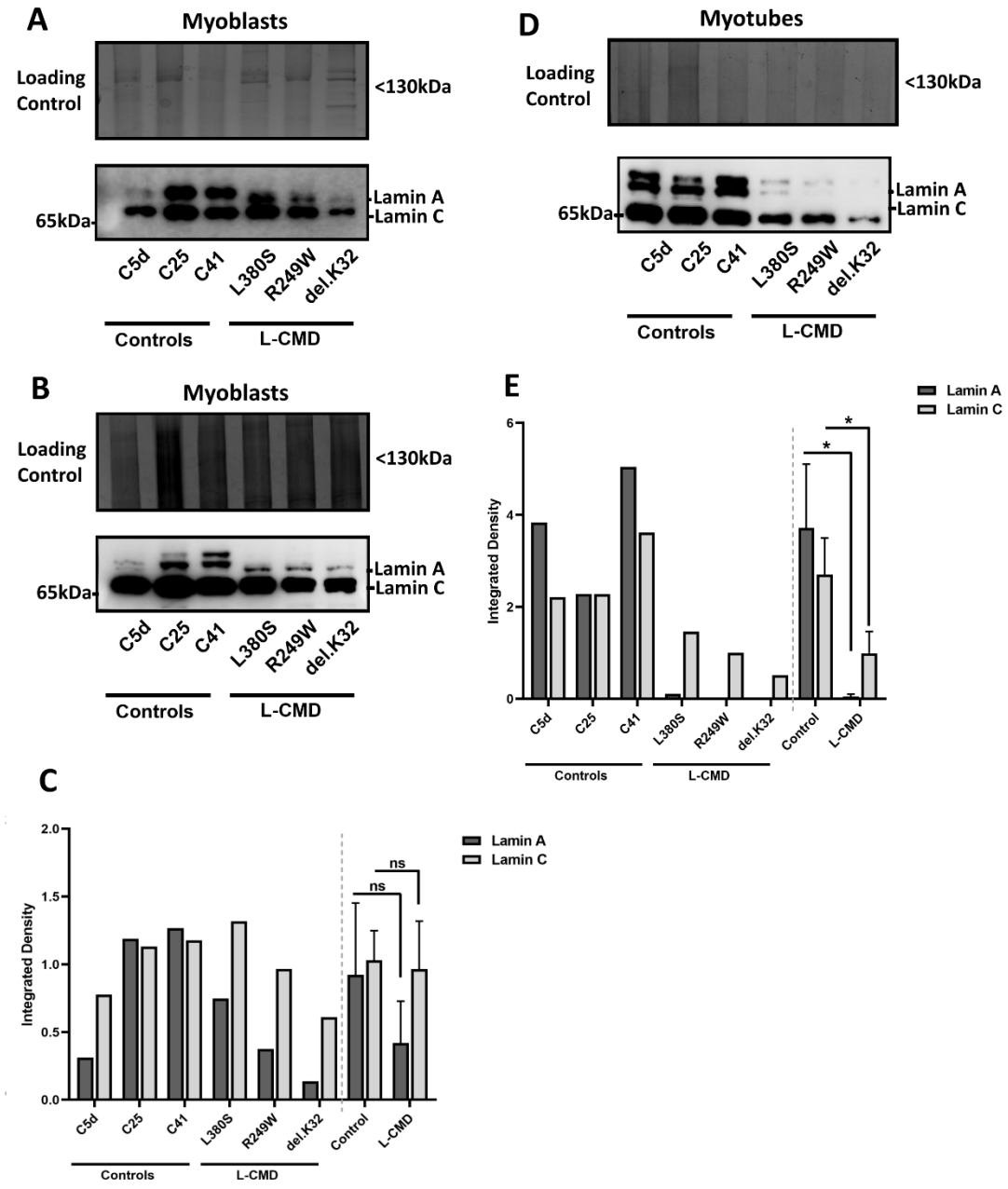

Figure 4.8- Comparison of lamin A/C expression in control and L-CMD myoblasts and myotubes. *Lamin A/C expression was compared in control (C5d, C25, C41) and L-CMD (R249W, del.K32, L380S) myoblasts (A,B,C) and myotubes (D,E). (A, C) In L-CMD myoblasts, lamin A appeared reduced compared to controls, although this finding was not statistically significant (54.55%, p=0.244), whilst lamin C did not appear obviously reduced (p=0.805). (B) However, it was noticed that lamin A was of a lower molecular weight in L-CMD myoblasts compared to controls. (D, E) In L-CMD myotubes, lamin A and C were both reduced with statistical significance compared to controls (98.68%, p=0.044, 63.29%, p=0.043). Two-tailed Student's t-test with unequal variance was used to determine significance, Asterisk (*) indicates significance, ns indicates not significant.*

4.2.7. Emerin was mislocalized to the cytoplasm in R249W L-CMD myoblasts

Emerin is an inner nuclear membrane protein and is part of the LINC complex, along with lamin A/C (Koch and Holaska, 2014). Immunostaining for emerin was done on L-CMD myoblasts and myotubes, as well as controls, to determine whether emerin was correctly localized in L-CMD cells.

In all control myoblast and myotube cell lines, emerin was easily identified at the nuclear envelope (**Fig 4.9**). Emerin was also detected at the nuclear rim in all L-CMD myoblast and myotubes, but in the L-CMD R249W myoblasts, some emerin was also found to be mislocalized. In the L-CMD R249W myoblasts, in approximately 33% of cells (out of 30 cells that were counted), emerin granules appeared to be mislocalized to the cytoplasm, or maybe to the endoplasmic reticulum (ER) within the cytoplasm. Further clarification with an ER-specific marker such as calreticulin or COL1A1 is needed to confirm the exact structure that emerin has mislocalized to. Previously, emerin has been found to be specifically mislocalized to the ER in *Lmna*$^{-/-}$ fibroblasts (Raharjo *et al.*, 2001).

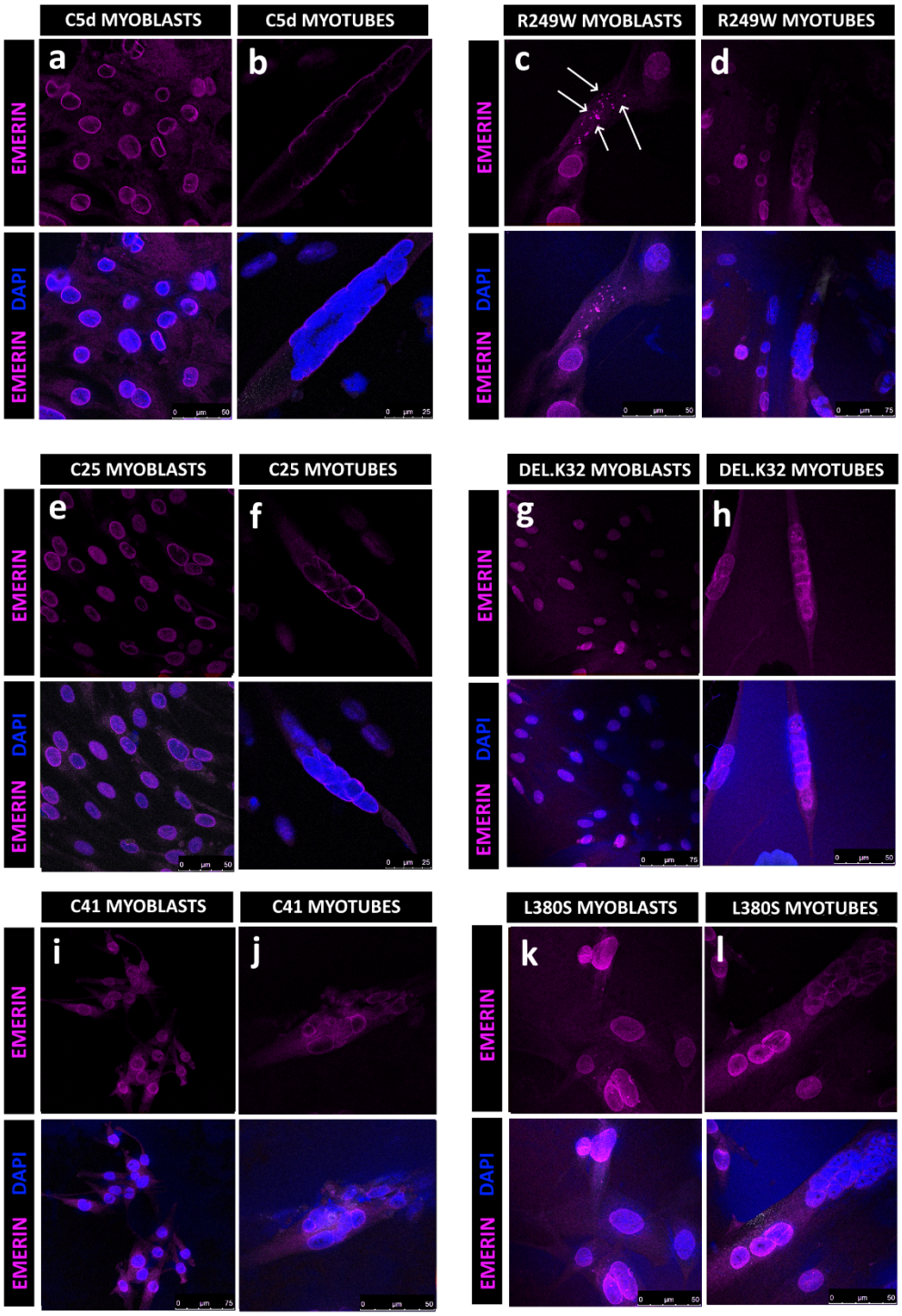

Figure 4.9- Immunofluorescent labelling of emerin in L-CMD and control myoblasts and myotubes. *Representative immunocytochemistry images showing emerin (magenta) and DAPI (blue) staining in control (C5d, C25, C41) and L-CMD (R249W, del.K32, L380S) myoblasts and myotubes. Emerin was found to be correctly localized at the nuclear envelope across all control myoblasts and myotubes, and all L-CMD myoblasts and myotubes except R249W L-CMD myoblasts where emerin found to be mislocalized. In the L-CMD R249W myoblasts, in approximately 33% of cells (out of 30 cells that were counted), emerin granules appeared to be mislocalized to the cytoplasm, or maybe to the endoplasmic reticulum (ER) within the cytoplasm.*

4.2.8. Emerin expression patterns during differentiation may be altered in L-CMD cell lines compared to controls

As emerin is a binding partner of lamin A/C and was found to be mislocalized in the L-CMD R249W myoblasts, it is plausible that emerin expression might be dysregulated in L-CMD cells.

Before characterizing emerin expression during differentiation in L-CMD cells, it was important to establish emerin expression in control myoblasts during differentiation, as it was unclear from the literature whether this had previously been defined. As described in Section 4.2.5., emerin expression was characterized across seven time-points during myoblast differentiation. Once emerin expression patterns had been identified in healthy controls, this could be compared to emerin levels in L-CMD cells.

Using quantitative western blotting, it was observed that emerin expression mostly appeared to be decreased on average by 81.37% in control myotubes (time-points six and seven), compared to in proliferating and differentiating myoblasts (time-points one to five) (**Fig. 4.10**). Although, control myoblast cell line C79 was a slight outlier, as emerin expression also appeared reduced in time-point one, to a similar level as was seen at time-points six and seven in this cell line. In the del.K32 L-CMD cells, emerin appeared reduced in the myotubes also, however emerin expression levels in L380S and R249W myotubes appeared similar to earlier time-points.

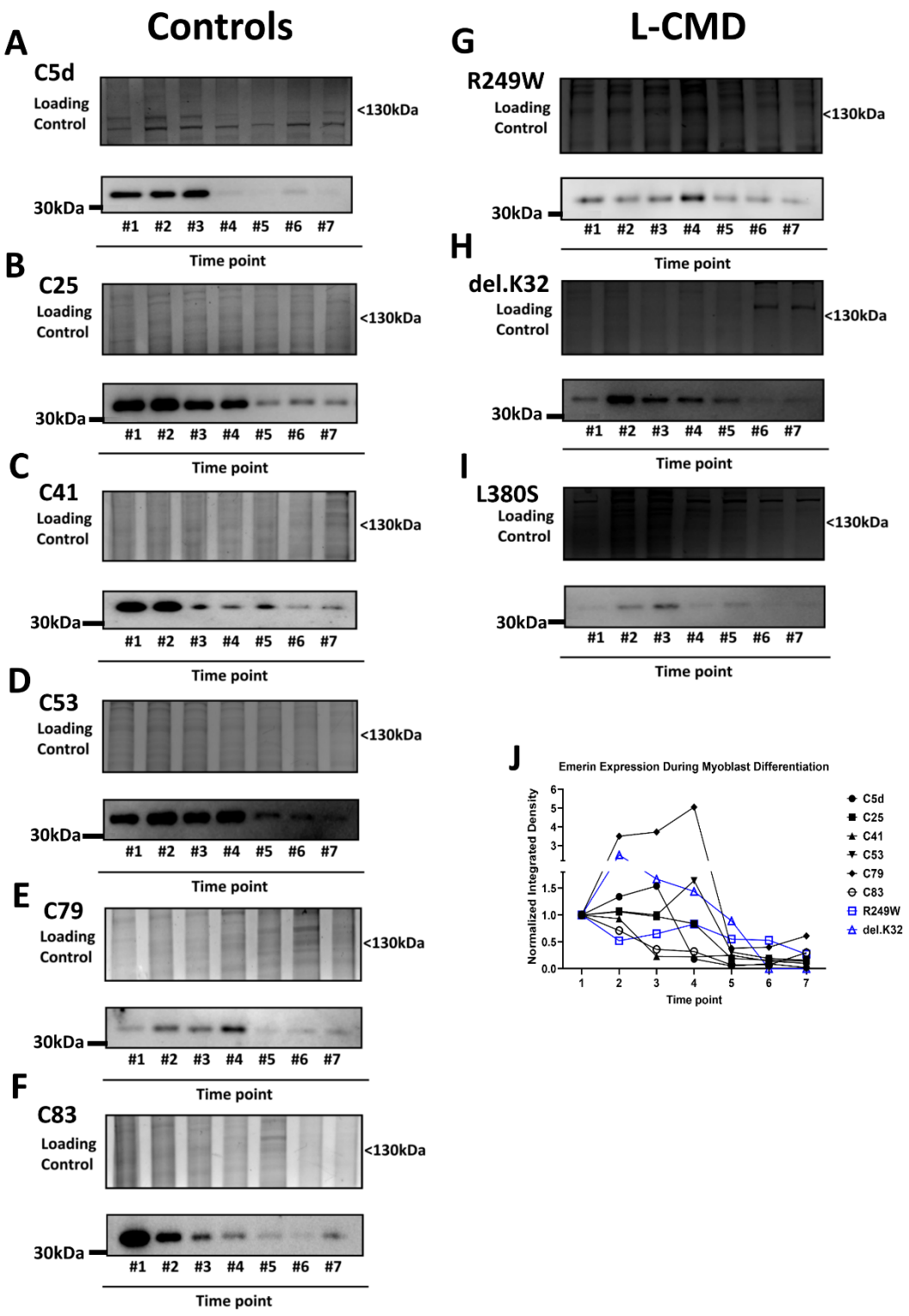

Figure 4.10- Emerin expression was found to decrease in control and L-CMD myotubes compared to myoblasts. *Emerin expression during myoblast differentiation in control cell lines (C5d, C25, C41, C53, C79 and C83) and L-CMD cell lines (R249W, del.K32 and L380S). Emerin was found to decrease once myotubes had formed at time-points 6 and 7 across all control and L-CMD cell lines. (A) Emerin expression during differentiation in each control myoblast cell line versus each L-CMD cell line. The L-CMD L380S cell line is absent from graph J as it was difficult to measure bands due to low signal.*

4.2.9. Emerin expression is not significantly reduced in L-CMD cells compared to controls

Emerin expression was then analysed in L-CMD myoblasts and myotubes and directly compared to the controls that were closest in age (C5d, C25, C41). Emerin expression was not significantly reduced across the L-CMD myoblasts (R249W, del.K32, L380S) compared to controls (C5d, C25, C41) (58.00%, *p*=0.097) (**Fig. 4.11, A, B**), however in L-CMD myotubes, emerin was significantly reduced compared to controls (74.25%, *p*=0.040) Out of the three L-CMD cell lines, the R249W, which exhibited emerin mislocalization, did not appear to show a significant difference in the level of emerin expression compared to the other two L-CMD cells (**Fig. 4.11, C, D**).

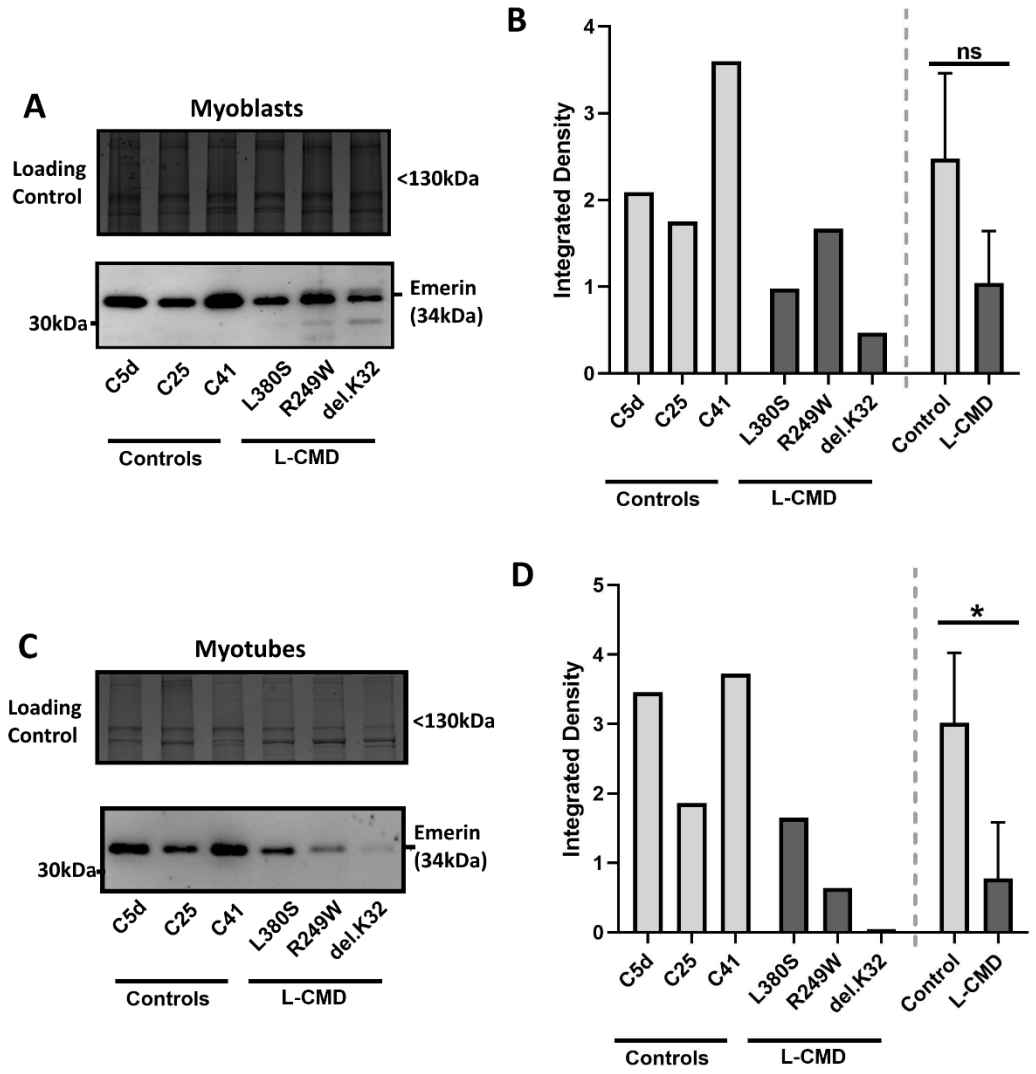

Figure 4.11- Comparison of emerin expression in control and L-CMD myoblasts and myotubes. *(A, B) Emerin was not found to be significantly reduced in L-CMD myoblasts (L380S, R249W, del.K32) compared to age matched controls (C5d, C25, C41) (58.00%, p=0.097). (C, D) Emerin was however significantly decreased L-CMD myotubes compared to controls (74.25%, p=0.040). Two-tailed Student's t-test with unequal variance was used to determine significance, Asterisk (*) indicates significance, ns indicates not significant.*

4.2.10. SUN2 was correctly localized at the nuclear rim in L-CMD cells, but was less detectable compared to healthy controls

As it has been demonstrated that SUN2 interacts with lamin A at the INM in HeLa cells (Crisp, Liu, Roux, J. B. Rattner, *et al.*, 2006), and that SUN2 is dependent on lamin A for its correct localization at the NE (Haque *et al.*, 2010), there is the possibility that

mutations in *LMNA* could affect this interaction and cause SUN2 to be mislocalized in the L-CMD cells. Here, control and L-CMD myoblasts and myotubes were fluorescently labelled for SUN2 (**Fig 4.12**). SUN2 was visualized at the nuclear envelope in the control cells and the L-CMD cells, suggesting that the *LMNA* mutations harboured in the L-CMD cells do not affect SUN2 localization. An unexpected observation is that the intensity of SUN2 staining appeared reduced in L-CMD myoblasts and myotubes compared to in control myoblasts and myotubes, when imaged using a consistent laser intensity. When measured, it was found that in L-CMD myoblasts, SUN2 staining intensity was reduced by 32.23% compared to controls, however this reduction was not statistically significant (p= 0.439). In L-CMD myotubes, however, SUN2 staining was reduced by 85.35%, which was found to be statistically significant (p= 0.010) (**Fig 4.13**).

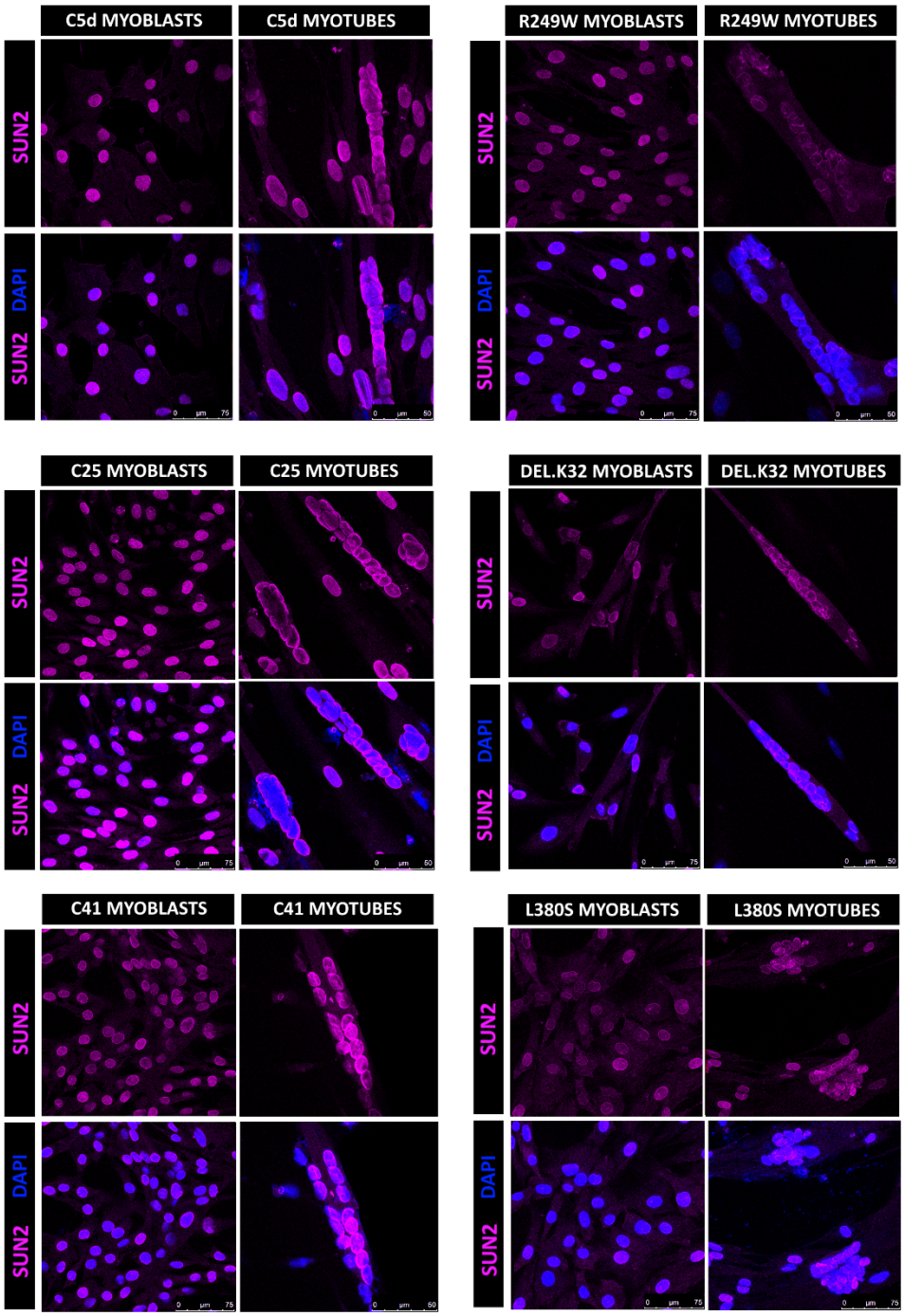

Figure 4.12- Immunofluorescent labelling of SUN2 in L-CMD and control myoblasts and myotubes. *Representative immunocytochemistry images showing SUN2 (magenta) and DAPI (blue) staining in control (C5d, C25, C41) and L-CMD (R249W, del.K32, L380S) myoblasts and myotubes. SUN2 was correctly localized at the nuclear envelope across all control myoblasts and myotubes, and all L-CMD myoblasts and myotubes. There however appeared to be reduced staining of SUN2 across L-CMD cells.*

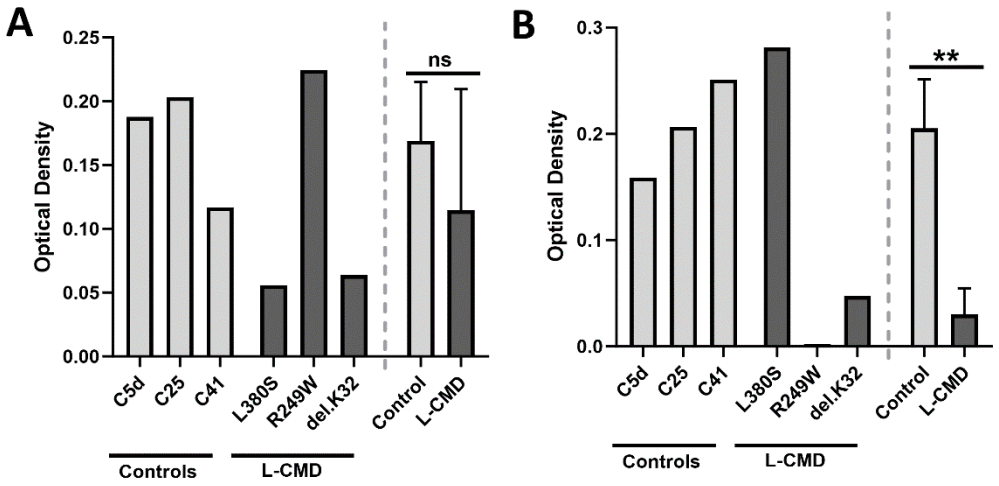

Figure 4.13- Measurements of SUN2 staining intensity in control and L-CMD myoblasts and myotubes. *SUN2 staining visually appeared reduced across the L-CMD myoblasts and myotubes compared to control myoblasts and myotubes. When measured, SUN2 staining was reduced in L-CMD myoblasts compared to controls, but this was not stastically significant (32.23%, p=0.439). However, in L-CMD myotubes, SUN2 staining was found to be reduced with statistical significance (85.35%, p=0.010). Two-tailed Student's t-test with unequal variance was used to determine significance, Asterisk (*) indicates significance, ns indicates not significant.*

4.2.11. SUN2 expression patterns during differentiation were similar in L-CMD cell lines compared to controls, though potential SUN2 isoform may be differentially expressed during differentiation

SUN2 expression during muscle cell differentiation was ascertained using quantitative western blotting (**Fig. 4.14, 4.15, 4.16**). The main isoform of SUN2 has a predicted MW of 80kDa, and this isoform was successfully detected on western blot in both control and L-CMD cell lines at each time-point during differentiation, albeit the signal was difficult to detect across all time-points in the L-CMD L380S cell line. There did appear to be slight differences in the intensity of the 80kDa SUN2 bands at different time-points across all of the L-CMD and control cell lines, but more intriguingly, it was noticed that there were other lower MW bands detected in each of the cell lines (**Fig 4.14, 4.15**), ranging from 75-25kDa in size that seemed to appear during different points of differentiation. Although there was variation between cell lines in the

number of lower MW bands that were identified (**Fig 4.14, 4.15**), two bands around the 75kDa and 65kDa region appeared consistently in all cell lines, apart from the C5d control line and the L-CMD cell line harbouring an L380S mutation. In the C5d control line the 80kDa SUN2 band was strongly detected across all time-points, but no lower MW bands were detected. For the L380S L-CMD cell line, as previously mentioned, it was difficult to detect the 80kDa SUN2 band and there were also no other lower MW bands detected. The aforementioned 75kDa and 65kDa bands detected across the rest of the control and L-CMD cell lines only appeared at time-point 3 onwards, corresponding to the time at which differentiation media had been added to the confluent cell cultures. During the period following time-point 3, myoblasts underwent differentiation into fully formed myotubes (see Figure 4.12, above).

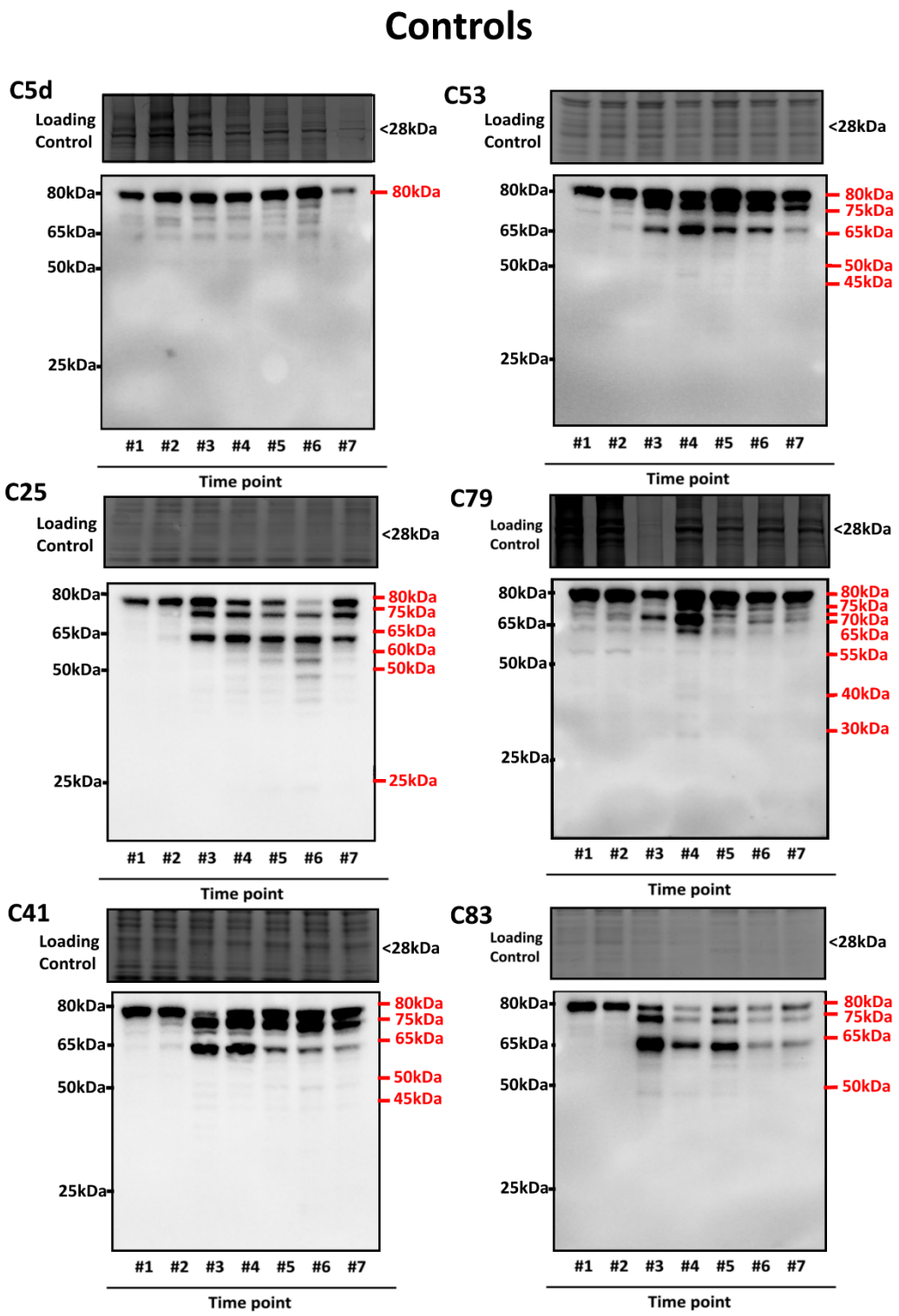

Figure 4.14- SUN2 expression during muscle cell differentiation in control cell lines. *The main isoform of SUN2 (80kDa) was detected across all control cell lines (C5d, C25, C41, C53, C79 and C83), as well as a number of smaller molecular weight bands. The number of smaller sized bands varied between each cell line, however the 65kDa and 75kDa bands appeared to be consistently present and was always seen to appear at time-point 3 onwards, coinciding with the point at which differentiation media was added to the cell cultures. The only exception to this was the C5d cell line, where only the main molecular weight SUN2 band was detected.*

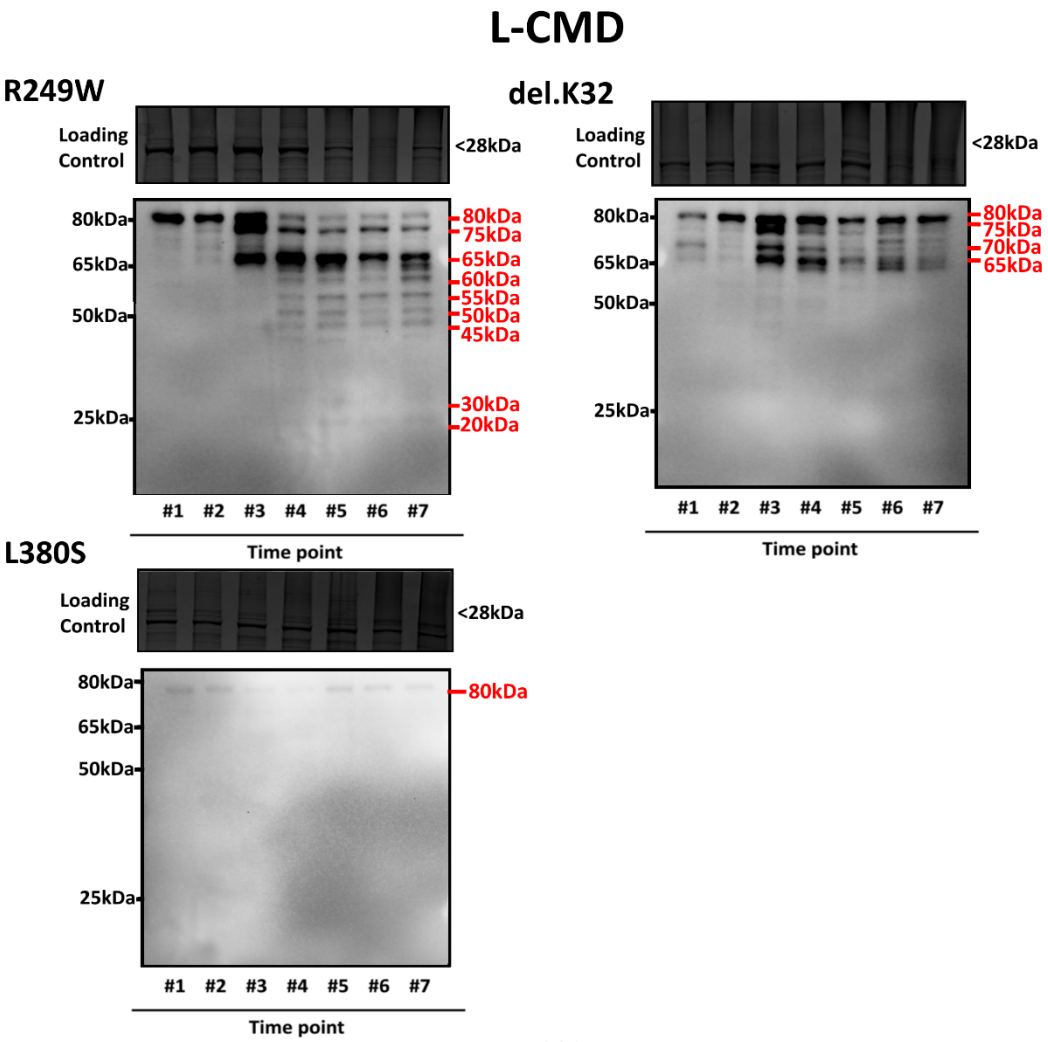

Figure 4.15- SUN2 expression during muscle cell differentiation in L-CMD cell lines. *Similarly, to the control cell lines, lower molecular weight bands were also detected in the L-CMD cell lines (R249W, del.K32, L380S). Again, the 65kDa and 75kDa bands were present. SUN2 was only barely detectable in the L-CMD cell line harbouring a L380S mutation, and only a faint band at 80kDa was observed.*

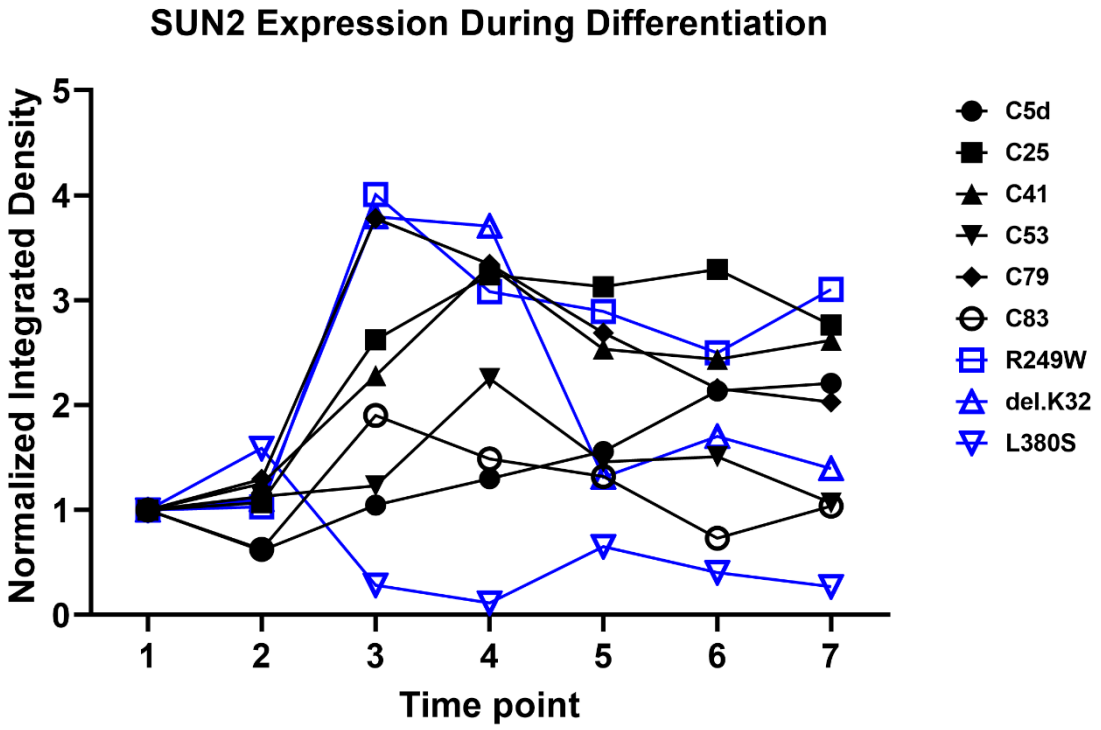

Figure 4.16- SUN2 expression during differentiation across L-CMD and control cells. *SUN2 expression during myoblast differentiation was determined by measuring all bands present in each lane to deduce a total SUN2 quantity at each time-point. There was high variation in SUN2 expression between all L-CMD and control cell lines, perhaps owing to differences in the amount of lower MW SUN2 bands present in each cell line.*

Considering that SUN2 staining appeared reduced in L-CMD myoblasts and myotubes (refer to Section 4.2.9.), SUN2 protein expression was also quantified and directly compared by running L-CMD and control myoblast, and L-CMD and control myotube extracts, side by side on the same western blot. On the resulting blots, the 80kDa band, representing the main SUN2 isoform was measured across all samples. In a separate measurement, the 80kDa band together with any other lower MW bands in each lane were measured, referred to as "total SUN2". This was done to capture any expression changes in the main SUN2 isoform or in all SUN2 isoforms ("total SUN2") in the L-CMD samples. Expression of the main SUN2 isoform did not appear to be reduced in L-CMD myoblasts compared to controls (19.19%, p= 0.401) (**Fig 4.17, A, B**).

However, lower MW SUN2 bands were detected strongly in L-CMD myoblasts which were not detected in the control samples, resulting in total SUN2 being statistically significantly increased in L-CMD myoblasts compared to controls (39.40%, p= 0.022) (**Fig 4.17, A, B**). In the myotube samples, on the other hand, main SUN2 isoform expression was statistically significantly reduced in L-CMD myotubes compared to controls (52.21%, p=0.049), but total SUN2 was not significantly reduced (36.45%, p=0.184) (**Fig 4.17, C, D)**.

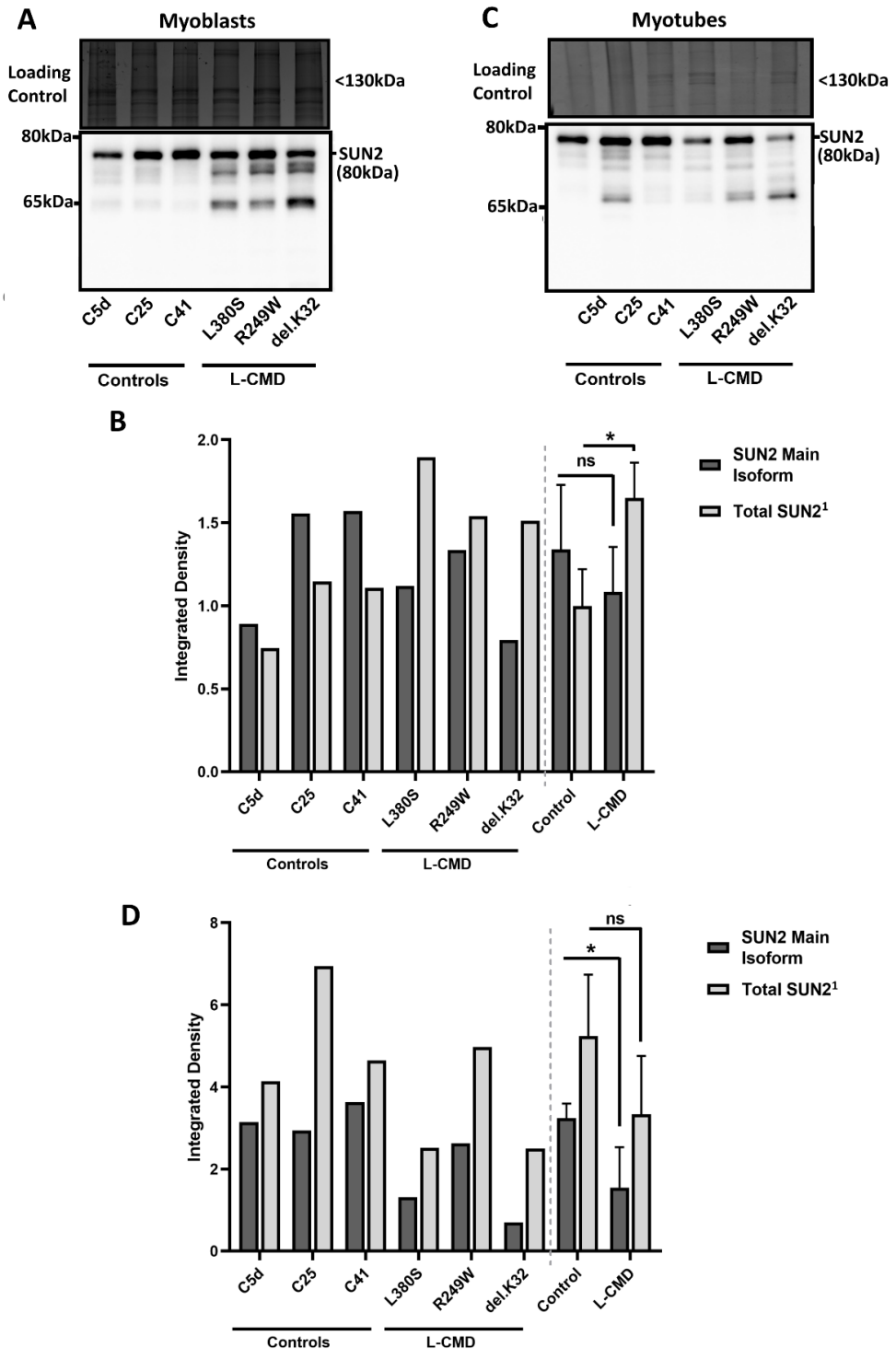

Figure 4.17- Quantification and comparison of SUN2 expression in L-CMD and control myoblasts and myotubes. *(A, B) Expression of the main isoform of SUN2 was not found to be reduced in L-CMD myoblasts compared to controls (19.19%, p=0.401), however total SUN2 was significantly increased in the L-CMD myoblasts compared to controls (39.40%, p=0.022). (C, D) In myotubes, expression of the SUN2 main isoform was significantly decreased (52.21%, p=0.049), but total SUN2 was not significantly changed in expression (36.45%, p=0.184). [1]Total SUN2 is a measurement of all the immunoreactive bands within each lane, as well as the main SUN2 isoform. Two-tailed Student's t-test with unequal variance was used to determine significance, Asterisk (*) indicates significance, ns indicates not significant.*

To clarify whether the lower MW SUN2 bands were cross-reactions of the primary antibody, a polyclonal SUN2 antibody was tested on western blot. Previously a monoclonal antibody had been used, which was specific to amino acid 700 to the C-terminus. The polyclonal antibody was raised against a different region of SUN2, amino acid 391 to 541. If the lower MW SUN2 bands were products of cross-reactions of the monoclonal antibody, these would not be expected to be detected with the polyclonal antibody. It was found that the western blot using the SUN2 polyclonal antibody produced an identical result to the western blot using the SUN2 monoclonal antibody, and the lower MW SUN2 bands were again detected, suggesting that these bands are less likely to be cross-reactions of the antibodies (**Fig 4.18**). The C25 control cell extract used for both western blots using the two different antibodies were also stored and handled identically at the same time, so it is unlikely that there would be differential degradation during sample processing. Although, the possibility that a cellular process is degrading SUN2 at different development stages *in-vitro* cannot be ruled out. The consistent identification of the 65kDa/75kDa bands in particular using western blot may represent lower MW SUN2 isoforms that are being differentially expressed during muscle cell differentiation.

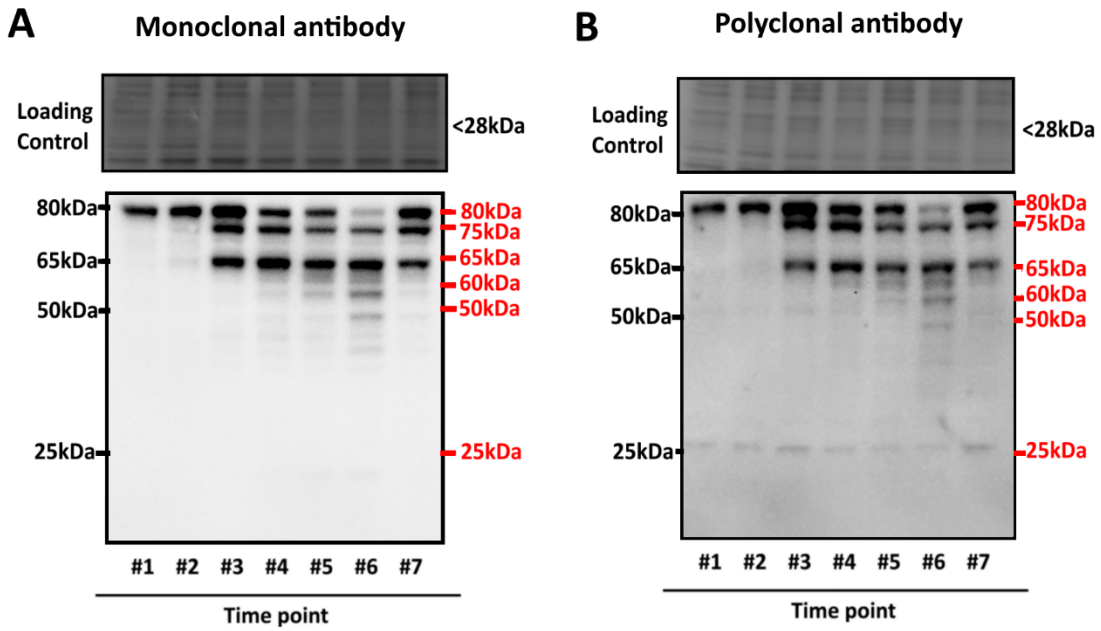

Figure 4.18- Comparative western blots using two different SUN2 antibodies on control cell extracts. *(A) Monoclonal SUN2 antibody and (B) Polyclonal SUN2 antibody produced identical results using C25 control cell extracts on western blot, ruling out the possibility that lower MW bands are cross-reactions of the antibodies.*

The National Centre for Biotechnology Information (NCBI) reports that there are a total of 11 predicted isoforms of SUN2 (**Fig 4.19**), and 22 transcript variants for SUN2 isoforms (Sayers *et al.*, 2022) (**Table 4.2**). For a number of SUN2 isoforms, including isoforms 1, 2, 4, 6, 8, and 11, more than one transcript variants exist which differ from each other by their base pair length. As a number of transcripts are believed to encode the same SUN2 isoform, they likely differ only in the "untranslated regions", whilst their coding sequence and resulting protein are the same. The canonical sequence, or main isoform, of a protein is usually termed "isoform 1". However, in a number of sources, the main isoform of SUN2 is documented as being 717aa in length (Malone *et al.*, 1999; Hoffenberg *et al.*, 2000; Wang *et al.*, 2006), which corresponds to "isoform 2" in the NCBI database. From this point onwards, the SUN2 isoforms will be referred

to as they are described on the NCBI database, therefore the canonical main isoform of SUN2 will be referred to as “isoform 2”.

Very little is known about these SUN2 isoforms other than basic structural parameters. The predicted isoforms range in length from 525-748 amino acids and have MWs of between 58.1kDa and 82.5kDa (**Fig 4.19**). Isoforms 1, 3, and 4 have longer N-termini than the main isoform, due to the presence of an extra exon in their gene sequences. Isoform 5 is also larger than the main isoform due to an exon insertion affecting the length of the C-terminus. This isoform additionally has a unique C-terminus sequence. The remaining isoforms (isoforms 7, 8, 9, and 11) have unique deletions causing the N-termini to be shorter, and isoform 10 also has a unique N-terminus sequence. Isoform 6 is the most similar to the main SUN2 isoform, as the gene sequence for it only differs by a single amino acid.

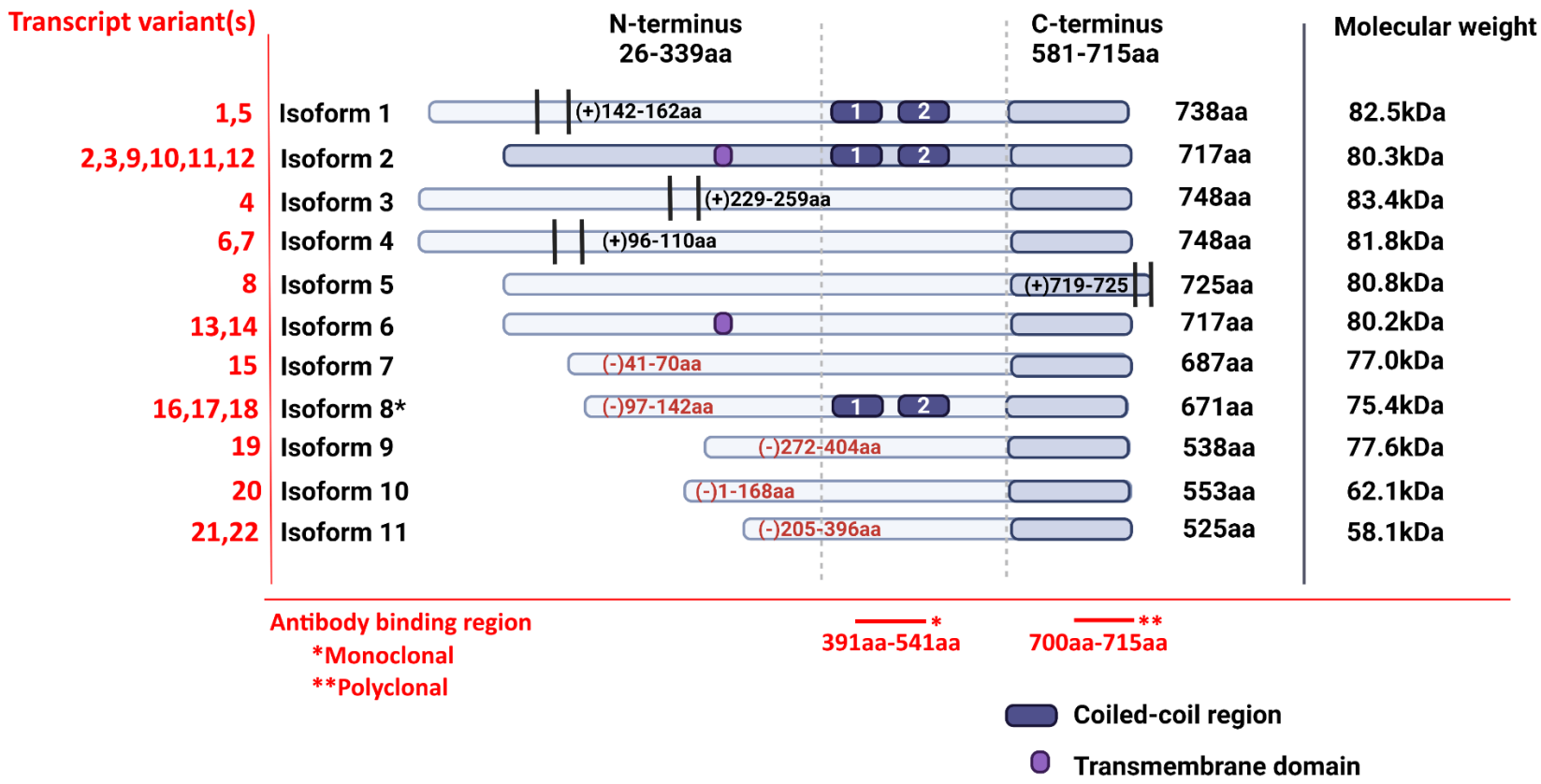

Figure 4.19- Predicted SUN2 isoforms. *There are 11 predicted SUN2 isoforms, ranging in length from 525-748 amino acids, and with molecular weights of between 58.1kDa and 82.5kDa. The main SUN2 isoform is known here as "isoform 2" and is depicted in the figure as being a darker shade of blue. The N- and C-termini for the isoforms were mapped onto their structures and domains and regions are labelled where possible. Isoforms 1, 3, and 4 each have longer N-termini than the main SUN2 isoform, whilst isoform 5 has a longer C-terminus. Isoforms 7, 8, 9, and 11 all have shorter N-termini due to exon deletions, as does isoform 10, as well as possessing a unique N-terminus sequence. Isoform 6 only differs from the main isoform by a single amino acid. The area where the monoclonal and polyclonal antibodies used for western blot may bind to are indicated on the main isoform (isoform 2).*

Table 4.2- Predicted SUN2 isoforms along with their corresponding transcript variant(s)

SUN2 isoform	Transcript variants	Transcript variant used for PCR primer design
Isoform 1	Variants 1, 5	Variant 1
Isoform 2 (main SUN2 isoform)	Variants 2, 3, 9, 10, 11, 12	N/A*
Isoform 3	Variant 4	Variant 4
Isoform 4	Variants 6, 7	Variant 6
Isoform 5	Variant 8	Variant 8
Isoform 6	Variants 13, 14	Variant 14
Isoform 7	Variant 15	Variant 15
Isoform 8	Variants 16, 17, 18	Variant 16
Isoform 9	Variant 19	N/A*
Isoform 10	Variant 20	Variant 20
Isoform 11	Variant 21, 22	Variant 21

In the table, each SUN2 isoform is listed along with its corresponding transcript variant(s). In the final column it is stated which of the variants was used for PCR primer design. Information on SUN2 isoforms and corresponding variants was determined from the NCBI database (Sayers *et al.*, 2022). N/A and Asterisk (*) indicates it was not possible to design primers for these isoforms.

RT-qPCR was used to determine relative transcript expression levels of the isoforms in myoblasts and myotubes from a control cell line (C25), and with a view to identifying any isoforms with increased transcript expression in myotubes compared to myoblasts, corresponding to the western blot results that were previously described. As the 65/75kDa MW SUN2 bands were not detected on western blot at time-points 1 and 2 (when the cells would be proliferating myoblasts) but were present at time-point 3 onwards (when differentiation media was added to the myoblast cultures), it was expected that transcript expression levels of the corresponding SUN2 isoforms may be reduced in myoblasts (or absent) and increased in myotubes.

Unique oligonucleotide sequences (primers) were created for SUN2 isoforms. These were designed based on the transcript variants attainted from the NCBI database (**Table 4.2**). For each isoform, primers were designed based on only one variant. However, it wasn't possible to design primers within the specified parameters for SUN2 isoforms 2 and 9. This was because the sequence for isoform 2 didn't appear to possess any unique characteristics compared to the other isoforms, therefore primers designed for this isoform may be specific to other isoforms. It was not possible to design primers for isoform 9 that had the required GC content and an appropriate melting point whilst remaining unique to the primers for other isoforms. The RT-qPCR results showed that both isoforms 6 and 8 transcript expression levels were significantly increased in myotubes compared to myoblasts (corresponding to time-points 2 and 7) (34% p= 0.0001, 46% p= 0.0047, respectively) (**Fig 4.20**). Isoforms 5 and 7 transcript levels were also identified, although levels were similar in both myoblasts and myotubes.

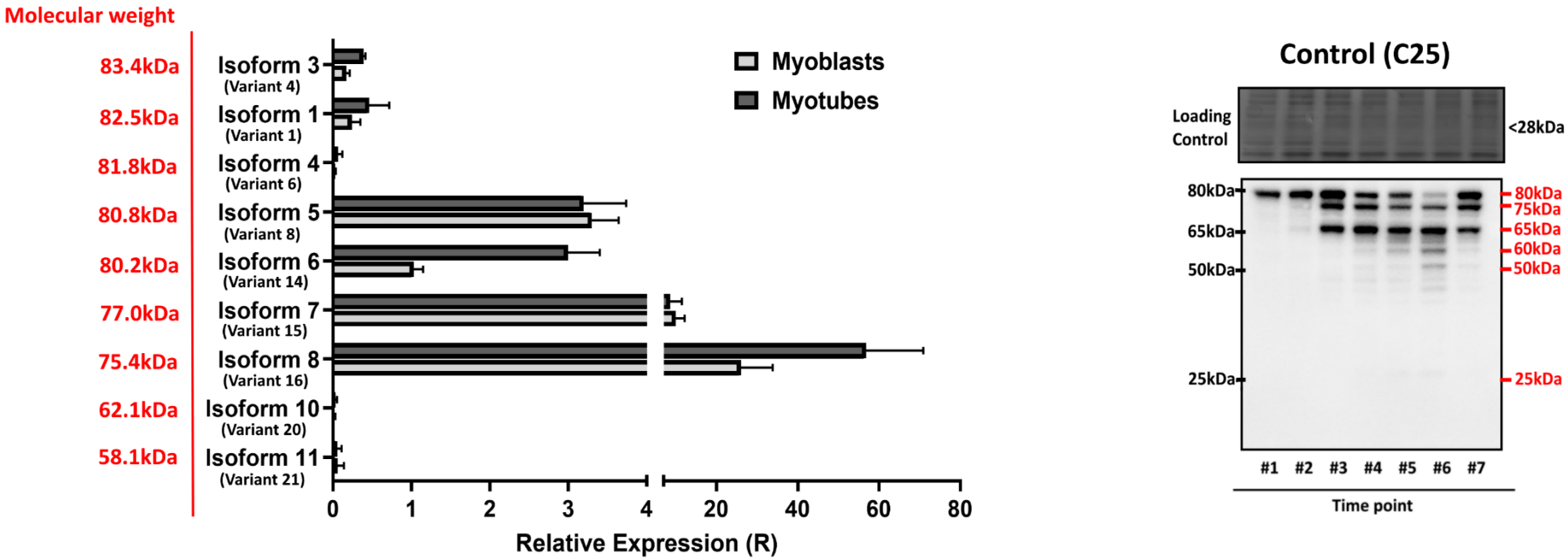

Figure 4.20- Relative expression of SUN2 isoforms in myoblasts versus myotubes. *Unique primers were designed for all SUN2 isoforms except for isoforms 2 and 9 based on transcript variants for SUN2 isoforms obtained from the NCBI database. This allowed the identification of specific SUN2 isoform transcript levels using RT-qPCR. Transcripts were detected for all isoforms, albeit isoform 4, 10, and 11 relative transcript expression levels were very low. Isoform 6 and 8 appeared to be significantly increased in expression in myotubes compared to myoblasts (p= 0.0001, p= 0.0047, respectively), whilst isoforms 5 and 7 were also successfully detected at similar levels in myoblasts and myotubes. Isoform 8 has a predicted molecular weight of 75.4kDa which could correspond to the 75kDa molecular weight band identified on western blot.*

Although the RT-qPCR results revealed that both isoforms 6 and 8 were highly expressed in myotubes compared to myoblasts, isoform 8 possessed characteristics which were fitting with the western blot results. Isoform 8 has a predicted MW of 75.4kDa, suggesting it could be represented by the 75kDa molecular weight band seen in myotubes on the western blots. In contrast, isoform 6 has a predicted molecular weight of 80.6kDa. However, isoform 9 also has a MW of 77.6kDa, meaning that this isoform could also be the 75kDa MW band seen on the western blot. As previously described, it was not possible to create unique primers for isoform 9, therefore isoform 9 expression levels were not evaluated in the RT-qPCR experiment.

Traditional PCR was then conducted on control (C25) myoblast and myotube extracts using the same primers used in RT-qPCR that were unique to isoform 8, and the PCR products were sent for DNA sequencing. If the nucleotide sequence ascertained from the PCR products were homologous to the isoform 8 sequence, this confirms that isoform 8 was the SUN2 isoform that was shown to be increased in expression in myotubes compared to myoblasts, as demonstrated using RT-qPCR. Once the PCR reaction was complete, the products were run on agarose gel electrophoresis to quantify the amount of PCR product in the samples. PCR products were then prepared in a number of different dilutions for DNA sequencing, and both forward and reverse primers were supplied. DNA sequencing reactions run forward and reverse primers as separate reactions. By using both forward and reverse primers, this often allows better coverage of the PCR product sequencing. The chromatograms generated from the DNA sequencing demonstrated that the samples containing the largest quantity of PCR product gave the best results, this was deduced from the chromatograms for these

sequencing reactions having clear, defined peaks, and the reactions having average intensities of 100-500 RFUs (relative fluorescence units) (**Fig 4.21, A**). This RFU value indicates that the reactions will give reasonable-good data, lower values denote weak signal strength and will give poor data (https://dnaseq.co.uk/resources/sequencing/retrieving-and-understanding-the-data). The sequence from the best reactions using the forward and reverse primers were then imputed into the basic local alignment search tool (BLAST) (Altschul *et al.*, 1990). A BLAST search enables a researcher to compare a subject protein or nucleotide sequence (called a query) with a library or database of sequences and identify database sequences that have similarity above a certain threshold (Altschul *et al.*, 1990). BLAST calculated that the forward and backward sequences had the highest similarities with transcript variants 16, 17, and 18, encoding isoform 8. However, an unusual observation was that the forward sequence had to be converted to its reverse complement for the sequence to match with the sequence of SUN2 isoform 8. Due to this, it is suspected that a reverse primer may have accidentally been used instead of the forward primer that was specified and so this result cannot be considered. The reverse sequence had 98.75% similarity with variants encoding isoform 8, and 90% query cover (the percentage of the query sequence length that aligns with the NCBI hit), whilst other SUN2 isoform variants, including the main SUN2 isoform, isoform 2, had between 98.73-98.72% similarity and 88% query cover (**Fig 4.21, B, C**). It was noted that whilst the similarity for the reverse sequence was higher for the transcripts encoding isoform 8, there was high similarity to transcripts for the other SUN2 isoforms. When aligning the sequence generated using the SUN2 isoform 8 reverse primer with the sequence of the main SUN2 isoform, isoform 2 (**Fig 4.21, B**), and then

with the sequence of SUN2 isoform 8 (**Fig 4.21, C**), it showed that the reverse sequence only mismatched with SUN2 isoform 2 by a couple of bases. This might be due to the SUN2 isoforms themselves being very similar, and having identical amino acid base sequences, only differing by insertions or deletions of exons (refer to **Fig 4.19**). However, because of this high similarity between the PCR product sequences and other SUN2 isoform variants as well as isoform 8, it is a possibility that other SUN2 isoforms might have been amplified using the primers that were designed to be specific for isoform 8 during the qPCR and subsequent PCR product sequencing. Therefore, these results cannot confirm that it is SUN2 isoform 8 that is differentially expressed during muscle cell differentiation. An approach that may be considered in future work is to design primers that have a longer length and span a larger area either side of the characteristic deletion in the SUN2 isoform 8 sequence. This would amplify a larger area of the SUN2 isoform 8 sequence that differs to the sequence of the other SUN2 isoforms, and consequently should have a higher similarity to the sequence of isoform 8.

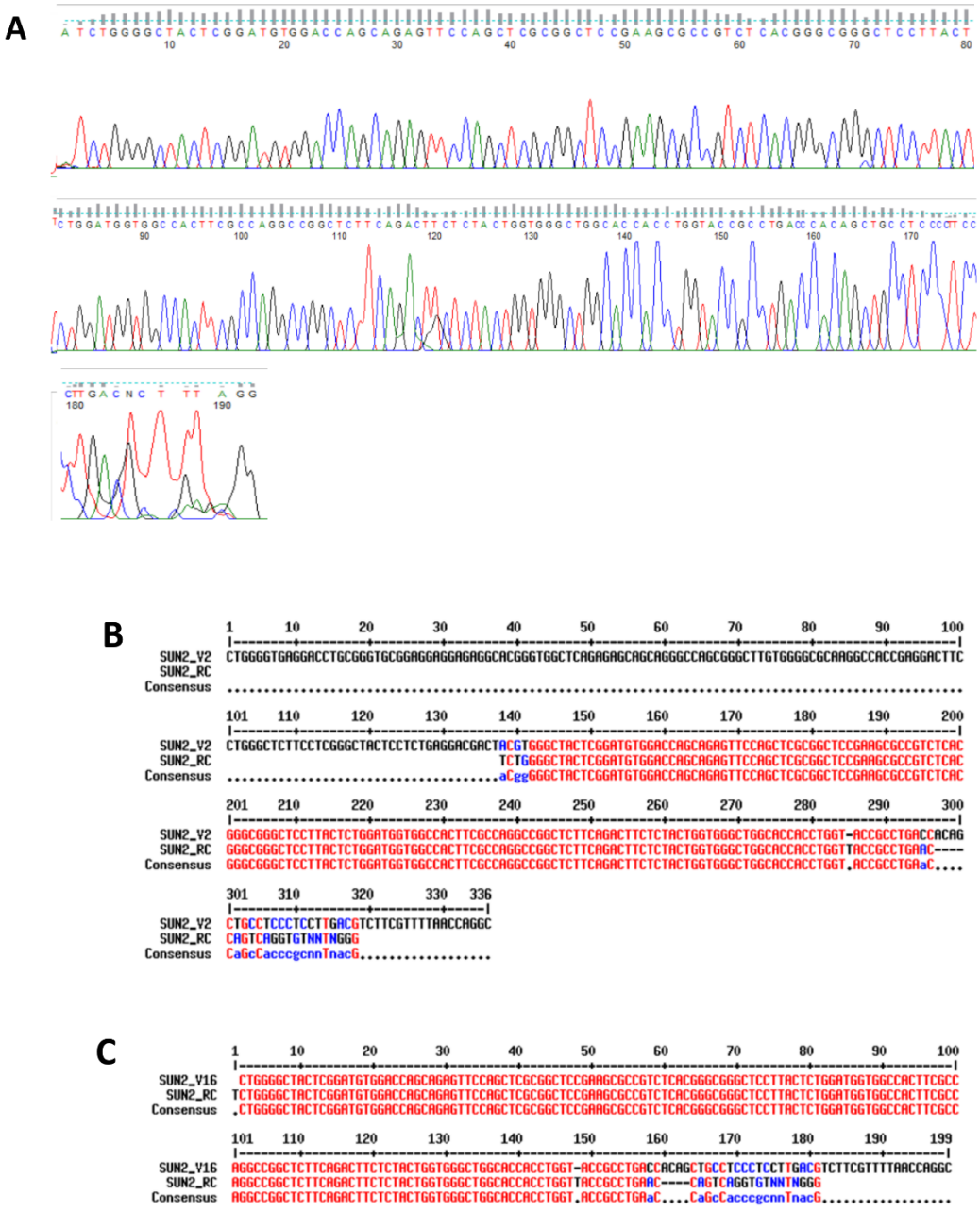

Figure 4.21- PCR product sequencing results. *(A) Chromatogram for the PCR product sequencing reaction using SUN2 isoform 8 reverse primer. This reaction had clear, defined peaks, and an average intensity of 100-500 RFUs (relative fluorescence units). This RFU value indicates that the reactions will give reasonable-good data, lower values denote weak signal strength and will give poor data. (B) Alignment of the sequence generated from using SUN2 isoform 8 reverse primer (reverse complement used) with the sequence of SUN2 isoform 2 (variant 2) (main SUN2 isoform). (C) Alignment of the sequence generated from SUN2 isoform 8 reverse primer with the sequence of SUN2 isoform 8 (variant 16).*

4.3. Summary of results

In culture, the morphology of L-CMD myoblasts do not appear visually different from control myoblasts, appearing as spindle shaped cells which then align and fuse to form multinucleated myotubes that also do not look different from healthy myotubes. Despite the similarities in appearance between the L-CMD cells and controls, a cell growth proliferation assay demonstrated that the L-CMD myoblasts grow at a slower rate than control myoblasts. Immunofluorescent labelling of lamin A/C, the product of the gene that is mutated in L-CMD cells, revealed that myoblasts and myotubes from each of the L-CMD cell lines exhibited abnormal nuclear morphologies, and lamin A/C was found to aggregate in the nucleoplasm in del.K32 L-CMD myoblasts. Lamin A/C expression patterns during myogenic differentiation were variable across all cell lines, and consequently, it was difficult to determine whether lamin A/C expression patterns were altered during differentiation in L-CMD cells. Quantitative comparison of lamin A/C expression in L-CMD and control cells however revealed that lamin A/C were significantly reduced in L-CMD myotubes compared to controls. Emerin, a binding partner of lamin A/C, was mislocalized in R249W L-CMD myoblasts and myotubes, and emerin expression was significantly decreased in L-CMD myotubes compared to controls. SUN2, another known lamin A interactor and integral component of the LINC complex, was correctly localized at the NE across all control and L-CMD cells, although SUN2 staining appeared weaker in L-CMD cells compared to controls. The main isoform of SUN2 was found to be significantly decreased in expression in L-CMD myotubes compared to controls, although there was no reduction of SUN2 in L-CMD myoblasts. SUN2 expression patterns were similar across L-CMD and control cell lines, although quantitative western blotting revealed a number of potential lower MW

SUN2 isoforms across all cell lines that appeared to be differentially expressed during differentiation. RT-qPCR and PCR product sequencing suggested that SUN2 isoform 8 may be highly expressed in myotubes compared to myoblasts during muscle cell differentiation, although further experiments are needed to corroborate this finding.

4.4. Discussion

4.4.1. L-CMD cells exhibited nuclear morphology defects that have been previously observed in cells harbouring *LMNA* mutations

In culture, L-CMD myoblasts and myotubes were indistinguishable from the healthy controls, based on their morphological appearance by microscopy. Immunofluorescent microscopy analysis, however, revealed that the L-CMD cells exhibited abnormal nuclear morphology. This is likely a result of a disrupted nuclear lamina due to mutations in *LMNA*, causing the nucleus to become unstable and fragile (Lammerding *et al.*, 2004). Abnormalities in nuclear structure are a well-known characteristic of *LMNA* mutations and have been previously observed in myoblasts from an Emery-Dreifuss muscular dystrophy (EDMD) patient with a confirmed *LMNA* mutation (Kandert *et al.*, 2009), myonuclei of muscle tissue from EDMD and Limb-Girdle (LGMD) muscular dystrophy patients carrying mutations in *LMNA* (Park *et al.*, 2009), as well as in skin fibroblasts from patients with a number of different laminopathies (Vigouroux *et al.*, 2001; Favreau *et al.*, 2003; Muchir, van Engelen, *et al.*, 2003; Muchir *et al.*, 2004), and in myogenic cells derived from induced pluripotent stem cells (iPSCs) from patients with skeletal muscle laminopathies including L-CMD (Steele-Stallard *et al.*, 2018). The L-CMD patient cell nuclei displayed various irregular shapes which were categorized into nuclear shape abnormalities (i.e., elongated and irregularly shaped nuclei), donuts, nuclear blebbing, and honeycomb structures. Abnormal nuclear morphologies seen in fibroblasts from laminopathy patients have previously been characterized according to these defects (Muchir *et al.*, 2004; van Tienen *et al.*, 2018). The nuclear morphology defects that were observed in the L-CMD cells are likely the consequences of a compromised NL in the cells. How this is linked to disease pathology has already been well-discussed in the form of the structural

hypothesis, with the idea that *LMNA* mutations lead to a weakened NL that results in the nucleus being unable to resist high mechanical strain in tissues exposed to tension, such as skeletal muscle (Davidson and Lammerding, 2014).

Across all of the L-CMD cell lines, it was found that on average around half of the myoblast and myotube nuclei were irregularly shaped. For the L-CMD R249W cell line, though, almost all myotube nuclei exhibited abnormalities, meaning that the number of abnormal nuclei was almost doubled in R249W myotubes compared to in myoblasts. This could suggest that nuclear abnormalities are exacerbated during differentiation in the R249W cells, which has previously not been described before. Some emerin was also found to be mislocalized to the cytoplasm, perhaps specifically the ER, in R249W myoblasts, and not in any other L-CMD cells. This may suggest that the R249W mutation in particular may cause more severe nuclear defects. Emerin was found to be correctly localized in R249W myotubes, however, maybe not supporting the finding that nuclear defects are worsened in R249W myotubes. Previously, emerin has been found to mislocalize and aggregate in foci in iPSC-derived myoblasts, and in the cytoplasm of C2C12 myoblasts harbouring R249W mutations (Steele-Stallard *et al.*, 2018; Gómez-Domínguez *et al.*, 2020).

Emerin has been seen to also be mislocalised to the cytoplasm, particularly the ER, previously in lamin A/C deficient mouse fibroblasts (Holt *et al.*, 2006), lamin A/C -/- mouse embryonic fibroblasts (MEFs) (Sullivan *et al.*, 1999), as well as in fibroblasts from LGMD patients (Muchir, van Engelen, *et al.*, 2003). In Chapter 4, emerin was identified as a well-characterised binding partner of lamin A/C, (Clements et al., 2000), and it has been found that lamin A is involved in tethering emerin to the NE (Vaughan

et al., 2001). Consequently, mutations in *LMNA* may disrupt this interaction and cause emerin to become mislocalized (how loss-of-interactions occur due to mutations is discussed further in Chapter 3, Section 3.3.2). In Chapter 3, Section 3.3.2.2., emerin was identified as a lamin A binding partner in each of the L-CMD cell lines. In addition to this, it is believed that the area of lamin A that binds to emerin is within the region of amino acids 384-566 of *LMNA* (Sakaki *et al.*, 2001; Haque *et al.*, 2010). None of the L-CMD mutations are predicted to affect this region of *LMNA,* therefore, it was not expected that emerin would be found to be mislocalized in any of the L-CMD cell lines. Here, even when some emerin was mislocalized in the R249W myoblasts, there was still a proportion of emerin that was correctly localized to the NE. These results both suggest that lamin A-emerin interactions are not entirely lost and are maybe just somewhat compromised by the *LMNA* mutations.

Loss of emerin from the NE could also have implications in L-CMD disease development, as correct localization is critical for a protein's function (Hegde and Zavodszky, 2019). If a protein is in the wrong environment, it is unlikely to fold or assemble properly, and may also trigger secondary consequences (e.g. protein degradation pathways) that could lead to further detrimental effects inside of the cell (Hegde and Zavodszky, 2019). It has previously been shown that mutant forms of emerin causing X-linked Emery-Dreifuss muscular dystrophy (EDMD) are mislocalised, and it has been proposed that an absence (caused by mutations that result in the deletion of *EMD*) or reduction of emerin at the NE may be responsible for the EDMD phenotype (Fairley, Kendrick-Jones and Ellis, 1999). It has also been found that COS-7 cells expressing mutant emerin (Del236-241, an *EMD* variant found in EDMD patients) that mainly localizes to the cytoplasm exhibit aberrant cell cycle length (Fairley *et al.*,

2002). Considering this has been linked to EDMD development, loss of emerin at the NE could also be contributing to L-CMD pathophysiology. This provides evidence that there may be some cross-over between the mechanisms behind EDMD and L-CMD disease pathways. This may not be surprising when AD and AR-EDMD are also caused by *LMNA* mutations.

Whilst emerin was found to be mislocalized in the R249W myoblasts, the del.K32 myoblasts were the only cells to exhibit mislocalization of lamin A/C. In the del.K32 myoblasts, lamin A/C appeared to be aggregated in nuclear foci within the nucleoplasm. Increased nucleoplasmic aggregation of lamin A/C has been previously observed in L-CMD fibroblasts harbouring the same del.K32 mutation, as well as primary myoblasts derived from the $Lmna^{dK32}$ mouse model of L-CMD (Bertrand *et al.*, 2020). In this study, myotubes harbouring the del.K32 mutation were also found to have almost exclusively nucleoplasmic localization of lamin A/C, although this was not observed here (Bertrand *et al.*, 2020). In the Bertrand *et al.* study, del.K32 myotubes were also found to have disrupted localization of other INM proteins such as emerin, lamin B1, SUN2 or nup153 (further information on where these proteins were mislocalized to is not provided), proving nuclear defects in cells harbouring the del.K32 *LMNA* mutation can also be severe (Bertrand *et al.*, 2020)

Absence of lamin A/C from the nuclear periphery and its accumulation in the nucleoplasm has been shown to be highly detrimental for myoblast differentiation in primary myoblasts derived from the $Lmna^{dK32}$ mouse (Bertrand *et al.*, 2012). This has been attributed to the inability of L-CMD post-mitotic myocytes to sequester muscle-specific NE transmembrane proteins in the nuclear envelope that are required for

chromatin remodelling (Bertrand *et al.*, 2012). Depending on their level of phosphorylation, A-type lamins are able to assemble under the INM (where they are primarily localized), but they may also reside in the nucleoplasm (Torvaldson, Kochin and Eriksson, 2015). A-type lamins at the nuclear periphery are necessary for the nuclear sequestration of NE transmembrane proteins (Sullivan *et al.*, 1999; Libotte *et al.*, 2005; P. Malik *et al.*, 2010; Thanisch *et al.*, 2017), and for the interaction with the cytoskeleton via the LINC complex (Crisp, Liu, Roux, J.B. Rattner, *et al.*, 2006). Other A-type lamin functions such as the regulation of gene transcription, DNA repair, and regulation of cell cycle and mechanotransduction also require lamin A/C to be correctly localized at the NL (Parnaik, 2008; Andrés and González, 2009; Ungricht and Kutay, 2015).

4.4.2. R249W and del.K32 *LMNA* variants exhibit more severe nuclear defects compared to L380S

Based on the evidence outlined above, it appeared that cells harbouring the R249W or del.K32 mutations had more severe nuclear defects than the L380S L-CMD patient cells. This could be a consequence of the region of the *LMNA* gene that is affected by the mutations. The R249W mutation is located at the ERK1/2 binding domain in *LMNA* and causes an arginine residue to be substituted with a tryptophan residue. Arginine and tryptophan have very different properties. Arginine is amphipathic, meaning it has both hydrophilic and hydrophobic parts, however it is often deemed to be the most hydrophilic of all amino acids and due to this it favours the surface of proteins (Betts and Russell, 2003). Tryptophan in comparison is extremely hydrophobic in nature and prefers to be buried in hydrophobic protein cores (Betts and Russell, 2003). As well as

this, tryptophan is the largest amino acid. Arginine is known to be common in binding sites, as its positive charge allows it to interact with negatively charged non-protein atoms (Betts and Russell, 2003). Therefore, if arginine is substituted with another amino acid with different properties, this may affect interactions at these domains. In this case, the R249W mutation could perturb ERK1/2 activity facilitated by an interaction with lamin A/C. Whilst ERK1/2 signaling has not been examined in the context of skeletal muscle laminopathies, ERK1/2 activity has been found to be hyperactivated in hearts from patients with cardiac disease caused by *LMNA* mutations, and in *Lmna*$^{H222P/H222P}$ mice, which is a model of *LMNA*-related cardiomyopathy (Muchir *et al.*, 2007; Muchir, Reilly, *et al.*, 2012). Additionally, *Lmna*$^{H222P/H222P}$ mice treated with an ERK1/2 inhibitor were found to have delayed onset of cardiac pathology and normal nuclear morphology was found to be restored in cardiomyocytes derived from the mice (Muchir, Reilly, *et al.*, 2012). There are 15 records of the R249W mutation causing human disease (The Universal Mutations Database, http://www.umd.be/LMNA/). Of these, 12 cases are related to L-CMD and two are associated with EDMD. Therefore, this mutation is one of the most notorious L-CMD-associated variants.

Unlike the other two *LMNA* mutations which are missense variants, the del.K32 mutation causes an in-frame deletion affecting a lysine residue. Lysine regularly has important structural roles and is involved in the formation of salt-bridges (Betts and Russell, 2003). Similarly, to arginine, lysine is also commonly found in protein binding sites (Betts and Russell, 2003). Lysine possesses a positively charged side chain which may facilitate the formation of hydrogen bonds with negatively charged non-protein atoms (Betts and Russell, 2003). The del.K32 variant is located in the head region of

lamin A/C, which is known to be involved in lamin assembly. Consequently, mutations in this region may lead to nuclear assembly defects, and as a result, a weakened NL, which has previously been observed in cells harbouring *LMNA* mutations (Ostlund *et al.*, 2001; Vigouroux *et al.*, 2001; Muchir, Van Engelen, *et al.*, 2003). The consequences of mutations in the head region of *LMNA* are examined in more detail in Chapter 6, Section 6.3.4.1. The del.K32 variant has been reported in six L-CMD patients, as well as some individuals with EDMD and Limb-Girdle muscular dystrophy. In a study where four L-CMD patients were identified as carriers of the del.K32 mutation, progressive flaccid paralysis was described as a specific phenotypic feature (Dadali *et al.*, 2016).

In comparison, the L380S variant causes a leucine residue to be changed to serine. There are some differences between these two amino acids. Leucine is hydrophobic, so similarly to tryptophan, it chooses to be within the centre of a protein (Betts and Russell, 2003). Serine, on the other hand, can be found both within the interior of a protein or on a protein's surface (Betts and Russell, 2003). Serine is a polar amino acid, but leucine is non-polar (Betts and Russell, 2003). The L380S mutation affects the HCD2 (highly conserved domain) region of *LMNA*, located at the end of the central rod domain, next to coil 2. The importance of this domain and predicted effects of mutations in this region remain unknown. This mutation has only been described in one L-CMD patient, who at seven years old was described as having no head or neck control, respiratory involvement (tracheostomy at 22 months), atrial tachycardia, contractures, and proximal and distal muscle weakness (Quijano-Roy *et al.*, 2008).

Comparing the consequences of each L-CMD *LMNA* mutation, it is likely that the R249W and del.K32 variants could be more damaging compared to the L380S

mutation, and this could be reflected by the finding that the R249W and del.K32 cells appear to exhibit worse nuclear defects compared to the L380S cells.

4.4.3. Lamin A/C expression may be reduced with age which might modulate disease progression in laminopathies

Lamin A/C expression patterns during differentiation appeared incredibly variable across all control and L-CMD cell lines, making it difficult to discern whether these expression patterns are changed in L-CMD cells. This variability could be due to experimental issues with extracting and solubilizing lamin A/C from cell extracts. It did appear, though, that lamin A/C was difficult to detect in the two oldest control cell lines, from donors aged 79 and 83 years old. This suggests that lamin A/C could be reduced in these cell lines, and therefore reduced as an individual ages. Lamin A/C mutations are well known to cause premature aging syndromes such as Hutchinson-Gilford progeria syndrome (HGPS). It is generally believed that mutations in *LMNA* that cause HGPS affect the ZMPSTE24 protease site, which results in the accumulation of truncated forms of prelamin A that remain farnesylated within cells (Pendás *et al.*, 2002; Mutesa *et al.*, 2007; Galant *et al.*, 2016). In particular, this accumulation of pre-lamin A has been attributed to the development of HGPS. Some evidence has suggested that this buildup of farnesyl-prelamin A may also be linked to normal aging, as inhibition of the ZMPSTE24 site has been shown to “reverse” the age phenotype (Scaffidi and Misteli, 2006). In addition to this, other defects observed in HGPS cells have been seen in healthy cells from older individuals such as changes in histone modifications and increased DNA damage (Scaffidi and Misteli, 2006). Reduction of lamin A/C levels have also previously been identified in fibroblasts from older healthy

individuals (81-96 years old) compared to younger healthy individuals (7-11 years old) (Scaffidi and Misteli, 2006).

In combination with laminopathy-causing mutations, a reduction in lamin A/C expression levels over time due to aging might modulate disease progression as a patient ages. As L-CMD is the most severe skeletal muscle laminopathy, patients usually have a very reduced life expectancy (on average, of 18 years, but often patients die much younger), therefore this may not contribute to L-CMD pathophysiology but may be relevant to other laminopathies. Future work might involve assessing lamin A protein expression levels in cells derived from laminopathy patients of different ages to determine whether lamin A is reduced in older patients. If possible, the disease severity could also be assessed in each patient to identify whether reduction of lamin A as a patient ages correlates with increased disease severity.

4.4.4. A gene therapy targeting upregulation of healthy lamin A/C may be a potential strategy to treat L-CMD

Lamin A/C were found to be significantly reduced in L-CMD myotubes compared to controls, and mutant lamin A appeared to be of a lower MW in L-CMD myoblasts compared to healthy lamin A in control myoblasts. In myoblasts and myotubes derived from *Lmna*$^{\Delta K32/\Delta K32}$ mice, a mouse model of L-CMD, reduced levels of lamin A/C protein have also been observed, although *LMNA* mRNA levels were not reduced, suggesting a reduced translation efficiency or higher rate of degradation of mutant lamin A/C (Bertrand *et al.*, 2012). Reduced lamin A/C levels could likely contribute to the L-CMD phenotype, as *Lmna*$^{\Delta K32/\Delta K32}$ mice present with an even more severe phenotype than

Lmna$^{-/-}$ mice (a lamin A/C deficient mouse model of AD-EDMD) (Bertrand *et al.*, 2012). Whilst *Lmna*$^{-/-}$ mice present with growth retardation, skeletal and cardiac muscle involvement, hypoglycemia and sudden cardiac death, this phenotype was exacerbated in *Lmna*$^{\Delta K32/\Delta K32}$ mice (Bertrand *et al.*, 2012). The result presented here that lamin A/C were reduced across all myotubes differentiated from each of the L-CMD cell lines harbouring different *LMNA* mutations corroborates Bertrand *et al.'*s findings and suggests reduced lamin A/C may be conserved across different L-CMD-causing mutations. Furthermore, the lower MW mutant lamin A observed in L-CMD myoblasts suggests that lamin A is also truncated. Truncated lamin A would not be able to function in the same way as healthy lamin A or interact with proteins within lamin A's interactome. It was unexpected that lamin A may be truncated in each of the cell lines as R249W and L380S are missense *LMNA* mutations (refer to Section 3.3.2. where the consequences of each mutation on the protein structure are discussed in detail), whilst truncated lamin A would more likely be produced from the del.K32 mutation.

These two findings may help to guide future research in L-CMD, as a therapeutic approach could be to upregulate lamin A/C production. It is important, however, to bare in mind that too much lamin A/C overexpression has toxic effects (Bechert *et al.*, 2003; Favreau *et al.*, 2003). Based on the finding that lamin A/C is reduced in *Lmna*$^{\Delta K32/\Delta K32}$ mice, spliceosome-mediated RNA trans-splicing (SMaRT), an approach that targets RNA at the pre-mRNA level and converts endogenous mutated sequences into wild type ones has already been used to target the del.K32 L-CMD mutation (Azibani *et al.*, 2018). To achieve this, 5'-RNA pre-*trans*-splicing molecules containing the first five exons of *Lmna* and targeting intron 5 of *Lmna* pre-mRNA were developed

and their efficacy at inducing *trans*-splicing events on *Lmna* were tested and confirmed at the protein level in C2C12 myoblasts (Azibani *et al.*, 2018). This approach was then tested *in-vivo* in newborn mice using adeno-associated virus (AAV) delivery, although the efficacy of *trans*-splicing events were low (Azibani *et al.*, 2018). Despite this, these results provide the first evidence for reprogramming *LMNA* mRNA *in vitro*.

4.4.5. Emerin expression patterns are variable in controls and L-CMD cells, but emerin is reduced in L-CMD myotubes

In control cells, it was found that generally emerin expression was decreased in myotubes compared to myoblasts. In comparison, in L-CMD cells, emerin appeared to be expressed at a more consistent level across time-points during differentiation, suggesting that emerin expression patterns during differentiation may be altered in L-CMD. A quantitative comparison of emerin expression in L-CMD and control myoblasts revealed that emerin expression levels were not found to be significantly decreased in L-CMD myoblasts but was significantly decreased in L-CMD myotubes compared to controls.

Emerin is known to be involved in processes in the early stages of myogenic differentiation, such as the regulation of myogenic signalling pathways including Wnt, IGF-1, TGF-ß, and Notch pathways which are involved in myogenic differentiation and muscle regeneration (Massagué *et al.*, 1986; Polesskaya, Seale and Rudnicki, 2003; Koch and Holaska, 2012). Furthermore, emerin has been shown to associate with genomic loci of muscle differentiation promoting factors in murine myogenic progenitors including *Myf5* and *MyoD,* as well as *Pax7* (Demmerle, Koch and Holaska, 2013). If emerin has more important roles during the beginning of myogenic

differentiation, maybe it is not as required in the later stages of differentiation, when myotubes are fully formed, and therefore is expressed at lower levels. In C2C12 myoblasts, however, it has been found that emerin was decreased in myoblasts, but was highly expressed in developing myotubes during the early stages of cell fusion (Lattanzi *et al.*, 2003). This does not align with the finding that across controls, emerin was generally reduced in myotubes compared to myoblasts. In the cell lines where emerin was reduced in myotubes, emerin was highly detectable in myoblasts. For the L-CMD cells, as well as one of the control cell lines, whilst emerin expression appeared more stable during differentiation, there was a slight increase in expression at the time-point where myoblasts begin to fuse together to form myotubes. This supports the finding by Lattanzi *et al.*. The discrepancies between emerin expression in controls and in the Lattanzi *et al.* study and L-CMD cells, therefore may be because emerin expression is generally variable during differentiation and does not follow a distinct pattern, or might be due to experimental differences. Further clarification is needed on the matter. To confirm whether emerin is reduced in control myotubes compared to myoblasts, RT-qPCR could be used to determine emerin transcript expression levels in the cells. As emerin was also found to be reduced in L-CMD myoblasts and myotubes compared to controls, but the reduction was not statistically significant, RT-qPCR could also be used to determine whether emerin transcript levels are also reduced in L-CMD myoblasts. Whilst emerin has been found to be mislocalized in various cells from laminopathy patients including L-CMD (as discussed in Section 3.3.1.), it is unclear whether the levels of emerin are altered in expression in these cells. As outlined in Section 3.3.1, reduced emerin expression or loss-of-interaction

between lamin A and emerin as a result of *LMNA* mutations could contribute to the mechanisms underpinning L-CMD.

4.4.6. SUN2 isoform 8 may be differentially expressed during muscle cell differentiation

SUN2 expression patterns were compared across L-CMD and control cell lines using western blotting. Generally, there appeared to be no obvious differences in SUN2 expression patterns during muscle cell differentiation across all L-CMD cells compared to controls. However, SUN2 was more difficult to detect using immunofluorescence microscopy in L-CMD myoblasts and myotubes compared to controls, and a quantitative comparison of SUN2 expression found that the main isoform of SUN2 was reduced in expression in L-CMD myotubes compared to controls. This suggests that, similarly to emerin, SUN2 expression is affected by *LMNA* mutations. It was also noticed that when comparing SUN2 expression in L-CMD myoblasts compared to controls, there were additional lower MW bands in the L-CMD myoblasts that were not present in control myoblasts. This could suggest that lower MW isoforms of SUN2 are expressed in L-CMD myoblasts that are not expressed in control myoblasts. Alternatively, these bands may indicate degradation of the main isoform of SUN2 in L-CMD myoblasts, which may be a result of interactions between SUN2 and lamin A becoming compromised due to *LMNA* mutations in L-CMD myoblasts.

Through assessing SUN2 expression patterns in L-CMD and control cells, lower MW bands were identified in most cell lines, indicating potential SUN2 isoforms. These lower MW bands appeared to coincide with the point where differentiation was induced in the cell cultures and were undetected in myoblasts. The canonical

sequence for the main SUN2 isoform is 717aa long, producing a product with a MW of 80kDa. There are a further 10 predicted isoforms of SUN2, mostly smaller in size and ranging in length from 525aa-748aa (Sayers *et al.*, 2022). Although the sequences for these isoforms are available in various databases, there are no published studies on them. Hence, there is little known about SUN2 isoforms other than their structure. The lower MW bands identified using western blot that consistently appeared across the majority of cell lines had a MW of 65kDa and 75kDa. The SUN2 isoform closest in MW to 65kDa is isoform 10, which is predicted to be 62.1kDa in size, whilst isoforms 7, 8 and 9 have MWs of 77.0kDa, 75.4kDa, and 77.6kDa, respectively, so could represent the 75kDa band. RT-qPCR identified that the only isoform to be significantly increased in expression in myotubes compared to myoblasts was isoform 8, and PCR product sequencing was used to confirm that isoform 8 was being identified using RT-qPCR. Therefore, taking these results together, SUN2 isoform 8 is likely differentially expressed during muscle cell differentiation. It is however important to consider that it was not possible to rule out that isoform 9 was the 75kDa band seen on western blots. This was because it was not possible to design primers that were both unique to isoform 9, and that had the optimum properties (i.e. appropriate GC content or melting point). As a result, the relative expression levels of isoform 9 could not be determined using RT-qPCR in myoblasts and myotubes.

RT-qPCR also revealed that SUN2 isoform 6 was highly expressed in myotubes compared to myoblasts, however this isoform has a predicted MW of 80.6kDa, therefore it would more likely correspond to the larger 80kDa band that was believed to be the main SUN2 isoform, instead of the lower 65kDa or 75kDa bands. Isoform 6 is almost identical in structure to the main isoform, only differing by a single amino acid.

It would be impossible to separate the main SUN2 isoform and isoform 6 bands on western blot, given their almost identical sizes.

SUN2, along with giant nesprins 1 and 2, form the main components of the LINC complex by interacting at the perinuclear space and forming the bridge between the INM and the ONM. Although previously SUN2 isoforms have not been found to be altered in expression during differentiation, nesprins have been found to switch isoforms at the NE during muscle development (Randles *et al.*, 2010). Considering their similar roles in linking the nucleus to the cytoskeleton, it may therefore be plausible that SUN2 isoforms similarly change isoforms during this period. The change in expression of nesprin-1 to nesprin-2 during muscle fibre maturation seems to coincide with the switch to mature patterns of gene expression that occurs during later foetal development (Randles *et al.*, 2010), therefore it is plausible that certain SUN2 isoforms could become more dominant when signaling pathways are being activated during muscle cell differentiation or myotube fusion.

During early myogenesis, nesprin-1 was found to be increased *in vitro*, however during the transition from immature to mature muscle fibres *in vivo*, nesprin-2 appeared to partly replaced nesprin-1 at the NE and short nesprin isoforms became dominant (Randles *et al.*, 2010). Unlike the SUN2 isoforms which differ in size from each other by 10-20kDa, short nesprin isoforms are much smaller than the giant counterparts. Giant nesprin-1/2 are huge 1000kDa proteins, whilst the smaller nesprin isoforms are 60kDa-120kDa in size (Randles *et al.*, 2010; Duong *et al.*, 2014). Nuclear rim staining was found to be very strong for both nesprins in myofiber nuclei in adult human skeletal muscle biopsy sections (Randles *et al.*, 2010). However, in regenerating fibres in

muscle biopsies from Becker muscular dystrophy patients, nesprin-1 staining was stronger than in surrounding fibres, suggesting that immature muscle fibres preferentially express nesprin-1 (Randles *et al.*, 2010). In contrast, SUN1 and SUN2 remained unchanged in regenerating fibres (Randles *et al.*, 2010). This difference was also shown on western blots of myotube cultures, where it was found that nesprin-1 was highly expressed whilst nesprin-2 expression remained low, reflecting what was seen *in-vivo* (Randles *et al.*, 2010). Shorter nesprin isoforms, including nesprin-1-α, nesprin-2-α and nesprin-2-α-2, were seen to be very prominent in human skeletal muscle extracts on western blot, whilst both nesprin giants appeared to be lower in expression in comparison (Randles *et al.*, 2010).

On western blot, it was observed that SUN2 isoform 8 was expressed from the time point where differentiation was initiated, to the point where myotubes were fully formed. SUN2 is known to be involved in rearward positioning of the nucleus, which contributes to centrosome orientation and polarity for migration and fusion of myoblasts and formation of myotubes (Chang *et al.*, 2015). When differentiation is initiated, myoblasts will begin to fuse with one another and as myotubes form, the mechanisms involved in nuclear positioning will be activated. Therefore, the expression of this isoform appears to coincide with the period of differentiation where SUN2 is known to have an active role in nuclear positioning. Whilst it may be necessary for the main SUN2 isoform to be consistently expressed in myoblasts and myotubes as it is needed to maintain the connection between the nucleus and the cytoskeleton, perhaps SUN2 isoform 8 primarily has a role in nuclear positioning, so is highly expressed during this time. Future work should aim to clarify the functions of SUN2 isoform 8, this could be assessed by “knocking-out” isoform 8 from control myoblasts

and determining whether nuclear-cytoskeleton connections and nuclear positioning are affected.

It is important to note that a limitation of this experiment was that it was not possible to determine the expression of the main SUN2 isoform in myoblasts and myotubes using RT-qPCR, as it was not possible to design primers that were unique to this isoform. It was also noticed that there was some discrepancy across different information sources over the nomenclature of the SUN2 isoforms. As mentioned previously, the NCBI database was used to derive nucleotide sequences for eleven SUN2 isoforms (Sayers *et al.*, 2022). The canonical sequence of SUN2 is described consistently across NCBI, UniProt, and published articles. This sequence encodes a 717aa protein. It would be expected that the main isoform of SUN2, produced from the canonical sequence would be labelled SUN2 isoform 1, however on NCBI, the main SUN2 isoform is identified as SUN2 isoform 2. Instead, NCBI list SUN2 isoform 1 as a 738aa protein. Other sources including UniProt and research articles describe the main 717aa SUN2 isoform as SUN2 isoform 1, which has an identical sequence to SUN2 isoform 2 listed on NCBI (Malone *et al.*, 1999; Hoffenberg *et al.*, 2000; Wang *et al.*, 2006). The differences in naming of SUN2 isoforms is extremely confusing, however, as SUN2 transcript variant sequences were derived from NCBI, and to avoid further confusion, within this study the isoforms are named to match how they are documented on NCBI. Therefore, the main 717aa SUN2 isoform was referred to throughout this experiment as SUN2 isoform 2.

Another observation was that the western blots revealed that the bands corresponding to the MW of isoform 8 (75kDa) appeared to not be present in

myoblast samples, however RT-qPCR detected isoform 8 in both myoblast and myotube samples from the C25 control cell line, albeit transcript levels were significantly higher in myotubes. In RT-qPCR, RNA is extracted from cell pellets and reverse transcribed into complementary DNA (cDNA). The cDNA is then used as a template for the qPCR reaction to analyse gene expression. In comparison, western blotting measures protein expression. It is widely known, however, that transcript and protein levels frequently do not correlate (Gry *et al.*, 2009; Edfors *et al.*, 2016; Jiang *et al.*, 2020). Therefore, this could be a reason why differences were seen between SUN2 isoform 8 protein levels on western blot, and SUN2 isoform 8 transcript levels detected by RT-qPCR.

4.5. Conclusions

Through characterising myoblasts and myotubes derived from L-CMD patients harbouring L380S, del.K32 and R249W *LMNA* mutations, it was observed that all L-CMD cell lines exhibited abnormal nuclear morphology. As well as this, expression of lamin A/C was significantly reduced in L-CMD myotubes, and lamin A/C binding partners emerin and SUN2 were significantly decreased in expression in L-CMD myotubes. These findings provide further evidence to guide the direction of future research and therapy development in L-CMD.

Abnormal nuclear morphology is likely due to a compromised NL. As this was a feature that was conserved across all L-CMD cells, future studies might aim to target the NL to make it more stable and resistant to damage. Other indicators of a lack of nuclear integrity were nucleoplasmic aggregation of lamin A/C in del.K32 myoblasts, and mislocalization of emerin in R249W myoblasts.

Lamin A/C expression was significantly decreased in L-CMD myotubes, aligning with previous findings that lamin A/C protein levels are reduced in myoblasts and myotubes from the *Lmna*$^{\Delta K32/\Delta K32}$ mouse. Significant reduction of lamin A binding partners, emerin and SUN2, in L-CMD myotubes also indicates that *LMNA* mutations affect expression of these proteins. This may be due to *LMNA* mutations affecting lamin A's affinity to interact with other proteins and anchor them at the NE. Consequently, if these proteins are mislocalized they may degrade and therefore be reduced in expression. However, emerin mislocalization was only observed in R249W myoblasts, and SUN2 was correctly localized across all L-CMD cell lines. A future approach to therapy in L-CMD could be to develop a gene therapy such as spliceosome-mediated RNA trans-splicing (SMaRT), an approach that has been attempted by Azibani *et al.* to correct the genetic defect and result in production of wild type lamin A/C instead of mutant lamin A/C (Azibani *et al.*, 2018). This would both increase the expression of lamin A/C, and produce functional, healthy lamin A/C that is able to correctly interact with its binding partners.

Chapter 5: Proteomic identification of differentially expressed proteins in L-CMD myoblasts and myotubes

5.1. Introduction

Proteomics is the large-scale study of the complete proteome within a sample; the proteome being the assortment of proteins produced at a specific time in a particular cell or tissue type. Proteomics aims to investigate how different proteins interact with one another and the roles they play within the cell or tissue sample. Using proteomics, the proteins that are expressed in a cell or tissue sample can be identified, then bioinformatics tools can be used to piece together molecular pathways that the identified proteins may be involved with. Whilst protein expression can be assessed using techniques such as western blotting, this requires prior knowledge of the protein(s) of interest, as well as multiple experiments. Proteomics allows the quantification of proteins within a sample using a global, unbiased approach. Proteomics typically employs the use of mass spectrometry (MS) for high-throughput identification of multiple proteins per sample, and with improvements in sensitivity and accuracy of MS technology in recent years, proteomics has become a popular technique used to conduct quantitative comparisons of tissues or cells derived from models of disease. This approach provides insight into the dysregulated processes underlying disease, by determining differentially expressed proteins in disease-relevant cells or tissues.

5.1.1. Proteomic studies in laminopathies and other neuromuscular diseases

Studies in L-CMD have mostly focused on characterising patient fibroblast cells (Barateau *et al.*, 2017), cells transfected with L-CMD-causing *LMNA* mutations (Bertrand *et al.*, 2020; Gómez-Domínguez *et al.*, 2020; Owens *et al.*, 2020), or mouse embryonic fibroblasts and tissue including skeletal muscle, the heart, and adipose

tissue from the *Lmna*$^{\Delta K32/\Delta K32}$ mouse model of L-CMD (Bertrand *et al.*, 2012), using techniques such as western blotting, histological staining, immunofluorescence microscopy, nuclear morphology evaluation methods, and cell assays to determine parameters including senescence rate and myogenic differentiation rate, as previously discussed in more detail in Chapter 4, Section 4.1.1. This has elucidated some mechanisms underlying L-CMD pathophysiology, however many of the molecular pathways downstream of the *LMNA* mutations remain unknown. Currently, there appear to be no obvious reports in the literature of quantitative proteomic studies in L-CMD. In addition to this, whilst proteomic studies are emerging in the wider field of laminopathy research, there seems to be no reports of proteomic analysis on muscle tissue or cells from skeletal muscle laminopathy patients.

In respect of proteomic studies of laminopathies more broadly, Magagnotti *et al.* produced the first proteomic study on cells from laminopathy patients (Magagnotti *et al.*, 2012). Skin fibroblasts from *LMNA* mutation carriers with personal or family history of skeletal or cardiac muscle disorder including Limb-girdle muscular dystrophy (LGMD), Emery-drefiuss muscular dystrophy (EDMD), familial partial lipodystrophy (FPLD) and dilated cardiomyopathy (DCM), arrhythmogenic right ventricular dysplasia (AVRD) or atrial fibrillation (AF), were subjected to proteomic analysis to identify differentially expressed proteins compared to controls (Magagnotti *et al.*, 2012). The control groups included patients affected by myopathy or muscular dystrophy not related to *LMNA* mutations (neuromuscular disease controls) and unaffected subjects (healthy controls) (Magagnotti *et al.*, 2012). GO and principal component analysis (PCA), together with western blot (WB) validation, suggested that *LMNA* defects affect primarily the expression of proteins that are involved in cytoskeleton organization,

energy metabolism and oxidative stress response, even when compared to other neuromuscular disorders (Magagnotti *et al.*, 2012). Although using patient fibroblasts is not necessarily pathologically relevant to skeletal muscle laminopathies, important insights into the mechanisms downstream of *LMNA* mutations in laminopathies can be made from this study.

In addition, Izquierdo *et al.* conducted a proteomic analysis of plasma samples from a family with an *LMNA* mutation related to DCM and sudden death (Izquierdo *et al.*, 2016). Plasma samples from four patients with clinical symptoms were compared to samples from healthy donors, and differentially regulated proteins were identified. In doing this, 14 differentially expressed proteins were identified that play a central role in the activation of the complement system and are involved in inflammatory response (Izquierdo *et al.*, 2016). Other dysregulated proteins were essential for the maintenance of haemostasis and platelet activation, blood coagulation, and thrombus formation (Izquierdo *et al.*, 2016). As well as these, clusterin, a ubiquitous anti-apoptotic protein involved in oxidative-stress protection was identified, along with essential components of the cytoskeleton and cell signalling proteins (Izquierdo *et al.*, 2016). For validation studies, five proteins were chosen that were related to cardiovascular events that were also upregulated in the DCM group. In doing this, vitamin-D binding protein, secreted clusterin, and antithrombin-III were confirmed as augmented in the DCM group and represent putative biomarkers for the evaluation of *LMNA*-DCM, as well as sudden death (Izquierdo *et al.*, 2016).

Away from research in disorders caused by mutations in *LMNA*, proteomics is a strategy that has gained momentum in other neuromuscular disorders and muscular

dystrophies. Duchenne muscular dystrophy (DMD) is the most common dystrophy, and the most thoroughly investigated using proteomics methodologies (Fuller, Graham, *et al.*, 2016). DMD is caused by mutations in the dystrophin gene, leading to ablation of the cytoskeleton protein, dystrophin (Bonilla *et al.*, 1988). A number of publications from several different research groups have utilized quantitative proteomics technologies to identify differentially expressed proteins in various models of DMD, including the mdx mouse model of DMD (Rayavarapu *et al.*, 2013), material from DMD patients (Cynthia Martin *et al.*, 2014; Rouillon *et al.*, 2014), and the golden retriever muscular dystrophy model (Guevel *et al.*, 2011), compared to control subjects. Proteomic studies in DMD have identified a number of proteins that are consistently changed in expression across multiple separate proteomic comparisons. For example, increased expression of type III intermediate filament proteins, desmin and vimentin, as well as other structural proteins including beta-tubulin, lamin A/C, lamin B1 and spectrin alpha chains, as well as proteins associated with protein assembly (Holland, Henry, *et al.*, 2015). This perhaps represents an attempted compensatory response to stabilize a weakened cytoskeleton (Holland, Henry, *et al.*, 2015). As well as this, several proteins associated with cell stress response were elevated in multiple proteomic studies of DMD tissue, such as heat shock proteins. The increased expression of these proteins correlates with their known involvement in dystrophin-deficient muscles (Brinkmeier and Ohlendieck, 2014). Increased levels of serum albumin have also been detected across multiple separate proteomic comparisons of DMD versus control tissues, which probably reflects the increased membrane permeability of the target tissues (Holland, Dowling, *et al.*, 2015). Increased membrane permeability is a characteristic feature of DMD and multiple

theories exist about what causes this including contraction-induced tears due to fragility of the already weakened membrane, oxidative damage to membranes, or altered regulation of calcium ion channels (Allen and Whitehead, 2011).

In the case of DMD, as well as other neuromuscular disorders where a large number of proteomic studies have been done, the use of a variety of different experimental models and sample types can unavoidably result in the identification of model or tissue-specific pathogenic patterns that are difficult to isolate from core molecular disease pathways. Consequently, translation of these findings into other experimental models can therefore be challenging and demands careful examination and selection of targets from a long list of protein changes. Whilst this is a complexity that is brought about by the ability to generate large datasets, the identification of commonalities across multiple studies can, however, strengthen findings and highlight things that may have previously been overlooked.

As well as DMD, a number of studies utilizing proteomics have emerged in the literature surrounding less prevalent muscular dystrophies, with the aim of furthering our understanding of the molecular mechanisms underlying the downstream effects of causative mutations by comparing protein expression in human patient tissue to controls, to try and distinguish dysregulated proteins in these muscular dystrophy subtypes (Fuller, Graham, *et al.*, 2016). This has enabled the discovery of differentially expressed proteins, which indicates potentially biological functions and pathways involved in the pathogenesis of these diseases, as well as potential biomarkers for monitoring disease progression and treatment efficacy.

5.1.2. Proteomic methods

There are a number of different acquisition approaches that have been developed for mass spectrometry (MS) analysis to allow the identification and/or quantification of peptides in a sample that have been generated by proteolysis. Two complementary strategies currently exist, targeted and untargeted. The untargeted method, often known as shotgun or discovery proteomics (Zhang *et al.*, 2013), aims at discovering unknown proteins of interest, whilst the targeted approach usually refers to multiple reaction monitoring (MRM), where multiple target peptides and their corresponding transition ions are selected manually for analysis with higher sensitivity and reproducibility (Picotti and Aebersold, 2012).

In each of the proteomic methods, a protein sample is digested into peptides, usually by trypsin, then the peptide mixture is fractionated by liquid chromatography before it is subjected to MS analysis. In MS, peptides are ionized and specific precursor ions are selected from the pool of detected peptide ions for fragmentation. The resulting product-ion mass spectra, commonly generated by collisional activation (where energy is put into the ions which gets distributed inside and bond cleavage can then take place, producing fragment ions), are recorded and used to determine the amino acid sequence of the selected peptides. Finally, the proteins present in the sample are deduced from the ensemble of identified peptides.

Shotgun proteomics analyses proteolytic proteins by data-dependent analysis (DDA) selection of precursor ions to generate fragment ion scans and allows the identification of thousands of proteins from a complex sample using database searching (Mann *et al.*, 2013). Stable-isotope labelling strategies can also be implemented for relative or absolute quantification of identified proteins using this

method (Yates and Washburn, 2013). In comparison, in MRM, a sample is queried for the presence and quantity of a limited set of peptides that have to be specified prior to data acquisition (Gillet *et al.*, 2012). MRM is a label-free approach and is believed to have enhanced quantification accuracy over other label-free methods (Addona *et al.*, 2009). The throughput of MRM, however, is limited as all of the transition ions have to be queued for measurement one after another (Huang *et al.*, 2015). This makes MRM useful for only studying a few target proteins. To summarise, shotgun proteomics is useful for discovering the maximal amount of proteins from one or more samples, whereas MRM, or targeted proteomics, is better suited for the reproducible detection and accurate quantification of specific sets of proteins (Gillet *et al.*, 2012).

Sequential window acquisition of all theoretical mass spectra (SWATH™) can be explained by MRM on a large-scale with increased throughput that is achieved by using data-independent acquisition (DIA) (Gillet *et al.*, 2012). SWATH continuously fragments all the peptides with stepped *m/z* windows (Huang *et al.*, 2015). The resulting transition ions are matched to a spectral library and generate peptide/protein identification and quantification results. SWATH™ method heavily relies on the peptide spectral library, which is required to be established beforehand usually by shotgun/DDA proteomics (Huang *et al.*, 2015). In terms of quantification power, SWATH™ combines the advantages of both DDA and MRM (**Table. 5.1**). Data acquisition is relatively easy, and it allows the identification of large numbers of proteins similarly to DDA, however the reproducibility and data consistency is similar to MRM. SWATH™ also allows for MS/MS-based label-free quantification and discrimination of isobaric peptides. The main drawback to this method is the difficulty of data analysis, as currently sophisticated software and large informatics resources

are required, whilst this is much easier for DDA and MRM proteomics (Ludwig *et al.*, 2018b).

Table 5.1- Comparing the advantages and disadvantages of SWATH™-MS, data-dependent acquisition (DDA) and targeted acquisition proteomics methods. *This table was reproduced from Ludwig et al.*

	Data-independent acquisition (DIA)-based SWATH-MS	Data-dependent acquisition (DDA) (Shotgun)	Targeted acquisition (MRM)
Ease of data acquisition	**Easy, requires definition of mass range to cover, precursor isolation window width and number of MS2 scans per cycle	***Easiest, the default set up on most mass spectrometers, requires definition of TopN method, MS2 trigger threshold and dynamic exclusion time	*Hardest, requires generation and optimisation of targeted peptide assays for data acquisition
Ease of data analysis	*Hardest, requires peptide query parameters, sophisticated software tools and large informatics resources	***Easiest, many resources available	**Easy, many software tools developed for automated and manual analysis
Breadth of protein and peptide detection/multiplexing	***10,000s of peptides per MS injection quantifiable	***10,000s of peptides per MS injection quantifiable	*10s to 1,000s of peptides per MS injection quantifiable
Selectivity/sensitivity/ dynamic quantification range	**4 orders of magnitude per MS injection	**4 orders of magnitude per MS injection	***4-5 orders of magnitude per MS injection
Reproducibility/data consistency	***High, due to peptide-centric scoring analysis	*Low, due to stochastic sampling in DDA	***High, due to targeted data acquisition
Retrospective targeting (using chromatogram extraction	***Possible on MS1 and MS2 level	**Possible on MS1 level only	*Not possible due to targeted data acquisition

Table lists different proteomic methods, comparing the advantages and disadvantages of eacb approach. This table was reproduced from Ludwig *et al.* (Ludwig *et al.*, 2018a).

The aim of this chapter was to use quantitative proteomics to use an unbiased approach to compare the whole proteome of L-CMD myoblasts and myotubes to control myoblasts and myotubes to elucidate the upstream or downstream molecular consequences of *LMNA* mutations in L-CMD cells, and to examine whether there is a core molecular signature of L-CMD that is shared across the three different *LMNA* mutations to identify potential therapeutic targets and/or biomarkers.

Specific objectives include:

- To use sequential window acquisition of all theoretical mass spectra (SWATH™-MS) to determine differentially expressed proteins in L-CMD myoblasts and myotubes, compared to control myoblasts and myotubes.
- To use ingenuity pathway analysis (IPA) to identify enriched molecular and cellular functions, as well as enriched canonical pathways that are associated with the dysregulated proteins.
- To verify selected dysregulated proteins/pathways identified using western blotting and drug treatment of L-CMD cells.
- Considering, from the literature, what is already known about the roles of differentially expressed proteins and the pathways which they are involved in, to investigate how this may relate to, or guide the direction of future research in L-CMD disease pathophysiology.

5.2. Results

5.2.1. SWATH-MS analysis revealed 124 differentially expressed proteins in L-CMD myoblasts, and 288 proteins in myotubes compared to healthy controls

To determine the downstream consequences of *LMNA* mutations in L-CMD (R249W, L380S, del.K32) myoblasts and myotubes, a quantitative proteomic comparison with control (C5d, C25, C41) myoblasts and myotubes was undertaken using Sequential window acquisition of all theoretical mass spectra (SWATH™-MS) as described in Section 2.8. This approach identified a total of 10977 proteins with a Mascot significance threshold for of $p<0.05$. To allow reliable quantification, proteins identified in SWATH-MS analysis from only one peptide were removed, then differentially expressed proteins were identified by the exclusion of proteins with a fold change that was >0.80 but <1.25 (less than a 25% change in expression). A t-test was then used to assign a *p*-value to the protein's fold changes, and proteins with a *p*-value of >0.05 were excluded. The raw SWATH-MS data and filtered lists of proteins can be found in **Supplementary file (2)**.

When compared to healthy controls, there were 124 differentially expressed proteins in the L-CMD myoblasts, and 228 proteins in the L-CMD myotubes, with only four proteins that were commonly changed in both L-CMD myoblasts and myotubes (**Fig 5.1, C**). There were 85 downregulated proteins in L-CMD myoblasts, and 171 in L-CMD myotubes, with two proteins, BCL7B (B-cell CLL/lymphoma 7 protein family member B) and transketolase, being commonly downregulated in both myoblasts and myotubes compared to controls (**Fig 5.1, A**). There were 96 upregulated proteins across the L-CMD myoblasts and L-CMD myotubes, therefore there were less upregulated proteins identified across the L-CMD samples than downregulated proteins. In L-CMD myoblasts, there were 39 upregulated proteins, and in L-CMD myotubes there were 57

upregulated proteins (**Fig 5.1, B**). None of the dysregulated proteins that were identified as upregulated in the L-CMD myoblasts were also identified as upregulated in the L-CMD myotubes, and vice versa. There was, however two proteins, DNA primase large subunit and F-box/LRR-repeat protein 3, that were upregulated in L-CMD myoblasts but downregulated in L-CMD myotubes.

The LINC complex proteins, lamin A/C, lamin B1 and B2, emerin, FHL1, SUN1 and SUN2, or nesprin-1 and nesprin 2, were each detected in the SWATH-MS analysis (**Table 5.2.**). Of these, only lamin A/C met the filtering criteria for being differentially expressed in L-CMD myotubes (ratio=0.450, *p*=0.038) (Chapter 2, Section 2.8.4.). This matches with findings discussed in Chapter 4, Section 4.2.6., where quantitative western blotting was used to compared lamin A/C expression in L-CMD myoblasts to control myoblasts, and L-CMD myotubes against control myotubes. In Chapter 4, it was found that lamin A and C were both reduced with statistical significance in L-CMD myotubes compared to controls (98.68%, *p*=0.044, 63.29%, *p*=0.043), although here lamin A and C were found to be reduced more than in the SWATH-MS analysis. In the SWATH-MS analysis, SUN2 was also found to be reduced in L-CMD myoblasts compared to controls, however narrowly missed the *p*-value cut off (ratio=0.601, *p*=0.083). This also aligns to Chapter 4, Section 4.2.9., where SUN2 staining intensity appeared reduced across all L-CMD myoblasts and myotubes when visualised using confocal microscopy, but contrasts results in Section 4.2.10. where a quantitative western blot measuring SUN2 protein expression found that SUN2 was not significantly reduced in L-CMD myoblasts compared to controls, despite the main isoform of SUN2 being found to be statistically significantly reduced in myotubes.

Table 5.2- List of LINC complex proteins that were detected in the SWATH-MS analysis

Protein name	L-CMD vs control myoblast ratio	*p*-value	L-CMD vs control myotube ratio	*p*-value
Lamin A/C	**0.548**	**0.217**	**0.450**	**0.038***
Lamin B1	0.865	0.743	0.911	0.719
Lamin B2	0.738	0.471	0.920	0.761
Emerin	0.724	0.335	0.794	0.152
FHL1	1.378	0.132	1.114	0.898
SUN1	0.736	0.498	1.081	0.757
SUN2	0.601	0.083	1.062	0.832
Nesprin-1	1.002	0.986	0.665	0.451
Nesprin-2	0.830	0.646	0.608	0.057

LINC complex proteins lamin A/C, lamins B1 and B2, emerin, FHL1, SUN1, SUN2 and nesprin-1/-2 were each detected in the SWATH-MS analysis. Of these proteins, only lamin A/C was identified as a dysregulated protein and was downregulated in L-CMD myotubes *(p=0.038).* Two-tailed Student's T-test with non-equal variance was used to determine significance, Asterisk (*) indicates significance.

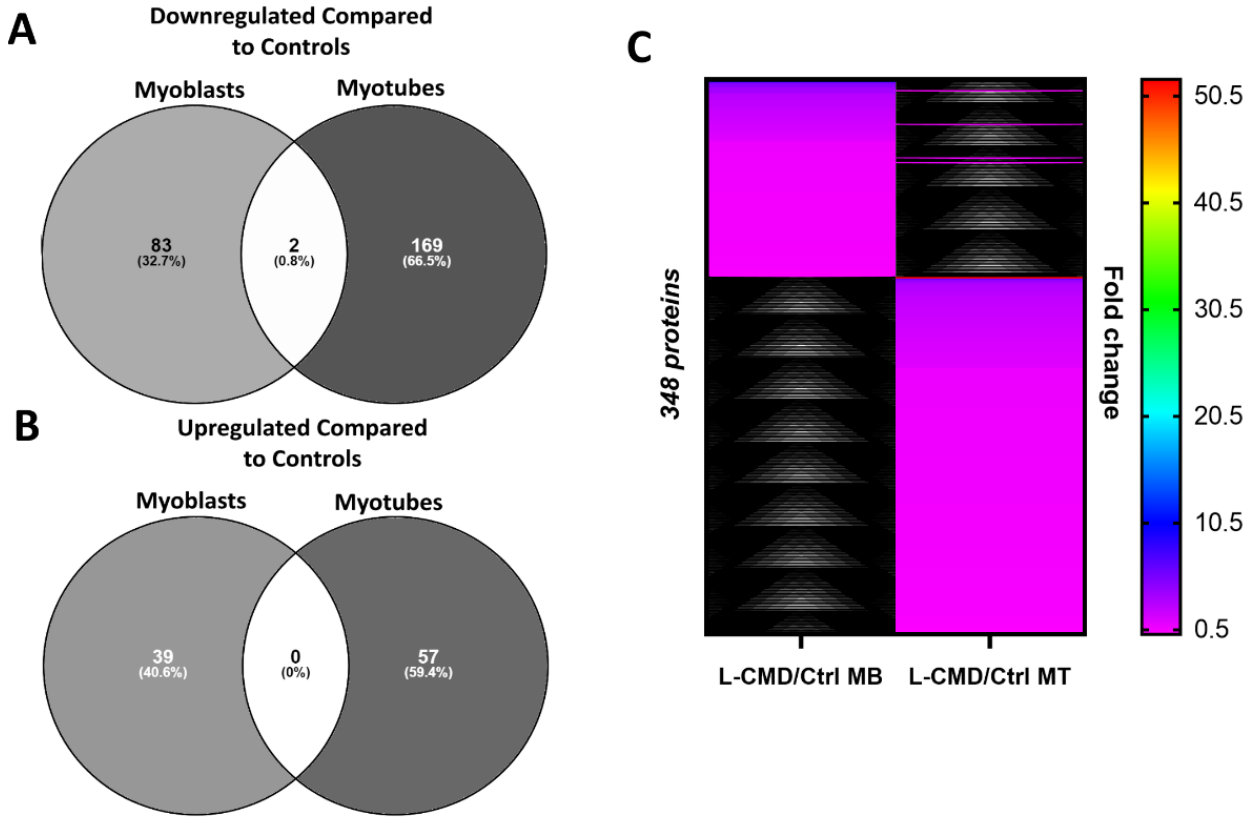

Figure 5.1- Quantitative proteomics analysis revealed 348 dysregulated proteins in L-CMD myoblasts and myotubes compared to healthy controls. *Using SWATH-MS analysis, dysregulated proteins were identified in L-CMD (R249W, L380S, del.K32) myoblasts and myotubes compared to controls (C5d, C25, C41). (A) Venn diagram illustrating the limited overlap of downregulated proteins that were identified in L-CMD myoblasts and L-CMD myotubes. (B) Venn diagram showing no overlap between the upregulated proteins identified in L-CMD myoblasts and L-CMD myotubes. (C) A total of 348 differentially expressed proteins were identified across the L-CMD myoblasts and L-CMD myotubes, there were four commonalities across the L-CMD samples, as mentioned previously, two proteins were both downregulated in L-CMD myoblasts and L-CMD myotubes, and two proteins were upregulated in L-CMD myoblasts but downregulated in L-CMD myotubes.*

5.2.2. Ingenuity pathway analysis revealed that dysregulated proteins identified in L-CMD cells were associated with pathways involved in cellular growth, development and proliferation, as well as cell death

The data acquired from the quantitative proteomic comparison of the L-CMD (R249W, L380S, del.K32) and control (C5d, C25, C41) myoblasts and myotubes was inputted into ingenuity pathway analysis (IPA) software, and this revealed molecular and cellular functions and top canonical pathways associated with the dysregulated proteins that were identified in the L-CMD cells.

Molecular and cellular functions that were most common to the dysregulated proteins were identified, providing insight into functions that may be abnormally controlled due to up or downregulation of proteins known to be associated with these pathways. The top molecular and cellular GO terms mostly differed between the differentially expressed proteins in the L-CMD myoblast and myotubes. The top five terms that the dysregulated proteins in L-CMD myoblasts were associated with were cell death and survival (n=11, p=1.18E-02-7.27E-04), cellular growth and proliferation (n=10, p=1.36E-02–3.19E-04), cell cycle (n=6, p=1.03E-02–3.92E-04), DNA replication, recombination, and repair (n=4, p=1.03E-02-3.92E-04), and cellular development (n=11, p=1.03E-02-3.19E-04) (**Table 5.3**). For the differentially expressed proteins in the L-CMD myotubes, cellular development (n=39, p=9.46E-03-7.13E-05) was also a top molecular and cellular pathway, although compared to the L-CMD myoblasts, a larger number of dysregulated proteins were related to this process in L-CMD myotubes. The other top molecular and cellular functions for the dysregulated proteins in the L-CMD myotubes included cell morphology (n=32, p=9.46E-03-7.13E-05), small molecule biochemistry (n=30, p=9.46E-03-1.56E-06), drug metabolism (n=6, p=9.46E-03-1.56E-06) and carbohydrate metabolism (n=31, p=1.18E-02-7.27E-04) (**Table 5.4**).

Table 5.3- Molecular and cellular functions associated with differentially expressed proteins in L-CMD myoblasts compared to control myoblasts

Myoblasts Molecular and Cellular Functions	*p*-value	Molecules
Cell death and survival	1.18E-02-7.27E-04	STAT1,TXN,SEC23B,FKBP1A,LTF,HFE, HPCA,ABL1,RAD51,COMP,PNP
Cell growth and proliferation	1.36E-02–3.19E-04	COL9A1,COMP,LTF,RBL1,STAT1,ABL1,TF, TXN,PNP,CMKLR1
Cell cycle	1.03E-02–3.92E-04	PSMC3IP,RAD51,PHF8,RBL1,STAT1, MAPK12
DNA replication, recombination and repair	1.03E-02-3.92E-04	PSMC3IP,RAD51,PNP, UCHL3
Cellular development	1.03E-02-3.19E-04	COL9A1,COMP,LTF,RBL1,STAT1,ABL1, TXN,PNP,MAPK12,MBD3, CMKLR1

Table showing enriched molecular and cellular functions associated with the differentially expressed proteins that were identified in L-CMD myoblasts compared to controls, alongside their *p*-value and molecules associated with each category.

Table 5.4- Molecular and cellular functions associated with differentially expressed proteins in L-CMD myotubes compared to control myotubes

Myotubes Molecular and Cellular Functions	*p*-value	Molecules
Cellular development	9.46E-03-7.13E-05	ID1, BCL10, CREBBP, RIGI, STAT3, ATXN1, LMNA, NEU1, VEGFC, ERBIN, TYRO3, HELLS, ATF1, FXN, HDGF, KAT2B, LOXL4, MEN1, NRCAM, PLAAT3, PLCD4, PSRC1, SMARCE1, UBTF, LGALS3, MAP2K4, APAF1, PRKD1, TWSG1, PIK3C2A, GPR89A/GPR89B, HDAC9, PKNOX1, PSMB8, OGT, SERPINE2, AKR1C3, CASP7, IQGAP2
Cell morphology	9.46E-03-7.13E-05	ID1,NEU1,STAT3,VEGFC, ABCD2,ERBIN,LMNA,MAPT,MARK2,NRCAM,OGT, DBNL, ATXN1,VAC14, MARK4,PARVA,FER, KIAA0586,LGALS3,PSMB10, ACOT11,MAF1, MEST,PLAAT3,SUMO1,CREBBP,RIGI, FHOD1, PIK3C2A,MARK1,MARK3,OPTN
Small molecule biochemistry	9.46E-03-1.56E-06	ID1,NEU1,STAT3,VEGFC,AKR1C1/AKR1C2, AKR1C3, AKR1C4, PTGR1, MTMR3, VAC14, ACOT11, PLAAT3, GALK1, GALM, CMAS, MDP1, OGT, ABCB10, EXOC6, FXN,

		PIK3C2A, H6PD, TKT, ASS1, BTD, CHMP1A, GBP2, ADAR, MAPT, DNPH1, APAF1, PTDSS2
Drug metabolism	9.46E-03-1.56E-06	LGALS3,PPIA,AKR1C3,AKR1C4, AKR1C1/AKR1C2,CBR3
Carbohydrate metabolism	1.18E-02-7.27E-04	AKR1C1/AKR1C2,AKR1C3,AKR1C4,CBR3, CMAS,CREBBP,GALK1,GALM,H6PD,MDP1,MTMR3,NEU1, OGT,OPTN,PIGB,PIK3C2A,PLCD4,PTDSS2,TKT,VAC14,VEGFC, ACOT11,APAF1,ATXN1, LGALS3,LMNA, MARK3,MEN1,PLAAT3,SNRPN,STAT3

Table showing enriched molecular and cellular functions associated with the differentially expressed proteins that were identified in L-CMD myotubes compared to controls, alongside their p-value and molecules associated with each category.

Having established enriched molecular and cellular functions associated with the differentially expressed proteins in L-CMD myoblasts and L-CMD myotubes, IPA was then used to determine the most significant enriched canonical pathways across the datasets. The significant values (*p*-value of overlap) for the canonical pathways are calculated by the right-tailed Fisher's Exact Test. This significance indicates the probability of association of molecules from the datasets with the canonical pathway by random chance alone. Another statistic, known as the z-score, is used to predict directionality (pathway activation or inhibition) based on the direction of expression change in the input dataset. This is achieved by comparing the IPA database, which tells us what to expect when upstream regulator interacts with its downstream target, to the direction of differential gene/protein expression that was observed in the input dataset. A z-score of ≥2 indicates predicted activation, while z-score ≤-2 represents predicted inhibition of a pathway. In some instances, pathways may be constructed by IPA in such a way that an activity prediction cannot be made.

In the dataset comparing L-CMD and control myoblasts, top enriched canonical pathways included the white adipose tissue browning pathway (n=3, p=0.034674), SNARE signalling pathway (n=3, p=0.033884), ferroptosis signalling pathway (n=3, p=0.0309), p38MAPK signalling (n=3, p=0.024547), ATM signalling (n=3, p=0.01479), apelin adipocyte signalling pathway (n=3, p=0.02344), PDGF signalling (n=3, p=0.01), and LPS/IL-1 mediated inhibition of RXR function (n=5, p=0.04266). For these pathways, IPA was not able to predict an activity pattern. The necroptosis pathway, however, had a z-score of -2, so was predicted to be downregulated (n=4, p=0.00912), whilst the synaptogenesis signalling pathway was assigned a z-score of 1.342, suggesting the pathway is upregulated (n=5, p=0.024547) (**Table 5.5**). There were no top canonical pathways that were associated with the differentially expressed proteins identified in both the L-CMD myoblasts and L-CMD myotubes. In the L-CMD versus control myotube dataset, top canonical pathways included the protein ubiquitination pathway (n=6, p=0.04677), sperm motility (n=6, p=0.034674), role of macrophages, fibroblasts and endothelial cells in rheumatoid arthritis (n=7, p=0.03715), xenobiotic metabolism signalling (n=8, p=0.006607), and RAR activation (n=10, p=0.000026303), for which no directionality could be predicted. HIF1α signaling (n=6, p=0.014454) and protein kinase A signalling (n=8, p=0.04169) had z-scores of 0, whilst the insulin secretion signalling pathway (n=6, p=0.04571) and Huntington's disease signalling (n=11, p=0.00008511) had positive z-scores, both of 0.816, suggesting activation, and the xenobiotic metabolism general signalling pathway (n=6, p=0.0024547) had a negative z-score of -0.816, predicting inhibition (**Table 5.6**).

Table 5.5- Canonical pathways associated with differentially expressed proteins in L-CMD myoblasts compared to control myoblasts

Myoblasts Ingenuity Canonical Pathways	-log(*p*-value)	Ratio	z-score	Molecules
White Adipose Tissue Browning Pathway	1.46	0.022	#NUM!	CACNA1S,MAPK12,PRKAB1
SNARE Signaling Pathway	1.47	0.022	#NUM!	NAPG,STXBP4,STXBP5
Ferroptosis Signaling Pathway	1.51	0.023	#NUM!	PRKAB1,RBL1,TF
p38 MAPK Signaling	1.61	0.025	#NUM!	HSPB7,MAPK12,STAT1
ATM Signaling	1.83	0.030	#NUM!	ABL1,MAPK12,RAD51
Apelin Adipocyte Signaling Pathway	1.93	0.033	#NUM!	GSTT2/GSTT2B,MAPK12,PRKAB1
PDGF Signaling	2	0.035	#NUM!	ABL1,INPP5B,STAT1
LPS/IL-1 Mediated Inhibition of RXR Function	1.37	0.016	#NUM!	CHST15,FABP3,FABP5,GSTT2/GSTT2B
Necroptosis Signaling Pathway	2.04	0.026	-2	FKBP1A,RBL1,STAT1,TOMM34
Synaptogenesis Signaling Pathway	1.61	0.016	1.342	COMP,NAPG,STXBP4,STXBP5,THBS4

Table showing enriched canonical pathways identified in L-CMD myoblasts compared to controls, alongside their corresponding *p*-value, ratio, z-score, and molecules identified in each canonical pathway. A positive z-score indicates pathway activation, whilst a negative score indicates inhibition. #NUM! indicates that IPA was not able to predict activity for a pathway.

Table 5.6- Canonical pathways associated with differentially expressed proteins in L-CMD myotubes compared to control myoblasts

Myotubes Ingenuity Canonical Pathways	-log(*p*-value)	Ratio	z-score	Molecules
Protein Ubiquitination Pathway	1.33	0.022	#NUM!	PSMA6,PSMB10,PSMB8,THOP1,UBE2V1,UBE2V2
Sperm Motility	1.46	0.024	#NUM!	FER,MAP2K4,PLAAT3,PLCD4,PRKD1,TYRO3
Insulin Secretion Signaling Pathway	1.34	0.022	0.816	CREBBP,PDHX,PIK3C2A,PLCD4,PRKD1,STAT3
HIF1α Signaling	1.84	0.029	0	CREBBP,MAP2K4,PIK3C2A,PRKD1,STAT3,VEGFC
Xenobiotic Metabolism General Signaling Pathway	2.61	0.042	-0.816	CREBBP,MAP2K4,MAP3K10,MGST1,PIK3C2A,PRKD1
Role of Macrophages, Fibroblasts and Endothelial Cells in Rheumatoid Arthritis	1.43	0.021	#NUM!	CREBBP,MAP2K4,PIK3C2A,PLCD4,PRKD1,STAT3,VEGFC
Xenobiotic Metabolism Signaling	2.18	0.028	#NUM!	ALDH7A1,CREBBP,MAP2K4,MAP3K10,MGST1,PIK3C2A,PRKD1,SUMO1
Protein Kinase A Signaling	1.38	0.020	0	ADD1,ATF1,CREBBP,DUSP22,MTMR3,PLCD4,PRKD1,PTPN18
RAR Activation	4.58	0.049	#NUM!	AKR1C1/AKR1C2,AKR1C3,AKR1C4,CREBBP,KAT2B,MAP2K4,NSD1,PRKD1,SMARCD2,SMARCE1
Huntington's Disease Signaling	4.07	0.039	0.816	APAF1,CASP7,CREBBP,HDAC9,MAP2K4,MAP3K10,PIK3C2A,PRKD1,PSMA6,PSMB10,PSMB8

Table showing enriched canonical pathways identified in L-CMD myoblasts compared to controls, alongside their corresponding p-value, ratio, z-score, and molecules identified in each canonical pathway. A positive z-score indicates pathway activation, whilst a negative score indicates inhibition. #NUM! indicates that IPA was not able to predict activity for a pathway.

The p38 MAPK signalling pathway and HIF1α signalling pathways, that were related to the dysregulated proteins in the L-CMD myoblasts and myotubes, are associated with cancer-related processes. Since these are likely unrelated to L-CMD, and instead likely reflect the high number of cancer-related studies comprising the IPA Knowledge Base, they were not considered pathways of interest. This however may be considered a limitation, as using this approach may lead to the exclusion of pathways of interest. Instead, canonical pathways which had significant z-scores for either activation or inhibition, and also appeared relevant to neuromuscular disease based on previous findings in the literature, were candidates for further verification. Of the canonical pathways associated with differentially expressed proteins in L-CMD myoblasts, both upregulation of the synaptogenesis signalling pathway and downregulation of the necroptosis signalling pathway and were intriguing. Synaptogenesis refers to the formation of synapses, which includes the neuromuscular junction (NMJ), a key player involved in muscle contraction, whilst necroptosis is a cell death process that has been implicated in other neuromuscular diseases (Bencze *et al.*, 2017; Chehade *et al.*, 2022). In L-CMD myotubes, dysregulated proteins were connected to upregulation of the insulin secretion signalling pathway and Huntington's disease signalling. The insulin secretion signalling is a carbohydrate metabolism process, and carbohydrate metabolism is a fundamental biochemical process that is responsible for providing a constant energy supply to cells, which is particularly important for muscle contraction (Hill, 1924). Further examination of the proteins implicated in Huntington's disease signalling identified dysregulated proteins that were involved in apoptosis, including PSMB8, PSMB10, PSMA6, APAF1 and CASP7. Dysregulation of apoptosis has also been

linked to the development diseases, such as neurological conditions (Sang et al., 2005; Yamazaki, Esumi and Nakano, 2005).

Due to time constraints, it was not possible to verify the dysregulation of all of the canonical pathways of interest that were identified in L-CMD myoblasts and myotubes. Instead, one pathway was selected for further study. Of particular interest was the necroptosis pathway that was identified in the dataset comparing L-CMD and control myoblasts. Necroptosis is a mode of regulated cell death that exhibits features of both apoptosis and necrosis (Degterev *et al.*, 2005). Apoptosis is a form of highly regulated "programmed" cell death, whilst necrosis is considered "unprogrammed" due to unregulated activity (Dhuriya and Sharma, 2018). Necroptosis is inhibited by necrostatin-1 by inhibiting the activity of receptor-interacting protein kinase 1 (RIPK1), suggesting that it is a well-regulated process, in other words, a programmed necrosis (Dhuriya and Sharma, 2018). The necroptosis pathway is emerging as an important feature of neuromuscular pathology, having previously been implicated in muscle degeneration in Duchenne muscular dystrophy (DMD) (Bencze *et al.*, 2017), and a recent study has identified that necroptosis plays a role in muscle fibre size and skeletal muscle development in SMA (Chehade *et al.*, 2022).

The necroptosis pathway had a significant negative z-score of -2 (n=4, p=0.00912), which predicts that it is downregulated in L-CMD myoblasts compared to controls. There were four dysregulated proteins associated with the necroptosis pathway, peptidyl-prolyl cis-trans isomerase FKBP1A (FKBP1A) (0.641-fold, p=0.027), retinoblastoma-like protein 1 (RBL1) (0.282-fold, p=0.045), signal transducer and

activator of transcription 1-alpha/beta (STAT1) (0.587-fold, p=0.017), and mitochondrial import receptor subunit TOM34 (TOMM34) (0.45-fold, p=0.02) (**Table 5.5**). Each of these proteins were found to have fold decreases across the L-CMD myoblasts compared to control myoblasts. Of these proteins, STAT1 and TOMM34 were selected as candidate for further verification. STAT1 appeared to be a good candidate as it was detected with a high peptide count (40 peptides detected). Peptide count indicates the number of distinct peptide sequences identified in a protein group. A higher peptide count indicates a higher certainty that the mass spectrometry instrument is identifying a particular protein. As well as this, STAT1 was found to be considerably reduced, which would be easier to demonstrate using western blotting compared to a protein that was less reduced. The other proteins were identified with similar numbers of peptides to one another, however TOMM34 and FKBP1A were more significantly reduced in L-CMD myoblasts compared to controls, making these proteins more preferable candidates. As TOMM34 was identified with slightly more peptides, this protein was chosen for further verification, along with STAT1. STAT1 and TOMM34 are also involved at different stages of the necroptosis pathway (**Fig 5.2**), therefore if dysregulation of both proteins can be validated, this reinforces dysregulation of the pathway. An attempt was also made to examine FKBP1A and RBL1 expression in L-CMD and control myoblasts and myotubes, however the FKBP1A antibody that was used detected bands that did not correspond to the molecular weight of FKBP1A. The RBL1 antibody did not detect any bands despite modification of the protocol which included increasing the antibody concentration and incubation time. For both FKBP1A and RBL1, there were limited alternative antibodies that were commercially available.

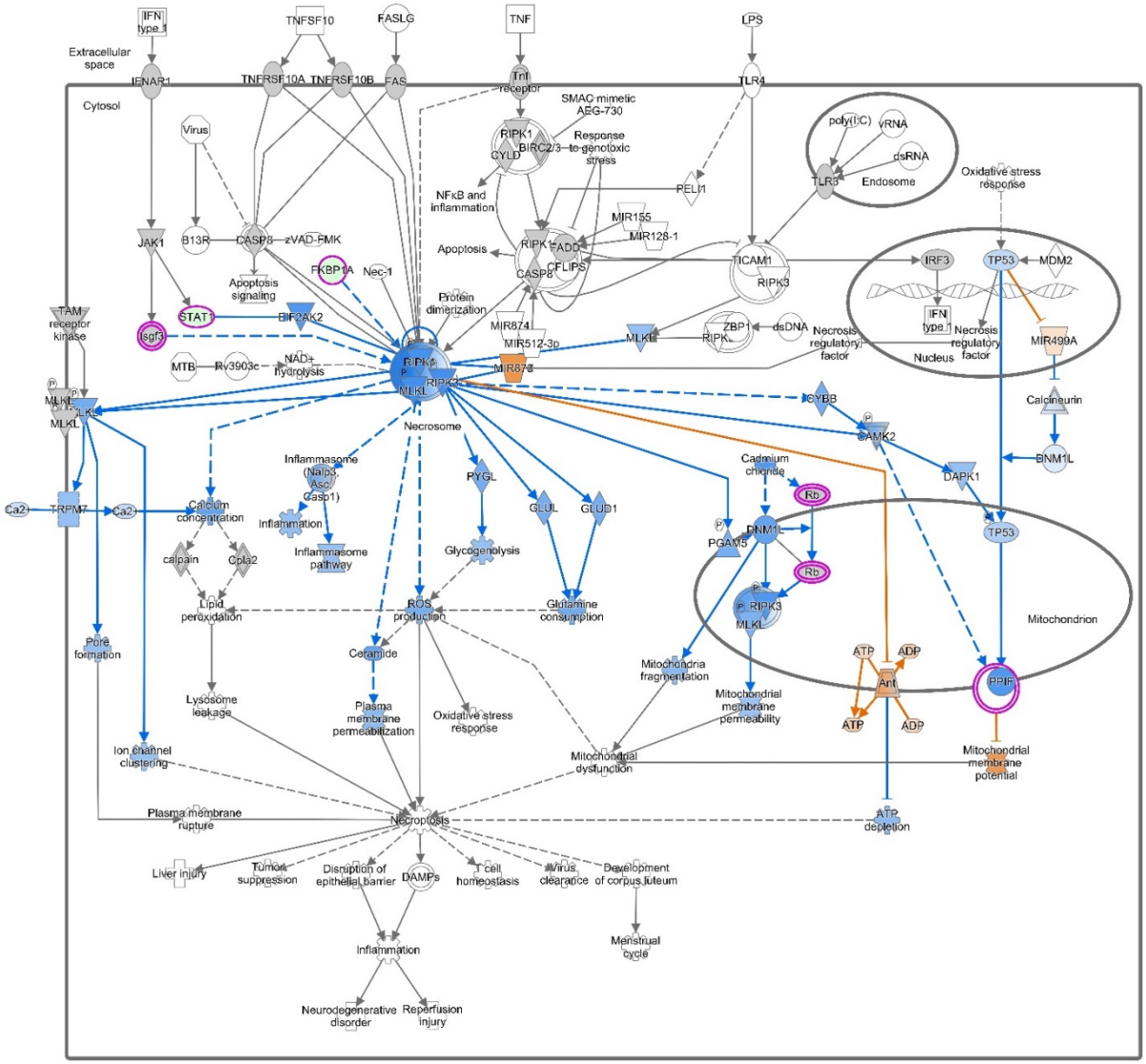

Figure 5.2- Schematic diagram of the necroptosis pathway. *Molecular pathways downstream of central component of the necroptosis pathway, RIPK1. Dysregulated proteins identified in SWATH-MS analysis are circled in purple. Blue lines indicate pathways that may be downregulated in L-CMD myoblasts, whilst orange lines indicate potentially upregulated pathways. Diagram generated with Ingenuity Pathway Analysis (IPA).*

Table 5.7- Dysregulated proteins associated with the necroptosis pathway in L-CMD myoblasts.

Protein Description	Peptide count	C5d Sum Total Area	C25 Sum Total Area	C41 Sum Total Area	L380S Sum Total Area	Del.K32 Sum Total Area	R249W Sum Total Area	Average Control Myoblasts	Average L-CMD Myoblasts	L-CMD vs Ctrl MB	*p*-Value
FKBP1A	4	1E+09	1E+09	7.7E+08	6E+08	6E.08	5E+08	9.1E+08	6E.08	0.641	0.027
RBL1	3	1.8E+07	1E+07	1.6E+07	3E+06	5E+06	4E+06	1.4E+07	4E+06	0.282	0.045
STAT1	40	1.2E+09	1.4E+09	1.6E+09	7.1E+08	9.8E+08	7.8E+08	1.4E+09	8.2E+08	0.587	0.017
TOMM34	6	1E+08	1.3E+08	1.3E+08	6.9E+07	6.9E+07	2.8E+07	1.2E+08	5.5E+07	0.453	0.020

Peptidyl-prolyl cis-trans isomerase FKBP1A (FKBP1A), retinoblastoma-like protein 1 (RBL1), signal transducer and activator of transcription 1-alpha/beta (STAT1), and mitochondrial import receptor subunit TOM34 (TOMM34) were each identified as components of the necroptosis pathway

Expression levels of STAT1 and TOMM34 were examined in L-CMD (L380S, R249W, del.K32) and control (C5d, C25, C41) myoblast samples using western blotting. STAT1 is a highly glycosylated protein (Schindler, Levy and Decker, 2007), and therefore instead of producing distinct bands like un-glycosylated proteins, it appears as a smear on western blot (**Fig 5.3, A**). In this case, instead of measuring each band for quantification, the whole smear in each lane was measured to calculate integrated density. It was clear that there was an abundance of STAT1 in the C5d and C41 myoblast samples, however, it was found that STAT1 was not decreased with statistical significance in the L-CMD myoblast cell lines compared to controls (90.40%, p=0.084) (**Fig 5.3, C**). This result is likely not significant due to STAT1 levels being very reduced in the C25 sample compared to the C5d and C41 samples, causing a large standard deviation between the controls. TOMM34 also appeared to be reduced in the L-CMD myoblasts compared to the controls, and this finding was statistically significant (57.34%, p=0.032) (**Fig 5.3, B, D**), closely matching the reduction of TOMM34 identified in L-CMD myoblasts in the SWATH-MS analysis (ratio=0.453, p=0.020). However, the band representing TOMM34 appeared to have a lower molecular weight, of around 30kDa, when TOMM34 has a molecular weight of 35kDa. A lower molecular weight band than expected can sometimes be a result of the target protein being degraded or cleaved, or the detection of a splice variant of the target protein. Care was taken to prevent samples from degradation, and splice variants of TOMM34 have not been confirmed. Another possibility is that there was not a high enough percentage of acrylamide in the gel, so the protein has moved too quickly due to a lack of resistance.

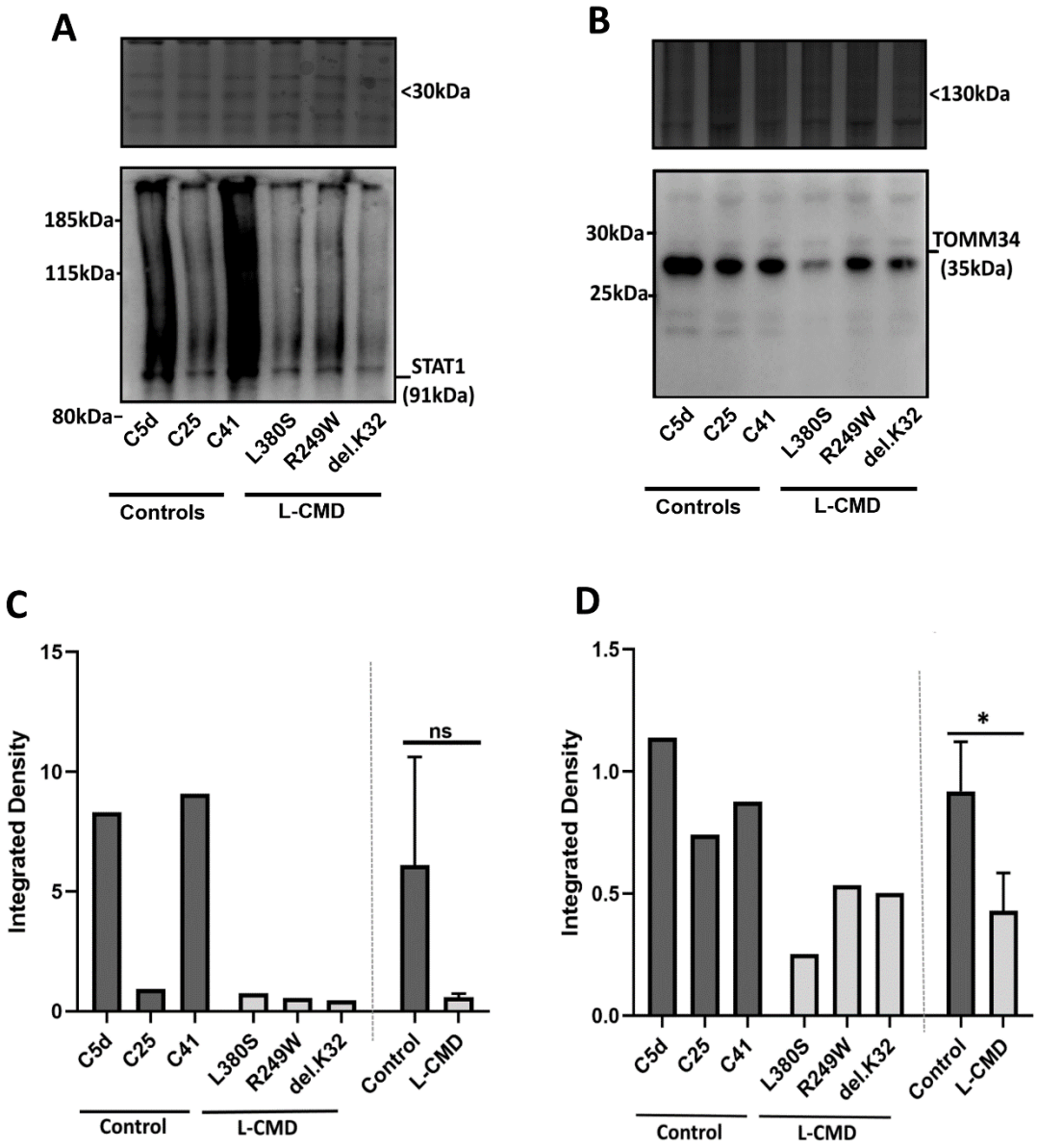

Figure 5.3- Examining dysregulation of the necroptosis pathway in L-CMD myoblasts. *(A, C) STAT1 expression was not found to be significantly decreased in L-CMD myoblasts (L380S, R249W, del.K32) compared to controls (C5d, C25, C41) (p=0.084). (B, D) TOMM34 expression was found to be significantly decreased in L-CMD myoblasts compared to controls (57.34%, p=0.032). Two-tailed Student's T-test with unequal variance was used to determine significance, Asterisk (*) denotes statistical significance, ns indicates not significant.*

5.2.3. Exploring the potential efficacy of Necrostatin-1 on STAT1 and TOMM34 expression levels in L-CMD myoblasts.

As previously mentioned, necrostatin-1 (Nec-1) is a specific RIPK1 inhibitor and inhibits

TNFα-induced necroptosis. It is believed that Nec-1 can inhibit the necroptosis

signalling pathway and ameliorate necroptotic cell death in disease development (Cao and Mu, 2021). As the necroptosis pathway was found to be downregulated in L-CMD myoblasts compared to controls, this suggests that a feature of L-CMD may be that necroptosis signalling is already inhibited, therefore Nec-1 may not be a potential therapeutic candidate for the treatment of this disease. However, due to Nec-1's targeting of the necroptosis signalling pathway, it was predicted that Nec-1 may further downregulate necroptosis in treated L-CMD myoblasts, consequently causing STAT1 and TOMM34 expression to be even more reduced. If true, this would help to further verify that the necroptosis pathway is downregulated in L-CMD myoblasts.

A drug study was designed to test the hypothesis that Nec-1 would further reduce STAT1 and TOMM34 expression in L-CMD myoblasts. The L-CMD myoblast lines (L380S, R249W, del.K32) were treated with Nec-1, at a concentration of 30µM for four hours. This concentration was determined as Nec-1 EC50=490nM for blocking necroptosis (EC50 refers to the concentration of a drug that induces a response halfway between the baseline and maximum), and previous studies have determined 30µM is the optimal concentration for this purpose (Liu *et al.*, 2011; Feyen *et al.*, 2013; D. Q. Lin *et al.*, 2020). Of closest relevance to human myoblasts, studies have used Nec-1 at this concentration to block necroptosis in human and murine cardiomyocytes, where Nec-1 used at 30µM was found to reduced necrotic cell death by between 37-45% compared to vehicle treated cells (Liu *et al.*, 2011; Feyen *et al.*, 2013). Using quantitative western blotting, STAT1 and TOMM34 expression was evaluated in Nec-1 treated, vehicle treated and untreated L-CMD myoblast extracts (**Fig 5.4**). Firstly, cell viability did not appear to be detrimentally affected by Nec-1 or vehicle (DMSO) treatment (**Fig 5.4, D**). The resulting western blots probed for STAT1 and TOMM34 in

these samples found that Nec-1 did not statistically significantly reduce the expression of these proteins in treated L-CMD myoblasts. STAT1 expression was not significantly changed between the Nec-1 treated, untreated or vehicle treated groups (p=0.233). Although STAT1 appeared slightly decreased in Nec-1 treated samples compared to untreated samples, this finding was not significant (43.49%, p=0.567). However, this result was hampered by technical issues with electrophoresing STAT1 as it appeared that there was still STAT1 within the wells of the polyacrylamide gel (**Fig 5.4, A, C**). It is uncertain as to why difficulties with electrophoresing STAT1 were experienced here when previously these issues were not encountered (refer to Section 5.2.3, **Fig 5.6**). This may be due to increased protein concentration in the drug study samples that were used for gel electrophoresis, compared to the samples probed for STAT1 previously in Section 5.2.3 which may have contained less protein. Consequently, the smears representing STAT1 may not be an accurate reflection of STAT1 expression in the samples if a proportion of STAT1 failed to travel out of the polyacrylamide gel wells. STAT1 also appeared highly increased in vehicle treated samples compared to untreated, although this was also significant, likely to the large standard deviation observed between the untreated controls (31.12%, p=0.546). This result, albeit not significant, could suggest that DMSO treatment increases STAT1 expression. In high doses, DMSO is known to be toxic to cell cultures, therefore could induce cell death pathways including apoptosis and necrosis (Awan *et al.*, 2020). However, cell viability was shown to not be reduced in DMSO treated cells, suggesting the concentration used here was not toxic (**Fig 5.4, D**). Perhaps even at used in concentrations that are not toxic to cells, DMSO still influences the necroptosis pathway. This, however, needs further confirmation.

TOMM34 expression was also not significantly changed across Nec-1 treated, untreated and vehicle treated groups (p=0.239). TOMM34 seemed to be slightly reduced in Nec-1 treated L-CMD myoblasts compared to untreated L-CMD myoblasts, but this finding was not statistically significant (23.41%, p=0.313) (**Fig 5.4, B,C**). TOMM34 also did not appear to be considerably affected by vehicle treatment, with an insignificant increase in expression being observed between vehicle treated and untreated samples (5.21%, p=0.919).

Although the concentration of Nec-1 used in this experiment was derived from previous studies (Liu *et al.*, 2011; Feyen *et al.*, 2013), a limitation was that a dose response was not tested, and perhaps a higher or lower dose would be found to have an effect. Due to time constraints, it was not possible to test multiple doses, however, this is something that should be considered in a future study. Another approach that could have been used to verify whether Nec-1 was effective at blocking necroptosis would be to examine RIPK1 expression in the Nec-1 treated, untreated, and vehicle treated L-CMD samples using western blotting. As RIPK1 is the main target of Nec-1 (Degterev *et al.*, 2005, 2008), it would be expected that RIPK1 expression would be reduced in Nec-1 treated cells.

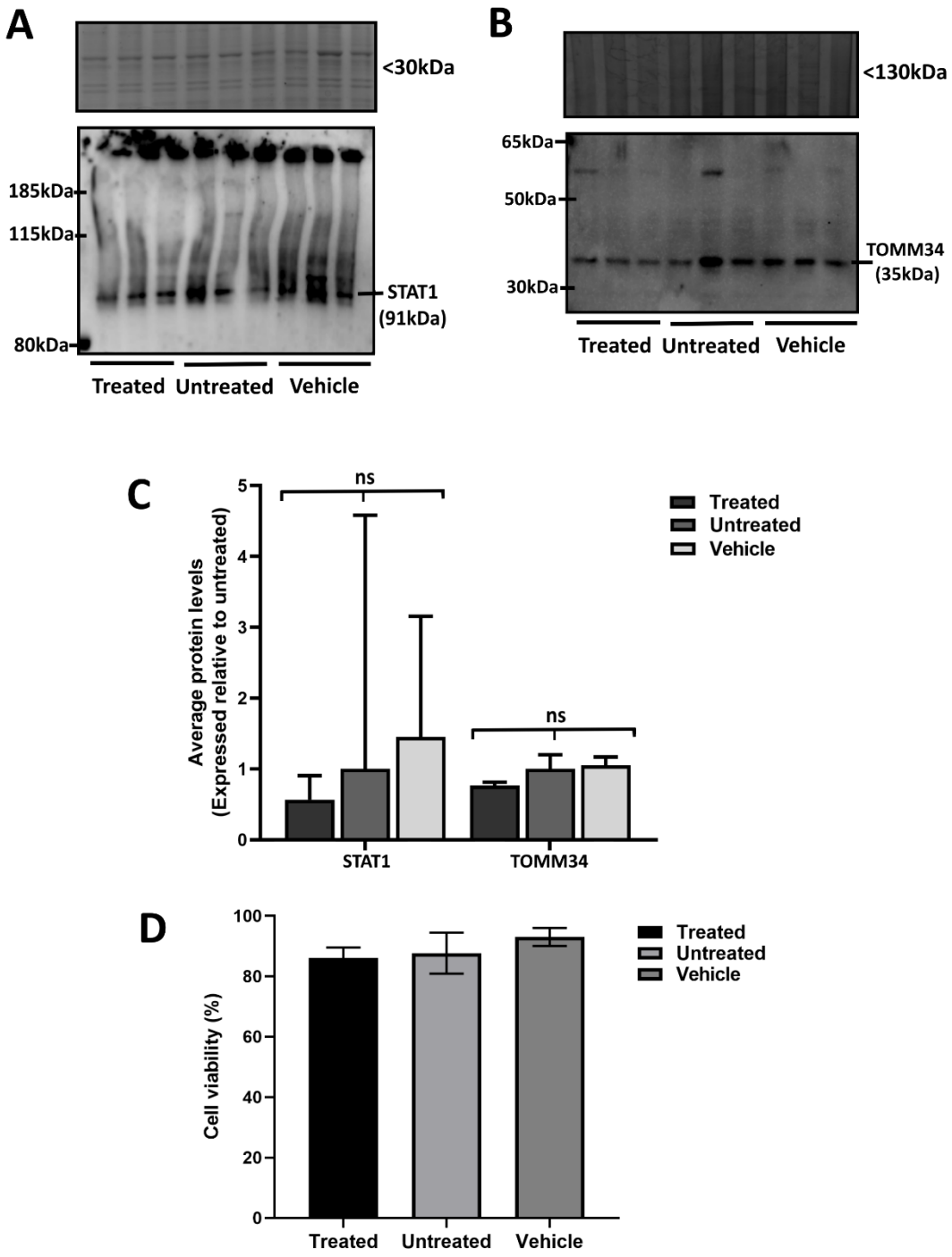

Figure 5.4- STAT1 and TOMM34 protein levels in L-CMD myoblasts after Necrostatin-1 (Nec-1) treatment. *(A, B) STAT1 and TOMM34 proteins levels in L-CMD (L380S) myoblasts treated with 30µM Nec-1, Three technical replicates were used in each group: untreated, vehicle treated (DMSO) and Nec-1. Coomassie stained gel was used as a total protein loading control. (C) Quantification of STAT1 and TOMM34 levels. Densitometry measurements of STAT1 and TOMM34 reactive bands were first normalised to densitometry measurements of Coomassie stained gel, then all samples were normalised to the average of untreated. Graphs are presented as average protein levels (expressed relative to untreated), with error bars showing standard deviation from the mean. Two-tailed Student's T-test with unequal variance was used to determine significance, ns indicates not significant. (D) Cell viability in L-CMD myoblasts treated with 30µM Nec-1 for four hours. Graphs are presented as average cell viability, with error bars showing standard deviation from the mean.*

5.2.4. Identification of potential upstream regulators for the dysregulated proteins identified in L-CMD myoblasts and myotubes

IPA is able to predict which upstream regulators are activated or inhibited to explain the up-regulated and down-regulated genes observed in a dataset. Knowledge of this regulatory cascade can help to further understand the biological activities occurring in the tissues or cells of interest. For the dysregulated proteins that were identified in the L-CMD myoblasts, a total of 204 upstream regulators were identified. Of these, IPA was able to predict the activity of three upstream regulators, two which were chemical drugs which were predicted to be activated, and one transcriptional regulator which was predicted to be inhibited. For the dysregulated proteins that were found in the L-CMD myotubes, a total of 264 upstream regulators were determined, 14 of which had predicted activity. Four upstream regulators for the L-CMD myotubes were predicted to be activated, these included two chemical drugs, a transcription regulator, and a kinase, whilst 10 upstream regulators were predicted to be inhibited. The inhibited regulators included two chemicals, four transcriptional regulators, a cytokine, an enzyme, a kinase and one molecule classes as a "group". For this study, upstream regulators were not further analysed, but may be explored in future work.

5.2.5. Differentially expressed proteins and enriched canonical pathways differed in L-CMD myotubes and control myotubes

Through examining the data generated from the comparative proteomic analysis of L-CMD versus control myoblasts and myotubes, it was noticed that a number of molecular and cellular pathways that were dysregulated in the L-CMD myoblasts or myotubes were associated with cell growth and development, cell proliferation and cell death and survival. These pathways could be related to impaired differentiation.

Considering that myoblasts are pre-differentiated cells that are undergo myogenesis in order to form myotubes, and that it is widely known that a number of different genes and proteins are differentially expressed in muscle cells during different points of muscle cell differentiation (Braun *et al.*, 1989; Shen *et al.*, 2003), it would be expected that there would be differentially expressed proteins in control myotubes compared to myoblasts. In fact, a comparative proteomic study has previously been conducted on proliferating immortalized murine myoblast C2C12 cells and fully differentiated myotubes, identifying a number of proteins that were changed in expression in myotubes compared to myoblasts (Tannu *et al.*, 2004). Myogenic differentiation impairments have previously been observed in L-CMD myoblasts (Gómez-Domínguez *et al.*, 2020), which could be due to impaired or dysregulated expression of proteins involved in myogenic differentiation. This was assessed by staining myotubes growing in 2D and 3D cultured that were differentiated from C2C12 cells harbouring L-CMD mutations for myosin heavy chain (MHC). MHC was undetected in some of the myotubes carrying L-CMD mutations, and myotubes differentiated from C2C12's harbouring the R249W mutation growing in 3D cultures exhibited an abnormal distribution of MHC (Gómez-Domínguez *et al.*, 2020). Based on this prior knowledge, the data acquired from the SWATH-MS analysis was examined to determine whether there were any differences in the differentially expressed proteins in L-CMD myotubes and myoblasts, compared to the control myotubes and myoblasts. This approach has previously been used to identify dysregulated proteins associated with differentiation and development in SMA, where quantitative proteomics was used to compare the proteome of SMA and control iPSC-derived motor neurons with the fibroblast lines from which they were originally derived (Fuller, Mandefro, *et al.*, 2016). As described

previously, in section 5.2.1, to allow reliable quantification, proteins identified in SWATH-MS analysis from only one peptide were removed, then differentially expressed proteins were identified by comparing the data from the L-CMD myotubes against L-CMD myoblasts, and the control myotubes against the control myoblasts, and excluding proteins with a fold change that was >0.80 but <1.25 (less than a 25% change in expression). A t-test was then used to assign a *p*-value to the protein's fold changes, and proteins with a *p*-value of >0.05 were excluded.

A total of 137 proteins were differentially expressed in control myotubes compared to myoblasts, whilst 571 proteins were differentially expressed in L-CMD myotubes compared to myoblasts. There was very little overlap between the differentially expressed proteins in L-CMD myotubes, compared to control myotubes. Only 31 proteins were identified to be changed in the same direction in L-CMD myotubes compared to control myotubes. Three proteins, dipeptidyl peptidase 2 (DPP7), histone H1.0, and SWI/SNF-related matrix-associated actin-dependent regulator of chromatin subfamily D member 2 (SMARCD2), were commonly upregulated in both L-CMD and control myotubes (**Fig 5.5, A)**, whilst 28 proteins were commonly downregulated (**Fig 5.5, B**) (**Table 5.6**).

Table 5.8- List of proteins that were commonly upregulated or downregulated in L-CMD myotubes and control myotubes

Protein name	Gene name	L-CMD myoblasts vs myotube ratio	*p*-value	Control myoblasts vs myotube ratio	*p*-value
Dipeptidyl peptidase 2	DPP7	2.087	0.008	1.960	0.044
Histone H1.0	H1-0	2.219	0.008	2.355	0.040
SWI/SNF-related matrix-associated actin-dependent regulator of chromatin subfamily D member 2	SMARCD2	2.483	0.035	2.921	0.009
Lactotransferrin	LTF	0.073	0.005	0.124	0.010
Syntenin-1	SDCBP	0.143	0.002	0.163	0.048
Interferon-stimulated 20 kDa exonuclease-like 2	ISG20L2	0.158	0.043	0.233	0.006
Dysbindin	DTNBP1	0.211	0.009	0.364	0.038
BTB/POZ domain-containing protein 9	BTBD9	0.270	0.048	0.327	0.049
Mitogen-activated protein kinase 6	MAPK6	0.271	0.047	0.322	0.007
Fibroblast growth factor receptor 4	FGFR4	0.272	0.044	0.371	0.010
Proto-oncogene tyrosine-protein kinase ROS	ROS1	0.273	0.047	0.326	0.009
Fibroblast growth factor receptor 2	FGFR2	0.273	0.049	0.339	0.017
Fibroblast growth factor receptor 3	FGFR3	0.276	0.049	0.344	0.016
Cyclin-dependent kinase 14	CDK14	0.277	0.049	0.341	0.022
Cyclin-dependent kinase 3	CDK3	0.286	0.049	0.355	0.021
Tyrosine-protein kinase Lck	LCK	0.289	0.049	0.365	0.015
Nucleoredoxin	NXN	0.289	0.006	0.385	0.003
Tyrosine-protein kinase Lyn	LYN	0.294	0.049	0.361	0.020
Interleukin-1 receptor-associated kinase 1	IRAK1	0.305	0.048	0.456	0.013
Dihydrofolate reductase 2, mitochondrial	DHFR2	0.306	0.033	0.139	0.023
Cyclin-dependent kinase 12	CDK12	0.313	0.047	0.386	0.015
Serotransferrin	TF	0.314	0.002	0.356	0.022
B-cell CLL/lymphoma 7 protein family member B	BCL7B	0.316	0.018	0.385	0.014

Table showing proteins that were commonly dysregulated in L-CMD myotubes and control myotubes compared to their respective myoblasts. Each protein is listed alongside its gene name, ratio between L-CMD myoblasts versus L-CMD myotubes, or control myoblasts versus control myotubes and the respective p-values.

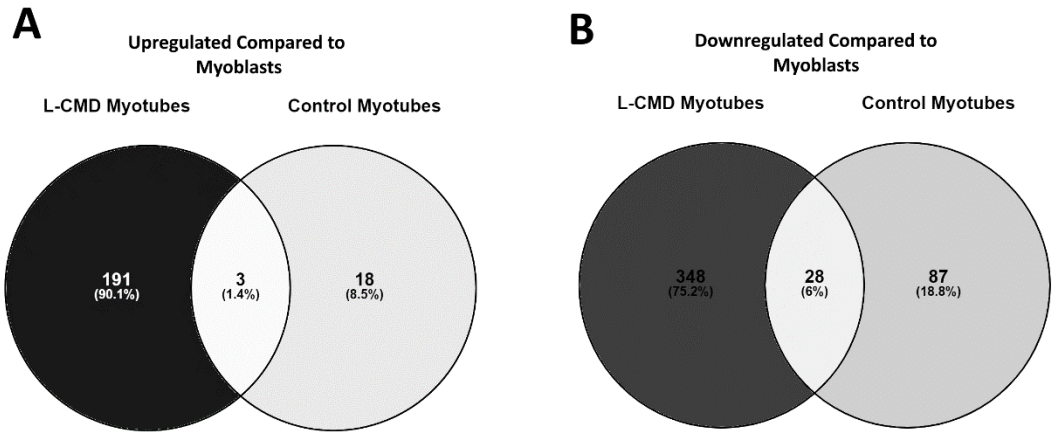

Figure 5.5- Differentially expressed proteins identified in L-CMD myoblasts compared to myotubes, and control myoblasts compared to myotubes. *There was limited overlap between the differentially expressed proteins that were identified in L-CMD myoblasts versus L-CMD myotubes, compared to control myoblasts versus control myotubes. (A) Only 3 proteins were commonly upregulated in L-CMD and control myoblasts compared to L-CMD and control myotubes, (B) whilst 28 proteins were commonly downregulated.*

The lack of overlap of differentially expressed proteins in the L-CMD myotubes, compared to the control myotubes, could suggest that proteins that are involved at different points during muscle cell differentiation are dysregulated in L-CMD myoblasts and/or myotubes. Consequently, this could impair differentiation. IPA analysis was used to reveal enriched canonical pathways for all differentially expressed proteins that were identified in the L-CMD myotubes and the control myotubes compared to their respective myoblasts. Top canonical pathways for the differentially expressed proteins in the control myotubes compared to control myoblasts included cell cycle control of chromosomal replication (p=1.31E-15, n=15), ID1 signalling pathway (p=1.87E-07, n=15), IL-15 production (p=1.89E-07, n=12), and reelin signalling in neurons (p=7.16E-07, n=12), which had negative z-scores of -3.4, -3.4, -3.5, and -2.1, respectively, indicating predicted inhibition, whilst role of tissue factor in cancer (p=9.88E-08, n=12) was also an enriched pathway, but had no predicted activity (**Table**

5.7). For the proteins identified in the L-CMD myotubes compared to L-CMD myoblasts, top enriched canonical pathways were very different and included dilated cardiomyopathy signalling pathway (p=5.18E-24, n=41) and calcium signalling (p=9.92E-20, n=44), which had z-scores of -5 and -0.6, suggesting inhibition, actin cytoskeleton signalling (p=1.79E-22, n=50) and oxidative phosphorylation (p=1.32E-19, n=32) which had z-scores of 2.2 and 5.7, suggesting activation, and mitochondrial dysfunction (p=2.05E-21, n=41), for which activity could not be predicted (**Table 5.8**). Whilst top canonical pathways for the differentially expressed proteins in the control myotubes included ID1 signalling and IL-15 production, which are pathways known to be involved in muscle cell differentiation or skeletal muscle hypertrophy (Jen, Weintraub and Benezra, 1992; Quinn *et al.*, 2002), the top canonical pathways for the differentially expressed proteins in the L-CMD myotubes included pathways associated with disease states including dilated cardiomyopathy signalling and mitochondrial dysfunction (Pieczenik and Neustadt, 2007).

Table 5.9- Canonical pathways associated with the dysregulated proteins identified in control myotubes

Control myotubes Ingenuity Canonical Pathways	**-log(*p*-value)**	**Ratio**	**z-score**	**Molecules**
Cell Cycle Control of Chromosomal Replication	14.9	0.268	-3.357	CDK1,CDK10,CDK12,CDK13,CDK14,CDK16,CDK17,CDK18,CDK3,CDK4,CDK5,CDK6,CDK9,MCM4,POLD1
Role of Tissue Factor in Cancer	7.01	0.103	#NUM!	CCN1,CFL1,CFL2,FGR,FRK,FYN,HCK,LCK,LYN,MAPK12,RALB,YES1
ID1 Signalling Pathway	6.73	0.075	-3.357	CDK4,FGFR1,FGFR2,FGFR3,FGFR4,FGR,FRK,FYN,HCK,LCK,LYN,MAPK12,PLXNB2,RALB,YES1
IL-15 Production	6.72	0.098	-3.464	FGFR1,FGFR2,FGFR3,FGFR4,FGR,FRK,FYN,HCK,LCK,LYN,ROS1,YES1

Reelin Signalling in Neurons	6.15	0.086	-2.111	ARHGEF28,CDK5,CFL1,FGR,FRK,FYN,HCK,ITGA5,LCK,LYN,MAPK12,YES1

Table showing enriched canonical pathways identified in L-CMD myoblasts compared to controls, alongside their corresponding p-value, ratio, z-score, and molecules identified in each canonical pathway. A positive z-score indicates pathway activation, whilst a negative score indicates inhibition. #NUM! indicates that IPA was not able to predict activity for a pathway.

Table 5.10- Canonical pathways associated with the dysregulated proteins identified in L-CMD myotubes

L-CMD myotubes Ingenuity Canonical Pathways	**-log(*p*-value)**	**Ratio**	**z-score**	**Molecules**
Dilated Cardiomyopathy Signalling Pathway	23.3	0.277	-5	ACTA1,ACTA2,ACTB,ACTC1,ACTG1,ACTG2,ATP2A2,CAMK1,CAMK1D,DES,KDM1A,MAPK14,MYH1,MYH10,MYH11,MYH13,MYH14,MYH2,MYH3,MYH4,MYH6,MYH7,MYH7B,MYH8,MYL1,MYL2,MYL3,MYL4,MYL6,MYL6B,MYL9,PRKAR1A,PRKAR1B,SCN5A,TNNC1,TNNI1,TNNT1,TNNT2,TNNT3,TPM1,TTN
Actin Cytoskeleton Signalling	21.7	0.204	2.188	ACTA1,ACTA2,ACTB,ACTC1,ACTG1,ACTG2,ARPC5,BCAR1,CFL1,CFL2,CRKL,CYFIP2,DIAPH1,EZR,F2,GRB2,IQGAP2,ITGA3,ITGA5,ITGA7,ITGB1,MSN,MYH1,MYH10,MYH11,MYH13,MYH14,MYH2,MYH3,MYH4,MYH6,MYH7,MYH7B,MYH8,MYL1,MYL10,MYL12A,MYL12B,MYL2,MYL3,MYL4,MYL6,MYL6B,MYL9,PIK3C2A,PXN,RALA,RALB,RDX,TTN
Mitochondrial Dysfunction	20.7	0.24	#NUM!	AIFM1,APP,ATP5F1A,ATP5F1B,ATP5F1C,ATP5F1D,ATP5ME,ATP5MF,ATP5MG,ATP5PD,ATP5PO,COX4I1,COX5A,COX5B,COX6B1,COX7A2,COX7A2L,CYC1,GSR,HSD17B10,MT-ATP6,NDUFA2,NDUFA6,NDUFA9,NDUFB10,NDUFB4,NDUFB7,NDUFS1,NDUFS5,NDUFS7,NDUFV1,PDHA1,PRDX3,RHOT2,SDHA,UQCRC1,UQCRC2,UQCRFS1,UQCRH,VDAC1,VDAC2
Calcium Signalling	19	0.202	-0.577	ACTA1,ACTA2,ACTC1,ATP2A1,ATP2A2,ATP2A3,ATP2B2,ATP2B3,ATP2C1,CAMK1,CAMK1D,CASQ2,CREBBP,HDAC9,LETM1,MCU,MYH1,MYH10,MYH11,MYH13,MYH14,MYH2,MYH3,MYH4,MYH6,MYH7,MYH7B,MYH8,MYL1,MYL2,MYL3,MYL4,MYL6,MYL6B,MYL9,PRKAR1A,PRKAR1B,TNNC1,TNNI1,TNNT1,TNNT2,TNNT3,TPM1,TPM3

Oxidative Phosphorylation	18.9	0.288	-0.577	ACTA1,ACTA2,ACTC1,ATP2A1,ATP2A2,ATP2A3,ATP2B2,ATP2B3,ATP2C1,CAMK1,CAMK1D,CASQ2,CREBBP,HDAC9,LETM1,MCU,MYH1,MYH10,MYH11,MYH13,MYH14,MYH2,MYH3,MYH4,MYH6,MYH7,MYH7B,MYH8,MYL1,MYL2,MYL3,MYL4,MYL6,MYL6B,MYL9,PRKAR1A,PRKAR1B,TNNC1,TNNI1,TNNT1,TNNT2,TNNT3,TPM1,TPM3

Table showing enriched canonical pathways identified in L-CMD myoblasts compared to controls, alongside their corresponding p-value, ratio, z-score, and molecules identified in each canonical pathway. A positive z-score indicates pathway activation, whilst a negative score indicates inhibition. #NUM! indicates that IPA was not able to predict activity for a pathway.

5.2.6. Summary of results

In summary, SWATH-MS revealed 124 differentially expressed proteins in the L-CMD myoblasts, and 228 proteins in the L-CMD myotubes, with only four proteins that were commonly changed in both L-CMD myoblasts and myotubes. Of the differentially expressed proteins, only two (BCL7B and transketolase) were changed in the same direction (both downregulated) across both L-CMD myoblasts and myotubes. Examination of the LINC complex proteins additionally found that although these proteins were detected, none appeared to be significantly changed in expression in L-CMD cells compared to controls. IPA revealed enriched molecular and cellular functions, as well as enriched canonical pathways associated with the differentially expressed proteins (**Fig 5.6**). Particular canonical pathways of interest included upregulation of the synaptogenesis signalling pathway and downregulation of the necroptosis signalling pathway in L-CMD myoblasts, and upregulation of the insulin secretion signalling pathway and Huntington's disease signalling pathway in L-CMD myotubes. Of these pathways, the necroptosis pathway was selected for further validation because of its implication in other neuromuscular diseases. The verification of the dyregulated proteins associated with the necroptosis pathway (FKBP1A, RBL1,

STAT1, TOMM34) was impeded by the availability of appropriate antibodies for use on western blot. Specifically, an FKBP1A antibody was trialled, but gave rise to multiple immunoreactive bands, whilst an RBL1 antibody that was used resulted in the detection of no bands on western blot, despite trialling increased antibody concentrations. Expression of STAT1 appeared reduced in L-CMD myoblasts compared to controls on western blot, but this was not found to be a significant reduction, whilst TOMM34 expression was found to be significantly reduced in L-CMD myoblasts compared to controls. To further explore dysregulation of the necroptosis pathway, L-CMD myoblasts were treated with Nec-1, a known inhibitor of necroptosis, however this was not found to significantly affect STAT1 or TOMM34 expression. For the dysregulated proteins identified in the L-CMD myoblasts and myotubes, IPA also identified a number of potential upstream regulators which may be explored in a further study. After identifying that many of the dysregulated proteins in L-CMD myoblasts and myotubes were associated with cellular growth and development, cell proliferation and cell death and survival, the SWATH-MS data was analysed to determine differentially expressed proteins in control myotubes and myoblasts, compared to L-CMD myotubes and myoblasts. This revealed that top canonical pathways for the differentially expressed proteins in control myotubes included ID1 signalling and IL-15 production pathways known to be involved in muscle cell differentiation or skeletal muscle hypertrophy (Jen, Weintraub and Benezra, 1992; Quinn et al., 2002), whilst the top canonical pathways for the L-CMD myotubes included pathways associated with disease states including dilated cardiomyopathy signalling and mitochondrial dysfunction.

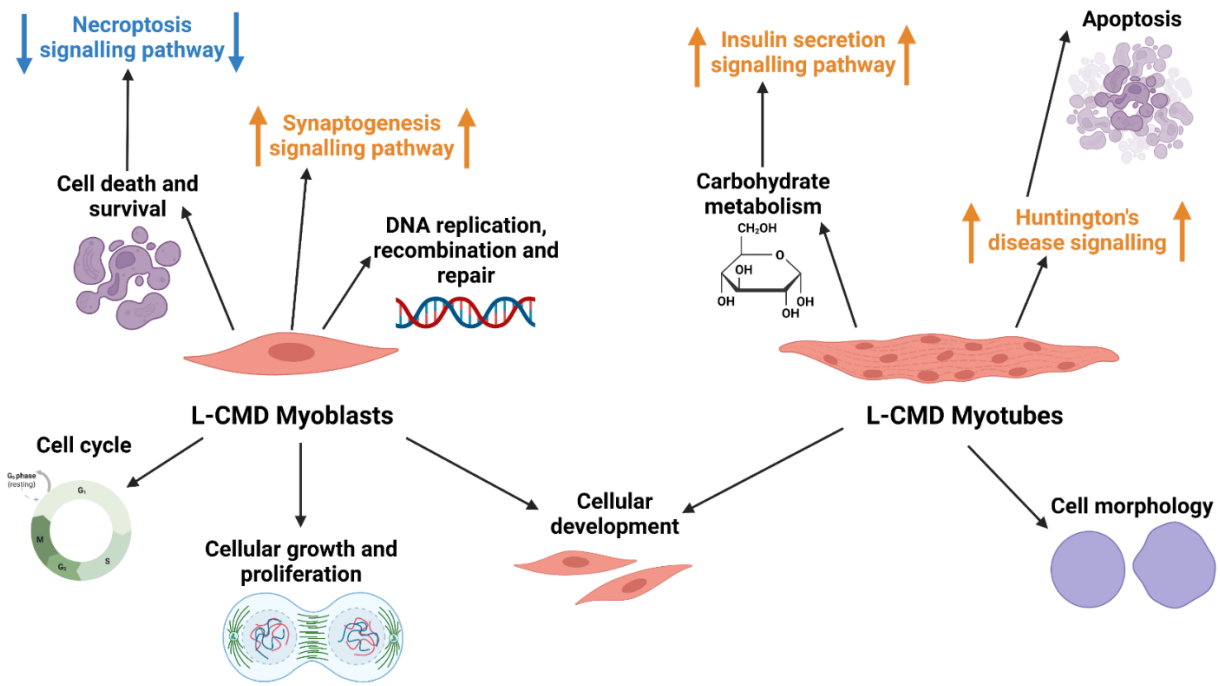

Figure 5.6- Overview of molecular and cellular processes and canonical pathways that may be dysregulated in L-CMD myoblasts and myotubes. *Molecular and cellular processes associated with differentially expressed proteins that were identified in L-CMD myoblasts compared to controls included cell cycle, cellular growth and proliferation, cellular development, DNA replication, recombination and repair, and cell death and survival. Cell death and survival might be related to downregulation of the necroptosis signalling pathway, and synaptogenesis signalling also appeared to be upregulated in L-CMD myoblasts. Cellular development was also related to differentially expressed proteins found in L-CMD myotubes, as well as cell morphology and carbohydrate metabolism. Carbohydrate metabolism could be linked to upregulation of the insulin secretion signalling pathway in L-CMD myotubes. Additionally, Huntington's disease signalling was elevated in L-CMD myotubes, and some of the proteins involved in this pathway were implicated in apoptosis.*

5.3. Discussion

In the past couple of decades, proteomics methods have gained popularity as a useful method for identifying and quantifying all the proteins within a biological sample on a large-scale in an unbiased manner. Proteomic studies have advanced our understanding of cellular signalling networks and have improved diagnosis and molecular understanding of disease mechanisms. By comparing the proteome of L-CMD cells to controls using SWATH-MS, a total of 124 differentially expressed proteins were identified in the L-CMD myoblasts, and 228 proteins were identified in the L-CMD myotubes, which could be potentially linked to the development of the disease. It was noted that there were more dysregulated proteins in the L-CMD myotubes than the L-CMD myoblasts, compared to controls, maybe suggesting that processes are more impaired in L-CMD myotubes. There was also found to be very little cross over between the dysregulated proteins that were identified in the L-CMD myoblasts and myotubes. This implies the processes and signalling pathways that are dysregulated in L-CMD myoblasts and myotubes differ. This was substantiated by the finding that the molecular and cellular pathways and the canonical pathways associated with the dysregulated proteins were different for the L-CMD myoblasts and myotubes.

5.3.1. B-cell CLL/lymphoma 7 protein family member B and transketolase were the only proteins found to be commonly downregulated in both L-CMD myoblasts and myotubes

Only two proteins were found to be changed in the same direction (downregulated) across the L-CMD myoblasts and myotubes, BCL7B (B-cell CLL/lymphoma 7 protein family member B) and transketolase. The human *BCL7* gene family have been implicated in cancer incidence, progression and development (Zani *et al.*, 1996; Potter

et al., 2008; Morton *et al.*, 2009), but it has also been identified that BCL7B has roles in negatively regulating the Wnt-signalling pathway and positively regulating the apoptotic pathway (Uehara *et al.*, 2015). Previously, in section 5.2.2., it was mentioned that pathways associated with cancer-related processes were not regarded as pathways of interest, although this may be seen as a limitation. Here, BCL7B is a good example of how filtering out cancer pathways may have removed interesting findings, as BCL7B is implicated in cancer development, but may play a role in other diseases through its involvement in apoptosis. *BCL7B* overexpression in human cancer cells (KATO III) was found to modulate cell proliferation, as cells overexpressing *BCL7B* died two days after transfection (Uehara *et al.*, 2015). This suggests overexpression of *BCL7B* may promote apoptosis. The expression of apoptosis inhibitors was additionally examined in *BCL7B*-knockdown cancer cells, and these were found to be upregulated (Uehara *et al.*, 2015). Collectively these results suggest BCL7B is a positive regulator of apoptosis. Interestingly other regulators of apoptosis were found to be dysregulated in L-CMD myotubes, which is later discussed in Section 5.3.6. In *BCL7B*-knockdown human cancer cells members of the Wnt signalling pathway, including β-catenin and high-mobility group A1 (HMGA1), were also significantly increased in expression (Uehara *et al.*, 2015). The Wnt signaling pathway is an evolutionarily conserved pathway that regulates crucial aspects of cell fate determination, cell migration, cell polarity, neural patterning and organogenesis during embryonic development (Nayak, Bhattacharyya and De, 2016). As BCL7B increases β-catenin expression, one approach could be to use quercetin, a known anti-tumor agent which is known to inhibit the transcriptional activity of β-catenin (Park *et al.*, 2005), and study the effects of quercetin treatment on L-CMD myoblasts and myotubes. Quercetin treatment has

previously been shown to be effective in models of SMA (Wishart *et al.*, 2014). Considering regulators of apoptosis have been found to be dysregulated in L-CMD myoblasts and myotubes, it would be useful to determine whether cell viability is decreased in the L-CMD cells compared to controls. Whilst this was not assessed in this thesis, it should be considered in future work.

Transketolase (TKT), on the other hand, is an enzyme that participates in the pentose phosphate pathway. The pentose phosphate pathway is a metabolic pathway that is parallel to glycolysis and generates NADPH and pentose, as well as ribose 5-phosphate, a precursor for the synthesis of nucleotides. TKT has been reported to be involved in the regulation of multiple cancer-related events, such as metastasis, invasion, cancer cell proliferation, epithelial-mesenchymal transition, chemoradiotherapy resistance, and patient survival (Hao *et al.*, 2022). TKT inhibitors have shown promise as effective cancer treatment drugs (Hao *et al.*, 2022), however, as TKT was downregulated in L-CMD myoblasts and myotubes, a TKT activator might be beneficial. Currently, no compounds are available that are known activators of TKT.

5.3.2. Of the LINC complex proteins, only lamin A/C appeared to be significantly changed in expression in L-CMD myotubes compared to controls

Although the LINC complex proteins, lamin A/C, lamin B1 and B2, emerin, FHL1, SUN1/SUN2, and nesprin-1/2, were detected in the SWATH-MS analysis, only lamin A/C met the criteria for differential expression, and this was found only in L-CMD myotubes compared to controls.

In Chapter 3, it was hypothesized that due to the L-CMD cells harbouring mutations in *LMNA,* the expression and localization of lamin A/C, as well as its known binding

partners, emerin and SUN2 may be changed in the L-CMD cells. Matching the results of the SWATH-MS analysis, using quantitative western blotting, lamin A/C was found to be statistically significantly reduced in L-CMD myotubes. As previously discussed, in Chapter 3, Section 3.3.4., lamin A/C has also previously been found to be reduced in myoblasts and myotubes derived from *Lmna*$^{\Delta K32/\Delta K32}$ mice (Bertrand *et al.*, 2012). These results together corroborate the hypothesis that lamin A/C is reduced in L-CMD cells, further highlighting that a potential therapy in L-CMD may aim to target or upregulate lamin A/C production (this is discussed in further detail in Chapter 3, Section 3.3.4.).

In Chapter 3, it was also found using western blotting that emerin and the main isoform of SUN2 were significantly reduced in expression in L-CMD myotubes compared to myoblasts. However, these two proteins were not found to be meet the criteria for differential expression in L-CMD myotubes in the SWATH-MS analysis. Although it was surprising that these results did not entirely match, it was noticed that in the case of emerin and SUN2, there was a lot of variability within the total sum areas for each peptide identified. To determine whether a protein was significantly dysregulated in the L-CMD cells, the total sum area was averaged across the three cell lines and tested for significance. The high variability would have increased the standard deviation of the L-CMD samples, resulting in emerin and SUN2 not being significantly changed in expression in L-CMD myotubes.

5.3.3. IPA analysis revealed top molecular and cellular pathways associated with the differentially expressed proteins that were identified in L-CMD myoblasts and myotubes

5.3.3.1. Dysregulated proteins associated with terms including cellular development, cell cycle and cell growth and proliferation suggest myotube formation could be compromised in L-CMD

Through imputing the data from the proteomics experiment into IPA, molecular and cellular pathway GO terms were generated which were most common to the dysregulated proteins. The most common GO terms for the dysregulated proteins in the L-CMD myoblasts and myotubes mostly differed, however cell development was a top term associated with the proteins in both groups. A larger number of proteins involved in cellular development were found to be dysregulated in L-CMD myotubes, therefore this process may be more impaired in L-CMD myotubes compared to L-CMD myoblasts. The GO term "cell development" is defined by the European Bioinformatics Institute as "the process whose specific outcome is the progression of the cell over time, from its formation to the mature structure". If proteins associated with this process are not functioning correctly, this perhaps suggests that L-CMD myoblasts may fail to develop and mature properly, which might affect their ability to then fuse and form myotubes. This may also affect the maturation and integrity of L-CMD myotubes. Previously it has been observed that C2C12 cells expressing L-CMD related *Lmna* exon 4 mutations have reduced differentiation capacity (Gómez-Domínguez *et al.*, 2020), and it has been observed that C2C12 myoblasts expressing lamin A linked muscular dystrophy mutations (R453W, W514) produce fewer myotubes per field and had reduced multinucleation per myofiber (Dutta and Vasudevan, 2022). This was not directly assessed in the L-CMD myotubes, and should be examined in future studies . Linked to cell development, cell cycle was also a top molecular and cellular pathway for the dysregulated proteins identified in the myoblasts. This term would not be

expected to be associated with the proteins found in the myotubes, as myotubes are terminally differentiated cells that are formed when proliferating myoblasts exit the cell cycle and fuse together, and expression of the myogenic program requires previous exit from the cell cycle (Andrés and Walsh, 1996). As the dysregulated proteins in the L-CMD myoblasts were associated with the cell cycle, this may allude to dysregulation of the cell cycle in these cells. It has previously been demonstrated that lamin A/C and emerin are critical for skeletal muscle satellite cell differentiation, that myoblasts lacking lamin A/C or emerin have decreased levels of proteins important for muscle cell differentiation, and that myoblasts with reduced lamin A/C (*Lmna*$^{-/-}$ myoblasts) are delayed in their ability to exit the cell cycle (Frock *et al.*, 2006). If proliferating myoblasts fail to exit the cell cycle, they will be unable to form myotubes. A number of dysregulated proteins in L-CMD myoblasts were also associated with cell growth and proliferation. If L-CMD myoblasts fail to proliferate properly, this could also affect their ability to form multinucleated myotubes. This links to a previous observation in Chapter 4, Section 4.2.1., where it was found that cell proliferation rate was significantly decreased in the L-CMD cells compared to healthy controls. However, in Chapter 4, Section 4.2.1., it was found that L-CMD myotubes contained a similar amount of nuclei than the controls, suggesting that L-CMD myotubes did appear to form correctly to some extent. It was noticed though, that the del.K32 myotubes did contain less nuclei than the other L-CMD myotubes and control myotubes. This may suggest that the del.K32 myotubes do not develop properly.

Overall, the association of differentially expressed proteins in L-CMD myoblasts and myotubes with cell development, and as a number of dysregulated proteins in L-CMD myoblasts are related to cell cycle and cell growth and proliferation, this may suggest

that myotube formation is somewhat compromised in L-CMD cells. In Chapter 4, the L-CMD myoblasts were able to fuse and form myotubes, and the myotubes visually appeared similar to control myotubes when growing in culture. Although in this Chapter, it was also revealed that each of the L-CMD cell lines exhibited abnormal nuclei in both myoblasts and myotubes. In particular, it was found that 95% of nuclei in R249W myotubes were abnormally shaped, compared to 54% of R249W myoblasts nuclei exhibiting abnormalities. This suggests that "faulty" myoblasts with abnormal nuclei still get incorporated into myotubes, and consequently this may impact myotube formation and development.

5.3.3.2. A number of differentially expressed proteins in L-CMD myotubes were linked to cell morphology, which may be related to nuclear defects observed in L-CMD cells as well as myotube morphology

It was found that a large number of dysregulated proteins in L-CMD myotubes were related to cell morphology. This could be linked to the finding that a large number of dysregulated proteins are involved in cell development, as if myotubes do not develop properly, their morphology may also be compromised, or vice versa. Interestingly, this term was not associated with the proteins that were dysregulated in the L-CMD myoblasts. This perhaps suggests that cell morphology defects may be worsened in myotubes. Whilst it was noted that the whole cell morphology of L-CMD myoblasts and myotubes did not appear different to controls when growing in culture (Chapter 4, Section 4.2.1.), they exhibited abnormally shaped nuclei when the nuclei were examined using immunofluorescence microscopy, which is a known characteristic of cells harbouring *LMNA* mutations, as further discussed in Chapter 4, Section 4.2.2. and 4.3.2. It was observed that L-CMD R249W myotubes had a larger percentage of abnormal nuclei compared to undifferentiated R249W myoblasts, providing some

evidence that cell morphology defects, in particular nuclear shape abnormalities, are exacerbated in L-CMD myotubes compared to myoblasts (Chapter 4, Section 4.2.2.). Bertrand *et al.* have also previously observed that nuclear defects are exacerbated with differentiation of myoblasts harbouring the *LMNA* del.K32 mutation (Bertrand *et al.*, 2012), and this is discussed in more detail in Chapter 4, Section 4.3.1. It is important to note, however, that some of the proteins identified in relation to cell morphology may be involved in maintaining cell morphology in cell types that are different from myogenic cells. In these other cell types, the regulation of these proteins may be more pertinent for cell morphology than in muscle cells.

5.3.3.3. Other top molecular and cellular terms associated with dysregulated proteins found in L-CMD myoblasts included DNA replication, recombination and repair and cell death and survival

DNA replication, recombination and repair was also a common term for the dysregulated proteins in the myoblasts. Interestingly, it was found in Chapter 3, Section 3.2.1. that a number of known lamin A interactors were proteins involved in DNA repair processes, and following on from this, in Section 3.2.3., X-ray repair cross complementing 6 protein was identified as a putative lamin A interactor using mass spectrometry analysis of L-CMD and control pull-down extracts. These results previously discussed suggest that lamin A is involved in DNA repair processes through interactions with other proteins. As the dysregulated proteins identified in L-CMD myoblasts were also associated with these terms, it is possible that *LMNA* mutations affect DNA replication, recombination and repair processes. Another top GO term associated with the proteins identified in the myoblasts was cell death and survival. This term alludes to processes including apoptosis and necroptosis. The necroptosis pathway was found to be downregulated in L-CMD myoblasts compared to controls,

which is discussed further in Section 5.3.5. Proteins involved in apoptosis may also be dysregulated in L-CMD myoblasts. Although apoptosis was not a canonical pathway associated with the differentially expressed proteins in the L-CMD myoblasts, dysregulated apoptosis is a feature of Huntington's disease, and Huntington's disease signalling was elevated in L-CMD myotubes compared to healthy myotubes. Apoptosis is also related to DNA repair processes, as it is a secondary response to DNA damage (Wang, 2001). A large number of the dysregulated proteins in the L-CMD myotubes only were also associated with carbohydrate metabolism, and this links to upregulation of the insulin secretion pathway which was also identified in L-CMD myotubes. This is examined and discussed further in Section 5.5.4.

5.3.4. Carbohydrate metabolism and the insulin secretion pathway may be dysregulated in L-CMD myotubes

A substantial number of the dysregulated proteins in myotubes were linked to carbohydrate metabolism. Carbohydrate metabolism encompasses the biological processes responsible for the metabolic formation, breakdown, and interconversion of carbohydrates in living organisms. The two major energy sources for muscle contraction are glycogen and fatty acids, whose metabolic pathways converge into actyl-CoA for final oxidation via the Krebs cycle and the respiratory chain, therefore carbohydrate metabolism is important for muscle function (Hill, 1924). This is highlighted by the existence of muscle diseases that are carbohydrate metabolism disorders, such as glycogen storage diseases. These include McArdle disease and Pompe disease which are attributed to the inability to breakdown glycogen within muscle cells (Kishnani and Howell, 2004; Andreu *et al.*, 2007). Metabolic dysfunction has been observed in Duchenne muscular dystrophy, and is characterised by reduced

glycolytic and oxidative enzymes, decreased and abnormal mitochondria, decreased ATP, and increased oxidative stress (Chi *et al.*, 1987; Sharma *et al.*, 2003; Onopiuk *et al.*, 2009; Timpani, Hayes and Rybalka, 2015; Nghiem *et al.*, 2017; Schneider *et al.*, 2018). These alterations in dystrophic muscle have been found to lead to a "metabolic crisis" and reduced capacity to respond to metabolic demands such as muscle contraction (Schneider *et al.*, 2018). Abnormal carbohydrate metabolism and reduced glucose metabolism have also been found to be features of the canine golden retriever muscular dystrophy (GRMD) model for Duchenne muscular dystrophy (Amaral *et al.*, 2017; Schneider *et al.*, 2018), suggesting glucose metabolism could be monitored and potentially utilized as a pre-clinical biomarker to assess disease progression and normalization of muscle metabolism in GRMD dogs following various treatments (Schneider *et al.*, 2018). Alterations in carbohydrate metabolism are often associated with neuromuscular disorders (Martin and Freeze, 2003), therefore it may not be a direct consequence of *LMNA* mutations in L-CMD, and instead may be a result of muscle damage or abnormal function. There is some supporting evidence that metabolic function may be aberrant in L-CMD, as a bioengineered 3D myotube contraction monitoring chip modelling L-CMD was shown to have reduced contraction (Rose *et al.*, 2023), however further investigation is needed to verify this finding. If carbohydrate metabolism is affected in L-CMD myotubes, perhaps similarly to DMD, it should be investigated for biomarker purposes.

Interestingly the insulin secretion signalling pathway, which is also a component of carbohydrate metabolism, was additionally found to be upregulated in L-CMD myotubes compared to controls. It has been demonstrated that this insulin signalling is involved in myogenesis through the action of microRNAs (Litwiniuk *et al.*, 2016; Luo

et al., 2019). MicroRNAs (miRNAs) are small non-coding RNAs that are required for the post-transcriptional control of gene expression and play a key role in modulating muscle regeneration and stem cell behaviour (Catalanotto, Cogoni and Zardo, 2016). The miRNAs- insulin signalling pathway has been implicated in the maintenance of myoblast proliferation (Wei *et al.*, 2016). Analysis of C2C12s has demonstrated that myoblast proliferation is induced partially by repression of miR-195 and miR-497, which is mediated by proliferative inductors including NF-κB, leading to an increase of miR-195-miR-497 targets such as cell cycle genes (Ccne1, Ccnd2), and the mitogens insulin-like growth factor I receptor (Igf1r) and insulin receptor (Insr) (Wei *et al.*, 2016). miR-128a targets key elements within the insulin signalling pathway such as insulin receptor substrate 1 (Irs1) and phosphoinositide-3-kinase regulatory subunit 1 (Pik3r1), and it has also been shown that the inhibitory effects of pro-inflammatory cytokine TNF-α on miR-128a facilitates myoblast divisions (Motohashi *et al.*, 2013). miR-128a inhibition in mice also lead to an increase in skeletal muscle mass and fiber size (Motohashi *et al.*, 2013). Another important element of the insulin signalling pathway, Foxo1, is a target for miR-16, and downregulation of this miRNA is required to maintain FOXO1 protein expression in proliferating myoblasts (Jia *et al.*, 2017). Aside from being involved in myoblast proliferation, the insulin signalling pathway is also important in differentiating myotubes, which is more relevant to its dysregulation in L-CMD myotubes. miR-206 enhances satellite cell differentiation by targeting important inhibitors of myogenesis, such as Hdac4, notch receptor 3 (Notch3) and insulin-like growth factor binding protein 5 (Igfbp5), and inducing cell cycle arrest through the repression of DNA polymerase alpha 1 catalytic subunit (Hak *et al.*, 2006; Winbanks *et al.*, 2011; Liu *et al.*, 2012). miRNAs are emerging as a potential target to

improve muscle regeneration in the context of DMD alongside gene therapies (Liu *et al.*, 2012). Although none of the targets of these miRNAs were identified in the proteomics analysis, these specific targets could be explored in L-CMD in future work, considering their role in the insulin signalling pathway and myogenesis.

5.3.5. Synaptogenesis signalling dysregulation in could lead to neuromuscular junction defects in L-CMD

The synaptogenesis signalling pathway was found to be elevated in L-CMD myoblasts compared to controls. Synaptogenesis is the formation of synapses between neurons in the nervous system. The most well-characterized synapse is the neuromuscular junction (NMJ), which is composed of three cell types: the motor neuron, the myofiber, and the Schwann cell, and is an important part of the neuromuscular system (Engel, 2008) (**Fig 5.7**). The NMJ allows the motor neuron to transmit a signal to the muscle fibre, causing muscle contraction. Muscles require innervation to function, and even to just maintain muscle tone, preventing atrophy. Synaptic transmission at the NMJ begins when an action potential reaches the presynaptic terminal of a motor neuron. This activates voltage-gated calcium channels, allowing calcium ions to enter the neuron. Calcium ions bind to synaptotagmins (sensor proteins) on synaptic vesicles, triggering vesicle fusion with the cell membrane and the subsequent release of acetylcholine (ACh) neurotransmitter from the motor neuron into the synaptic cleft (Roghani *et al.*, 1994). ACh then binds to nicotinic acetylcholine receptors on the cell membrane of the muscle fibre, also known as the sarcolemma (**Fig 5.7**).

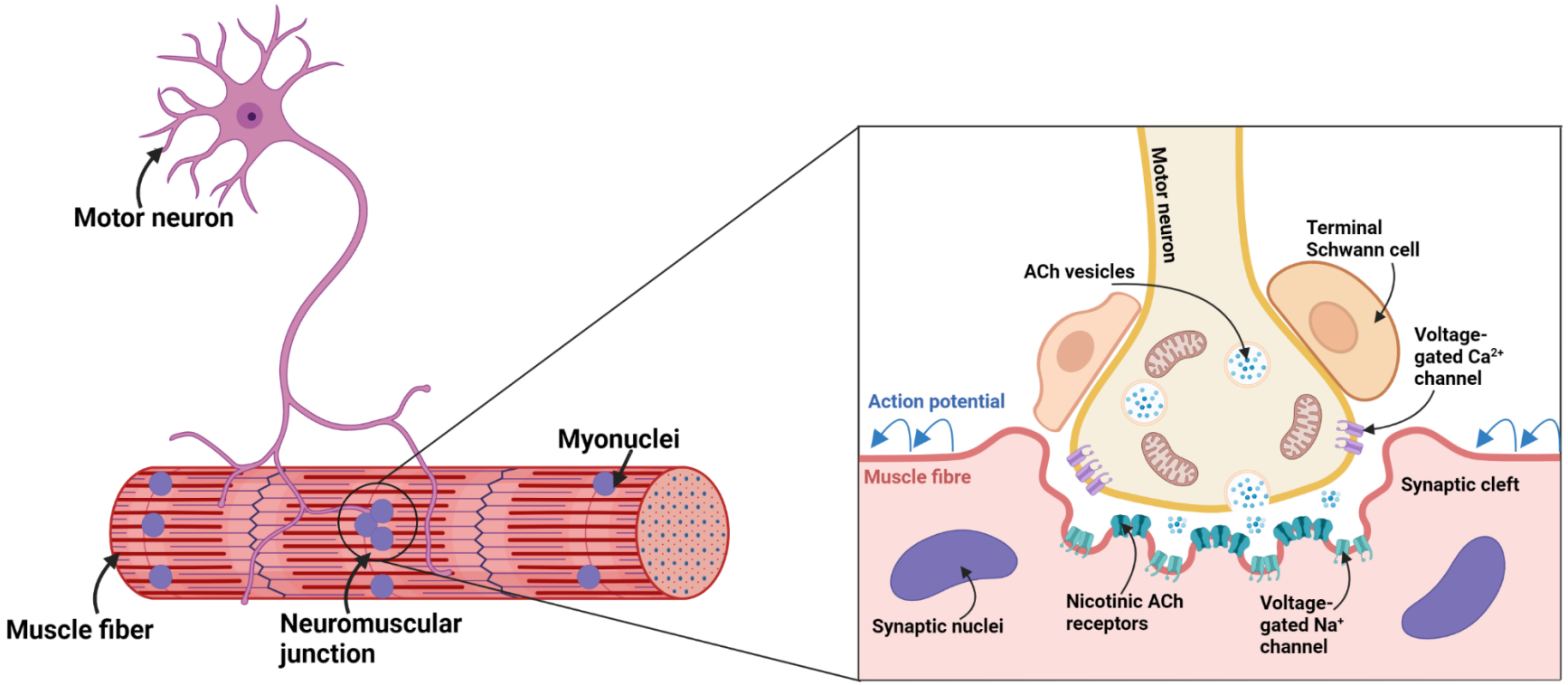

Figure 5.7- The neuromuscular junction (NMJ). *The NMJ allows the motor neuron to transmit a signal to the muscle fibre, causing muscle contraction. Synaptic transmission begins when an action potential reaches the presynaptic terminal of a motor neuron. This activates voltage-gated calcium channels, allowing calcium ions to enter the neuron. Calcium ions trigger vesicle fusion with the cell membrane and release of acetylcholine (ACh) neurotransmitter into the synaptic cleft. ACh then binds to nicotinic acetylcholine receptors on the cell membrane of the muscle fibre, also known as the sarcolemma. Adapted from Castets, Ham and Rüegg, 2020. Created using Biorender.*

For a long time, researchers have pondered whether it is the motorneurons or the muscle fibres that determine where and how NMJ are formed (Wu, Xiong and Mei, 2010). In mouse aneural muscle fibres, ACh receptors (AChRs) are initially evenly distributed, then accumulate in the middle of the fibres, where innervation occurs (Braithwaite and Harris, 1979; Ziskind-Conhaim and Bennett, 1982; Creazzo and Sohal, 1983). However, *in vitro* studies of synapse formation indicated, that spinal neuron axons ignore such pre-existing AChR clusters on co-cultured muscle fibres and form synapses at different locations (Anderson and Cohen, 1977). This suggests a dominant role for motorneurons determining where NMJs are formed (Wu, Xiong and Mei, 2010). Although, other *in vivo* studies have revealed that AChR clusters are located in the central region of muscle fibres prior to the arrival of motorneuron axons (Lin *et al.*, 2001; Yang *et al.*, 2001). This is known as prepatterning and appears to be nerve independent, also occurring in mice lacking motor nerves (Yang *et al.*, 2001). These findings suggest that muscle fibres may play an active role in NMJ formation, therefore it is possible that defective signaling pathways within muscle cells could affect this process (Kummer, Misgeld and Sanes, 2006; Wu, Xiong and Mei, 2010).

Skeletal muscle tissue comprises of multinucleated fibres formed by the fusion of mononucleated myoblasts during development. Among the hundreds of nuclei within a muscle fibre, approximately four to eight nuclei are specialized for the transcription of the components of the synapse at the NMJ (Schaeffer, de Kerchove d'Exaerde and Changeux, 2001; Méjat *et al.*, 2003). Synaptic nuclei are recruited within the area of the postsynaptic membrane during muscle differentiation, and their proper

positioning is crucial for NMJ establishment and maintenance (Ruegg, 2005). The positioning of synaptic nuclei is dependent on the cytoskeleton and several nuclear envelope (NE) proteins including nesprin and SUN proteins (Grady *et al.*, 2005; X. Zhang *et al.*, 2007). Double knock out of both nesprin-1 and nesprin-2 in mice leads to the absence of nuclei recruited to the synapses of diaphragm muscles, demonstrating the important of NE proteins in the positioning of synaptic nuclei (X. Zhang *et al.*, 2007).

NMJ defects have been previously observed in models of autosomal dominant Emery-Dreifuss muscular dystrophy (AD-EDMD), which, similarly to L-CMD, is caused by *LMNA* mutations (Méjat *et al.*, 2009). Two AD-EDMD mouse models *($Lmna^{H222P/H222P}$, $Lmna^{-/-}$)* were found to show innervation defects including misexpression of electrical activity-dependent genes and altered epigenetic chromatin modifications, as well as aberrant NMJ architecture (Méjat *et al.*, 2009). Synaptic nuclei were also not properly recruited to the NMJ due to mislocalisation of several NE components, including SUN2 and nesprin-1 (Méjat *et al.*, 2009). These same defects were present in biopsies from AD-EDMD patients, indicating that these defects are relevant to human disease (Méjat *et al.*, 2009). Considering these results, it is plausible that NMJ defects contribute to L-CMD pathophysiology, and this is something that has not yet been investigated. In Chapter 4, Section 4.3.5, localization of SUN2 was examined in L-CMD myoblasts and myotubes, and unusually, SUN2 was detected very weakly at the NE, but it did not appear to be mislocalized to another part of the cell. The reasons for this are explored in more detail in Chapter 4, Section 4.3.5. The localization of nesprin-1 was not explored and has not been previously characterized in L-CMD cells. In future, it would be insightful to clarify whether SUN and nesprin proteins are mislocalized in L-CMD

myoblasts and myotubes, it would be even more relevant to determine whether these proteins are mislocalized in L-CMD patient muscle, however obtaining muscle biopsies is difficult. Given there are L-CMD mouse models available (such as the *Lmna*$^{\Delta K32}$ mouse) (Azibani *et al.*, 2018), perhaps in future, a study could be conducted to establish whether the same innervation and NMJ architecture defects are present, and whether synaptic nuclei positioning is also affected.

5.3.6. Apaf-1, a key component of the intrinsic apoptotic pathway, may be upregulated in L-CMD myotubes

In multicellular organisms, there are a number of different cell death mechanisms. Necrosis is an unregulated process that usually occurs as a result of acute cellular injury and is a form of traumatic cell death. Apoptosis, on the other hand, is a highly regulated and controlled form of programmed cell death.

Apoptosis dysregulation has been identified as a feature of a number of neurodegenerative diseases, including Huntington's disease (Hickey and Chesselet, 2003; Sang *et al.*, 2005; Vis *et al.*, 2005; Yang *et al.*, 2010), a condition characterized by progressive motor, psychiatric and cognitive impairment that is attributed to nerve cell damage and atrophy of the brain tissue (McColgan and Tabrizi, 2018). Huntington's disease signalling was upregulated in L-CMD myotubes compared to controls, and upon further examination of the dysregulated proteins involved in this pathway, two proteins that are involved in apoptosis were of particular interest; apoptotic protease-activating factor 1 (Apaf-1) and caspase-7. Apaf-1 was increased in L-CMD myotubes, whilst Casp-7 was downregulated. Apaf-1 is a component of the mitochondrial-mediated or intrinsic apoptotic pathway that is triggered by intracellular stress (Danial

and Korsmeyer, 2004) (**Fig 5.8**). When there is an absence of stress signals, cytochrome c associates with the outer surface of the inner membrane of mitochondria, while Apaf-1, procaspase-9 monomers as well as procaspase-3 dimers are present in the cytosol (Shakeri, Kheirollahi and Davoodi, 2021). In response to intracellular stress, mitochondrial membranes become permeable, and cytochrome c is released to the cytosol (Shakeri, Kheirollahi and Davoodi, 2021). Cytochrome c binds to Apaf-1 and promotes a conformational change that leads to the Apaf-1 oligomerization and procaspase-9 binding, forming a large complex known as apoptosome (Shakeri, Kheirollahi and Davoodi, 2021). Procaspase-3 is then recruited and cleaved by the active caspase-9 on the apoptosome complex (Shakeri, Kheirollahi and Davoodi, 2021). Once active, caspase-9 can also directly cleave and activate caspase-3 and caspase-7 (Li *et al.*, 1997). Caspase-3 and -7 are effector caspases which are responsible for initiating the hallmarks of the degradation phase of apoptosis including DNA fragmentation, cell shrinkage, and membrane blebbing (Woo *et al.*, 1998; Shi, 2002). Effector caspases perform the actual destruction of the cell and initiate “the point of no return” in the apoptotic “death cascade”.

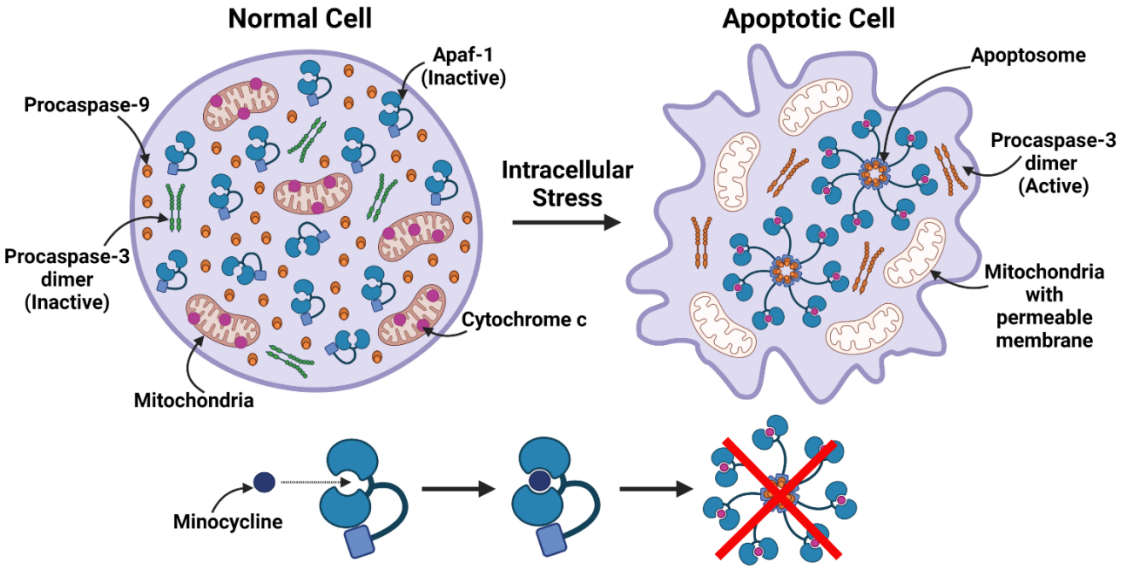

Figure 5.8- The intrinsic apoptotic pathway*. The intrinsic apoptotic pathway is triggered by intracellular stress. When stress signals are not present, cytochrome c is found on the outer surface of the inner membrane of mitochondria, while Apaf-1, procaspase-9 as well as procaspase-3 are in the cytosol. The membrane of mitochondria become permeable in response to intracellular stress, and cytochrome c is released to the cytosol. Cytochrome c binds to Apaf-1 and promotes a conformational change that leads to the Apaf-1 oligomerization and procaspase-9 binding, forming a large complex known as apoptosome. Then, procaspase-3 is recruited and cleaved by the active caspase-9 on the apoptosome complex. When active, caspase-9 can also directly cleave effector caspases, initiating destruction of the cell. Minocycline is an Apaf-1 inhibitor and binds to Apaf-1, preventing the formation of the apoptosome and hence preventing apoptosis. Adapted from Shakeri, Kheirollahi and Davoodi, 2021. Created using Biorender.*

Differentiated cells including cardiomyocytes, skeletal myocytes and neurons exhibit low levels of Apaf-1 (Burgess *et al.*, 1999; Yakovlev *et al.*, 2001; Sanchis *et al.*, 2003), suggesting that downregulation of Apaf-1 is important in contributing to the resistance of these cells to apoptosis. Alterations of Apaf-1 have been reported in different diseases. Downregulation of Apaf-1 has been associated with cancer (Shakeri, Kheirollahi and Davoodi, 2021), whilst upregulation of Apaf-1 has been identified in pathologies associated with enhanced neuronal cell death such as Huntington's

disease and amyotrophic lateral sclerosis (ALS) (Sang *et al.*, 2005; Yamazaki, Esumi and Nakano, 2005). This suggests that upregulation of Apaf-1 in L-CMD myotubes may make them susceptible to cell death. It has been shown that inhibition of Apaf-1 allows cells to escape apoptosis and recover (Gortat *et al.*, 2015), and suppresses unwanted apoptotic cell death in animal models of apoptotic damage (Orzáez *et al.*, 2014). This has been accomplished through endogenous inhibitors, microRNAs and epigenetic alterations (Shakeri, Kheirollahi and Davoodi, 2021). Amongst these is minocycline ((7-dimethylamino-6-dimethyl-6-deoxytetracycline), a tetracycline that has been used for over 40 years for its antibiotic properties which is already licensed for the treatment of conditions including rheumatoid arthritis, acne and other bacterial infections. Minocycline binds to Apaf-1, preventing apoptosome formation and apoptosis induction, and directly inhibits the release of cytochrome c from the mitochondria (Zhu *et al.*, 2002; Sancho *et al.*, 2011) (**Fig 5.8**). Minocycline has been shown to slow ALS progression in mice (Zhu *et al.*, 2002), and can increase survival and reduce motor neuron loss in transgenic mouse models of ALS (Swash, 2007). In preclinical studies in Huntington's disease animal models, however, minocycline has shown differing levels of efficacy. Some studies have reported significant biochemical and behavioural improvements (Chen *et al.*, 2000; Stack *et al.*, 2006; Sancho *et al.*, 2011; Kalonia, Mishra and Kumar, 2012), suggesting minoclycline has a neuroprotective effect, although some studies have shown no improvement in mice models (Smith *et al.*, 2003; Mievis *et al.*, 2007; Menalled *et al.*, 2010). Despite this, knowledge of Apaf-1 inhibitors could be applied and tested on L-CMD myotubes to determine whether apoptosis can firstly be suppressed, then an Apaf-1 inhibitor could perhaps be tested in a mouse model of L-CMD (as previously described), to determine

whether the muscular dystrophy phenotype is improved. Minoclycline is an attractive candidate for drug repurposing in L-CMD due to its known safety and tolerability, although it is important to bare in mind that over suppression of apoptosis could lead to an increased risk of tumor development.

5.3.7. Necroptosis may be dysregulated in L-CMD myoblasts, however verification of this pathway is proving difficult

Necroptosis is another method of cell death which combines aspects of necrosis and apoptosis and can be known as a programmed form of necrosis. In L-CMD myoblasts, it was found that the necroptosis pathway was significantly downregulated, and four dysregulated proteins were implicated in this pathway, signal transducer and activator of transcription 1 (STAT1), translocase of outer mitochondrial membrane 34 (TOMM34), peptidyl-prolyl cis-trans isomerase FKBP1A (FKBP1A), retinoblastoma-like protein 1 (RBL1). Necroptosis can be caused by Toll-like receptor (TLR)-3 and TLR-4 agonists, tumor necrosis factor (TNF), certain microbial infections, and T cell receptors (Yu *et al.*, 2021). Necroptosis signaling is modulated by receptor-interacting protein kinase (RIPK) 1 when the activity of caspase-8 becomes compromised (Yu *et al.*, 2021). Activated death receptors (DRs) cause the activation of RIPK1 and RIPK1 kinase activity-dependent formation of an RIPK1-RIPK3-mixed lineage kinase domain-like protein (MLKL), which is complex II (Yu *et al.*, 2021). RIPK3 phosphorylates MLKL, ultimately leading to necrosis through plasma membrane disruption and cell lysis (Yu *et al.*, 2021).

Necroptosis has been found to be of central pathophysiological relevance in a variety of disease states including myocardial infarction and stroke (Smith *et al.*, 2007;

Degterev *et al.*, 2008), atherosclerosis (Lin *et al.*, 2013), ischemia-reperfusion injury (Linkermann *et al.*, 2012; Oerlemans *et al.*, 2012), pancreatitis (D. W. Zhang *et al.*, 2009; Wu *et al.*, 2013), inflammatory bowel diseases (Welz *et al.*, 2011), as well as neurological disorders (Ito *et al.*, 2016; S. Zhang *et al.*, 2019). More recently, necroptosis has been implicated in neuromuscular diseases including Duchenne muscular dystrophy (DMD) and SMA (Bencze *et al.*, 2017; Chehade *et al.*, 2022). DMD is caused by a deficiency in dystrophin (Bonilla *et al.*, 1988). Dystrophin-deficient muscles are characterized by progressive myofiber necrosis, and necroptosis has been identified as a mechanism underlying myofiber death in muscle lacking dystrophin (Morgan *et al.*, 2018). RIPK1, RIPK3 and MLKL have been found to be upregulated in dystrophic mouse myofibres (Morgan *et al.*, 2018). Furthermore, genetic ablation of *Ripk3* in the mdx mouse model of DMD reduces myofiber degeneration, inflammatory infiltrate, and muscle fibrosis, and eventually improves muscle function (Morgan *et al.*, 2018). These findings provided the first evidence of necroptotic cell death in a disease affecting skeletal muscle (Morgan *et al.*, 2018). SMA, on the other hand, is caused by reduced levels of the survival motor neuron (SMN) protein. Chehade *et al.* evaluated the role of necroptosis in SMA by generating a triple mutant knock out (TKO), $Smn^{2B/-}$; $Ripk3^{-/-}$; $Casp1^{-/-}$ mouse (Chehade *et al.*, 2022). TKO mice displayed a robust increase in survival and improved motor function compared to $Smn^{2B/-}$ mice (Chehade *et al.*, 2022). Whilst it was found that there was no protection against motor neuron loss or NMJ pathology, larger muscle fibers were also observed in TKO mice compared to $Smn^{2B/-}$ mice (Chehade *et al.*, 2022). This study concluded that necroptosis modulated survival, motor behaviour and muscle fiber size independent of SMN levels and independent of neurodegeneration (Chehade *et al.*, 2022). Considering the

necroptosis pathway's emerging role in neuromuscular conditions as well as identification of its dysregulation in L-CMD myoblasts, it appeared to be a strong candidate for further verification.

Another factor that made the necroptosis pathway a contender for further study was the feasibility of being able to target the pathway using available pharmacological compounds. Several specific necroptosis inhibitors aimed at the central components of the necroptosis pathway have been discovered or developed, such as RIPK1 inhibitors Necrostatin-1 (Nec-1), Necrostatin 2 racemate (Nec-1s), and Compound 27 (furo[2,3-d]pyrimidines) (cpd27), and RIPK3 inhibitor GSK872. Studies of these necroptosis inhibitors have shown therapeutic effects in various inflammatory disease. In animal models of traumatic brain injury, Nec-1 inhibits apoptosis and autophagy (Wang *et al.*, 2012), Nec-1 also reduces amyloid beta, the main components of amyloid plaques found in the brains of people with Alzheimer's disease, and tau protein abnormalities in an Alzheimer's disease animal model (Yang *et al.*, 2017). The use of a necroptosis inhibitor is yet to be tested in a model of neuromuscular disease. As the necroptosis pathway was found to be decreased in L-CMD myoblasts, a necroptosis inhibitor may not be a potential therapeutic treatment. However, as there are currently no compounds that target upregulation of the pathway, L-CMD myoblasts were treated with Nec-1 in an attempt to verify dysregulation of the necroptosis pathway in these cells.

It was theorized that Nec-1 treatment would further reduce levels of STAT1 and TOMM34, which were identified by IPA as components of the necroptosis pathway and reduced in expression in L-CMD myoblasts. Despite this, results suggested that

STAT1 and TOMM34 may not be decreased in expression in treated cells compared to untreated and vehicle treated. This may be a consequence of technical experimental difficulties and/or STAT1 and TOMM34 not being components of the pathway cascades downstream of Nec-1's target (RIPK1). When verifying the expression levels of STAT1 in Nec-1 treated, untreated and vehicle treated L-CMD myoblasts using western blotting, there were technical difficulties electrophoresing STAT1. It appeared that there may have been issues solubilizing STAT1 and therefore the protein may not have migrated properly out of the wells during sodium dodecyl sulfate-polyacrylamide gel electrophoresis (SDS-PAGE), this makes quantifying STAT1 difficult. An indication of this was that the resulting western blot image showed distinct bands that were located in the area corresponding to where the wells of the gel were transferred to the nitrocellulose. If STAT1 failed to migrate out of the wells into the SDS-PAGE gel then the resulting bands may not accurately reflect the quantity of STAT1 in the samples. Prior to the drug study, in the previous experiment where western blotting was used to explore STAT1 expression in L-CMD myoblasts versus control myoblasts, STAT1 did appear to successfully electrophorese despite running the SDS-PAGE gel under identical conditions (using the same type of gels, buffer system and voltage). However, in the drug study, more protein may have been loaded into the wells, consequently making it more difficult to electrophorese and separate STAT1 from the samples. STAT1 is a heavily glycosylated protein, and glycosylation often heavily impacts protein migration during SDS-PAGE gel electrophoresis. Unlike non-glycosylated proteins which have a distinct singular band, glycosylated proteins often appear as a characteristic "smear" on SDS-PAGE gel due to the heterogeneity in the glycosylation, meaning that the mass of the protein can change dramatically by several thousand

daltons as the extent of protein glycosylation can vary drastically. The smears produced by glycosylated proteins are additionally hard to accurately measure and quantify using software such as ImageJ compared to clean, distinct single bands produced by non-glycosylated proteins.

Overall, dysregulation of the necroptosis pathway in L-CMD myoblasts, as revealed using quantitative proteomics, was incredibly difficult to verify using quantitative western blotting. This was not only due to the issues surrounding the Nec-1 drug study, as discussed above, but also because there are very few antibodies available that target the necroptosis pathway proteins that were found to be dysregulated, and of these antibodies, there was a lack of publications verifying their efficacy. As a consequence, many antibodies were tried and tested but failed to work on western blot. This meant that it was only possibly to verify two (STAT1 and TOMM34) of the four dysregulated proteins.

5.4. Conclusion and future work

As a quantitative proteomics study in L-CMD is not currently evident within the literature, the results generated here are potentially particularly insightful into L-CMD pathophysiology. This approach has revealed differential expression of 124 differentially expressed proteins in the L-CMD myoblasts, and 228 proteins in the L-CMD myotubes, with only four proteins that were commonly changed in both L-CMD myoblasts and myotubes , and potential dysregulation of a number of different molecular and cellular processes and signalling pathways.

Amongst these, it was noted that molecular and cellular processes included common to dysregulated proteins identified in L-CMD myoblasts and or myotubes included cellular development, cell cycle and cellular growth and repair, which may affect the ability of myoblasts to fuse and form multinucleated myotubes. Previously, in Chapter 4, L-CMD myotubes were observed to visually be indistinguishable from healthy myotubes, however future work could clarify whether myogenic markers of differentiation are altered in the L-CMD myoblasts and myotubes.

Additionally, it has been revealed that carbohydrate metabolism and insulin secretion signalling may be dysregulated in L-CMD myotubes. If this can be verified, insulin signalling may be a targetable pathway for future therapy development. The use of miRNAs to target aspects of the insulin signalling pathway are currently being studied for use in combination with other therapies for DMD, this could perhaps be also applied to L-CMD. The results here also suggest that components of the synaptogenesis pathway may be dysregulated in L-CMD myoblasts, this may be insightful into disease pathophysiology but is not a pathway that is necessarily targetable.

Cell death and survival related processes also seemed to re-occur in both L-CMD myoblasts and myotubes. A number of proteins involved in apoptosis may be dysregulated in L-CMD myotubes, and the necroptosis pathway may be downregulated in myoblasts. Verification of the necroptosis pathway was attempted, however this was hindered by technical difficulties and lack of antibodies available. If it is possible to confirm dysregulation of either apoptosis or necroptosis, either of these pathways may be potential therapeutic targets. It is important, however, to consider

cell death processes may be a result of the muscle being dystrophic and not functioning correctly, rather than a direct consequence of the causative mutation.

Finally, both an advantage and drawback of proteomics is the quantity of data generated from the experiment, as although thousands of proteins can be identified, often interesting findings can be overlooked. No doubt there may be pathways or proteins of interest within the data generated in this study that have been missed. Although, once the data has been produced, it remains as a valuable resource for future research.

Chapter 6: Genotype-phenotype correlations in human diseases caused by mutations of LINC complex-associated genes: a systematic review and meta-summary

6.1. Introduction

As well as *LMNA*, mutations in genes encoding other nuclear envelope (NE) proteins have additionally been associated with a range of human disorders that are collectively known as "nuclear envelopathies" (Nagano and Arahata, 2000; Somech *et al.*, 2005; Chi, Chen and Jeang, 2009). In some cases, mutations in the genes encoding NE proteins lead to the development of multiple diseases, and it is uncertain why this occurs. Many of these nuclear envelopathies are rare diseases and their pathophysiology is not fully understood. As a result, there are few or no treatment options available for these conditions.

6.1.1. Mutations in the *LMNA* gene cause a spectrum of human diseases with vastly different phenotypes

LMNA mutations are responsible for more than 15 tissue-specific laminopathies that can be classified into two groups; neuromuscular disorders affecting skeletal muscle, cardiac muscle and/or the peripheral nervous system, and secondly partial lipodystophy syndromes with or without developmental abnormalities and premature aging (Bertrand *et al.*, 2011). Congenital muscular dystrophy (L-CMD) (Quijano-Roy *et al.*, 2008), autosomal dominant and recessive Emery-dreifuss muscular dystrophy (EDMD) (Bonne *et al.*, 1999), and Limb-girdle muscular dystrophy type 1B (LGMD1B) (Muchir *et al.*, 2000), are all skeletal muscle disorders caused by *LMNA* variants, whilst dilated cardiomyopathy (DCM) is a laminopathy that affects the heart (Fatkin *et al.*, 1999). These muscular dystrophies differ in their age of onset, muscle group involvement, disease progression and other associated symptoms, although they do share some clinical similarities. Categorised as muscular dystrophies, these diseases primarily involve muscle weakness

and wasting, in some cases joint contractures, and cardiac abnormalities including cardiomyopathy, which as mentioned, is a stand-alone laminopathy (Muchir *et al.*, 2000; Quijano-Roy *et al.*, 2008; Scharner *et al.*, 2011; Madej-Pilarczyk, 2018). Another *LMNA*-related neuromuscular disorder is autosomal recessive axonal Charcot-Marie-Tooth type 2B1 (CMT2B1) (De Sandre-Giovannoli *et al.*, 2002). CMT2B1 is a peripheral nervous system disease that mainly affects the hands, arms, legs and feet, leading to muscle weakness and decreased sensation in these regions of the body (Bernard *et al.*, 2006). Although CMT2B1 is a disease affecting the peripheral nervous system, it is important to highlight that similarly to the muscular dystrophies, CM2B1 manifests as muscle weakness and atrophy, sometimes with cardiac involvement (Bernard *et al.*, 2006).

Familial partial lipodystrophy (FPLD) falls into the second category of laminopathies. FPLD is a metabolic disease associated with reduced adipose tissue, particularly in the limbs and trunk (Vantyghem *et al.*, 2004). Individuals with FPLD may also be predisposed to metabolic abnormalities including insulin-resistant diabetes mellitus, hypertriglyceridemia and menstrual abnormalities (Garg, 2004). Premature aging disorders including Hutchinson-Gilford progeria syndrome (HGPS) (De Sandre-Giovannoli *et al.*, 2003), mandibuloacral dysplasia type A and B (MAD-A/B), restrictive dermopathy (RD), and atypical Werner syndrome are classified together with FPLD as individuals with premature aging diseases often also have reduced adipose tissue as is seen in lipodystrophies. HGPS is a rare, fatal childhood condition with features resembling premature aging. Affected children experience profound growth delays and have a distinctive facial appearance characterised by a disproportionately small face compared to the head, an

underdeveloped jaw, small nose, and a bluing around the mouth (Ahmed *et al.*, 2018). Other characteristics of HGPS that affected children may develop include atherosclerosis, cardiovascular disease, and stroke (Ahmed *et al.*, 2018). Unlike the other laminopathies, HGPS is a multi-system disorder affecting a number of different tissues and organ systems.

It remains a conundrum to scientists researching *LMNA*-related disorders as to how mutations in this one gene can cause a wide range of diseases. In the case of HGPS, however, a link has been made between the disease phenotype and the genotype which is different to other laminopathies. Whilst lamin C is directly translated from *LMNA*, lamin A is first synthesised as a precursor known as pre-lamin A which undergoes post-translational processing to become mature lamin A protein. Prelamin A contains a C-terminal CAAX motif that is farnesylated, followed by cleavage of the last three residues and carboxymethylation of the terminal cysteine (Sinensky *et al.*, 1994; Gonzalo, Kreienkamp and Askjaer, 2017). Finally, the 15 C-terminal residues are cleaved by the endoprotease Zmpste24 (FACE-1), producing mature lamin A (Sinensky *et al.*, 1994; Gonzalo, Kreienkamp and Askjaer, 2017). Mutations causing HGPS activate a cryptic splice site, leading to an in-frame deletion near the C-terminus of prelamin A (De Sandre-Giovannoli *et al.*, 2003; Eriksson *et al.*, 2003). This abnormal protein is known as "progerin" and retains the CAAX motif, is farnesylated and carboxymethylated, but lacks the site for endoproteolytic cleavage so remains permanently farnesylated within cells (Gonzalo, Kreienkamp and Askjaer, 2017). This discovery has allowed the development of the first therapy to treat HGPS, a farnesyltransferase inhibitor (FTI) called lonafarnib

(brand name Zokinvy™), which received its first approval in the USA in November 2020 (Dhillon, 2021). Ionafarnib works by preventing the farnesylation and subsequent accumulation of progerin (Dhillon, 2021). Despite thorough research, the relationship between different laminopathy phenotypes, besides HGPS, and genotypes remain poorly understood.

6.1.2. Nuclear envelope proteins and their associated diseases

Unlike *LMNA*, which is well known to cause a greater variety of genetic disorders than any other gene (Broers *et al.*, 2006), *LMNB1* and *LMNB2,* encoding B-type lamins, have been linked to far fewer diseases. Mutations in *LMNB2* have been implicated in acquired partial lipodystrophies, whilst *LMNB1* related diseases are only just appearing to emerge. Adult-onset autosomal dominant leukodystrophy (ADLD) is a slowly progressive, rare, demyelinating neuropathy, with a phenotype that bares resemblance to chronic progressive multiple sclerosis (Padiath *et al.*, 2006). Genomic duplications of the *LMNB1* gene have been found to be responsible for ADLD, where affected individuals carry an extra copy of the gene, resulting in increased expression of lamin B1 mRNA and protein expression in brain tissue from individuals with ADLD (Padiath *et al.*, 2006). ADLD was the first disease that was found to be attributed to *LMNB1* mutations (Padiath *et al.*, 2006). Even more recently, *LMNB1* variants have been identified in patients with neural tube defects (NTDs) including spina bifida, anencephaly and microcephaly (Robinson *et al.*, 2013).

EMD, encoding inner nuclear membrane protein emerin, was the first gene found to be responsible for EDMD (Bione *et al.*, 1994). Since then, mutations in *TMEM43* (also known as LUMA) (Liang *et al.*, 2011), *FHL1B* (Ziat and Bertrand, 2015), *SYNE1/SYNE2* (encoding nesprin 1 and 2) (Q. Zhang *et al.*, 2007a), have been linked to EDMD (as well as *LMNA,* as previously mentioned). *SUN1/SUN2* have also been identified as disease severity modifiers of EDMD (Meinke *et al.*, 2014). In addition to causing EDMD, *SYNE1* variants are known to cause autosomal recessive cerebellar ataxia (SCAR8) (Dupré *et al.*, 2007). SCAR8 manifests as pure cerebellar atrophy, ataxia and dysarthria with late-onset and a slow progression (Dupré *et al.*, 2007). Mutations in *SYNE1* can also cause arthrogryposis multiplex congenita (AMC), which causes infantile-onset musculoskeletal disease, bilateral club foot, scoliosis and restrictive lung disease (Attali *et al.*, 2009). Although, it has been debated whether AMC is just a continuation of SCAR8 rather than a distinct phenotype.

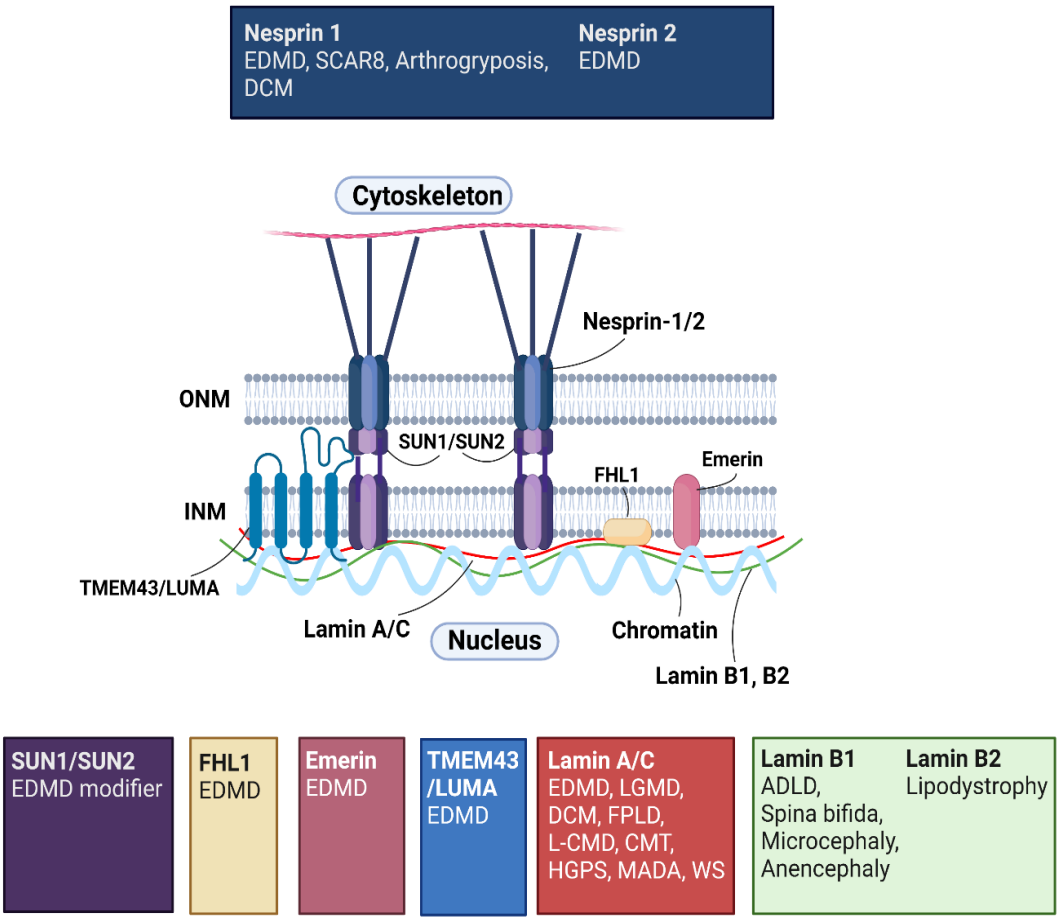

Figure 6.1- The Linker of Nucleoskeleton and Cytoskeleton (LINC) complex and associated human diseases. *The Linker of Nucleoskeleton and Cytoskeleton (LINC) complex primarily consists of SUN1/SUN2 and nesprin proteins, situated at the inner nuclear membrane (INM) and outer nuclear membrane (ONM), respectively. The Sad-UNC-84 and Klarsicht/Anc-1/Syne homology domains of the respective proteins interact in the perinuclear space (PNS), creating a physical connection between the nuclear lamina (NL) and the cytoskeleton. The NL comprises of type-V intermediate filament proteins, the nuclear lamins. Lamins A/C are A-type nuclear lamins, whilst lamin B1/B2 are B-type lamins. Various other NE proteins interact with the LINC complex including integral INM protein emerin, TMEM43/LUMA and isoforms of four-and-a-half LIM domain protein 1 (FHL1). Mutations in the genes encoding these proteins have been associated with a range of diseases exhibiting different phenotypes. Abbreviations: Emery-Dreifuss muscular dystrophy (EDMD), cerebellar ataxia (SCAR8), dilated cardiomyopathy (DCM), limb-girdle muscular dystrophy (LGMD), familial partial lipodystrophy (FPLD), congenital muscular dystrophy (L-CMD), Charcot-Marie-Tooth disease (CMT), Hutchinson-Gilford progeria syndrome (HGPS), mandibuloacral dysplasia (MADA), atypical Werner syndrome (WS). Created with BioRender.com.*

6.1.3. Theories on how mutations in one gene can cause multiple diseases

Although there is some understanding of the structure of LINC complex proteins and how they interact with one another and neighbouring NE proteins (Storey *et al.*, 2020), it is unclear how mutations in genes encoding them can simultaneously cause the same disease, and different diseases with entirely different phenotypes. As mentioned, mutations in *LMNA*, *EMD, SYNE1/SYNE2*, *TMEM43* and *FHL1B* all cause EDMD, yet mutations in *SYNE1* also cause SCAR8, and *LMNA* mutations cause a multitude of different diseases. To explain how mutations in *LMNA* cause many different conditions despite being ubiquitously expressed, the structural and gene hypotheses were proposed, which may not be two mutually exclusive theories, as previously discussed in detail in Chapter 1 (Sullivan *et al.*, 1999; Nikolova *et al.*, 2004). The structural hypothesis is not a sound theory on its own. It may explain the existence of multiple laminopathies that affect load-bearing tissues such as straited muscle, cardiovascular tissue, bone and cartilage, but doesn't account for metabolic disorders or peripheral nervous system diseases which affect tissues that are not exposed to high tension. The most logical explanation is that the structural and gene expression hypotheses are connected, and that there is a link between structural abnormalities of the nucleus caused by *LMNA* mutations, and chromatin modifications and reorganisation (Crasto, My and Di Pasquale, 2020).

There has been speculation that certain phenotypes may correlate to different regions of the *LMNA* gene, similarly to the HGPS phenotype as discussed earlier. There have been studies that have attempted to make correlations between the genotype and phenotype of laminopathies. These have identified mutation "hot-spots" (Perrot *et al.*, 2009; Botto *et*

al., 2010), which may either be mutations that are common in certain regions of the *LMNA* gene, or specific point mutations that frequently cause the same gene. However, these studies have mostly focused on a certain disease, and/or conclusions have mostly been drawn from a relatively small patient population. Further complicating the situation, identical mutations in *LMNA* have been found to cause different conditions. A clinical report on a group of five patients across three muscle centres in England found that although all patients carried the same p.Glu358Lys mutation in *LMNA*, three had classical EDMD features, whilst one exhibited symptoms of L-CMD and another had muscle weakness alongside FPLD attributes (Mercuri *et al.*, 2004). In a similar case report, nine patients were found to have extreme phenotypic diversity that were all carrying the p.Arg644Cys *LMNA* variant. In this report, three patients had insulin resistance, two of which also had lipodystrophy, one patient had motor neuropathy, one had dilated cardiomyopathy, one had severe scoliosis with contractures and one patient had LGMD (Rankin *et al.*, 2008).

It is also unclear how mutations in *SYNE1* cause multiple diseases, and whether other NE protein genes, which are relatively less researched than *LMNA*, also cause multiple diseases. If so, it may be possible to determine genotype-phenotype correlations can be for these NE protein genes. Identifying links between phenotypes of diseases and where mutations that cause those diseases are situated on the genome may aid the development of therapies for these diseases, as was seen in the development of Zokinvy™ for HGPS. Whilst research attempting to provide insight into laminopathies has been thorough, studies surrounding the development of diseases associated with mutations

affecting other LINC complex proteins and their relation to human diseases is mostly dispersed across many articles and has not been recently synthesised.

The aim of this chapter was to conduct a systematic review following PRISMA guidelines into published mutations of genes encoding NE proteins associated with the LINC complex. These include: *LMNA* (lamin A/C), *LMNB1/LMNB2* (lamin B1/B2), *EMD* (emerin), *TMEM43* (LUMA), *SYNE1/SYNE2* (nesprin-1/2). This was done to determine whether any genotype-phenotype correlations exist between the location of mutations on the NE protein gene, and different disease phenotypes. Although some genotype-phenotype studies have previously focused on specific NE protein genes and/or diseases, a study investigating each of the LINC complex proteins and all the diseases they are known to cause has never been conducted before. If any patterns do exist, this will guide research into the development of therapies for nuclear envelopathies.

Specific objectives include:

- To generate a list of mutations associated with LINC complex proteins along with information on associated diseases, clinical presentation and number of reports of the mutation.
- To determine where within the gene each mutation is located, and what structures and domains each mutation may affect.
- To determine whether any patterns exist between genetic sequence variants and clinical aspects of diseases.

6.2. Results

6.2.1. Study Selection

Bibliographic databases Medline (n=2048), CINAHLPlus (n=165) and AMED (n=5) were searched, yielding a total of 2218 records. Before screening, duplicate records (n=875) were removed. The remaining 1342 records were subjected to blind screening by two reviewers, based on the inclusion and exclusion criteria previously outlined. There were 878 records that were excluded during the first round of screening, this left 464 records that were sought for retrieval. Three reports were not retrieved and were excluded at this stage as they were duplicates which had been overlooked during the initial deduplication process. In the final round of screening, 461 reports were assessed for eligibility. Records were excluded due to one of the following reasons: the article was in a foreign language (n=12), multiple mutations in different proteins were described as causing the same disease in the report (n=6), the mutation was not specified, was unrelated to the study or unclear (n=42), the disease type was excluded as stated in the exclusion criteria (n=2). As a result, 402 records were included in the review. (**Fig. 6.2**).

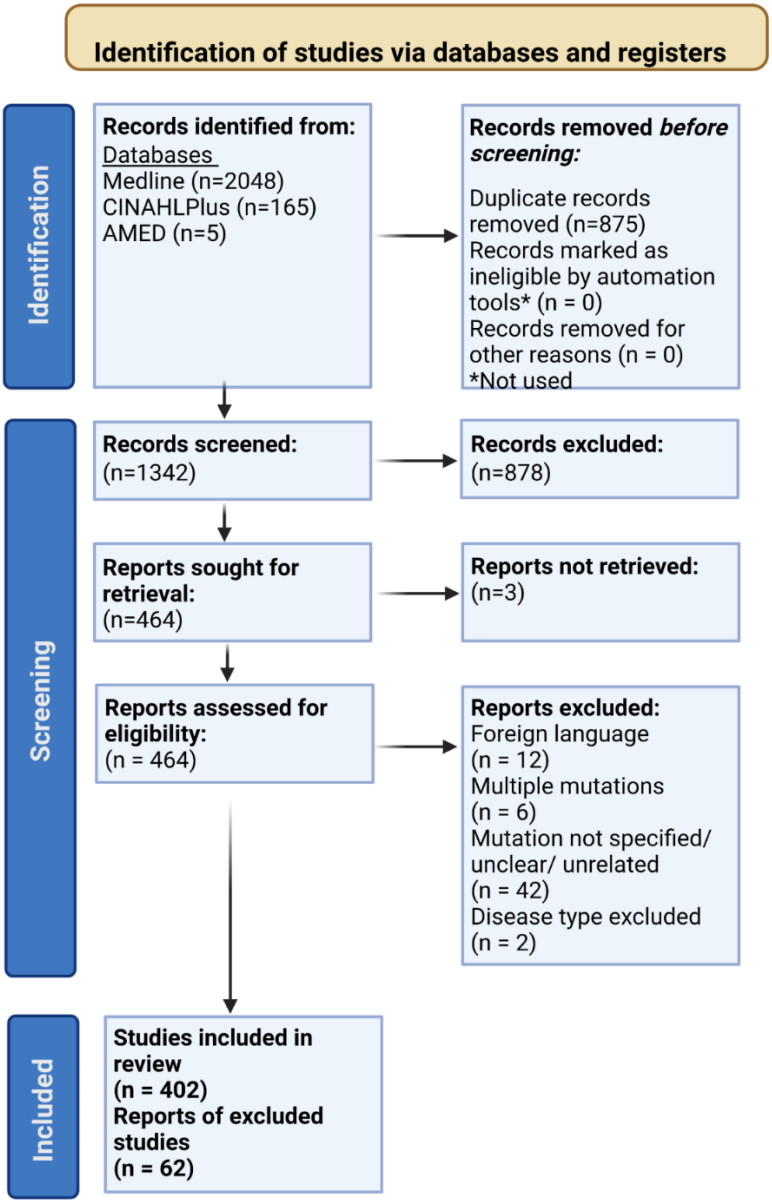

Figure 6.2- PRISMA flow diagram outlining the search and selection process of identifying records for the systematic review. *The databases that were searched were Medline (n=2048), CINAHPlus (n=165) and AMED (n=5), yielding a total of 2218 records. Duplicate records (n=875) were removed prior to screening, then 1254 records were subjected to blind screening by two independent reviewers. 878 reports were excluded during the first round of screening, and 464 records were retrieved. Three reports were not retrieved as they were duplicates that had previously been overlooked. This left a total of 464 reports that were assessed for eligibility. There were 402 studies that were included in the review, whilst 62 were excluded. Reports were excluded for the following reasons: foreign language (n=12), multiple mutations (n=6), mutations were not specified, unclear or unrelated (n=42) or contained a disease type that was listed within the exclusion criteria (n=2). Created with BioRender.com.*

6.2.2. Nuclear Lamins

6.2.2.1. A high density of *LMNA* mutations at exons 1 and 6 cause striated muscle disease, whilst mutations causing metabolic disease increase in frequency from exon 7 onwards

In total, 519 unique mutations in *LMNA*, the gene that encodes the alternatively spliced products, lamins A and C, were identified. Four mutations were found to be lamin C specific. Lamin C is derived from *LMNA* using an alternative splice site located in intron 10, therefore the C-terminus of lamin C differs to that of lamin A(Lin and Worman, 1993).

While mutations in *LMNA* have already been associated with more than 15 different phenotypes(Crasto, My and Di Pasquale, 2020), this study revealed 37 conditions related to *LMNA* variants (**Fig. 6.3, A**). Moreover, identical mutations were found to give rise to different conditions. An astonishing 201 mutations were associated with more than one phenotype, and 99 mutations were linked to disorders affecting entirely different tissues and/or organ systems. Notorious examples of this include the variants p.Arg644Cys, p,Arg453Trp, p.Arg527Pro and p.Ser573Leu which were associated with 11, 6, 5 and 5 different diseases, respectively, each affecting multiple tissues (**Table 6.1.**). One of the widest ranging examples among these is the p.Arg644Cys variant which has been linked to EDMD, LGMD, L-CMD, atrioventricular block (AVB), DCM, arrhythmogenic right ventricular cardiomyopathy, left ventricular noncompaction, insulin resistance, FPLD, and CMT (Mercuri *et al.*, 2005; Rankin *et al.*, 2008; Perrot *et al.*, 2009; Quarta *et al.*, 2012; Parent, Towbin and Jefferies, 2015; Dohrn *et al.*, 2017; Avila *et al.*, 2021).

Table 6.1- Examples of LMNA mutations known to cause distinct phenotypes.

Protein nomenclature	c.DNA nomenclature	Associated diseases				Min. number of reports of variant	References
		Skeletal Muscle	**Cardiac**	**Metabolic**	**Nervous system**		
Arg644Cys	1930C>T	EDMD, muscular dystrophy, LGMD, L-CMD	AVB, DCM, ARVC, LVNC	IR, FPLD	CMT	23	(Mercuri *et al.*, 2005; Rankin *et al.*, 2008; Pasotti *et al.*, 2008; Møller *et al.*, 2009; Perrot *et al.*, 2009; Liang *et al.*, 2011; Quarta *et al.*, 2012; Parent, Towbin and Jefferies, 2015; Dohrn *et al.*, 2017; Ditaranto *et al.*, 2019; E. W. Lin *et al.*, 2020)
Arg453Trp	1357C>T	EDMD, LGMD, L-CMD, CFTD	DCM	FPLD		37	(Bonne *et al.*, 1999, 2000; Sewry *et al.*, 2001; Colomer *et al.*, 2002; Sanna *et al.*, 2003; Vytopil *et al.*, 2003, 2004; Favreau *et al.*, 2003; Muchir *et al.*, 2004; Astejada *et al.*, 2007; Kandert *et al.*, 2009; Park *et al.*, 2009; Magagnotti *et al.*, 2012; Kajino *et al.*, 2014; Díaz-Manera *et al.*, 2016; Ge *et al.*, 2019; Refaat *et al.*, 2019; Choi *et al.*, 2019; Liang *et al.*, 2020; E. W. Lin *et al.*, 2020; Ebert *et al.*, 2020; Sanga *et al.*, 2021; Fan *et al.*, 2021)
Arg527Pro	1580G>C	EDMD, LGMD, L-CMD	DCM	FPLD		21	(Bonne *et al.*, 1999, 2000; Raffaele Di Barletta *et al.*, 2000; Muchir *et al.*, 2004; Astejada *et al.*, 2007; Makri *et al.*, 2009; Tan *et al.*, 2015; Choi *et al.*, 2019; Ditaranto *et al.*, 2019; Ge *et al.*, 2019; E. W. Lin *et al.*, 2020; Fan *et al.*, 2021)

Ser573Leu	1718C>T	LGMD	DCM, AVB	Diabetes, FPLD		14	(Rudnik-Schöneborn *et al.*, 2007; Pasotti *et al.*, 2008; Francisco *et al.*, 2017; Gigli *et al.*, 2019; E. W. Lin *et al.*, 2020)

Table listing *LMNA* mutations known to cause different distinct disease phenotypes. Each mutation is listed using protein nomenclature as well as c.DNA nomenclature, along with its associated diseases categorised into either skeletal muscle, cardiac, metabolic or nervous system disease. The minimum number of reports in the literature for each variant is listed alongside relevant references.

The Arg644Cys variant was associated with 11 phenotypes affecting skeletal and cardiac muscle, metabolism, and the nervous system. Whilst the Arg453Trp, Arg527Pro and Ser537Leu mutations each caused diseases associated with three different tissue or organ systems. Abbreviations: Emery-Dreifuss muscular dystrophy (EDMD), limb-girdle muscular dystrophy (LGMD), congenital muscular dystrophy (L-CMD), atrioventricular block (AVB), dilated cardiomyopathy (DCM), arrhythmogenic right ventricular cardiomyopathy (ARVC), left ventricular noncompaction (LVNC), insulin resistance (IR), familial partial lipodystrophy (FPLD), Charcot-Marie-Tooth disease (CMT), congenital fibre type disproportion myopathy (CFTD).

There were 477 mutations located in the coding region of the *LMNA* gene (91.92%), and 42 intronic splice-site mutations (8.09%) (**Fig. 6.3, B**). The most frequently occurring type of mutations were missense mutations (n=342), accounting for 71.70% of the mutations found in the coding region of *LMNA.* Frameshift (n=59, 12.37), nonsense (n=30, 6.29%), deletion (28, 5.87%), deletion/insertion (n=7, 1.47%), insertion (n=6, 1.26%) and duplication (n=5, 1.05%%) mutations were also identified (**Fig. 6.3, C**). Arginine residues were found to be mutated more often than other amino acids, with 24.32% (n=116) of coding region mutations being the result of arginine mutations. Mutations were distributed across all 12 exons of the *LMNA* gene. The most mutations were found to be located on exon 1, (n=105, 22.01%) and exon 6 (n=75, 15.72%). Very few mutations (n=8) were found within exons 12 and 10. Only one (0.22%) mutation was found to be situated in exon 12, and seven mutations were found in exon 10 (1.51%).

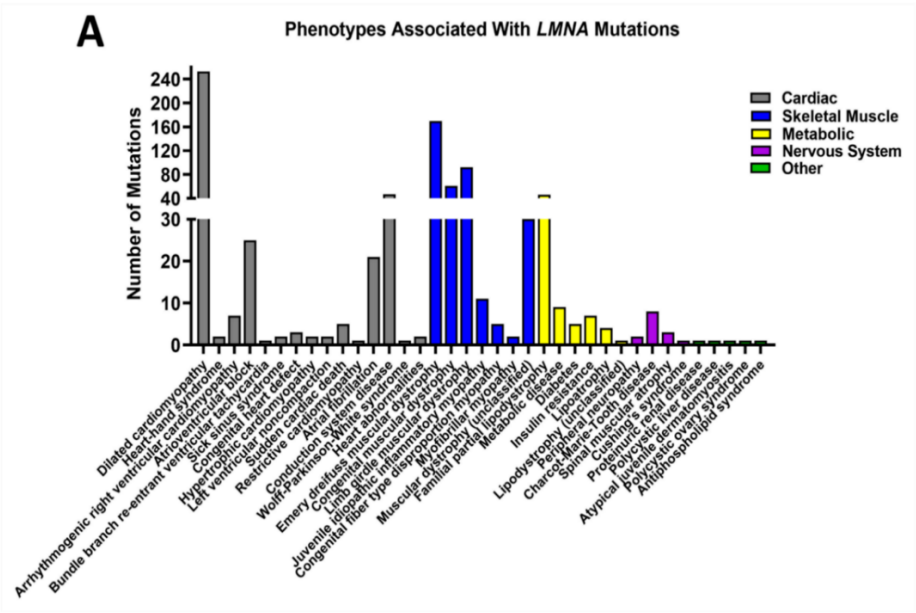
A
Phenotypes Associated With LMNA Mutations
Number of Mutations
240
200
160
120
80
40
30
20
10
0
Cardiac
Skeletal Muscle
Metabolic
Nervous System
Other
Dilated cardiomyopathy
Heart-hand syndrome
Arrhythmogenic right ventricular cardiomyopathy
Atrioventricular block
Bundle branch re-entrant ventricular tachycardia
Sick sinus syndrome
Congenital heart defect
Hypertrophic cardiomyopathy
Left ventricular noncompaction
Sudden cardiac death
Restrictive cardiomyopathy
Atrial fibrillation
Conduction system disease
Wolff-Parkinson-White syndromeEmery dreifuss muscular dystrophy
Congenital muscular dystrophy
Heart valve malformations
Limb girdle muscular dystrophy
Juvenile idiopathic inflammatory myopathy
Congenital fiber type disproportion myopathy
Myofibrillar myopathy
Muscular dystrophy (unclassified)
Familial partial lipodystrophy
Metabolic disease
Diabetes
Insulin resistance
Lipoatrophy
Lipodystrophy (unclassified)
Peripheral neuropathy
Charcot-Marie-Tooth disease
Spinal muscular atrophy
Cushing's syndrome
Progeroid syndrome
Polycystic liver disease
Atypical juvenile dermatomyositis
Polycystic ovary syndrome
Antiphospholipid syndrome

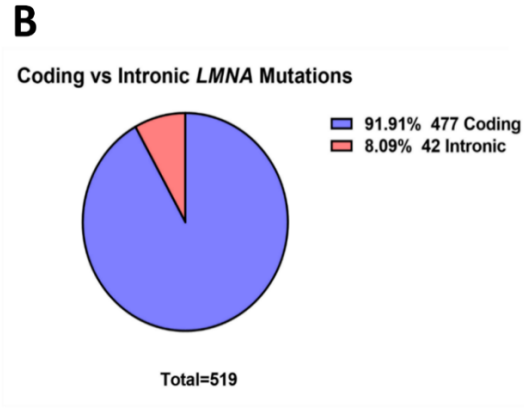
B
Coding vs Intronic LMNA Mutations
91.91% 477 Coding
8.09% 42 Intronic
Total=519

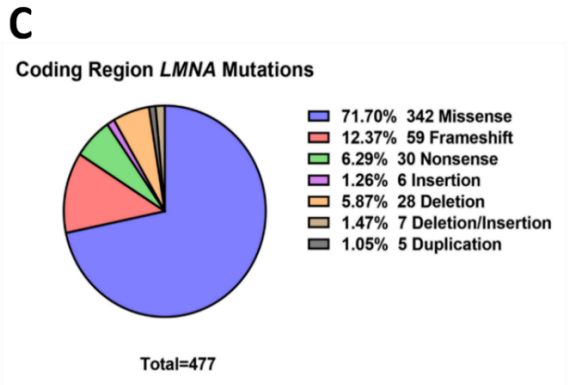
C
Coding Region LMNA Mutations
71.70% 342 Missense
12.37% 59 Frameshift
6.29% 30 Nonsense
1.26% 6 Insertion
5.87% 28 Deletion
1.47% 7 Deletion/Insertion
1.05% 5 Duplication
Total=477

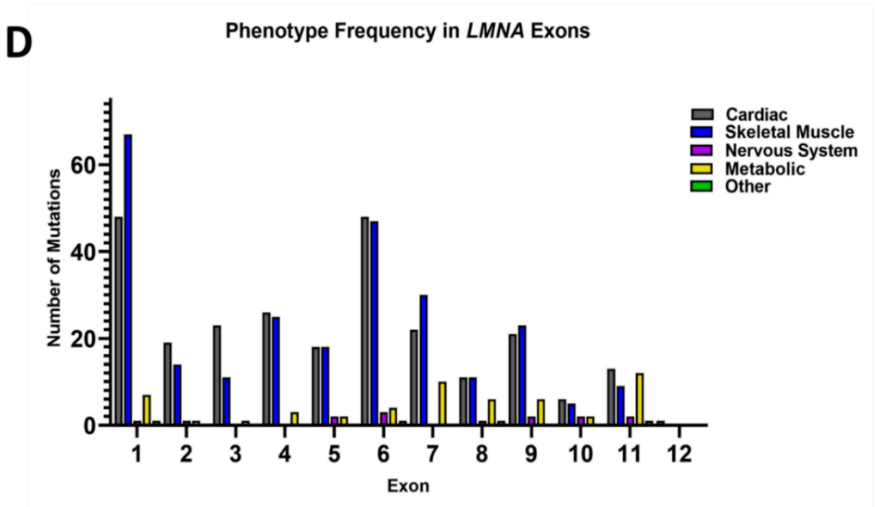
D
Phenotype Frequency in LMNA Exons
Number of Mutations
60
40
20
0
1
2
3
4
5
6
7
8
9
10
11
12
Exon
Cardiac
Skeletal Muscle
Nervous System
Metabolic
Other

Figure 6.3- LMNA mutations. (A) Phenotypes associated with LMNA mutations. *There were 37 different conditions that were found to be associated with LMNA mutations, some which were caused by identical LMNA variants. These can be broadly classified into diseases affecting cardiac muscle, skeletal muscle, the metabolic system and the nervous system. A few variants caused diseases that fell into other categories.* ***(B) Coding vs intronic mutations.*** *A total of 519 LMNA mutations were identified. 477 (91.91%) were coding mutations, whilst 42 (8.09%) were splice-site variants.* ***(C) Coding region mutations.*** *Missense mutations were the most frequently occurring type of LMNA mutations (342, 71.70%). Frameshift (59, 12.37%), nonsense (30, 6.29%), deletion (28, 5.87%), deletion/insertion (7, 1.47%), insertion (6, 1.26%) and duplication (5, 1.05%) mutations were also identified.* ***(D) Mutations associated with different disease types and their frequency in LMNA exons.*** *The most commonly occurring disease types arising from LMNA mutations were diseases affecting skeletal (262) and cardiac (260) muscle. These disease types clustered at exons 1 and 6. A total of 55 mutations were associated with metabolic disease, and these mostly appeared to increase in frequency from exon 7 onwards. Only 16 mutations caused nervous system disease and four caused other conditions which fell into different disease categories. Created with GraphPad Prism.*

Given that *LMNA* mutations cause a broad range of diseases, analysis was next performed to determine whether genotype influenced disease phenotype. Using MeSH terms, each laminopathy identified in this study was classified into one of the following disease categories; skeletal muscle disease, cardiac disease, metabolic disease, nervous system disease or other. Each individual *LMNA* mutation was then assigned a disease category, based on the disease(s) that it was found to cause. If a mutation caused more than one disease type, it was counted in more than one category (for example, if a mutation caused DCM and EDMD, it would be categorised as causing skeletal muscle disease and cardiac disease). Disease phenotype was then examined in relation to the position of the causative mutation on the *LMNA* gene, and consequently the affected protein structures and domains.

The most frequently occurring disease categories associated with *LMNA* mutations were skeletal muscle diseases (n=262 mutations) and cardiac diseases (n=260 mutations). These

two disease types seemed to occur most often in exons 1 and 6 (**Fig. 6.3, D)**. It was found that 67 mutations causing skeletal muscle disease were in exon 1, and 47 were found to be within exon 6, whilst 48 cardiac disease-associated mutations were located in exon 1, and exon 6 also harboured 48 variants (**Fig. 6.3, D and Fig. 6.4**). Interestingly, in cases where a single mutation caused multiple disease types, most commonly cardiac and skeletal muscle diseases were found to be caused by the same mutation. It is important to also consider that skeletal muscle diseases including EDMD, L-CMD and LGMD do also often cause cardiac abnormalities, therefore there may be some crossover between skeletal and cardiac disease phenotypes. Of 99 mutations known to cause diseases affecting multiple tissues or organ systems, 63 (64.29%) were found to cause both cardiac and skeletal muscle disease, whilst 11 (11.22%) mutations caused cardiac and skeletal muscle disease along with another type of disease(s). There were 55 mutations associated with diseases of the metabolic system. These mutations were distributed throughout the 12 exons of the *LMNA* gene (**Fig. 6.3, D and Fig. 6.4**). The frequency of metabolic disease mutations, however, generally appears to increase from exon 7 onwards (besides the mutations found in exon 1). Exon 7 through to 12 encode the tail region of lamin A (**Fig. 4**). Only 16 mutations were found to cause nervous system disease, whilst 4 mutations caused other conditions which fell into other disease categories.

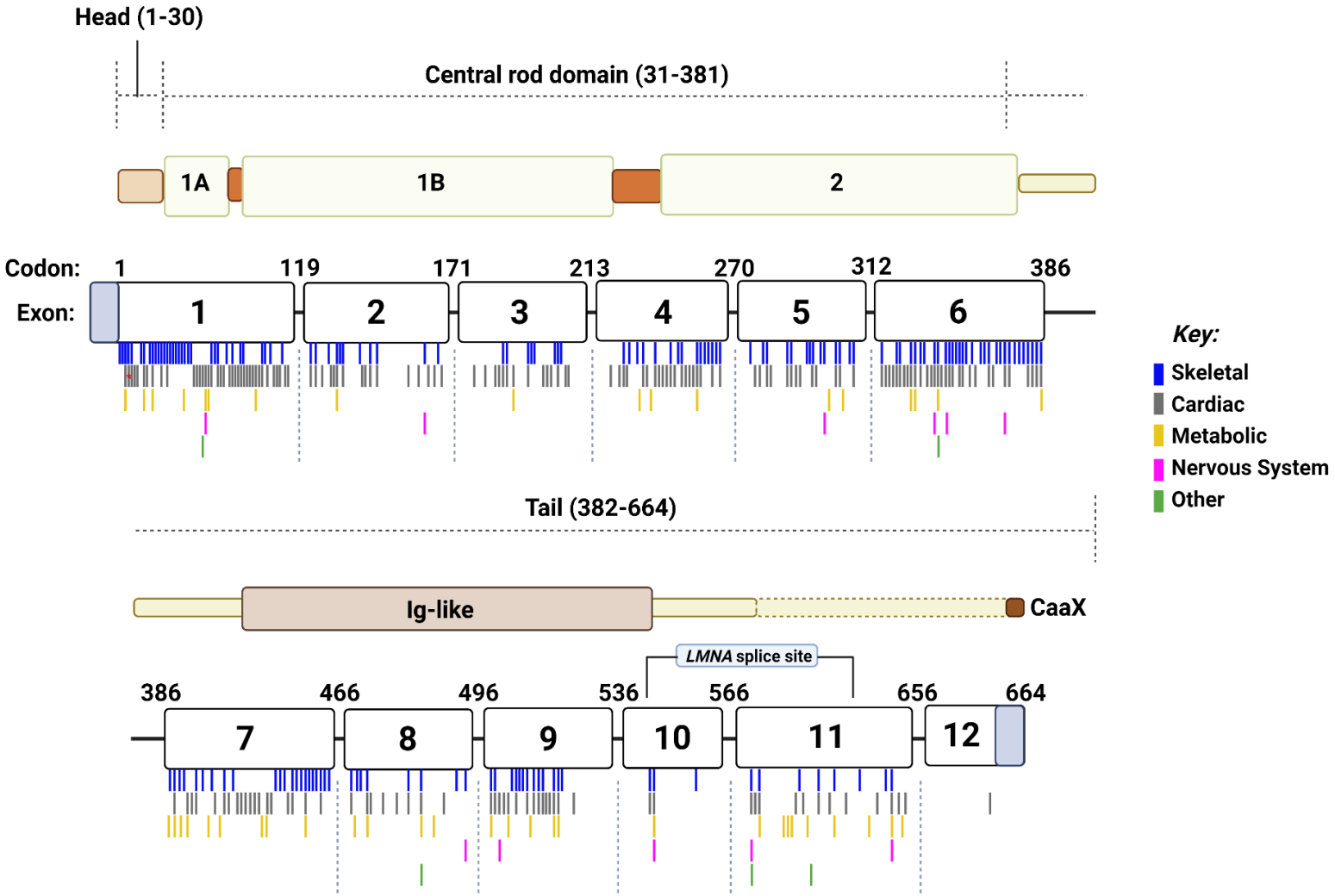
Head (1-30)
Central rod domain (31-381)
1A
1B
2
Codon:
Exon:
1
119
171
213
270
312
386
1
2
3
4
5
6
Key:
Skeletal
Cardiac
Metabolic
Nervous System
Other
Tail (382-664)
Ig-like
CaaX
LMNA splice site
386
466
496
536
566
656
664
7
8
9
10
11
12

Figure 6.4- The structure of the LMNA gene and protein product lamin A. *LMNA encodes lamin A/C. Lamin C is produced via a splice site located at intron 10 and therefore it's C-terminus differs to lamin A. LMNA consists of 12 exons. Each coding region LMNA mutation was assigned to a disease category based on the disease type it caused. If it caused more than one type of disease, it was considered in multiple categories. These mutations were then marked below the LMNA gene at the appropriate codon, in a colour that corresponds to its related disease type(s). Above the LMNA gene is the structure of lamin A, consisting of a head, central rod and tail domain. Created with BioRender.com.*

6.2.2.2. Fewer mutations are reported in B-type lamins compared to lamin A/C

Despite their relatively similar size, very few mutations were found in B-type lamins compared to lamins A and C. There were 13 mutations associated with *LMNB1*, all causing neural tube defects (NTDs) including microcephaly (n=5), spina bifida (n=7) and anencephaly (n=1). Only 4 mutations were identified in *LMNB2*, and these were associated with acquired partial lipodystrophy.

6.2.3. Inner Nuclear Membrane

6.2.3.1. *EMD* is implicated in diseases other than Emery-Dreifuss muscular dystrophy and has a mutation hot-spot at exon 6

There were 83 mutations found in *EMD*, the gene encoding emerin. We found that 92.86% (n=78) of *EMD* mutations were attributed to EDMD. This study also found that mutations in emerin have been linked to the development of DCM, cardiac conduction disease (CCD), atrial fibrillation (AF), LGMD and rigid spine syndrome (RSS). It is important to note that DCM, CCD and AF are often manifestations of EDMD, although in these cases they have been recorded as isolated diseases, not symptoms of EDMD. Only eleven *EMD* mutations were splice site variants, the remaining 72 (86.25%) mutations were found in the coding region (**Fig. 6.5, A**). Within the coding region of the gene, many mutations

were frameshift (n=32, 44.44%), deletion (n=9, 12.50%) and nonsense (n=15, 20.83%) variants. A notable proportion of missense mutations (n=14, 19.44%) were also identified (**Fig. 6.5, B**). *EMD* consists of 6 exons, and mutations were found throughout the emerin gene. However, 39.75%(n=33) mutations were found in exon 6, suggesting that this region is mutation hot-spot (**Fig. 6.5, C**).

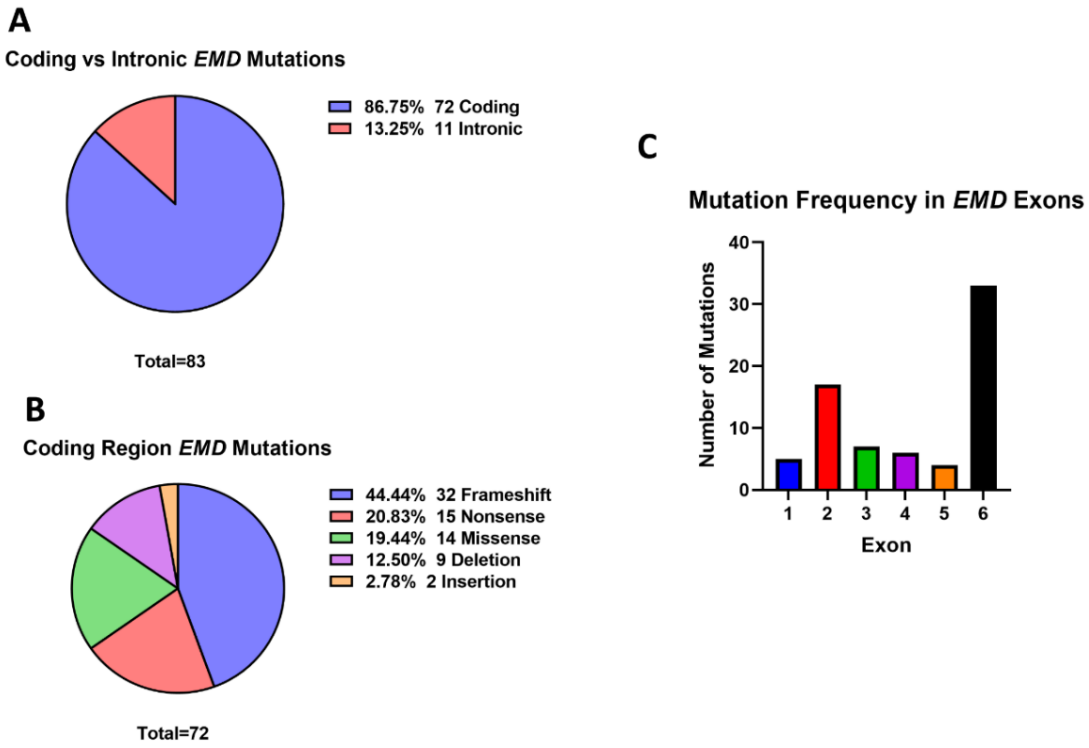

Figure 6.5- EMD mutations. (A) Coding vs intronic mutations. *A total of 83 EMD mutations were identified. 73 (86.75%) were coding region mutations and eleven (13.25%) were intronic variants.* ***(B) Coding region mutations.*** *The largest percentage of coding region mutations were frameshift (32, 44.44%), deletion (9, 12.50%) and nonsense (15, 20.83%) variants. Missense mutations (14, 19.44%) also accounted for a considerable proportion of the mutations identified. A couple of insertion (2, 2.78%) mutations were also identified.* ***(C) Mutation frequency in EMD exons****. Mutations most frequently occurred within exon 6, accounting for 45.21% (33) of total coding region mutations. Exon 2 contained the second highest proportion of mutations (17, 23.29%), followed by exons 3 (7, 9.59%) and 4 (6, 8.22%). Exon 1 and 5 contained the fewest EMD variants (5, 6.85% and 4, 5.48%, respectively). Created with GraphPad Prism.*

6.2.3.2. Mutations in Inner Nuclear Membrane Protein, TMEM43, and Integral LINC Complex Components SUN1/SUN2, Are Also Linked to Emery-Dreifuss Muscular Dystrophy

In this study, mutations in the INM protein TMEM43 were also found to be linked to the development of EDMD. Only two mutations in TMEM43 were identified in the literature, however the evidence linking the mutations to EDMD is weak. No other diseases were found to be associated with mutations in this gene. Although we found no mutations in SUN1/SUN2 that were directly found to cause disease, SUN1/SUN2 variants have been identified as disease severity modifiers in EDMD when mutations in LMNA or EMD are present (P. Li *et al.*, 2014).

6.2.4. Outer Nuclear Membrane

6.2.4.1. Most often, nesprin-1 nonsense mutations cause nervous system disorders, particularly spinocerebellar ataxia 8 (SCAR8)

In total, 141 mutations in *SYNE1* were identified. Out of these, four mutations were found to specifically affect the expression of short isoform nesprin-1α. Only three mutations were identified in *SYNE2.* Most of the *SYNE1* mutations were coding region mutations (n=127, 90.07%), with only 14 intronic mutations being identified (9.93%) (**Fig. 6.6, A**). 48.82% (n=62) of mutations in the coding region of the gene were nonsense (**Fig. 6.6, B**). Additionally, missense (n=32, 25.20%), frameshift (n=30, 23.62%) and deletion (n=3, 2.36%) mutations were identified (**Fig. 6.6, B**). No duplication or insertion mutations were discovered. These mutations were found to be distributed mostly throughout the region of the gene that encodes the spectrin repeats (SRs), with seven mutations being found in the N-terminal calponin homology (CH) domain and three in the KASH domain.

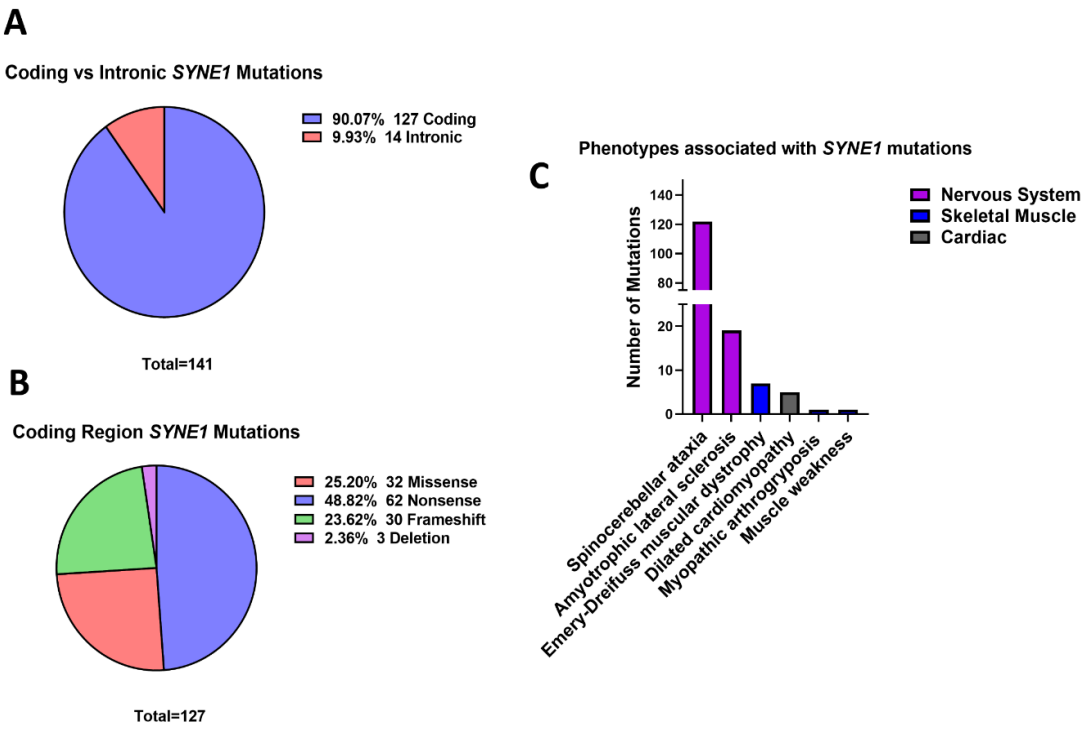

Figure 6.6- SYNE1 mutations. (A) Coding vs intronic mutations. *There were 127 (90.07%) mutations identified in the coding region of SYNE1 and 14 (9.93%) were intronic.* ***(B) Coding region mutations.*** *Almost half (48.82%, 62) of coding region mutations were nonsense. Many mutations were also missense (32, 25.20%) and frameshift (30, 23.62%) variants. Three (2.36%) deletion mutations were also identified.* ***(C) Diseases associated with SYNE1 variants.*** *The most common disease resulting from SYNE1 variants was autosomal recessive spinocerebellar ataxia (SCAR8). 122 (85.82%) mutations were related to this disease. Amyotrophic lateral sclerosis was also found to be frequently caused by SYNE1 mutations (19, 13.48%). Seven cases of Emery-Dreifuss muscular dystrophy (EDMD) were related to SYNE1 variants, and a handful of mutations were associated with myopathic arthrogryposis (2), dilated cardiomyopathy (DCM) (5) and general muscle weakness (1). Created with GraphPad Prism.*

Mutations in *SYNE1* predominantly cause diseases of the nervous system. Of the mutations identified, 122 were associated with SCAR8, whilst 19 mutations were found to cause ALS (**Fig. 6.6, C**). Fewer mutations were related to the development of EDMD (n=7), myopathic arthrogryposis (n=1), generalized muscle weakness (n=1), and DCM (n=5) (**Fig.**

6.6, C). Two of the *SYNE2* mutations caused EDMD, whilst a single mutation was found to cause ALS.

6.3. Discussion

In this study, known mutations in genes encoding LINC complex-associated proteins that are related to human disease were systematically reviewed and summarised, providing a useful resource for researchers in this field. It was demonstrated that there appear to be no obvious correlations between the position of lamin A/C mutations on the *LMNA* gene and different disease phenotypes. However, it was found that a high frequency of striated muscle disease-causing *LMNA* variants located within exons 1 and 6, whilst mutations associated with metabolic diseases often occurred in exon 7 onwards. An emerin mutation "hot-spot" was also identified within exon 6 of *EMD*. It has also been observed that most often *SYNE1* nonsense variants lead to the development of nervous system disease.

6.3.1. Genetic disease modifiers may be responsible for the phenotypic diversity seen in laminopathies

LMNA variants were associated with 35 different conditions, and in some cases, identical mutations caused diseases with entirely different phenotypes. A notorious example of this is the mutation p.Arg644Cys, which causes 11 different disease phenotypes affecting skeletal and cardiac muscle (Mercuri *et al.*, 2005; Perrot *et al.*, 2009; Quarta *et al.*, 2012; Parent, Towbin and Jefferies, 2015; Avila *et al.*, 2021), the metabolic system (Rankin *et al.*,

2008), and the nervous system (Dohrn *et al.*, 2017). It remains unclear how this could be, and no answers have arisen from studying the position of known mutations on the *LMNA* gene in relation to different disease phenotypes. This study has, however, revealed that there are no instances in which an identical mutation in the other nuclear envelope genes studied here is responsible for causing so many distinct diseases. One explanation for this could be that other genetic disease modifiers are present in addition to *LMNA* mutations, which may affect the phenotypic outcome of the disease-causing variant.

6.3.1.1. Expressivity modifiers that alter disease severity have been previously identified in EDMD

Expressivity modifiers which modulate disease severity have already been identified in conjunction with *LMNA* mutations. The presence of *SUN1/SUN2* variants alongside other Emery-Dreifuss muscular dystrophy EDMD-related genes, including *LMNA,* cause a more severe EDMD phenotype (Meinke *et al.*, 2014), and the synergistic effects of *LMNA* and *DES* (encoding desmin) or *EMD* mutations have also been found to alter EDMD disease severity (Muntoni *et al.*, 2006; Ben Yaou *et al.*, 2007; Granger *et al.*, 2011).

Meinke *et al.,* screened an undisclosed number of unrelated patients with EDMD who had previously been identified as carriers of mutations in *LMNA, EMD* or *SYNE1/SYNE2* to determine if a mutation in *SUN1* or *SUN2* influences disease severity. Using PCR, five patients (three with previously diagnosed *LMNA* mutations, and two with *EMD* mutations) were identified as carriers of non-synonymous variants with evidence of pathogenicity in *SUN1* and *SUN2* (Meinke *et al.*, 2014). These mutations were classified as pathogenic due to their ability to disrupt nuclear-cytoskeleton connections and nuclear positioning

(Meinke *et al.*, 2014). The *SUN1/SUN2* variants were also found to be present in family members of the patients, however alone these variants did not cause disease (Meinke *et al.*, 2014). It is logical that a disruption of the LINC complex as a result of *SUN1/SUN2* mutations could likely have detrimental effects at the NE and contribute to increased EDMD severity, but it is questionable why these same mutations do not cause disease on their own, without mutations in other NE being present. Particularly given that *SYNE1/SYNE2* variants cause diseases, possibly through a similar disruption of the LINC complex (Q. Zhang *et al.*, 2007b; Nikolova-Krstevski *et al.*, 2011; Zhou *et al.*, 2017). Maybe a compensatory mechanism exists when *LMNA* or *EMD* mutations are also present to prevent disease from occurring. For example, it has been found that depletion of nesprin-1 in endothelial increases the number of focal adhesions in cells, suggesting a compensatory mechanism to maintain cellular structure when the LINC complex is compromised (Chancellory *et al.*, 2010).

Granger *et al.* mapped *DES* as a modifier locus of EDMD by genotyping 291 microsatellite markers in 59 individuals of a large French family and performing a linkage study using a range of techniques. Within this family 19 patients carried the exact same mutation in *LMNA* but exhibited a wide range of age of disease onset (Granger *et al.*, 2011). Prior to this study, Mutoni *et al*. identified a *DES* mutation in a EDMD patient with a previously diagnosed *LMNA* mutation after observing that there were unusual accumulations of desmin in the cardiac tissue of the individual. In the same study, a patient with an unusually severe form of X-EDMD who also presented with cardiac features similar to those with AD-EDMD, was also found to carry a mutation in *LMNA* as well as *EMD*

(Muntoni *et al.*, 2006). Another study then found coincidence of *EMD* and *LMNA* mutations in 14 members of a family with EDMD who each had a variable combination of skeletal muscle, cardiac and nerve involvement, when screening the individuals for mutations in *LMNA* and *EMD* (Ben Yaou *et al.*, 2007). Seen as mutations in *EMD* alone are responsible for X-EDMD, it is logical that mutations in both *EMD* and *LMNA* would give rise to a more severe phenotype. Although, the instance of coincidence of *EMD* and *LMNA* variants in EDMD patients must be extremely rare due to the likelihood of mutations in both these genes being identified in regular screening of EDMD patients for EDMD-related genes.

6.3.1.2. Modifier genes present in combination with *LMNA* mutations may have pleiotopic effects

Modifier effects may also influence pleiotropy, causing individuals that share the same target allele to show a range of phenotypes (Riordan and Nadeau, 2017; Cerrone *et al.*, 2019). Pleiotropy is the phenomenon whereby a single locus affects two or more apparently unrelated pheotypic traits and is often identified as a single mutation that affects two or more wild-type traits (Stearns, 2010). This pleiotropism can lead to different disease manifestations, though such variation in disease phenotypes resulting from one gene, such as *LMNA,* has never been attributed to modifiers before. *MKS1*, the gene encoding the protein associated with Meckel syndrome type 1, has been identified as a pleiotropic modifier gene in Bardet-Biedl syndrome (BBS). BBS-patients harbouring mutations in both *MKS* and *BBS* (BBS gene) were found to suffer with seizures, which are

not typically associated with either MKS or BBS. Hence, the combination of the two mutations generated a novel phenotype (Leitch *et al.*, 2008). It is, however, important to note that MKS and BBS are both multisystem diseases which cause affected individuals to have some neurological impairment, therefore the novel phenotype described by a combination of mutations in *MKS* and *BBS* does not affect entirely different tissues or organ systems. Individual modifier genes with pleiotropic effects have also been found to increase the risk of cystic fibrosis (CF) patients developing various co-morbidities (W. Li *et al.*, 2014). Although, these co-morbidities are directly related to the downstream consequences of mutations in *CFTR* (cystic fibrosis transmembrane conductance regulator) that primarily cause CF, hence these modifier genes are only associated with an increased risk of developing such co-morbidities.

Perhaps laminopathy patients also carry modifier genes which have pleiotropic effects, whereby different modifier genes give rise to diseases affecting different tissue and organ systems. As mentioned, though, examples of diseases where pleiotropic modifiers have been identified have not been found to produce phenotypes affecting completely different tissues.

6.3.2. Fewer diseases may be associated with B-type lamins because loss of lamin B1/B2 is incompatible with postnatal life

Interestingly, few mutations were identified in B-type lamins, lamin B1 and B2, compared to lamin A/C. This may be because a loss of B-type lamins is incompatible with postnatal life, as it has been argued that due to their vital roles in neurodevelopment, B-type lamins

are indispensable in mammalian cells (Yang *et al.*, 2011) . Histological analysis of *Lmnb1*$^{\Delta/\Delta}$ mice brains revealed abnormalities including absence of layering of neurons in the cerebral cortex, reduced numbers of cortical neurons, no lamination was observed in the hippocampus, and the cerebellum was reduced in size (Coffinier *et al.*, 2011). These neurodevelopmental abnormalities suggest *Lmnb1* is important in embryonic development. Additionally, severe nuclear shape abnormalities were observed in the cerebral cortex of *Lmnb1*$^{\Delta/\Delta}$ embryos, and *Lmnb2*$^{-/-}$ neurons were also found to have elongated nuclei (Coffinier *et al.*, 2011). These nuclear morphology defects are similar to those observed in cells lacking *LMNA* or harbouring *LMNA* mutations (Vigouroux *et al.*, 2001; Favreau *et al.*, 2003; Muchir, van Engelen, *et al.*, 2003; Muchir *et al.*, 2004), and suggest reduced integrity of the NL. It has also been found that *Lmnb1*$^{\Delta/\Delta}$ mice do not survive long after birth due to severe developmental abnormalities in the lungs and skeleton (Vergnes *et al.*, 2004),

The forebrain of *Lmnb2*$^{-/-}$ embryos have also been found to have dramatic neuronal layering defects, and cortical neuron migration was perturbed (Coffinier, Chang, *et al.*, 2010). Neuronal migration is one of the most fundamental processes during development where functional brain circuits are constructed (Hatanaka and Hirata, 2020). Excitatory neurons are born within the ventricular zone in the cerebral cortex and migrate toward their final positions where they form a specific layered structure (Hatanaka and Hirata, 2020). Moreover, *Lmnb2*$^{-/-}$ mice died within 15-60 minutes after birth (Coffinier, Chang, *et al.*, 2010).

The phenotype that these mouse models exhibit is a result of a complete lack of lamin B1 or B2, which in humans would correspond to perhaps a deletion or nonsense mutation. In this study, one deletion mutation was identified in *LMNB1*, however the other mutations were missense. A missense mutation would still result in production of *LMNB1/LMNB2*, but the resulting protein may have limited functions. Perhaps there is specifically a lack of deletion or nonsense mutations as these may have catastrophic effects during neurodevelopment. The missense mutations in *LMNB1*, on the other hand, are associated with the development of NTDs; microcephaly, spina bifida, and anencephaly. NTDs occur when the neural tube, which forms the early brain and spine, does not close properly (Botto *et al.*, 1999). This occurs in utero, usually before an individual is aware that they are pregnant. Considering lamin B1's roles in neurodevelopment, it is plausible that aberrant lamin B1 may cause NTDs, given that they are conditions affecting the brain during embryonic development.

As mentioned previously, it was out of the scope of this review to include ADLD caused by a genomic duplication of *LMNB1*, however it is important to mention the effects of overexpression of *LMNB1* also. ADLD is also a neurological disorder characterised by widespread myelin loss in the central nervous system, with a phenotype similar to multiple sclerosis (Padiath *et al.*, 2006). Increased expression of *LMNB1* has also been found to result in a degenerative phenotype in *Drosophila melanogaster*, and HEK293 and HeLa cells expressing high levels of *LMNB1* exhibited abnormal nuclear morphology including extensive folding and blebbing of the nuclear membrane (Padiath *et al.*, 2006). These results, along with the results from the studies using *Lmnb1*-null mice, suggest that

a balance of *LMNB1* expression within a certain range is necessary for proper neurodevelopment.

Another explanation for a lack of mutations in *LMNB1/LMNB2* may be that the expression of A-type lamins compensate when B-type lamins are not present. Some evidence from studying neurodevelopment in mouse models supports this theory, suggesting that low levels or absence of lamin A/C may exacerbate the effects of lamin B deficiency. An absence of *Lmna* in neurons of *Lmnb1/b2* mouse embryos is associated with abnormal nuclear shape and severe neuropathology (Coffinier *et al.*, 2011), whereas fibroblasts from the same mouse models deficient in lamin B1/B2 exhibit normal nuclei, but *Lmna* expression is robust in the skin of these mice. A reduction in *Lmna* in these mice also does not appear to be a result of a lack of B-type lamins as *Lmna* expression has previously been found to be reduced in brain tissue of healthy mice (Röber, Weber and Osborn, 1989).

An alternative hypothesis may be that the loss of one of either lamin B1 or B2 is compensated by the other. A study using $Lmnb1^{B2/B2}$ and $Lmnb2^{B1/B1}$ mice (mice that make lamin B2 from the *Lmnb1* locus and vice-versa), however, found that increased production of one B-type lamin doesn't appear to fully compensate the other, as both mouse models exhibited neuronal abnormalities (Lee *et al.*, 2014).

6.3.3. *LMNA* mutations may cause distinct phenotypes due to lamin A/C having highly complex and varied roles compared to other nuclear envelope proteins

In contrast to the spectrum of diseases caused by *LMNA* mutations, we observed that *EMD* mutations cause multiple diseases with overlapping clinical phenotypes. Mutations in *EMD* have long been associated with causing EDMD (Bione *et al.*, 1994), but are also attributed to DCM, AF, CCD and RSS. Whilst these have presented as isolated diseases in certain cases, they are also known symptoms of EDMD (Emery, 1989b; Boriani *et al.*, 2003). A possible explanation as to why *LMNA* mutations cause conditions with very distinct phenotypes, whilst other NE proteins do not, could be due to the highly complex and varied roles of lamin A/C. Besides having structural functions, such as maintaining the integrity of the NE (Broers *et al.*, 2004; Lammerding *et al.*, 2004), lamin A/C has also been implicated in DNA replication, chromatin organisation, cell differentiation, and is known to interact with several transcription factors (Ellis *et al.*, 1997; Hutchison, 2002; Zastrow, Vlcek and Wilson, 2004). The consequences of mutations on any or all these processes could have a range of effects. Additionally, lamin A/C is known to interact with a number of different proteins that may be expressed with high tissue specificity themselves (Schirmer and Gerace, 2005; Dittmer *et al.*, 2014). For example, lamin A/C is known to interact with nesprin-2 (Libotte *et al.*, 2005), which is highly expressed in skeletal muscle, as well as proliferating cell nuclear antigen (PCNA) (Shumaker *et al.*, 2008), which has enhanced tissue expression in the bone marrow. Mutations in *LMNA* may therefore lead to differential interactions of mutant lamins and their associated proteins (Kubben *et al.*, 2010). Commonly laminopathies are caused by missense mutations, and arginine residues were found to be frequently substituted. Mutations at arginine and glycine residues

together are responsible for around 30% of genetic diseases (Vitkup, Sander and Church, 2003). This is a result of the high mutability of arginine due to the deamination of 5'-CpG dinucleotides in arginine codons (Cooper and Youssoufian, 1988), the relatively high frequency of arginine in human proteins and the fact that arginine mutates to other residues with very different chemical properties(Vitkup, Sander and Church, 2003). Variants affecting arginine residues may have devastating effects on protein stability, as arginine is frequently involved in the formation of salt bridges, and may disrupt and interfere with protein interactions and post-translational modification sites as arginine is also common in protein-active or binding sites (Betts and Russell, 2003).

6.3.4. *LMNA* mutation clusters found in different exons of the gene may have specific effects as they affect different structures of lamin A

6.3.4.1. Mutations in exons 1 and 6 of *LMNA* may lead to nuclear assembly defects and consequently, a weak nuclear lamina

Clusters of mutations corresponding to different laminopathies were also found at different exons of the *LMNA* gene. Many mutations causing skeletal myopathies or cardiac diseases occurred within exons 1 and 6. The N-terminal head of lamin A/C is encoded within a region of exon 1, whilst exon 6 corresponds to coil 2 within the central rod domain. These structures have both been implicated in lamin assembly, therefore mutations in these regions may impede this process.

Initially, it was believed that lamin dimers longitudinally associate “head-to-tail” (Stuurman, Sasse and Fisher, 1996; Stuurman, Heins and Aebi, 1998), whereby the N- and C-terminals of lamin interact (**Fig 6.7, B**). To date, the assembly mechanisms of nuclear

lamins have are poorly understood. However, research into lamin assembly at the molecular level has gained momentum within the past ten years, partially due to advances in technology, revealing that the central rod domains of lamins have a high propensity to form "coiled-coil" dimers (Chernyatina, Guzenko and Strelkov, 2015; Turgay *et al.*, 2017; Ahn *et al.*, 2019). In the Ahn *et al.* study, they first determined the crystal structure of an N-terminal fragment of human lamin A/C. This fragment spanned the N-terminus, coil 1a, L1, coil 1b, L12 and the first half of coil 2. This unit consisted of four protomers (a protomer being the structural unit of an oligomeric protein, composed of at least two protein chains), which were bundled by a pair of helical dimers (Ahn *et al.*, 2019). This is also referred to as a tetramer. Asides from identifying the tetrameric arrangement of the unit, the study also clarified the existence of coiled-coil dimers, and identified two different interactions which facilitate their formation (**Fig 6.7, C**). The A_{11} interaction involves an Ala146 residue at the centre of coil1b forming a disulphide bond by changing to a cysteine (Ala146Cys) to form anti-parallel coiled coil dimers (Ahn *et al.*, 2019). The eA_{22} interaction is whereby introducing a cysteine at an Arg388 site at the C-terminal end of coil 2, Cys388 forms a covalent bond with a lysine residue (Lys171) within coil 1b to produce extensive anti-parallel binding between coil 2s (Ahn *et al.*, 2019) (**Fig 6.7, C**). This work is valuable in providing insight into the assembly of lamins, and the formation and existence of coiled-coil lamin dimers have convincing supporting evidence which derails the "head-to-tail" conformation of lamin dimers. Therefore, perhaps it is more likely that *LMNA* mutations in exon 6 (which correspond to coil 2) may disrupt nuclear assembly than those mutations in exon 1 (within the head/N-terminus).

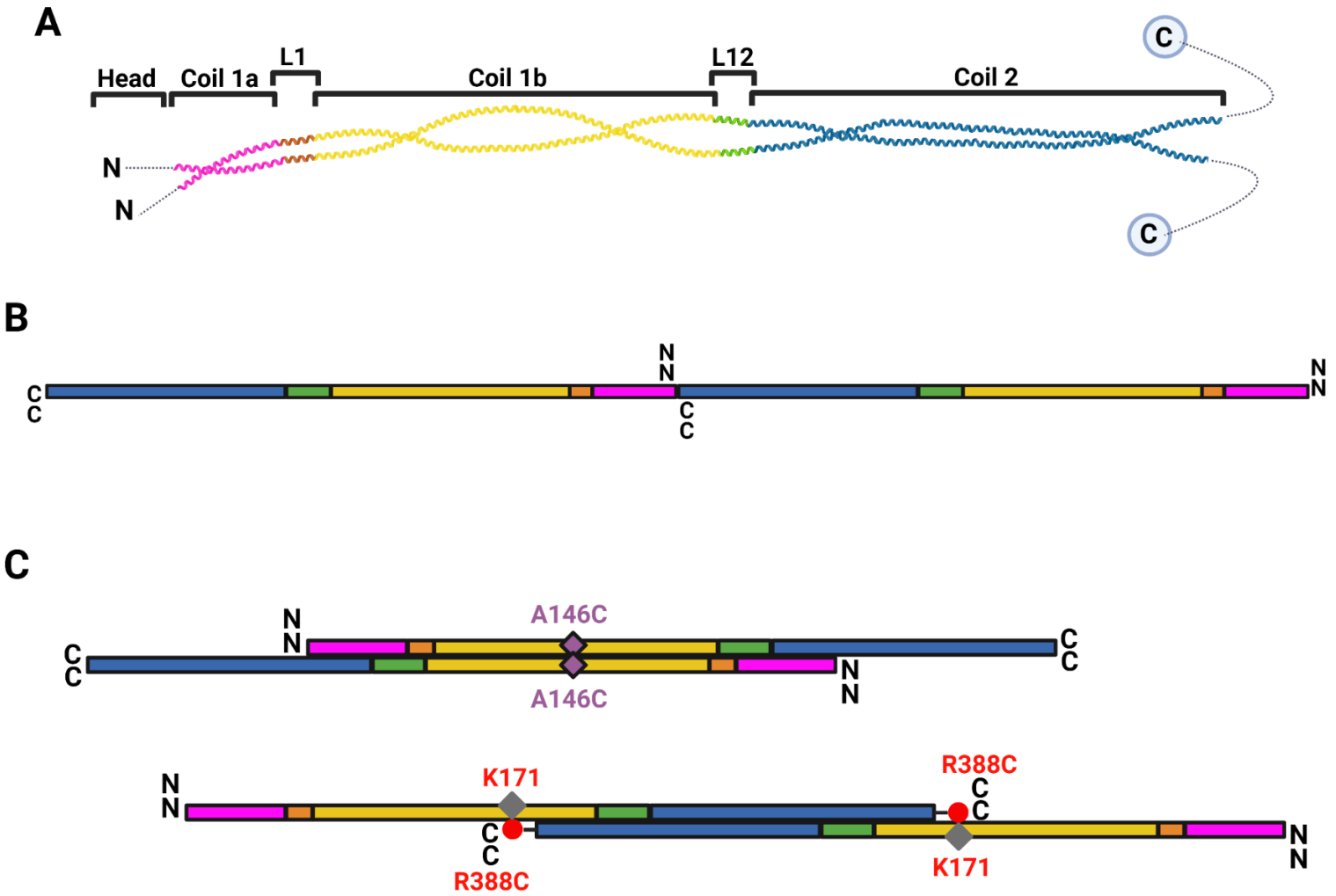
A
Head
Coil 1a
L1
Coil 1b
L12
Coil 2
C
N
N
C
B
N
N
C
C
N
N
C
C
C
A146C
N
N
C
C
N
N
A146C
K171
R388C
N
N
C
C
R388C
K171
N
N

Figure 6.7- The assembly of nuclear lamins. (A) The structure of lamin A. *The unstructured regions including the NLS, and C-terminal tail are illustrated using dotted lines. N represents the N-terminal region, whilst C denotes the C-terminus. The colours in (B) and (C) correspond to those used in this structure.* ***(B) "Head-to-tail" assembly of lamins.*** *Lamins were thought to associate longitudinally, by forming interactions between there N- and C-terminal domains.* ***(C) Coiled-coil dimer formation of lamins.*** *Lamins have now been found to form coiled-coil dimers through two interactions. The A_{11} interaction is facilitated by the Ala146 residue being changed to a cysteine (A146C) and therefore being able to form a disuphide bond. The eA_{22} interaction involves the Arg388 residues being changed by a cysteine (R388C) and forming a covalent bond with lysine residues (K171).*

Defects in lamina structure and assembly have been previously observed in cells harbouring *LMNA* mutations. Raharjo *et al.* found that *LMNA* variants p.Leu85Arg and p.Asn195Lys that cause DCM, and p.Leu530Pro, which is associated with EDMD, were found to modify the lamin assembly. In contrast, an FPLD-associated variant, p.Arg482Trp did not appear to have an affect on lamin assembly (Raharjo *et al.*, 2001). These variants were introduced into lamin A/C and expressed in both wild-type and *Lmna*-null cells, and assembly defects were determined by immunofluorescence analysis of cells expressing HA-tagged forms of each lamin A allele (Raharjo *et al.*, 2001). Incorrect lamin assembly may then lead to a compromised NL, as previously observed in cells harbouring *LMNA* mutations (Ostlund *et al.*, 2001; Vigouroux *et al.*, 2001; Muchir, Van Engelen, *et al.*, 2003). As per the "structural hypothesis" theory, a fragile NL leads to structural weakness resulting in the nucleus being unable to withstand high mechanical stress within cells (Osmanagic-Myers and Foisner, 2019). This is particularly pertinent within striated muscle, which is exposed to high mechanical tension.

6.3.4.2. *LMNA* mutations located in exon 7 may disrupt interactions between lamin A and other proteins

LMNA mutations related to metabolic diseases also appeared to generally increase in frequency from exon 7 onwards, the area which encodes the C-terminal tail region of lamin A. It is understood that the tail domain contains the binding sites for most lamin-binding proteins. Lamin A interacts with and tethers emerin to the NE via a binding site in this region(Clements *et al.*, 2000; Lee *et al.*, 2001; Sakaki *et al.*, 2001). This interaction could be altered by mutations, displacing emerin from the NE and as a result, affecting emerin function. Mutations in the tail region of lamin A have previously been shown to affect emerin binding *in vivo*, however these variants were related to cardiomyopathy and EDMD(Holt *et al.*, 2003). Emerin may be involved in metabolic processes (Mziaut *et al.*, 2001; Dharmaraj *et al.*, 2019), although the evidence is limited. Mziaut *at al.* found that the induction of stearoyl CoA desaturase is associated with high-level induction of emerin RNA. Stearoyl CoA desaturase is a key enzyme in the synthesis of unsaturated fatty acyl-CoAs during fatty acid metabolism. The emerin variant, p.Asp149His has also been associated with a “healthy” lipid phenotype and traits including; reduced triglycerides, reduced waist circumference, as well as high-impact reductions in LDL cholesterol and cholesterol (Dharmaraj *et al.*, 2019). This is a phenotype which is opposite to what is seen in *LMNA*-associated lipodystrophy, metabolic syndrome and insulin resistance. The Dharmaraj *et al.* study was the first to discover that emerin directly influences metabolism, since then no further work has been published in the literature linking emerin to metabolic processes. Lamin A is also thought to regulate 12-lipogenase (12-LOX) through an interaction at a binding site located in the lamin A tail domain (Tang *et al.*, 2000). Mounting evidence has shown that 12-LOX contributes to the progression of diabetes,

and therapeutic interventions to limit pro-inflammatory 12-LOX metabolites may positively impact on outcomes for diabetes co-morbidities (Prasad *et al.*, 2003; Grzesik *et al.*, 2015; Dobrian *et al.*, 2019; Dong *et al.*, 2020). *LMNA* variants that affect this binding region may result in a dysregulation of 12-LOX which may contribute to diabetes pathology. Other notable binding sites in this region include actin and DNA(Sasseville and Langelier, 1998; Stierlé *et al.*, 2003; Zastrow, Vlcek and Wilson, 2004), but it is unclear how these interactions may be linked to metabolic disease pathology.

As well as lamin A/C mutation clusters being identified within specific exons of *LMNA*, emerin mutations appeared to most often occur within exon 6 of *EMD* suggesting this region of the gene may be a mutation "hot-spot". As the majority of these variants are frameshift, deletion and nonsense mutations, they will most likely result in the loss of, or the production of a non-functional truncated form of emerin (Bione *et al.*, 1994; Manilal *et al.*, 1998; Koch and Holaska, 2014). This is because frameshift mutations disrupt the reading frame, causing the entire gene sequence following the mutation to be incorrectly read (Streisinger *et al.*, 1966). This may result in the addition of a stop codon which prevents a full-length protein from being produced (Streisinger *et al.*, 1966). A nonsense mutation is where a sequence change results in a stop codon instead of an amino acid, also resulting in the production of a shorter protein which is likely non-functional (Engelhardt *et al.*, 1965). Deletion mutations are simply the removal of at least one nucleotide in a sequence. Deletion mutations may be small and only remove a few nucleotides, or large and remove entire sequences. Large deletions may cause complete deletion of a gene. When diagnosing patients with EDMD in resource-restricted settings, it may be useful to consider first sequencing exon 6, given

the large number of emerin mutations located in this region. It is important to bear in mind, though, that many *EMD* mutations were located in other exons of the gene.

6.3.5. Stop-codon readthrough therapy could be used to treat SCAR8 caused by nonsense *SYNE1* mutations

Most disease-causing *SYNE1* variants result in the production of a truncated form of nesprin-1 due to nonsense mutations. Mutations impairing nesprin-1 function may affect its affinity to interact with LINC complex proteins including both SUN1/SUN2 at the PNS, and with the cytoskeleton in the cytoplasm (Crisp, Liu, Roux, J. B. Rattner, *et al.*, 2006; Zhou *et al.*, 2017). Three GFP-tagged wild-type (WT) and mutant nesprin-1 constructs (Arg8272Gln, Ser8381Cys, Asn8406Lys) were generated and transfected into human osteocarcinoma cells (U2OS) and were subjected to immunofluorescence staining which revealed that all three mutants caused weaker staining of SUN2 at the NE (Zhou *et al.*, 2017). These results suggest that nesprin-1 mutants affect the localisation of SUN2. GST-tagged nesprin-1α_2 constructs lacking the KASH domain were also found to have significantly reduced binding to lamin A/C and SUN2 when subjected to GST pull-down, further indicating that nesprin-1 mutations disrupt interactions between nesprin-1 and LINC complex proteins (Zhou *et al.*, 2017). Reduced interactions between nesprin-1 and LINC complex proteins, especially SUN1/SUN2 may result in the dissolution of the LINC complex, causing the connection between the NL and cytoskeleton to become weakened.

SYNE1 mutations commonly cause SCAR8, suggesting that nesprin-1 is indispensable in the brain. *Syne-1/Syne-2* double knock down (DKD) mice exhibit a severe phenotype,

failed to breathe and died shortly after birth (X. Zhang *et al.*, 2009). The brains of these mice displayed a number of defects including enlarged lateral ventricles, inverted layers in the cerebral cortex, loss of the pyramidal cell layer in hippocampus, loss of the Purkinje cell layer in cerebellum, and laminary defects in the midbrain, brain stem, and many other brain regions (X. Zhang *et al.*, 2009). Nesprin-1/2 have been found to be crucial for proper neurodevelopment, and the LINC complex has been found to be the main mediator coupling the nucleus to the cytoskeleton in migrating postmitotic neurons (X. Zhang *et al.*, 2009). Loss of *Syne-1/Syne-2* has been found to lead to severe defects in the laminary structures of many brain regions. Analysis of the neocortex in DKD *Syne-1/2* mice discovered radial neuronal migration defects, which is likely a result of laminary defects (X. Zhang *et al.*, 2009). Neuronal migration, as discussed previously, is a fundamental process in neurodevelopment. These findings, however, are the result of loss of both *Syne-1* and *Syne-2* together. There is currently not a mouse model of loss of *Syne-1* alone that exhibits a neurological phenotype. *Syne-1*$^{-/-}$ mice brains were also found to have no obvious defects, whilst *Syne-2*$^{-/-}$ mice had impaired laminary structures, similar to as seen in *Syne-1/Syne-2* DKD mice. This suggests that perhaps the phenotype seen in *Syne-1/Syne-2* DKD mice is mostly due to loss of Syne-2. Interestingly, *SYNE2* has only been associated with very few cases of human disease, which is surprising given the above results as well as *Syne-2*$^{-/-}$ mice having severe defects in learning and memory. Syne-2 has also been found to form complexes with SUN1 and SUN2 to mediate centrosome-nucleus coupling during radial neuronal migration in the cerebral cortex.

The finding here that almost 50% of *SYNE1* coding region mutations are nonsense suggests that stop-codon readthrough (also known as suppression therapy) should be

considered as a treatment option for nesprin-1 related disorders. Suppression therapy utilises pharmacological compounds, which are often aminoglycoside antibiotics, that suppress translation termination at in-frame premature termination codons to restore the translation of a full-length, functional peptide(Wilschanski *et al.*, 2000; Clancy *et al.*, 2001; Politano *et al.*, 2003; James *et al.*, 2005; V. Malik *et al.*, 2010; Taguchi *et al.*, 2017; Hamada *et al.*, 2019). A number of clinical trials have been conducted where aminoglycoside antibiotics have been administered to patients carrying nonsense mutations with diseases including cystic fibrosis(Wilschanski *et al.*, 2000, 2009; Clancy *et al.*, 2001), hemophilia(James *et al.*, 2005) and Hailey-Hailey disease(Kellermayer *et al.*, 2006) showing varying effects including the partial restoration of full-length, functional protein. Moreover, a nonaminoglycoside known as ataluren (previously PTC124) was the first stop-codon readthrough therapy to gain global approval in 2014 for treatment of nonsense mutation Duchenne muscular dystrophy(Inc., 2014; McDonald *et al.*, 2017). Stop-codon readthrough may also be applicable for other NE proteins whereby a significant proportion of causative mutations are nonsense.

6.3.6. The LINC complex as a whole may also be involved in disease pathophysiology

In this study, we focused on examining how the individual proteins associated with the LINC complex contribute to human disease, but the LINC complex as a whole may also be involved in disease pathophysiology. The LINC complex is involved in rearward nuclear movement and contributes to centrosome orientation. This is facilitated by SUN2 and nesprin-2 assembling into transmembrane-associated nuclear (TAN) lines that link actin cables to the nucleus at the INM through anchorage by emerin and A-

type lamins (Folker *et al.*, 2011). Depletion of SUN2, nesprin-2, or lamin A/C in C2C12 cells hindered nuclear movement, and in particular, reduction of nesprin-2 also interfered with cell migration and myoblast fusion into myotubes (Chang *et al.*, 2015). This suggests that the LINC complex is important for proper myogenic differentiation. The LINC complex is also involved in mechanotransduction, the process by which mechanical stimuli is translated into biochemical signals, allowing cells to adjust their structure and function to the physical environment around them, by allowing force transmission across the NE (Lombardi *et al.*, 2011; Kirby and Lammerding, 2018). When exploring nuclear lamin expression in response to external stimuli, it was found that the expression of lamin A/C, relative to B-type lamins, have been found to scale with substrate stiffness both *in-vivo* and *in-vitro* (Swift *et al.*, 2013). Furthermore, interference of the LINC complex is known to impair intracellular force transmission from the cytoskeleton to the nucleus (Brosig *et al.*, 2010). When taken together, these findings imply that mutations in any of the LINC complex proteins may also disrupt the LINC complex and its associated functions, which could be related to disease development. From *in-vitro* studies of cells derived from patients, we also know that mutations in certain LINC complex proteins have implications on others, due to their involvement as components of a protein structure. For example, emerin has been found to be mislocalized in fibroblasts from LGMD patients harbouring *LMNA* mutations, therefore it is important to consider the effect of mutations in LINC complex components on the LINC complex itself (Osmanagic-Myers and Foisner, 2019). The LINC complex has also been implicated in other disease-related processes, and whilst this was not within the scope of this study, considering the role of these proteins in other biological conditions does allow us to understand more about their

function (Matsumoto *et al.*, 2015). Mutations in *SYNE1*, for example, have been implicated in human glioblastoma progression and survival (Masica and Karchin, 2011), and *SYNE1* has also been identified as a potential driver gene in cervical cancer development (Xu *et al.*, 2021). Disruption of the LINC complex in glandular epithelial cells was also found to cause the development of aberrant glandular acini, suggesting the LINC complex is important in maintaining tissue architecture, which could be related to cancer pathophysiology (Q. Zhang *et al.*, 2019). In addition, imbalanced nucleoskeletal connections have been found to create cell polarity defects in HGPS as well as normal physiological aging. As mentioned previously, HGPS is caused by an accumulation of truncated pre-lamin A also known as “progerin” (De Sandre-Giovannoli *et al.*, 2003). Progerin affects the mobility of LINC complex-associated proteins, SUN2, nesprin-2 and emerin, which in turn causes defective nuclear positioning and cell polarity which is essential for migration (Chang *et al.*, 2019).

6.3.7. Limitations of the study

It is understood that many mutations are reported directly to genetic databases and as a result are not published in journal articles. This may be a limitation to this study and as a result a number of mutations may not be recorded and therefore missing in the final analysis. However, there are also limitations to database searching. We found that it was not possible to easily filter mutations by disease or phenotype, therefore it was more appropriate to conduct a systematic review into the literature where we could find clinical details within journal articles. It is also important to consider that some patients with mutations in genes encoding NE proteins displayed “like-phenotype” symptoms. These may not necessarily be strictly classified as diseases but

may be diseases mimicking the phenotypes of other diseases. This is particularly relevant to the many diseases associated with *LMNA* variants. It is necessary to include these phenotypes within this study as it is interesting and valuable to report that these phenotypes are linked to mutations in these genes, even if these cases don't allow for a full clinical classification. This could be considered a limitation of the literature, and what is reported within the literature.

6.4. Conclusion

Overall, many unanswered questions remain surrounding *LMNA* mutations, and why faults with this one protein can cause a spectrum of different diseases, especially since this phenomenon is not seen with in other NE proteins. Despite these uncertainties, other observations were made which offer some insight into the potential downstream consequences of lamin A/C mutations. Striated muscle diseases appear to be most frequent in exons 1 and 6 of *LMNA*, which correspond to areas of the protein involved in lamin-lamin interactions. Subsequently, mutations located in these exons may prevent correct lamin assembly. Variants associated with metabolic diseases generally increase in frequency within the area of *LMNA* which encodes the tail domain of lamin A/C. This region facilitates interactions between numerous proteins and lamin A/C. These interactions could be disrupted by mutations that affect these binding sites. Additionally, exon 6 of *EDM* appears to be an emerin mutation "hot-spot", which is perhaps useful to know when diagnosing EDMD, while nonsense *SYNE1* mutations are frequently the cause of SCAR8, suggesting a compromised LINC complex particularly disrupts processes in the brain. Stop-codon read-through therapy may be a beneficial treatment option for SCAR8 and more research may be needed in

this area. When taken together, these results provide insight into the varied roles of LINC-complex proteins in human disease and provide direction for future gene-targeted therapy development. Moreover, identifying conditions affected by mutations in different NE proteins may allow for sharing of therapies or therapeutic development strategies.

Chapter 7: General discussion and conclusion

It is evident from the literature that there is an urgent need for the development of innovative, effective therapies to treat *LMNA*-associated congenital muscular dystrophy (L-CMD). Current treatment approaches focus only on alleviating symptoms, for example by using surgical interventions or physiotherapy (Macquart *et al.*, 2016). Due to a lack of efficacious treatment options, the disease is able to progress and individuals with L-CMD eventually develop life-threatening complications that eventually become fatal (Quijano-Roy *et al.*, 2008). Therapy development in L-CMD has been hampered by the molecular mechanisms underpinning the disease not being fully understood, therefore the main aim of this thesis was to identify core mechanisms that were conserved across three myoblast cell lines derived from L-CMD patients, each harbouring different *LMNA* mutations (L380S, R249W, del.K32), using a variety of different experimental techniques, to elucidate potential therapeutic targets or biomarkers that may be used to track disease and/or treatment progression. The discoveries within this thesis have helped to both strengthen previous findings in L-CMD research and have also provided new information on conserved characteristics of L-CMD patient-derived myoblasts and myotubes.

Using co-immunoprecipitation (Co-IP) and mass spectrometry (MS) analysis, putative lamin A interactors were identified in L-CMD and healthy myoblast cell lines. A number of putative lamin A interactors were identified exclusively across all L-CMD myoblast cell lines that were not present in the healthy controls, suggesting binding partners that may be gained as a result of *LMNA* mutations. GO analysis revealed mutant lamin A may gain potential new roles through these gained interactors. Further experiments such as Co-IP followed by western blotting are needed to verify that these interactions are detected in L-CMD myoblasts, and to determine whether they can be detected in

control myoblasts. “Knocking-out” proteins that were exclusively identified across all L-CMD myoblasts, and studying whether this alleviates the L-CMD phenotype in myoblasts may also help to determine whether gained interactors contribute to L-CMD pathophysiology. Putative lamin A interactors were also identified that were only present across all healthy control myoblast cell lines, that were not present in the L-CMD myoblasts. There may represent lamin A interactors that are lost as a result of *LMNA* mutations in L-CMD. Whilst it is difficult to verify lost interactions, immunofluorescence microscopy could be used to determine whether these proteins are mislocalized in L-CMD myoblasts, if they are seen to usually co-localize in healthy control myoblasts. This future work may provide insight on whether L-CMD mutations cause gain-of or loss-of-function, as has been previously debated (Liu, Jin and Zhou, 2012). Interactions that are lost of gained between lamin A and other proteins could be further explored to determine whether the molecular pathways downstream of these interactions are dysregulated in L-CMD myoblasts, which may be targeted for future therapy development.

It was observed that L-CMD myoblasts and myotubes had abnormal nuclear morphology, as has been previously seen in myoblasts and myotubes derived from the *Lmna*$^{\Delta K32/\Delta K32}$ mouse model of L-CMD (Bertrand *et al.*, 2012), C2C12 myoblasts transfected with L-CMD *LMNA* mutations (Gómez-Domínguez *et al.*, 2020), as well as in fibroblasts derived from other laminopathy patients (Vigouroux *et al.*, 2001; Favreau *et al.*, 2003; Muchir, van Engelen, *et al.*, 2003; Muchir *et al.*, 2004), indicating a lack of integrity of the nuclear lamina (Lammerding *et al.*, 2004). Additionally, R249W L-CMD myoblasts exhibited emerin mislocalization from the nuclear envelope (NE) to the cytoplasm. Although not identified across all L-CMD cell lines, this is also a symptom of

a weakened nuclear lamina and highlights that a lack of nuclear integrity is a hallmark of the disease. The nuclear lamina is also a critical structure for the stability and proper nuclear distribution of DNA (Guelen *et al.*, 2008). A weakened nuclear envelope can affect the integrity of DNA, inducing the accumulation of DNA damage (Gómez-Domínguez *et al.*, 2020). This is a feature that has previously been linked to laminopathies (Earle *et al.*, 2020). In C2C12 myoblasts transfected with the R249W *LMNA* mutation, significantly elevated levels of DNA damage have been observed. DNA damage was quantified by detection of γH2AX (phosphor-H2A.X Variant Histone) (Gómez-Domínguez *et al.*, 2020). In future work this same technique could be used to determine if DNA damage is a feature of all the L-CMD myoblast cell lines.

Reduced lamin A/C expression was identified across all L-CMD cell line myotubes using western blotting and SWATH-MS quantitative proteomics, which has previously been observed in myoblasts and myotubes derived from the *Lmna*$^{\Delta K32/\Delta K32}$ mouse model of L-CMD (Bertrand *et al.*, 2012). This emphasizes that this may also be a key feature of L-CMD. In *Lmna*$^{\Delta K32/\Delta K32}$ mice, *LMNA* mRNA levels were not reduced alongside lamin A/C protein levels, suggesting reduced translation efficiency or higher rate of degradation of lamin A/C (Bertrand *et al.*, 2012). In myoblasts derived from *Lmna*$^{\Delta K32/\Delta K32}$ mice, lamin A/C accumulation in nuclear aggregates was also observed, which may be due to nuclear assembly defects and could contribute to increased degradation of the protein (Bertrand *et al.*, 2012). In this thesis, lamin A/C aggregation was only detected in del.K32 L-CMD myoblasts.

Reduced lamin A/C levels could have a range of different molecular consequences in myotubes and skeletal muscle tissue and may contribute to the weakened nuclear

lamina observed in the L-CMD cells. Considering these findings, one approach to L-CMD treatment could be to upregulate wild-type lamin A/C expression using a gene therapy. Previously, spliceosome-mediated RNA *trans*-splicing (SMaRT), an approach that targets RNA at the pre-mRNA level and converts endogenous mutated sequences into wild type ones has been used to target the del.K32 L-CMD mutation (Azibani *et al.*, 2018). This approach was found to partially rescued the phenotype of myotubes derived from an L-CMD patient, but the efficacy of *trans*-splicing events were low when delivered to newborn wild-type mice using adeno-associated virus (AAV) delivery (Azibani *et al.*, 2018). Despite this, these results are promising, and other methods to increase lamin A/C production in L-CMD should be explored and their efficacy determined as it could be an effective approach to treating L-CMD. Another feature that was conserved across all L-CMD cell lines was that emerin and the main isoform of SUN2 were both reduced in expression in L-CMD myotubes. Future work may also aim to determine whether upregulation of lamin A/C also rescues emerin and SUN2 expression.

Through characterising nuclear envelope (NE) protein expression in L-CMD and control myoblasts during differentiation, a lower molecular weight isoform of SUN2 that could potentially be SUN2 isoform 8 was identified as being differentially expressed and increased in expression once differentiation is initiated in the majority of L-CMD and control myoblast cell lines. Very little is known about SUN2 isoform 8, so this finding is potentially very insightful into SUN2's roles in muscle cell differentiation. Whilst an endeavor was made to verify this result, follow up experiments are needed to provide further evidence. After this has been done, experiments investigating the roles of this isoform in myoblasts and myotubes may be considered. This could involve "knocking-

out" SUN2 isoform 8 from human myoblasts and studying the consequences of this on muscle cell differentiation.

Within this thesis, SWATH-MS quantitative proteomics was used to identify dysregulated proteins in L-CMD myoblasts and myotubes compared to controls, and molecular, cellular and canonical pathways associated with these proteins were elucidated using Ingenuity Pathway Analysis (IPA), providing insight into the molecular consequences downstream of *LMNA* mutations in L-CMD cells. Due to time constraints, it was not possible to explore all pathways of interest, so further work is needed to investigate these. It was found that carbohydrate metabolism and the insulin signalling pathway, which have previously been linked to other neuromuscular disorders, may be dysregulated in L-CMD myotubes. It would be interesting to explore these pathways as if verified, abnormal carbohydrate metabolism could be used as a biomarker for tracking L-CMD disease progression, or treatment efficacy. Elements of apoptosis pathways including BCL7B (B-cell CLL/lymphoma 7 protein family member B) and Apaf-1, a key component of the intrinsic apoptotic pathway (Danial and Korsmeyer, 2004), were also found to be dysregulated in L-CMD myotubes. It would be interesting to also investigate these proteins further by targeting them with pharmacological compounds and studying the effects on L-CMD cells to determine whether this improves their phenotype. Of course, it is also important to consider that dysregulation of apoptosis may be a consequence that is very far downstream of the effects of *LMNA* mutations in L-CMD, and may be a general repercussion of damaged, unhealthy muscle.

It was found that a number of the dysregulated proteins that were identified in either L-CMD myoblasts or myotubes were associated with terms such as cellular development, cell cycle and cell growth and proliferation. A number of experiments could be conducted in future work to further assess whether these processes are abnormal in L-CMD cells. To determine whether the L-CMD cells had effectively undergone differentiation, L-CMD myotubes could be immunostained for markers of differentiation, such as myosin heavy chain (MHC) or myogenin and visualised using confocal microscopy. As previously, C2C12 cells transfected with the R249W L-CMD mutation were found to have an abnormal distribution of, as well as reduced MHC staining (Gómez-Domínguez *et al.*, 2020). Another method of determining the differentiation capacity of L-CMD myoblasts would be to use RT-qPCR to analyse the expression of a number of both early and late markers of differentiation. To determine whether the L-CMD myoblasts fail to properly exit the cell cycle and to assess the proportion of cells within different stages of the cell cycle, staining with propidium iodide (PI) could be used and analysed using flow cytometry. PI binds to DNA, and the amount of fluorescent signal emitted is directly proportionate to the amount of DNA. Because of the alterations that occur during the cell cycle, analysis of DNA content allows discrimination between G1, S, G2 and M phases.

From the SWATH-MS, IPA was also able to predict which upstream regulators are inhibited or activated for the dysregulated proteins that were identified in the L-CMD myoblasts and myotubes. This information was generated but was not explored in this thesis, therefore should be investigated in future work to determine whether any upstream regulators can be targeted in L-CMD cells.

LMNA mutations are known to cause multiple tissue-specific diseases with vastly varying phenotypes including skeletal muscle, cardiac, metabolic and nervous system pathologies (Worman and Bonne, 2007). It remains unknown how faults with one protein can cause so many diseases. As part of this thesis, a systematic review was conducted to determine whether mutations in NE proteins other than lamin A/C, including lamin B1 and B2, emerin, nesprin-1 and -2, SUN1/SUN2 and FHL1, also caused different diseases (Nagano and Arahata, 2000; Somech *et al.*, 2005; Chi, Chen and Jeang, 2009), and whether any correlations could be made between NE protein disease phenotypes and the region of the gene affected by disease-associated mutations. In doing this, it was revealed that *LMNA* mutations causing striated muscle diseases clustered in exons 1 and 6 of *LMNA*, corresponding to regions involved in lamin-lamin interactions. These mutations may disrupt lamin-lamin binding, and consequently affect lamin assembly. Myoblasts derived from the $Lmna^{\Delta K32/\Delta K32}$ mouse model of L-CMD have been observed to have increased nucleoplasmic aggregation of lamin A/C which is indicative of defective nuclear assembly (Bertrand *et al.*, 2012), and in Chapter 4, nucleoplasmic aggregation of lamin A/C was also observed in del.K32 L-CMD myoblasts. In contrast, *LMNA* variants associated with metabolic diseases also appeared to increase in frequency in areas of *LMNA* encoding the tail domain of lamin A/C, where there are regions that facilitate interactions with other proteins and lamin A/C. This could suggest that a contributing mechanism behind the development of metabolic laminopathies is loss of lamin A interactors. From Chapter 3, it was revealed that whilst some lamin A interactors were only present across all healthy control myoblasts, and not present in L-CMD myoblast cell lines, suggesting some lamin A interactions may be lost in L-CMD myoblasts, this was only a small number of proteins.

In metabolic disorders caused by *LMNA* mutations, a larger amount of lamin A interactions may be disrupted. Research in metabolic laminopathies may benefit from a study similar to the one conducted in Chapter 3, where Co-IP and MS was used to identify lamin A interactors in L-CMD and control myoblasts. A comparison of lamin A interactors in cells from familial partial lipodystrophy (FPLD) patients harbouring *LMNA* mutations with cells from controls may clarify whether lamin A interactions are lost in this condition. Perhaps lamin A interactors in FPLD patient cells could additionally be compared to lamin A interactors identified in L-CMD myoblasts to determine whether there are differences or similarities in interaction partners.

The systematic review revealed that *LMNA* was the only NE protein gene found to cause so many diseases with different phenotypes, but regarding other NE proteins, exon 6 of *EMD* was revealed as an emerin mutation "hot-spot", which may aid in diagnosing X-linked EDMD. It was also observed that nonsense *SYNE1* (encoding nesprin-1) mutations frequently cause cerebellar ataxia (SCAR8), suggesting a compromised LINC complex is especially damaging in brain tissue. Further research into stop-codon read-through therapy may be beneficial in SCAR8 caused by *SYNE1* mutations, as this is an effective therapy currently being used for Duchenne muscular dystrophy (DMD) caused by nonsense mutations (Inc., 2014; McDonald *et al.*, 2017).

Throughout this thesis, immortalized human myoblast cell lines derived from healthy subjects and L-CMD patients were used in experiments. It is important to point out that cell lines are not entirely representative of what occurs *in-vivo*. Human skeletal muscle is a complex 3D tissue consisting of highly compact and aligned myotubes, is vascularize and has a contractile system. Therefore, molecular findings within

myoblasts and myotubes may not necessarily translate in muscle tissue. In addition to this, throughout this thesis the three L-CMD immortalized myoblast cell lines (L380S, R249W, del.K32) were often compared to the C5d, C25, and C41 immortalized control myoblast cell lines. Out of the control myoblasts available, these three were from the youngest donors and closest in age to the donors of the L-CMD myoblasts. Despite this, the C25 and C41 control myoblasts, taken from a 25- and 41-year-old, respectively, were still from donors that were considerably older than the L-CMD patients (3-12 years old). The donors of the L-CMD and control myoblasts also differed in sex, and the cells were derived from different muscles. It is important to consider that age, sex, and donor muscle may influence results as, for example, the expression of proteins can differ with age and within different muscles. Here, immortalized human myoblasts were used as L-CMD is an incredibly rare disease, so it is difficult to attain human muscle samples from L-CMD patients. Furthermore, whilst there may be concerns over whether immortalization of cell lines has an effect on the processes that occur within the cells, it is incredibly difficult to isolate pure populations of myoblasts from muscle biopsies as often fibroblasts contaminate the myoblast cultures. Taking this into account, immortalized myoblasts were the most suitable tool to be used in this thesis to study L-CMD. Perhaps in future, it would be possible to collaborate with other L-CMD research groups to verify the findings here in another model of L-CMD.

In the introduction to this thesis, it was discussed how there is some overlap between L-CMD and Emery-Drefiuss muscular dystrophy (EDMD) in terms of the two diseases clinical features and some findings on the molecular level. As previously discussed in Chapter 6, mutations in *LMNA* notoriously also cause a wide range of different human diseases, and in some cases, identical mutations cause different conditions. If the

resources were available, future work may seek to determine whether dysregulated pathways that were identified in L-CMD myoblasts and myotubes are similarly dysregulation in EDMD myoblasts and myotubes, or in other laminopathies. This could help to identify differences in downstream mechanisms underpinning the different laminopathies and help us to understand how one gene can cause multiple diseases. Or alternatively, this may reveal common aberrant pathways across the different diseases which could be targeted in future for therapy development.

References

Addona, T. A. *et al.* (2009) 'Multi-site assessment of the precision and reproducibility of multiple reaction monitoring-based measurements of proteins in plasma', *Nature biotechnology*. Nat Biotechnol, 27(7), pp. 633–641. doi: 10.1038/NBT.1546.

Aguilar-Agon, K. W. *et al.* (2019) 'Mechanical loading stimulates hypertrophy in tissue-engineered skeletal muscle: Molecular and phenotypic responses', *Journal of Cellular Physiology*. Wiley-Liss Inc., 234(12), pp. 23547–23558. doi: 10.1002/jcp.28923.

Ahmed, M. S. *et al.* (2018) 'Hutchinson-Gilford Progeria Syndrome: A Premature Aging Disease.', *Molecular neurobiology*, 55(5), pp. 4417–4427. doi: doi.org/10.1007/s12035-017-0610-7.

Ahn, J. *et al.* (2019) 'Structural basis for lamin assembly at the molecular level', *Nature Communications*. Nature Publishing Group, 10(1), pp. 1–12. doi: 10.1038/s41467-019-11684-x.

Allen, D. G. and Whitehead, N. P. (2011) 'Duchenne muscular dystrophy - What causes the increased membrane permeability in skeletal muscle?', *International Journal of Biochemistry and Cell Biology*, 43(3), pp. 290–294. doi: 10.1016/j.biocel.2010.11.005.

Alsharidah, M. *et al.* (2013) 'Primary human muscle precursor cells obtained from young and old donors produce similar proliferative, differentiation and senescent profiles in culture', *Aging Cell*, 12(3), pp. 333–344. doi: 10.1111/acel.12051.

Altschul, S. F. *et al.* (1990) 'Basic local alignment search tool', *Journal of molecular biology*. J Mol Biol, 215(3), pp. 403–410. doi: 10.1016/S0022-2836(05)80360-2.

Amaral, A. R. *et al.* (2017) 'Abnormal carbohydrate metabolism in a canine model for

muscular dystrophy', *Journal of Nutritional Science*. Cambridge University Press, 6, pp. 1–6. doi: 10.1017/JNS.2017.59.

Anderson, M. J. and Cohen, M. W. (1977) 'Nerve-induced and spontaneous redistribution of acetylcholine receptors on cultured muscle cells', *The Journal of physiology*. J Physiol, 268(3), pp. 757–773. doi: 10.1113/JPHYSIOL.1977.SP011880.

Andrés, V. and González, J. M. (2009) 'Role of A-type lamins in signaling, transcription, and chromatin organization.', *The Journal of cell biology*. The Rockefeller University Press, 187(7), pp. 945–57. doi: 10.1083/jcb.200904124.

Andrés, V. and Walsh, K. (1996) 'Myogenin expression, cell cycle withdrawal, and phenotypic differentiation are temporally separable events that precede cell fusion upon myogenesis.', *Journal of Cell Biology*. The Rockefeller University Press, 132(4), pp. 657–666. doi: 10.1083/JCB.132.4.657.

Andreu, A. L. *et al.* (2007) 'McArdle disease: molecular genetic update', *Acta Myologica*. Pacini Editore, 26(1), p. 53.

Arimura, T. *et al.* (2005) 'Mouse model carrying H222P-Lmna mutation develops muscular dystrophy and dilated cardiomyopathy similar to human striated muscle laminopathies.', *Human molecular genetics*, 14(1), pp. 155–169. doi: doi.org/10.1093/hmg/ddi017.

Astejada, M. N. *et al.* (2007) 'Emerinopathy and laminopathy clinical, pathological and molecular features of muscular dystrophy with nuclear envelopathy in Japan.', *Acta myologica : myopathies and cardiomyopathies : official journal of the Mediterranean Society of Myology*, 26(3), pp. 159–164.

Attali, R. *et al.* (2009) ‘Mutation of SYNE-1, encoding an essential component of the nuclear lamina, is responsible for autosomal recessive arthrogryposis.’, *Human molecular genetics*, 18(18), pp. 3462–3469. doi: doi.org/10.1093/hmg/ddp290.

Auguste, G. *et al.* (2018) ‘Suppression of Activated FOXO Transcription Factors in the Heart Prolongs Survival in a Mouse Model of Laminopathies’, *Circulation research*. Circ Res, 122(5), pp. 678–692. doi: 10.1161/CIRCRESAHA.117.312052.

Avila, G. M. *et al.* (2021) ‘Is the Next Generation Sequencing the Essential Tool for the Early Diagnostic Approach in Congenital Muscular Dystrophy? New Mutation in the Gene LMNA Associated with Serious Phenotype.’, *Neurology India*, 69(6), pp. 1835–1837. doi: 10.4103/0028-3886.333448.

Awan, M. *et al.* (2020) ‘Dimethyl sulfoxide: A central player since the dawn of cryobiology, is efficacy balanced by toxicity?’, *Regenerative Medicine*. Future Medicine Ltd., 15(3), pp. 1463–1491. doi: 10.2217/rme-2019-0145.

Azibani, F. *et al.* (2018) ‘Gene Therapy via Trans-Splicing for LMNA-Related Congenital Muscular Dystrophy’, *Molecular therapy. Nucleic acids*. Mol Ther Nucleic Acids, 10, pp. 376–386. doi: 10.1016/J.OMTN.2017.12.012.

Bakay, M. *et al.* (2006) ‘Nuclear envelope dystrophies show a transcriptional fingerprint suggesting disruption of Rb–MyoD pathways in muscle regeneration’, *Brain*, 129(4), pp. 996–1013. doi: 10.1093/brain/awl023.

Bank, E. M. *et al.* (2011) ‘A laminopathic mutation disrupting lamin filament assembly causes disease-like phenotypes in Caenorhabditis elegans’, *Molecular Biology of the Cell*. The American Society for Cell Biology , 22(15), pp. 2716–2728. doi:

10.1091/mbc.E11-01-0064.

Barateau, A. *et al.* (2017) 'A Novel Lamin A Mutant Responsible for Congenital Muscular Dystrophy Causes Distinct Abnormalities of the Cell Nucleus.', *PloS one*, 12(1), p. e0169189. doi: doi.org/10.1371/journal.pone.0169189.

Baumann, M. *et al.* (2017) 'Homozygous SYNE1 mutation causes congenital onset of muscular weakness with distal arthrogryposis: a genotype-phenotype correlation.', *European journal of human genetics*, 25(2), pp. 262–266. doi: doi.org/10.1038/ejhg.2016.144.

Bechert, K. *et al.* (2003) 'Effects of expressing lamin A mutant protein causing Emery-Dreifuss muscular dystrophy and familial partial lipodystrophy in HeLa cells', *Experimental Cell Research*. Academic Press Inc., 286(1), pp. 75–86. doi: 10.1016/S0014-4827(03)00104-6.

Bedell, V. M., Westcot, S. E. and Ekker, S. C. (2011) 'Lessons from morpholino-based screening in zebrafish', *Briefings in Functional Genomics*, 10(4), pp. 181–188. doi: doi.org/10.1093/bfgp/elr021.

Ben-Harush, K. *et al.* (2009) 'The Supramolecular Organization of the C. elegans Nuclear Lamin Filament', *Journal of Molecular Biology*. Academic Press, 386(5), pp. 1392–1402. doi: 10.1016/j.jmb.2008.12.024.

Bencze, M. *et al.* (2017) 'Necroptosis, a programmed form of necrosis, participates in muscle degeneration in Duchenne muscular dystrophy', *Neuromuscular Disorders*. Elsevier BV, 27, p. S98. doi: 10.1016/j.nmd.2017.06.029.

Bernadotte, A., Mikhelson, V. M. and Spivak, I. M. (2016) 'Markers of cellular

senescence. Telomere shortening as a marker of cellular senescence', *Aging (Albany NY)*. Impact Journals, LLC, 8(1), p. 3. doi: 10.18632/AGING.100871.

Bernard, R. *et al.* (2006) 'Molecular genetics of autosomal-recessive axonal Charcot-Marie-Tooth neuropathies.', *Neuromolecular medicine*, 8(1–2), pp. 87–106. doi: doi.org/10.1385/NMM:8:1-2:87.

Bertrand, A. T. *et al.* (2011) 'Laminopathies: one gene, several diseases', *Biologie aujourd'hui*, 205(3), pp. 147–162. doi: 10.1051/jbio/2011017.

Bertrand, A. T. *et al.* (2012) 'DelK32-lamin A/C has abnormal location and induces incomplete tissue maturation and severe metabolic defects leading to premature death', *Human Molecular Genetics*. Oxford Academic, 21(5), pp. 1037–1048. doi: 10.1093/HMG/DDR534.

Bertrand, A. T. *et al.* (2014) 'Cellular microenvironments reveal defective mechanosensing responses and elevated YAP signaling in LMNA-mutated muscle precursors.', *Journal of cell science*, 127(13), pp. 2873–2884. doi: doi.org/10.1242/jcs.144907.

Bertrand, A. T. *et al.* (2020) 'Lamin A/C Assembly Defects in LMNA -Congenital Muscular Dystrophy Is Responsible for the Increased Severity of the Disease Compared with Emery-Dreifuss Muscular Dystrophy.', *Cells*, 9(4), p. 844. doi: doi.org/10.3390/cells9040844.

Betts, M. J. and Russell, R. B. (2003) 'Amino Acid Properties and Consequences of Substitutions', in Barnes, M. R. and Gray, I. C. (eds) *Bioinformatics for Geneticists*. John Wiley & Sons, Ltd, pp. 289–316. doi: 10.1002/0470867302.CH14.

Biggar, W. D. *et al.* (2001) 'Deflazacort treatment of Duchenne muscular dystrophy', *The Journal of Pediatrics*. Mosby, 138(1), pp. 45–50. doi: 10.1067/MPD.2001.109601.

Bione, S. *et al.* (1994) 'Identification of a novel X-linked gene responsible for Emery-Dreifuss muscular dystrophy', *Nature Genetics*. Nature Publishing Group, 8(4), pp. 323–327. doi: 10.1038/ng1294-323.

Bodine, S. C. *et al.* (2001) 'Identification of ubiquitin ligases required for skeletal Muscle Atrophy', *Science*, 294(5547). doi: 10.1126/science.1065874.

Bodnar, A. G. *et al.* (1998) 'Extension of life-span by introduction of telomerase into normal human cells', *Science*, 279(5349), pp. 349–352. doi: 10.1126/science.279.5349.349.

Bogan, A. A. and Thorn, K. S. (1998) 'Anatomy of hot spots in protein interfaces', *Journal of Molecular Biology*, 280(1), pp. 1–9. doi: 10.1006/jmbi.1998.1843.

Bonati, U. *et al.* (2014) 'Congenital muscular dystrophy with dropped head phenotype and cognitive impairment due to a novel mutation in the LMNA gene', *Neuromuscular Disorders*. Elsevier Ltd, 24(6), pp. 529–532. doi: 10.1016/j.nmd.2014.02.004.

Bone, C. R. *et al.* (2014) 'The Caenorhabditis elegans SUN protein UNC-84 interacts with lamin to transfer forces from the cytoplasm to the nucleoskeleton during nuclear migration', *Molecular Biology of the Cell*. American Society for Cell Biology, 25(18), pp. 2853–2865. doi: doi.org/10.1091/mbc.e14-05-0971.

Bonello-Palot, N. *et al.* (2014) 'Prelamin A accumulation in endothelial cells induces premature senescence and functional impairment', *Atherosclerosis*. Elsevier, 237(1), pp. 45–52. doi: 10.1016/J.ATHEROSCLEROSIS.2014.08.036.

Bonifacino, J. S., Dell'Angelica, E. C. and Springer, T. A. (1999) 'Immunoprecipitation', *Current Protocols in Protein Science*. John Wiley & Sons, Ltd, 18(1), pp. 9.8.1-9.8.28. doi: 10.1002/0471140864.PS0908S18.

Bonilla, E. *et al.* (1988) 'Duchenne muscular dystrophy: Deficiency of dystrophin at the muscle cell surface', *Cell*. Cell Press, 54(4), pp. 447–452. doi: 10.1016/0092-8674(88)90065-7.

Bonne, G. *et al.* (1999) 'Mutations in the gene encoding lamin A/C cause autosomal dominant Emery-Dreifuss muscular dystrophy', *Nature Genetics*, 21(3), pp. 285–288. doi: 10.1038/6799.

Bonne, G. *et al.* (2000) 'Clinical and molecular genetic spectrum of autosomal dominant Emery-Dreifuss muscular dystrophy due to mutations of the lamin A/C gene', *Annals of Neurology*. John Wiley & Sons, Ltd, 48(2), pp. 170–180. doi: 10.1002/1531-8249(200008)48:2<170::AID-ANA6>3.0.CO;2-J.

Bonne, G., Leturcq, F. and Yaou, R. Ben (2019) *Emery-Dreifuss Muscular Dystrophy*, *Gene Reviews*. University of Washington, Seattle. Available at: https://www.ncbi.nlm.nih.gov/books/NBK1436/ (Accessed: 25 January 2023).

Boriani, G. *et al.* (2003) 'Clinical relevance of atrial fibrillation/flutter, stroke, pacemaker implant, and heart failure in Emery-Dreifuss muscular dystrophy: A long-term longitudinal study', *Stroke*. Lippincott Williams & Wilkins, 34(4), pp. 901–908. doi: 10.1161/01.STR.0000064322.47667.49.

Bossi, A. and Lehner, B. (2009) 'Tissue specificity and the human protein interaction network', *Molecular Systems Biology*, 5(1). doi: 10.1038/msb.2009.17.

Botto, L. D. *et al.* (1999) 'Neural-Tube Defects', *N Engl J Med*. Massachusetts Medical Society, 341(20), pp. 1509–1519. doi: 10.1056/NEJM199911113412006.

Botto, N. *et al.* (2010) 'A novel LMNA mutation (R189W) in familial dilated cardiomyopathy: evidence for a "hot spot" region at exon 3: a case report.', *Cardiovascular ultrasound*, 8(9), p. 7681. doi: doi.org/10.1186/1476-7120-8-9.

Brachner, A. *et al.* (2005) 'LEM2 is a novel MAN1-related inner nuclear membrane protein associated with A-type lamins', *Journal of Cell Science*. The Company of Biologists, 118(24), pp. 5797–5810. doi: 10.1242/JCS.02701.

Braithwaite, A. W. and Harris, A. J. (1979) 'Neural influence on acetylcholine receptor clusters in embryonic development of skeletal muscles', *Nature*. Nature, 279(5713), pp. 549–551. doi: 10.1038/279549A0.

Braun, T. *et al.* (1989) 'Differential expression of myogenic determination genes in muscle cells: possible autoactivation by the Myf gene products.', *The EMBO Journal*. John Wiley & Sons, Ltd, 8(12), pp. 3617–3625. doi: 10.1002/J.1460-2075.1989.TB08535.X.

Brero, A. *et al.* (2005) 'Methyl CpG–binding proteins induce large-scale chromatin reorganization during terminal differentiation', *The Journal of Cell Biology*. Rockefeller University Press, 169(5), pp. 733–743. doi: 10.1083/JCB.200502062.

Brinkmeier, H. and Ohlendieck, K. (2014) 'Chaperoning heat shock proteins: Proteomic analysis and relevance for normal and dystrophin-deficient muscle', *Proteomics - Clinical Applications*, 8(11–12), pp. 875–895. doi: 10.1002/prca.201400015.

Broers, J. L. V *et al.* (2004) 'Decreased mechanical stiffness in LMNA-/- cells is caused

by defective nucleo-cytoskeletal integrity: implications for the development of laminopathies.', *Human molecular genetics*, 13(21), pp. 2567–2580. doi: 10.1093/hmg/ddh295.

Broers, J. L. V *et al.* (2006) 'Nuclear lamins: laminopathies and their role in premature ageing.', *Physiological reviews*, 86(3), pp. 967–1008. doi: doi.org/10.1152/physrev.00047.2005.

Brosig, M. *et al.* (2010) 'Interfering with the connection between the nucleus and the cytoskeleton affects nuclear rotation, mechanotransduction and myogenesis', *The international journal of biochemistry & cell biology*. Int J Biochem Cell Biol, 42(10), pp. 1717–1728. doi: 10.1016/J.BIOCEL.2010.07.001.

Brown, S. J. *et al.* (2022) 'The Proteome Signatures of Fibroblasts from Patients with Severe, Intermediate and Mild Spinal Muscular Atrophy Show Limited Overlap', *Cells*. MDPI, 11(17), p. 2624. doi: doi.org/10.3390/cells11172624.

Brull, A. *et al.* (2018) 'The pathogenesis and therapies of striated muscle laminopathies', *Frontiers in Physiology*, 9. doi: 10.3389/fphys.2018.01533.

Brussino, A. *et al.* (2010) 'A family with autosomal dominant leukodystrophy linked to 5q23.2-q23.3 without lamin B1 mutations.', *European journal of neurology*, 17(4), pp. 541–549. doi: doi.org/10.1111/j.1468-1331.2009.02844.x.

Bulaj, G. (2005) 'Formation of disulfide bonds in proteins and peptides', *Biotechnology advances*. Biotechnol Adv, 23(1), pp. 87–92. doi: 10.1016/J.BIOTECHADV.2004.09.002.

Burgess, D. H. *et al.* (1999) 'Human skeletal muscle cytosols are refractory to cytochrome c-dependent activation of type-II caspases and lack APAF-1', *Cell Death*

and Differentiation, 6(3), pp. 256–261. doi: 10.1038/sj.cdd.4400489.

Burns, J. A. *et al.* (2002) 'Selective reduction of disulfides by tris(2-carboxyethyl)phosphine', *Journal of Organic Chemistry*. American Chemical Society, 56(8), pp. 2648–2650. doi: 10.1021/JO00008A014.

Cadot, B., Gache, V. and Gomes, E. R. (2015) 'Moving and positioning the nucleus in skeletal muscle – one step at a time', *Nucleus*. Taylor & Francis, 6(5), pp. 373–381. doi: 10.1080/19491034.2015.1090073.

Cain, N. E. *et al.* (2018) 'Conserved SUN-KASH Interfaces Mediate LINC Complex-Dependent Nuclear Movement and Positioning', *Current Biology*. Cell Press, 28(19), pp. 3086–97.e4. doi: 10.1016/j.cub.2018.08.001.

Cao, L. and Mu, W. (2021) 'Necrostatin-1 and necroptosis inhibition: Pathophysiology and therapeutic implications', *Pharmacological Research*. Academic Press, 163, p. 105297. doi: 10.1016/J.PHRS.2020.105297.

Carson, J. A., Nettleton, D. and Reecy, J. M. (2002) 'Differential gene expression in the rat soleus muscle during early work overload-induced hypertrophy', *The FASEB Journal*. John Wiley & Sons, Ltd, 16(2), pp. 1–21. doi: 10.1096/FJ.01-0544FJE.

Catalanotto, C., Cogoni, C. and Zardo, G. (2016) 'MicroRNA in control of gene expression: An overview of nuclear functions', *International Journal of Molecular Sciences*, p. 1712. doi: 10.3390/ijms17101712.

Cattin, M.-E. *et al.* (2013) 'Heterozygous LmnadelK32 mice develop dilated cardiomyopathy through a combined pathomechanism of haploinsufficiency and peptide toxicity.', *Human molecular genetics*, 22(15), pp. 3152–3164. doi:

10.1093/hmg/ddt172.

Cerrone, M. *et al.* (2019) 'Beyond the One Gene–One Disease Paradigm', *Circulation*. Lippincott Williams & WilkinsHagerstown, MD, 140(7), pp. 595–610. doi: 10.1161/CIRCULATIONAHA.118.035954.

Chai, R. J. *et al.* (2021) 'Disrupting the LINC complex by AAV mediated gene transduction prevents progression of Lamin induced cardiomyopathy', *Nature Communications*, 12, p. 4722. doi: 10.1038/s41467-021-24849-4.

Chancellory, T. J. *et al.* (2010) 'Actomyosin Tension Exerted on the Nucleus through Nesprin-1 Connections Influences Endothelial Cell Adhesion, Migration, and Cyclic Strain-Induced Reorientation', *Biophysical Journal*. The Biophysical Society, 99(1), p. 115. doi: 10.1016/J.BPJ.2010.04.011.

Chang, H. H. Y. *et al.* (2017) 'Non-homologous DNA end joining and alternative pathways to double-strand break repair', *Nature Reviews Molecular Cell Biology*, 18(8), pp. 495–506. doi: 10.1038/nrm.2017.48.

Chang, W. *et al.* (2015) 'Linker of nucleoskeleton and cytoskeleton (LINC) complex-mediated actin-dependent nuclear positioning orients centrosomes in migrating myoblasts.', *Nucleus*, 6(1), pp. 77–88. doi: 10.1080/19491034.2015.1004947.

Chang, W. *et al.* (2019) 'Imbalanced nucleocytoskeletal connections create common polarity defects in progeria and physiological aging', *Proceedings of the National Academy of Sciences of the United States of America*. National Academy of Sciences, 116(9), pp. 3578–3583. doi: doi.org/10.1073/pnas.1809683116.

Chapman, M. A. *et al.* (2014) 'Disruption of both nesprin 1 and desmin results in

nuclear anchorage defects and fibrosis in skeletal muscle.', *Human molecular genetics*. Oxford University Press, 23(22), pp. 5879–92. doi: 10.1093/hmg/ddu310.

Chehade, L. *et al.* (2022) 'Suppression of the necroptotic cell death pathways improves survival in Smn2B/− mice', *Frontiers in Cellular Neuroscience*. Frontiers Media S.A., 16, p. 408. doi: doi.org/10.3389/fncel.2022.972029.

Chen, C.-Y. *et al.* (2012) 'Accumulation of the inner nuclear envelope protein Sun1 is pathogenic in progeric and dystrophic laminopathies.', *Cell*, 149(3), pp. 565–577. doi: 10.1016/j.cell.2012.01.059.

Chen, M. *et al.* (2000) 'Minocycline inhibits caspase-1 and caspase-3 expression and delays mortality in a transgenic mouse model of Huntington disease', *Nature Medicine*, 6(7), pp. 797–801. doi: 10.1038/77528.

Chernyatina, A. A., Guzenko, D. and Strelkov, S. V. (2015) 'Intermediate filament structure: the bottom-up approach', *Current Opinion in Cell Biology*. Elsevier Current Trends, 32, pp. 65–72. doi: 10.1016/J.CEB.2014.12.007.

Chi, M. M. Y. *et al.* (1987) 'Effect of Duchenne muscular dystrophy on enzymes of energy metabolism in individual muscle fibers', *Metabolism*. W.B. Saunders, 36(8), pp. 761–767. doi: 10.1016/0026-0495(87)90113-2.

Chi, Y. H., Chen, Z. J. and Jeang, K. T. (2009) 'The nuclear envelopathies and human diseases', *Journal of Biomedical Science*, 16(1), p. 96. doi: 10.1186/1423-0127-16-96.

Choi, J. C. *et al.* (2012) 'Temsirolimus activates autophagy and ameliorates cardiomyopathy caused by lamin A/C gene mutation.', *Science translational medicine*, 4(144), pp. 144–102. doi: 10.1126/scitranslmed.3003875.

Choi, S. A. *et al.* (2019) 'Importance of early diagnosis in LMNA-related muscular dystrophy for cardiac surveillance.', *Muscle & nerve*, 60(6), pp. 668–672. doi: 10.1002/mus.26700.

Clancy, J. P. *et al.* (2001) 'Evidence that systemic gentamicin suppresses premature stop mutations in patients with cystic fibrosis', *American journal of respiratory and critical care medicine*. Am J Respir Crit Care Med, 163(7), pp. 1683–1692. doi: 10.1164/AJRCCM.163.7.2004001.

Clements, L. *et al.* (2000) 'Direct interaction between emerin and lamin A.', *Biochemical and biophysical research communications*, 267(3), pp. 709–714. doi: 10.1006/bbrc.1999.2023.

Coffinier, C., Chang, S. Y., *et al.* (2010) 'Abnormal development of the cerebral cortex and cerebellum in the setting of lamin B2 deficiency', *Proceedings of the National Academy of Sciences*. National Academy of Sciences, 107(11), pp. 5076–5081. doi: 10.1073/PNAS.0908790107.

Coffinier, C., Jung, H. J., *et al.* (2010) 'Direct synthesis of lamin A, bypassing prelamin a processing, causes misshapen nuclei in fibroblasts but no detectable pathology in mice', *Journal of Biological Chemistry*, 285(27). doi: 10.1074/jbc.M110.128835.

Coffinier, C. *et al.* (2011) 'Deficiencies in lamin B1 and lamin B2 cause neurodevelopmental defects and distinct nuclear shape abnormalities in neurons', *Molecular Biology of the Cell*. The American Society for Cell Biology, 22(23), pp. 4683–4693. doi: 10.1091/mbc.E11-06-0504.

Collins, C. M., Ellis, J. A. and Holaska, J. M. (2017) 'MAPK signaling pathways and

HDAC3 activity are disrupted during differentiation of emerin-null myogenic progenitor cells', *Disease Models & Mechanisms*, 10(4), pp. 385–397. doi: 10.1242/dmm.028787.

Collins, J. and Bönnemann, C. G. (2010) 'Congenital muscular dystrophies: Toward molecular therapeutic interventions', *Current Neurology and Neuroscience Reports*. Springer, pp. 83–91. doi: 10.1007/s11910-010-0092-8.

Collomp, K. *et al.* (2016) 'Glucocorticoid administration in athletes: Performance, metabolism and detection', *Steroids*. doi: 10.1016/j.steroids.2016.09.008.

Colomer, J. *et al.* (2002) 'Autosomal dominant Emery-Dreifuss muscular dystrophy: a new family with late diagnosis.', *Neuromuscular disorders : NMD*, 12(1), pp. 19–25. doi: 10.1016/s0960-8966(01)00239-5.

Cooper, D. N. and Youssoufian, H. (1988) 'The CpG dinucleotide and human genetic disease', *Human Genetics 1988 78:2*. Springer, 78(2), pp. 151–155. doi: 10.1007/BF00278187.

Corpet, F. (1988) 'Multiple sequence alignment with hierarchical clustering', *Nucleic acids research*. Nucleic Acids Res, 16(22), pp. 10881–10890. doi: 10.1093/NAR/16.22.10881.

Cossu, G., Tajbakhsh, S. and Buckingham, M. (1996) 'How is myogenesis initiated in the embryo?', *Trends in Genetics*, 12(6), pp. 218–213. doi: 10.1016/0168-9525(96)10025-1.

Crasto, S., My, I. and Di Pasquale, E. (2020) 'The Broad Spectrum of LMNA Cardiac Diseases: From Molecular Mechanisms to Clinical Phenotype.', *Frontiers in physiology*,

11, p. 761. doi: 10.3389/fphys.2020.00761.

Creazzo, T. L. and Sohal, G. S. (1983) 'Neural control of embryonic acetylcholine receptor and skeletal muscle', *Cell and Tissue Research*. Springer-Verlag, 228(1), pp. 1–12. doi: 10.1007/BF00206259/METRICS.

Crisp, M., Liu, Q., Roux, K., Rattner, J.B., *et al.* (2006) 'Coupling of the nucleus and cytoplasm: Role of the LINC complex', *The Journal of Cell Biology*, 172(1), pp. 41–53. doi: 10.1083/jcb.200509124.

Crisp, M., Liu, Q., Roux, K., Rattner, J. B., *et al.* (2006) 'Coupling of the nucleus and cytoplasm: Role of the LINC complex', *The Journal of Cell Biology*, 172(1), pp. 41–53. doi: 10.1083/jcb.200509124.

Culetto, E. and Sattelle, D. B. (2000) 'A role for Caenorhabditis elegans in understanding the function and interactions of human disease genes', *Human Molecular Genetics*. Oxford Academic, 9(6), pp. 869–877. doi: 10.1093/HMG/9.6.869.

Cynthia Martin, F. *et al.* (2014) 'Fibronectin is a serum biomarker for Duchenne muscular dystrophy', *Proteomics - Clinical Applications*, 8(3–4), pp. 269–278. doi: 10.1002/prca.201300072.

D'Amico, A. *et al.* (2005) 'Two patients with "Dropped head syndrome" due to mutations in LMNA or SEPN1 genes', *Neuromuscular Disorders*, 15(8), pp. 521–524. doi: 10.1016/j.nmd.2005.03.006.

Dadali, E. L. *et al.* (2016) 'Clinical/genetic characteristics of patients with congenital muscular dystrophy caused by mutations in the LMNA gene', *Zhurnal nevrologii i psikhiatrii imeni S.S. Korsakova*. Zh Nevrol Psikhiatr Im S S Korsakova, 116(1), pp. 70–

75. doi: 10.17116/jnevro20161161170-75.

Dalziel, R. G., Mendelson, S. C. and Quinn, J. P. (1992) 'The nuclear autoimmune antigen Ku is also present on the cell surface', *Autoimmunity*, 13(4), pp. 265–267. doi: 10.3109/08916939209112334.

Dang, L. *et al.* (2009) 'Cancer-associated IDH1 mutations produce 2-hydroxyglutarate', *Nature*, 462(7274), pp. 739–744. doi: 10.1038/nature08617.

Danial, N. N. and Korsmeyer, S. J. (2004) 'Cell Death: Critical Control Points', *Cell*, 116(2), pp. 205–219. doi: 10.1016/S0092-8674(04)00046-7.

David, A. *et al.* (2012) 'Protein-protein interaction sites are hot spots for disease-associated nonsynonymous SNPs', *Human Mutation*, 33(2), pp. 359–363. doi: 10.1002/humu.21656.

Davidson, P. M. and Lammerding, J. (2014) 'Broken nuclei – lamins, nuclear mechanics, and disease', *Trends in Cell Biology*, 24(4), pp. 247–256. doi: 10.1016/j.tcb.2013.11.004.

Davis, R. J. (1993) 'The mitogen-activated protein kinase signal transduction pathway', *Journal of Biological Chemistry*. Elsevier, 268(20), pp. 14553–14556. doi: 10.1016/S0021-9258(18)82362-6.

Dechat, T. *et al.* (2000) 'Lamina-associated polypeptide 2alpha binds intranuclear A-type lamins', *Journal of Cell Science*. The Company of Biologists, 113(19), pp. 3473–3484. doi: 10.1242/JCS.113.19.3473.

Degterev, A. *et al.* (2005) 'Chemical inhibitor of nonapoptotic cell death with therapeutic potential for ischemic brain injury', *Nature Chemical Biology 2005 1:2*.

Nature Publishing Group, 1(2), pp. 112–119. doi: 10.1038/nchembio711.

Degterev, A. *et al.* (2008) 'Identification of RIP1 kinase as a specific cellular target of necrostatins', *Nature Chemical Biology*, 4(5), pp. 313–321. doi: 10.1038/nchembio.83.

Dell'Amore, A. *et al.* (2007) 'Heart Transplantation in Patients With Emery-Dreifuss Muscular Dystrophy: Case Reports', *Transplantation Proceedings*, 39(10), pp. 3538–3540. doi: 10.1016/j.transproceed.2007.06.076.

Demmerle, J., Koch, A. J. and Holaska, J. M. (2013) 'Emerin and histone deacetylase 3 (HDAC3) cooperatively regulate expression and nuclear positions of MyoD, Myf5, and Pax7 genes during myogenesis', *Chromosome Res*, 21, pp. 765–779. doi: 10.1007/s10577-013-9381-9.

Dharmaraj, T. *et al.* (2019) 'Rare BANF1 Alleles and Relatively Frequent EMD Alleles Including "Healthy Lipid" Emerin p.D149H in the ExAC Cohort.', *Frontiers in cell and developmental biology*, 7, p. 48. doi: 10.3389/fcell.2019.00048.

Dheda, K. *et al.* (2005) 'The implications of using an inappropriate reference gene for real-time reverse transcription PCR data normalization', *Analytical Biochemistry*, 344(1). doi: 10.1016/j.ab.2005.05.022.

Dhillon, S. (2021) 'Lonafarnib: First Approval', *Drugs*. Springer, 81(2), pp. 283–289. doi: 10.1007/S40265-020-01464-Z.

Dhuriya, Y. K. and Sharma, D. (2018) 'Necroptosis: a regulated inflammatory mode of cell death', *Journal of Neuroinflammation 2018 15:1*. BioMed Central, 15(1), pp. 1–9. doi: 10.1186/S12974-018-1235-0.

Díaz-Manera, J. *et al.* (2016) 'Muscle imaging in muscle dystrophies produced by

mutations in the EMD and LMNA genes.', *Neuromuscular disorders : NMD*, 26(1), pp. 33–40. doi: 10.1016/j.nmd.2015.10.001.

Ditaranto, R. *et al.* (2019) 'Differences in cardiac phenotype and natural history of laminopathies with and without neuromuscular onset.', *Orphanet journal of rare diseases*, 14(1), p. 263. doi: 10.1186/s13023-019-1245-8.

Dittmer, T. A. *et al.* (2014) 'Systematic identification of pathological lamin A interactors.', *Molecular biology of the cell*, 25(9), pp. 1493–1510. doi: 10.1091/mbc.e14-02-0733.

Dittmer, T. and Misteli, T. (2011) 'The lamin protein family', *Genome Biology*, 12(5), p. 222. doi: 10.1186/gb-2011-12-5-222.

Dobrian, A. D. *et al.* (2019) 'Role of the 12-lipoxygenase pathway in diabetes pathogenesis and complications', *Pharmacology & Therapeutics*. Pergamon, 195, pp. 100–110. doi: 10.1016/J.PHARMTHERA.2018.10.010.

Dohrn, M. F. *et al.* (2017) 'Frequent genes in rare diseases: panel-based next generation sequencing to disclose causal mutations in hereditary neuropathies.', *Journal of neurochemistry*, 143(5), pp. 507–522. doi: 10.1111/jnc.14217.

Dong, C. *et al.* (2020) '12-Lipoxygenase as a key pharmacological target in the pathogenesis of diabetic nephropathy', *European Journal of Pharmacology*. Elsevier, 879, p. 173122. doi: 10.1016/J.EJPHAR.2020.173122.

Dorner, D. *et al.* (2006) 'Lamina-associated polypeptide 2alpha regulates cell cycle progression and differentiation via the retinoblastoma-E2F pathway', *The Journal of cell biology*. J Cell Biol, 173(1), pp. 83–93. doi: 10.1083/JCB.200511149.

Dreuillet, C. *et al.* (2002) 'In vivo and in vitro interaction between human transcription factor MOK2 and nuclear lamin A/C', *Nucleic Acids Research*. Oxford Academic, 30(21), pp. 4634–4642. doi: 10.1093/NAR/GKF587.

Dubinska-Magiera, M., Zaremba-Czogalla, M. and Rzepecki, R. (2013) 'Muscle development, regeneration and laminopathies: how lamins or lamina-associated proteins can contribute to muscle development, regeneration and disease', *Cellular and Molecular Life Sciences*, 70(15), pp. 2713–2741. doi: 10.1007/s00018-012-1190-3.

DuBose, A. J. *et al.* (2018) 'Everolimus rescues multiple cellular defects in laminopathy-patient fibroblasts.', *Proceedings of the National Academy of Sciences of the United States of America*, 115(16), pp. 4206–4211. doi: 10.1073/pnas.1802811115.

Duong, N. T. *et al.* (2014) 'Nesprins: Tissue-specific expression of epsilon and other short isoforms', *PLoS ONE*, 9(4), p. e94380. doi: 10.1371/journal.pone.0094380.

Dupré, N. *et al.* (2007) 'Mutations in SYNE-1 lead to a newly discovered form of autosomal recessive cerebellar ataxia', *Medecine sciences : M/S*, 23(3), pp. 261–262. doi: 10.1038/ng1927.

Dutta, S. and Vasudevan, M. (2022) 'Interconnection between molecular regulators in LMNA related muscular dystrophy', *bioRxiv*. Cold Spring Harbor Laboratory. doi: 10.1101/2022.03.09.483617.

Earle, A. J. *et al.* (2020) 'Mutant lamins cause nuclear envelope rupture and DNA damage in skeletal muscle cells.', *Nature materials*, 19(4), pp. 464–473. doi: 10.1038/s41563-019-0563-5.

Ebert, M. *et al.* (2020) 'Prevalence and Prognostic Impact of Pathogenic Variants in

Patients With Dilated Cardiomyopathy Referred for Ventricular Tachycardia Ablation.', *JACC. Clinical electrophysiology*, 6(9), pp. 1103–1114. doi: 10.1016/j.jacep.2020.04.025.

Edfors, F. *et al.* (2016) 'Gene-specific correlation of RNA and protein levels in human cells and tissues', *Molecular Systems Biology*. European Molecular Biology Organization, 12(10), p. 883. doi: 10.15252/MSB.20167144.

Ellis, D. *et al.* (1997) 'GST-lamin fusion proteins act as dominant negative mutants in Xenopus egg extract and reveal the function of the lamina in DNA replication', *Journal of cell science*, 110, pp. 2507–2518. doi: 10.1242/jcs.110.20.2507.

Emery, A. E. H. (1989a) 'Emery-Dreifuss muscular dystrophy and other related disorders', *British Medical Bulletin*. Narnia, 45(3), pp. 772–787. doi: 10.1093/oxfordjournals.bmb.a072357.

Emery, A. E. H. (1989b) 'Emery-Dreifuss syndrome', *Syndrome of the month Journal of Medical Genetics*, 26, pp. 637–641. doi: 10.1136/jmg.26.10.637.

Engel, A. G. (2008) 'Chapter 3 The neuromuscular junction', *Handbook of Clinical Neurology*. Elsevier, 91, pp. 103–148. doi: 10.1016/S0072-9752(07)01503-5.

Engelhardt, D. L. *et al.* (1965) 'In vitro studies on the mechanism of suppression of a nonsense mutation.', *Proceedings of the National Academy of Sciences of the United States of America*. Proceedings of the National Academy of Sciences, 54(6), pp. 1791–1797. doi: 10.1073/pnas.54.6.1791.

Eriksson, M. *et al.* (2003) 'Recurrent de novo point mutations in lamin A cause Hutchinson-Gilford progeria syndrome.', *Nature*, 423(6937), pp. 293–298. doi:

10.1038/nature01629.

Fairley, E. A., Kendrick-Jones, J. and Ellis, J. A. (1999) 'The Emery-Dreifuss muscular dystrophy phenotype arises from aberrant targeting and binding of emerin at the inner nuclear membrane.', *Journal of cell science*, 112, pp. 2571–2582. doi: 10.1242/jcs.112.15.2571.

Fairley, E. A. L. *et al.* (2002) 'The cell cycle dependent mislocalisation of emerin may contribute to the Emery-Dreifuss muscular dystrophy phenotype.', *Journal of cell science*, 115(Pt 2), pp. 341–354. doi: 10.1242/jcs.115.2.341.

Fan, Y. *et al.* (2021) 'Clinical spectrum and genetic variations of LMNA -related muscular dystrophies in a large cohort of Chinese patients.', *Journal of medical genetics*, 58(5), pp. 326–333. doi: 10.1136/jmedgenet-2019-106671.

Fatkin, D. *et al.* (1999) 'Missense mutations in the rod domain of the lamin A/C gene as causes of dilated cardiomyopathy and conduction-system disease.', *The New England journal of medicine*, 341(23), pp. 1715–1724. doi: 10.1056/NEJM199912023412302.

Favreau, C. *et al.* (2003) 'Expression of lamin A mutated in the carboxyl-terminal tail generates an aberrant nuclear phenotype similar to that observed in cells from patients with Dunnigan-type partial lipodystrophy and Emery-Dreifuss muscular dystrophy', *Experimental cell research*. Exp Cell Res, 282(1), pp. 14–23. doi: 10.1006/EXCR.2002.5669.

Feng, X.-H. and Derynck, R. (2005) 'Specificity and versatility in TGF-β signaling through smads', *Annual Review of Cell and Developmental Biology*, 21, pp. 659–693. doi: 10.1146/annurev.cellbio.21.022404.142018.

Feyen, D. *et al.* (2013) 'Increasing short-term cardiomyocyte progenitor cell (CMPC) survival by necrostatin-1 did not further preserve cardiac function', *Cardiovascular Research*. Oxford Academic, 99(1), pp. 83–91. doi: 10.1093/CVR/CVT078.

Finkel, R. S. *et al.* (2017) 'Nusinersen versus sham control in infantile-onset spinal muscular atrophy', *New England Journal of Medicine*. Massachussetts Medical Society, 377(18), pp. 1723–1732. doi: 10.1056/NEJMoa1702752.

Fisher, D. Z., Chaudhary, N. and Blobel, G. (1986) 'cDNA sequencing of nuclear lamins A and C reveals primary and secondary structural homology to intermediate filament proteins', *Proceedings of the National Academy of Sciences of the United States of America*, 83(17), pp. 6450–6454. doi: 10.1073/pnas.83.17.6450.

Folker, E. S. *et al.* (2011) 'Lamin A variants that cause striated muscle disease are defective in anchoring transmembrane actin-associated nuclear lines for nuclear movement', *Proceedings of the National Academy of Sciences of the United States of America*. National Academy of Sciences, 108(1), pp. 131–136. doi: 10.1073/pnas.1000824108.

Fong, L. G. *et al.* (2006) 'Prelamin A and lamin A appear to be dispensable in the nuclear lamina', *Journal of Clinical Investigation*, 116(3), pp. 743–752. doi: 10.1172/JCI27125.

Francisco, A. R. G. *et al.* (2017) 'Complex phenotype linked to a mutation in exon 11 of the lamin A/C gene: Hypertrophic cardiomyopathy, atrioventricular block, severe dyslipidemia and diabetes.', *Revista portuguesa de cardiologia*, 36(9), pp. 669.e1-669.e4. doi: 10.1016/j.repc.2016.07.018.

Frock, R. L. *et al.* (2006) 'Lamin A/C and emerin are critical for skeletal muscle satellite cell differentiation.', *Genes & development*, 20(4), pp. 486–500. doi: 10.1101/gad.1364906.

Fuller, H. R. *et al.* (2010) 'The SMN interactome includes Myb-binding protein 1a', *Journal of Proteome Research*, 9(1), pp. 556–563. doi: 10.1021/pr900884g.

Fuller, H. R., Mandefro, B., *et al.* (2016) 'Spinal muscular atrophy patient iPSC-derived motor neurons have reduced expression of proteins important in neuronal development', *Frontiers in Cellular Neuroscience*. Frontiers Media S.A., 9, p. 506. doi: 10.3389/fncel.2015.00506.

Fuller, H. R., Graham, L. C., *et al.* (2016) 'Understanding the molecular consequences of inherited muscular dystrophies: advancements through proteomic experimentation', *Expert Review of Proteomics*. Taylor and Francis Ltd, 13(7), pp. 659–671. doi: 10.1080/14789450.2016.1202768.

Fuller, H. R., Gillingwater, T. H. and Wishart, T. M. (2016) 'Commonality amid diversity: Multi-study proteomic identification of conserved disease mechanisms in spinal muscular atrophy', *Neuromuscular Disorders*. Elsevier Ltd, 26(9), pp. 560–569. doi: 10.1016/j.nmd.2016.06.004.

Furukawa, K. *et al.* (2009) 'A-type and B-type lamins initiate layer assembly at distinct areas of the nuclear envelope in living cells', *Experimental Cell Research*. Academic Press, 315(7), pp. 1181–1189. doi: 10.1016/J.YEXCR.2008.12.024.

Galant, D. *et al.* (2016) 'A Heterozygous ZMPSTE24 Mutation Associated with Severe Metabolic Syndrome, Ectopic Fat Accumulation, and Dilated Cardiomyopathy.', *Cells*,

5(2), p. 21. doi: 10.3390/cells5020021.

Gao, J. *et al.* (2012) 'A Chinese patient with acquired partial lipodystrophy caused by a novel mutation with LMNB2 gene.', *Journal of pediatric endocrinology & metabolism*, 25(3–4), pp. 375–377. doi: 10.1515/jpem-2012-0007.

Garg, A. (2004) 'Acquired and Inherited Lipodystrophies', *N Engl J Med*. Massachusetts Medical Society, 350(12), pp. 1220–1234. doi: 10.1056/NEJMRA025261.

Ge, L. *et al.* (2019) 'Congenital muscular dystrophies in China.', *Clinical genetics*, 96(3), pp. 207–215. doi: 10.1111/cge.13560.

Gholobova, D. *et al.* (2018) 'Human tissue-engineered skeletal muscle: a novel 3D in vitro model for drug disposition and toxicity after intramuscular injection', *Scientific Reports*. Nature Publishing Group, 8(1), pp. 1–14. doi: 10.1038/s41598-018-30123-3.

Gigli, M. *et al.* (2019) 'Genetic Risk of Arrhythmic Phenotypes in Patients With Dilated Cardiomyopathy.', *Journal of the American College of Cardiology*, 74(11), pp. 1480–1490. doi: 10.1016/j.jacc.2019.06.072.

Gillet, L. C. *et al.* (2012) 'Targeted Data Extraction of the MS/MS Spectra Generated by Data-independent Acquisition: A New Concept for Consistent and Accurate Proteome Analysis', *Molecular & Cellular Proteomics : MCP*. American Society for Biochemistry and Molecular Biology, 11(6), pp. 401–407. doi: 10.1074/MCP.O111.016717.

Gilmour, D. S. *et al.* (1986) 'Topoisomerase I interacts with transcribed regions in Drosophila cells', *Cell*, 44(3). doi: 10.1016/0092-8674(86)90461-7.

Glare, E. M. *et al.* (2002) 'β-actin and GAPDH housekeeping gene expression in asthmatic airways is variable and not suitable for normalising mRNA levels', *Thorax*,

57(9). doi: 10.1136/thorax.57.9.765.

Goldspink, G. (2002) 'Gene expression in skeletal muscle', *Biochemical Society Transactions*. Portland Press, 30(2), pp. 285–290. doi: 10.1042/BST0300285.

Gómez-Domínguez, D. *et al.* (2020) 'Consequences of Lmna Exon 4 Mutations in Myoblast Function.', *Cells*, 9(5), p. 1286. doi: 10.3390/cells9051286.

Gonzalez, J. M. *et al.* (2011) 'A-type lamins and Hutchinson-Gilford progeria syndrome: Pathogenesis and therapy', *Frontiers in Bioscience - Scholar*, 3(3), pp. 1133–1146. doi: 10.2741/s216.

Gonzàlez, J. M. *et al.* (2008) 'Fast regulation of AP-1 activity through interaction of lamin A/C, ERK1/2, and c-Fos at the nuclear envelope', *Journal of Cell Biology*. The Rockefeller University Press, 183(4), pp. 653–666. doi: 10.1083/JCB.200805049.

Gonzalez, M. W. and Kann, M. G. (2012) 'Chapter 4: Protein Interactions and Disease', *PLoS Computational Biology*, 8(12), p. e1002819. doi: 10.1371/journal.pcbi.1002819.

Gonzalo, S. (2014) 'DNA damage and lamins', *Advances in Experimental Medicine and Biology*. Springer New York LLC, 773, pp. 377–399. doi: 10.1007/978-1-4899-8032-8_17.

Gonzalo, S., Kreienkamp, R. and Askjaer, P. (2017) 'Hutchinson-Gilford Progeria Syndrome: A premature aging disease caused by LMNA gene mutations', *Ageing Research Reviews*. Elsevier, 33, pp. 18–29. doi: 10.1016/J.ARR.2016.06.007.

Gortat, A. *et al.* (2015) 'Apaf1 inhibition promotes cell recovery from apoptosis', *Protein and Cell*, 6(11), pp. 833–843. doi: 10.1007/s13238-015-0200-2.

Grady, R. M. *et al.* (2005) 'Syne proteins anchor muscle nuclei at the neuromuscular junction', *Proceedings of the National Academy of Sciences*. National Academy of Sciences, 102(12), pp. 4359–4364. doi: 10.1073/PNAS.0500711102.

Granato, M. *et al.* (1996) 'Genes controlling and mediating locomotion behavior of the zebrafish embryo and larva', *Development*, 123(1), pp. 399–413. doi: 10.1242/dev.123.1.399.

Granger, B. *et al.* (2011) 'Modifier locus of the skeletal muscle involvement in Emery-Dreifuss muscular dystrophy.', *Human genetics*, 129(2), pp. 149–159. doi: 10.1007/s00439-010-0909-1.

Gruenbaum, Y. *et al.* (2002) 'The expression, lamin-dependent localization and RNAi depletion phenotype for emerin in C. elegans', *Journal of Cell Science*, 115(5), pp. 923–929. doi: 10.1242/jcs.115.5.923.

Gry, M. *et al.* (2009) 'Correlations between RNA and protein expression profiles in 23 human cell lines', *BMC Genomics*. BioMed Central, 10(1), pp. 1–14. doi: 10.1186/1471-2164-10-365.

Grzesik, W. J. *et al.* (2015) 'Expression Pattern of 12-Lipoxygenase in Human Islets With Type 1 Diabetes and Type 2 Diabetes', *The Journal of Clinical Endocrinology & Metabolism*. Oxford Academic, 100(3), pp. E387–E395. doi: 10.1210/JC.2014-3630.

Guelen, L. *et al.* (2008) 'Domain organization of human chromosomes revealed by mapping of nuclear lamina interactions', *Nature*, 453(7197), pp. 948–951. doi: 10.1038/nature06947.

Gueneau, L. *et al.* (2009) 'Mutations of the FHL1 Gene Cause Emery-Dreifuss Muscular

Dystrophy', *The American Journal of Human Genetics*. Cell Press, 85(3), pp. 338–353. doi: 10.1016/J.AJHG.2009.07.015.

Guevel, L. *et al.* (2011) 'Quantitative proteomic analysis of dystrophic dog muscle', *Journal of Proteome Research*, 10(5), pp. 2465–2478. doi: 10.1021/pr2001385.

Güttinger, S., Laurell, E. and Kutay, U. (2009) 'Orchestrating nuclear envelope disassembly and reassembly during mitosis', *Nature Reviews Molecular Cell Biology*. Nature Publishing Group, 10(3), pp. 178–191. doi: 10.1038/nrm2641.

Hak, K. K. *et al.* (2006) 'Muscle-specific microRNA miR-206 promotes muscle differentiation', *Journal of Cell Biology*. The Rockefeller University Press, 174(5), pp. 677–687. doi: 10.1083/JCB.200603008.

Håkelien, A.-M. *et al.* (2008) 'Expression of the myodystrophic R453W mutation of lamin A in C2C12 myoblasts causes promoter-specific and global epigenetic defects', *Experimental Cell Research*. Academic Press, 314(8), pp. 1869–1880. doi: 10.1016/J.YEXCR.2008.02.018.

Hamada, K. *et al.* (2019) 'New Negamycin-Based Potent Readthrough Derivative Effective against TGA-Type Nonsense Mutations', *ACS Medicinal Chemistry Letters*. American Chemical Society, 10(10), pp. 1450–1456. doi: 10.1021/acsmedchemlett.9b00273.

Han, M. *et al.* (2019) 'Lamin A mutation impairs interaction with nucleoporin NUP155 and disrupts nucleocytoplasmic transport in atrial fibrillation', *Human Mutation*. John Wiley and Sons Inc., 40(3), pp. 310–325. doi: 10.1002/HUMU.23691.

Hao, S. *et al.* (2022) 'The role of transketolase in human cancer progression and

therapy', *Biomedicine and Pharmacotherapy*. Elsevier Masson s.r.l., 154, p. 113607. doi: 10.1016/J.BIOPHA.2022.113607.

Haque, F. *et al.* (2006) 'SUN1 Interacts with Nuclear Lamin A and Cytoplasmic Nesprins To Provide a Physical Connection between the Nuclear Lamina and the Cytoskeleton', *Molecular and Cellular Biology*, 26(10), pp. 3738–3751. doi: 10.1128/MCB.26.10.3738-3751.2006.

Haque, F. *et al.* (2010) 'Mammalian SUN protein interaction networks at the inner nuclear membrane and their role in laminopathy disease processes', *Journal of Biological Chemistry*, 285(5), pp. 3487–3498. doi: 10.1074/jbc.M109.071910.

Harper, M. *et al.* (2009) 'Phosphorylation-dependent binding of human transcription factor MOK2 to lamin A/C', *The FEBS Journal*. John Wiley & Sons, Ltd, 276(11), pp. 3137–3147. doi: 10.1111/J.1742-4658.2009.07032.X.

Hatanaka, Y. and Hirata, T. (2020) 'How Do Cortical Excitatory Neurons Terminate Their Migration at the Right Place? Critical Roles of Environmental Elements', *Frontiers in Cell and Developmental Biology*. Frontiers Media S.A., 8, p. 1189. doi: 10.3389/fcell.2020.596708.

Hegde, R. S. and Zavodszky, E. (2019) 'Recognition and Degradation of Mislocalized Proteins in Health and Disease', *Cold Spring Harbor Perspectives in Biology*. Cold Spring Harbor Laboratory Press, 11(11), p. a033902. doi: 10.1101/CSHPERSPECT.A033902.

Hickey, M. A. and Chesselet, M. F. (2003) 'Apoptosis in Huntington's disease', *Progress in Neuro-Psychopharmacology and Biological Psychiatry*, 27(2), pp. 255-. doi: 10.1016/S0278-5846(03)00021-6.

Hill, A. V. (1924) ‘Muscular activity and carbohydrate metabolism’, *Science*. Science, 60(1562), pp. 505–514. doi: 10.1126/SCIENCE.60.1562.505.

Hoffenberg, S. *et al.* (2000) ‘A novel membrane-anchored Rab5 interacting protein required for homotypic endosome fusion’, *Journal of Biological Chemistry*, 275(32), pp. 24661–24669. doi: 10.1074/jbc.M909600199.

Holland, A., Henry, M., *et al.* (2015) ‘Comparative label-free mass spectrometric analysis of mildly versus severely affected mdx mouse skeletal muscles identifies annexin, lamin, and vimentin as universal dystrophic markers’, *Molecules*, 20(6), pp. 11317–11344. doi: 10.3390/molecules200611317.

Holland, A., Dowling, P., *et al.* (2015) ‘Label-free mass spectrometric analysis of the mdx-4cv diaphragm identifies the matricellular protein periostin as a potential factor involved in dystrophinopathy-related fibrosis’, *Proteomics*, 15(13), pp. 2318–2331. doi: 10.1002/pmic.201400471.

Holt, I. *et al.* (2003) ‘Effect of pathogenic mis-sense mutations in lamin A on its interaction with emerin in vivo’, *Journal of Cell Science*, 116(14), pp. 3027–3035. doi: 10.1242/jcs.00599.

Holt, I. *et al.* (2006) ‘Lamin A/C assembly defects in Emery-Dreifuss muscular dystrophy can be regulated by culture medium composition.’, *Neuromuscular disorders : NMD*, 16(6), pp. 368–373. doi: 10.1016/j.nmd.2006.03.014.

Holt, I. *et al.* (2020) ‘An interaction of heart disease-associated proteins POPDC1/2 with XIRP1 in transverse tubules and intercalated discs’, *BMC Molecular and Cell Biology*, 21(1), p. 88. doi: 10.1186/s12860-020-00329-3.

Howe, K. *et al.* (2013) 'The zebrafish reference genome sequence and its relationship to the human genome', *Nature*. Nature Publishing Group, 496(7446), pp. 498–503. doi: 10.1038/nature12111.

Hu, X. *et al.* (2017) 'Are mice good models for human neuromuscular disease? Comparing muscle excursions in walking between mice and humans', *Skeletal Muscle*, 7(1), p. 26. doi: 10.1186/s13395-017-0143-9.

Huang, D. W., Sherman, B. T. and Lempicki, R. A. (2008) 'Systematic and integrative analysis of large gene lists using DAVID bioinformatics resources', *Nature Protocols 2009 4:1*. Nature Publishing Group, 4(1), pp. 44–57. doi: 10.1038/nprot.2008.211.

Huang, Q. *et al.* (2015) 'SWATH enables precise label-free quantification on proteome scale', *PROTEOMICS*. John Wiley & Sons, Ltd, 15(7), pp. 1215–1223. doi: 10.1002/PMIC.201400270.

Huber, M. D., Guan, T. and Gerace, L. (2009) 'Overlapping Functions of Nuclear Envelope Proteins NET25 (Lem2) and Emerin in Regulation of Extracellular Signal-Regulated Kinase Signaling in Myoblast Differentiation', *Molecular and cellular biology*, 29(21), pp. 5718–5728. doi: 10.1128/MCB.00270-09.

Hutchison, C. J. (2002) 'Lamins: building blocks or regulators of gene expression?', *Nature reviews. Molecular cell biology*. Nat Rev Mol Cell Biol, 3(11), pp. 848–858. doi: 10.1038/NRM950.

Inc., P. T. (2014) 'PTC Therapeutics Receives Conditional Approval in the European Union for Translarna™ For the Treatment of Nonsense Mutation Duchenne Muscular Dystrophy | PTC Therapeutics, Inc.', 4 August. Available at:

https://ir.ptcbio.com/news-releases/news-release-details/ptc-therapeutics-receives-conditional-approval-european-union?ReleaseID=863914 (Accessed: 1 February 2022).

Ingram, V. M. (1956) 'A Specific Chemical Difference Between the Globins of Normal Human and Sickle-Cell Anæmia Hæmoglobin', *Nature*. Nature Publishing Group, 178(4537), pp. 792–794. doi: 10.1038/178792a0.

Irion, U., Krauss, J. and Nüsslein-Volhard, C. (2014) 'Precise and efficient genome editing in zebrafish using the CRISPR/Cas9 system', *Development (Cambridge)*. Company of Biologists Ltd, 141(24), pp. 4827–4830. doi: 10.1242/dev.115584.

Ito, Y. *et al.* (2016) 'RIPK1 mediates axonal degeneration by promoting inflammation and necroptosis in ALS', *Science*, 353(6299), pp. 603–608. doi: 10.1126/science.aaf6803.

Iyer, A., Koch, A. J. and Holaska, J. M. (2017) 'Expression Profiling of Differentiating Emerin-Null Myogenic Progenitor Identifies Molecular Pathways Implicated in Their Impaired Differentiation', *Cells*. Multidisciplinary Digital Publishing Institute, 6(4), p. 38. doi: 10.3390/cells6040038.

Izquierdo, I. *et al.* (2016) 'Proteomic identification of putative biomarkers for early detection of sudden cardiac death in a family with a LMNA gene mutation causing dilated cardiomyopathy.', *Journal of proteomics*, 148, pp. 75–84. doi: 10.1016/j.jprot.2016.07.020.

Jahn, D. *et al.* (2012) 'A truncated lamin A in the Lmna−/− mouse line: Implications for the understanding of laminopathies', *Nucleus*. Taylor & Francis, 3(5), p. 463. doi: 10.4161/NUCL.21676.

James, P. D. *et al.* (2005) 'Aminoglycoside suppression of nonsense mutations in severe hemophilia', *Blood*. Blood, 106(9), pp. 3043–3048. doi: 10.1182/BLOOD-2005-03-1307.

Jamin, A. and Wiebe, M. S. (2015) 'Barrier to Autointegration Factor (BANF1): interwoven roles in nuclear structure, genome integrity, innate immunity, stress responses and progeria', *Current opinion in cell biology*. NIH Public Access, 34, p. 61. doi: 10.1016/J.CEB.2015.05.006.

Janin, A. *et al.* (2018) 'SMAD6 overexpression leads to accelerated myogenic differentiation of LMNA mutated cells.', *Scientific reports*, 8(1), p. 5618. doi: 10.1038/s41598-018-23918-x.

Jen, Y., Weintraub, H. and Benezra, R. (1992) 'Overexpression of Id protein inhibits the muscle differentiation program: In vivo association of Id with E2A proteins', *Genes and Development*, 6(8), pp. 1466–1479. doi: 10.1101/gad.6.8.1466.

Jia, X. *et al.* (2017) 'miR-16 controls myoblast proliferation and apoptosis through directly suppressing Bcl2 and FOXO1 activities', *Biochimica et Biophysica Acta (BBA) - Gene Regulatory Mechanisms*. Elsevier, 1860(6), pp. 674–684. doi: 10.1016/J.BBAGRM.2017.02.010.

Jiang, L. *et al.* (2020) 'A Quantitative Proteome Map of the Human Body', *Cell*. Cell Press, 183(1), pp. 269-283.e19. doi: 10.1016/j.cell.2020.08.036.

Judge, D. P. *et al.* (2022) 'Long-Term Efficacy and Safety of ARRY-371797 (PF-07265803) in Patients With Lamin A/C–Related Dilated Cardiomyopathy', *The American Journal of Cardiology*. Excerpta Medica, 183, pp. 93–98. doi:

10.1016/J.AMJCARD.2022.08.001.

Kajino, S. *et al.* (2014) 'Congenital fiber type disproportion myopathy caused by LMNA mutations.', *Journal of the neurological sciences*, 340(1–2), pp. 94–98. doi: 10.1016/j.jns.2014.02.036.

Kalonia, H., Mishra, J. and Kumar, A. (2012) 'Targeting neuro-inflammatory cytokines and oxidative stress by minocycline attenuates quinolinic-acid-induced huntington's disease-like symptoms in rats', *Neurotoxicity Research*, 22(4), pp. 310–320. doi: 10.1007/s12640-012-9315-x.

Kandert, S. *et al.* (2009) 'Impaired nuclear functions lead to increased senescence and inefficient differentiation in human myoblasts with a dominant p.R545C mutation in the LMNA gene', *European Journal of Cell Biology*. Urban & Fischer, 88(10), pp. 593–608. doi: 10.1016/J.EJCB.2009.06.002.

Kaur, G. and Dufour, J. M. (2012) 'Cell lines', *Spermatogenesis*. Informa UK Limited, 2(1), pp. 1–5. doi: 10.4161/spmg.19885.

Kellermayer, R. *et al.* (2006) 'Aminoglycosides as potential pharmacogenetic agents in the treatment of Hailey-Hailey disease', *The Journal of investigative dermatology*. J Invest Dermatol, 126(1), pp. 229–231. doi: 10.1038/SJ.JID.5700031.

Keshet, Y. and Seger, R. (2010) 'The MAP kinase signaling cascades: a system of hundreds of components regulates a diverse array of physiological functions', *Methods in molecular biology (Clifton, N.J.)*. Methods Mol Biol, 661, pp. 3–38. doi: 10.1007/978-1-60761-795-2_1.

Khobta, A. *et al.* (2006) 'Early effects of topoisomerase I inhibition on RNA polymerase

II along transcribed genes in human cells', *Journal of Molecular Biology*, 357(1), pp. 127–138. doi: 10.1016/j.jmb.2005.12.069.

Kim, Y. and Zheng, Y. (2013) 'Generation and characterization of a conditional deletion allele for Lmna in mice', *Biochemical and Biophysical Research Communications*, 440(1), pp. 8–13. doi: 10.1016/j.bbrc.2013.08.082.

Kirby, T. J. and Lammerding, J. (2018) 'Emerging views of the nucleus as a cellular mechanosensor', *Nature Cell Biology*. Nature Publishing Group, 20(4), pp. 373–381. doi: 10.1038/s41556-018-0038-y.

Kishnani, P. S. and Howell, R. R. (2004) 'Pompe disease in infants and children', *Journal of Pediatrics*. Mosby Inc., 144(5 SUPPL.), pp. S35–S43. doi: 10.1016/j.jpeds.2004.01.053.

Kittisopikul, M. *et al.* (2021) 'Computational analyses reveal spatial relationships between nuclear pore complexes and specific lamins', *Journal of Cell Biology*, 220(4), p. e202007082. doi: 10.1083/JCB.202007082.

Koch, A. J. and Holaska, J. M. (2012) 'Loss of Emerin Alters Myogenic Signaling and miRNA Expression in Mouse Myogenic Progenitors', *PLoS ONE*, 7(5), p. 37262. doi: 10.1371/journal.pone.0037262.

Koch, A. J. and Holaska, J. M. (2014) 'Emerin in health and disease.', *Seminars in cell & developmental biology*, 29, pp. 95–106. doi: 10.1016/j.semcdb.2013.12.008.

Kohler, R. E. (1994) *Lords of the Fly: Drosophila Genetics and the Experimental Life*. University of Chicago Press. Available at: https://books.google.co.uk/books?hl=en&lr=&id=J57ht8TPP74C&oi=fnd&pg=PP7&ots

=esm6id4Lss&sig=eb4kq1BMjAw9qbXH6tuaqX-JRoo&redir_esc=y#v=onepage&q&f=false (Accessed: 26 January 2023).

Koike, M. (2002) 'Dimerization, translocation and localization of Ku70 and Ku80 proteins', *Journal of Radiation Research*, 43(3), pp. 223–236. doi: 10.1269/jrr.43.223.

Korfali, N. *et al.* (2010) 'The leukocyte nuclear envelope proteome varies with cell activation and contains novel transmembrane proteins that affect genome architecture', *Molecular and Cellular Proteomics*, 9(12), pp. 2571–2585. doi: 10.1074/mcp.M110.002915.

Korfali, N. *et al.* (2012) 'The nuclear envelope proteome differs notably between tissues', *Nucleus (United States)*, 3(6), pp. 552–564. doi: 10.4161/nucl.22257.

Kubben, N. *et al.* (2010) 'Identification of differential protein interactors of lamin A and progerin', *Nucleus*, 1(6), pp. 513–525. doi: 10.4161/nucl.1.6.13512.

Kubben, N. *et al.* (2011) 'Post-natal myogenic and adipogenic developmental: defects and metabolic impairment upon loss of A-type lamins.', *Nucleus*, 2(3), pp. 195–207. doi: 10.4161/nucl.2.3.15731.

Kummer, T. T., Misgeld, T. and Sanes, J. R. (2006) 'Assembly of the postsynaptic membrane at the neuromuscular junction: paradigm lost', *Current opinion in neurobiology*. Curr Opin Neurobiol, 16(1), pp. 74–82. doi: 10.1016/J.CONB.2005.12.003.

Laemmli, U. K. (1970) 'Cleavage of structural proteins during the assembly of the head of bacteriophage T4', *Nature*. Nature Publishing Group, 227(5259), pp. 680–685. doi: 10.1038/227680a0.

Lammerding, J. *et al.* (2004) 'Lamin A/C deficiency causes defective nuclear mechanics and mechanotransduction', *Journal of Clinical Investigation*, 113(3), pp. 370–378. doi: 10.1172/JCI19670.

Lashuel, H. A. *et al.* (1999) 'The most pathogenic transthyretin variant, L55P, forms amyloid fibrils under acidic conditions and protofilaments under physiological conditions', *Biochemistry*, 38(41), pp. 13560–13573. doi: 10.1021/bi991021c.

Lattanzi, G. *et al.* (2000) 'Emerin expression at the early stages of myogenic differentiation', *Differentiation*, 66(4–5), pp. 208–217. doi: 10.1111/j.1432-0436.2000.660407.x.

Lattanzi, G. *et al.* (2003) 'Association of emerin with nuclear and cytoplasmic actin is regulated in differentiating myoblasts', *Biochemical and Biophysical Research Communications*. Academic Press, 303(3), pp. 764–770. doi: 10.1016/S0006-291X(03)00415-7.

Lawson, M. A. and Purslow, P. P. (2000) 'Differentiation of Myoblasts in Serum-Free Media: Effects of Modified Media Are Cell Line-Specific', *Cells Tissues Organs*. Karger Publishers, 167(2–3), pp. 130–137. doi: 10.1159/000016776.

Lee, J. M. *et al.* (2014) 'Reciprocal knock-in mice to investigate the functional redundancy of lamin B1 and lamin B2', *Molecular Biology of the Cell*. American Society for Cell Biology, 25(10), p. 1666. doi: 10.1091/MBC.E14-01-0683.

Lee, K. K. *et al.* (2000) 'C. elegans nuclear envelope proteins emerin, MAN1, lamin, and nucleoporins reveal unique timing of nuclear envelope breakdown during mitosis', *Molecular Biology of the Cell*. American Society for Cell Biology, 11(9), pp. 3089–3099.

doi: 10.1091/mbc.11.9.3089.

Lee, K. K. *et al.* (2001) 'Distinct functional domains in emerin bind lamin A and DNA-bridging protein BAF', *Journal of Cell Science*. The Company of Biologists, 114(24), pp. 4567–4573. doi: 10.1242/JCS.114.24.4567.

Lefebvre, S. *et al.* (1995) 'Identification and characterization of a spinal muscular atrophy-determining gene', *Cell*, 80(1), pp. 155–165. doi: 10.1016/0092-8674(95)90460-3.

Leitch, C. C. *et al.* (2008) 'Hypomorphic mutations in syndromic encephalocele genes are associated with Bardet-Biedl syndrome', *Nature Genetics*, 40(4), pp. 443–448. doi: 10.1038/NG.97.

Li, P. *et al.* (1997) 'Cytochrome c and dATP-dependent formation of Apaf-1/caspase-9 complex initiates an apoptotic protease cascade', *Cell*, 91(4). doi: 10.1016/S0092-8674(00)80434-1.

Li, P. *et al.* (2014) 'Contribution of SUN1 mutations to the pathomechanism in muscular dystrophies.', *Human mutation*, 35(4), pp. 452–461. doi: 10.1002/humu.22504.

Li, W. *et al.* (2014) 'Unraveling the complex genetic model for cystic fibrosis: Pleiotropic effects of modifier genes on early cystic fibrosis-related morbidities', *Human Genetics*, 133(2), pp. 151–161. doi: 10.1007/S00439-013-1363-7.

Liang, W.-C. *et al.* (2011) 'TMEM43 mutations in Emery-Dreifuss muscular dystrophy-related myopathy.', *Annals of neurology*, 69(6), pp. 1005–13. doi: 10.1002/ana.22338.

Liang, W.-C. *et al.* (2020) 'Clinical, pathological, imaging, and genetic characterization

in a Taiwanese cohort with limb-girdle muscular dystrophy.', *Orphanet journal of rare diseases*, 15(1), p. 160. doi: 10.1186/s13023-020-01445-1.

Liberati, A. *et al.* (2009) 'The PRISMA statement for reporting systematic reviews and meta-analyses of studies that evaluate healthcare interventions: explanation and elaboration.', *BMJ*. British Medical Journal Publishing Group, 339, p. b2700. doi: 10.1136/bmj.b2700.

Libotte, T. *et al.* (2005) 'Lamin A/C–dependent Localization of Nesprin-2, a Giant Scaffolder at the Nuclear Envelope', *Molecular Biology of the Cell*. American Society for Cell Biology, 16(7), pp. 3411–3424. doi: 10.1091/MBC.E04-11-1009.

Lin, D. Q. *et al.* (2020) 'Optimal concentration of necrostatin-1 for protecting against hippocampal neuronal damage in mice with status epilepticus', *Neural Regeneration Research*, 15(5), pp. 936–943. doi: 10.4103/1673-5374.268903.

Lin, E. W. *et al.* (2020) 'Genotype-phenotype analysis of LMNA-related diseases predicts phenotype-selective alterations in lamin phosphorylation.', *FASEB*, 34(7), pp. 9051–9073. doi: 10.1096/fj.202000500R.

Lin, F. *et al.* (2005) 'MAN1, an integral protein of the inner nuclear membrane, binds Smad2 and Smad3 and antagonizes transforming growth factor-β signaling', *Human Molecular Genetics*, 14(3), pp. 437–445. doi: 10.1093/hmg/ddi040.

Lin, F. and Worman, H. J. (1993) 'Structural organization of the human gene encoding nuclear lamin A and nuclear lamin C', *Journal of Biological Chemistry*. Elsevier, 268(22), pp. 16321–16326. doi: 10.1016/S0021-9258(19)85424-8.

Lin, J. *et al.* (2013) 'A Role of RIP3-Mediated Macrophage Necrosis in Atherosclerosis

Development', *Cell Reports*, 3(1), pp. 200–210. doi: 10.1016/j.celrep.2012.12.012.

Lin, W. *et al.* (2001) 'Distinct roles of nerve and muscle in postsynaptic differentiation of the neuromuscular synapse', *Nature*. Nature, 410(6832), pp. 1057–1064. doi: 10.1038/35074025.

Linde, N. and Stick, R. (2010) 'Intranuclear membranes induced by lipidated proteins are derived from the nuclear envelope', *Nucleus*. Taylor and Francis Inc., 1(4), pp. 343–353. doi: 10.4161/nucl.1.4.12352.

Lindholm, P. F., Reid, R. L. and Brady, J. N. (1992) 'Extracellular Tax1 protein stimulates tumor necrosis factor-beta and immunoglobulin kappa light chain expression in lymphoid cells', *Journal of Virology*, 66(3), pp. 1294–1302. doi: 10.1128/jvi.66.3.1294-1302.1992.

Linkermann, A. *et al.* (2012) 'Rip1 (Receptor-interacting protein kinase 1) mediates necroptosis and contributes to renal ischemia/reperfusion injury', *Kidney International*, 81(8), pp. 751–761. doi: 10.1038/ki.2011.450.

Litwiniuk, A. *et al.* (2016) 'FOXO1 and GSK-3β are main targets of insulin-mediated myogenesis in C2C12 muscle cells', *PLoS ONE*, 11(1), p. e0146726. doi: 10.1371/journal.pone.0146726.

Liu, B. *et al.* (2005) 'Genomic instability in laminopathy-based premature aging', *Nature Medicine*, 11(7), pp. 780–785. doi: 10.1038/nm1266.

Liu, B., Jin, D. Y. and Zhou, Z. (2012) 'From loss to gain: Role for SUN1 in laminopathies', *Cell and Bioscience*, p. 21. doi: 10.1186/2045-3701-2-21.

Liu, J. *et al.* (2000) 'Essential roles for Caenorhabditis elegans lamin gene in nuclear

organization, cell cycle progression, and spatial organization of nuclear pore complexes', *Molecular Biology of the Cell*. American Society for Cell Biology, 11(11), pp. 3937–3947. doi: 10.1091/mbc.11.11.3937.

Liu, J. *et al.* (2011) 'MicroRNA-155 prevents necrotic cell death in human cardiomyocyte progenitor cells via targeting RIP1', *Journal of Cellular and Molecular Medicine*, 15(7), pp. 1474–1482. doi: 10.1111/j.1582-4934.2010.01104.x.

Liu, N. *et al.* (2012) 'microRNA-206 promotes skeletal muscle regeneration and delays progression of Duchenne muscular dystrophy in mice', *The Journal of Clinical Investigation*. American Society for Clinical Investigation, 122(6), pp. 2054–2065. doi: 10.1172/JCI62656.

Lombardi, M. L. *et al.* (2011) 'The interaction between nesprins and sun proteins at the nuclear envelope is critical for force transmission between the nucleus and cytoskeleton.', *The Journal of biological chemistry*, 286(30), pp. 26743–26753. doi: doi.org/10.1074/jbc.M111.233700.

Lourim, D. and Lin, J. J. C. (1989) 'Expression of nuclear lamin A and muscle-specific proteins in differentiating muscle cells in ovo and in vitro.', *Journal of Cell Biology*. The Rockefeller University Press, 109(2), pp. 495–504. doi: 10.1083/JCB.109.2.495.

Ludwig, C. *et al.* (2018a) 'Data-independent acquisition-based SWATH-MS for quantitative proteomics: a tutorial', *Molecular Systems Biology*. John Wiley & Sons, Ltd, 14(8), p. e8126. doi: 10.15252/MSB.20178126.

Ludwig, C. *et al.* (2018b) 'Data-independent acquisition-based SWATH-MS for quantitative proteomics: a tutorial', *Molecular Systems Biology*. European Molecular

Biology Organization, 14(8). doi: 10.15252/MSB.20178126.

Luo, W. *et al.* (2019) 'High glucose inhibits myogenesis and induces insulin resistance by down-regulating AKT signaling', *Biomedicine and Pharmacotherapy*, 120, p. 109498. doi: 10.1016/j.biopha.2019.109498.

Macquart, C. *et al.* (2016) 'Clinical features and therapeutic strategies for managing the striated muscle laminopathies', *Expert Opinion on Orphan Drugs*. Taylor and Francis Ltd, pp. 631–638. doi: 10.1080/21678707.2016.1180975.

Madej-Pilarczyk, A. (2018) 'Clinical aspects of emery-dreifuss muscular dystrophy', *Nucleus*. Taylor and Francis Inc., 9(1), pp. 314–320. doi: 10.1080/19491034.2018.1462635.

Maffioletti, S. M. *et al.* (2018) 'Three-Dimensional Human iPSC-Derived Artificial Skeletal Muscles Model Muscular Dystrophies and Enable Multilineage Tissue Engineering', *Cell Reports*. Elsevier B.V., 23(3), pp. 899–908. doi: 10.1016/j.celrep.2018.03.091.

Magagnotti, C. *et al.* (2012) 'Protein profiling reveals energy metabolism and cytoskeletal protein alterations in LMNA mutation carriers.', *Biochimica et biophysica acta*, 1822(6), pp. 970–979. doi: 10.1016/j.bbadis.2012.01.01.

Maggi, L., Carboni, N. and Bernasconi, P. (2016) 'Skeletal Muscle Laminopathies: A Review of Clinical and Molecular Features', *Cells*, 5(3), p. 33. doi: 10.3390/cells5030033.

Maji, A. *et al.* (2020) 'A Lamin-Associated Chromatin Model for Chromosome Organization', *Biophysical Journal*, 118(12), pp. 3041–3050. doi:

10.1016/j.bpj.2020.05.014.

Makri, S. *et al.* (2009) 'Germinal mosaicism for LMNA mimics autosomal recessive congenital muscular dystrophy', *Neuromuscular Disorders*. Elsevier Ltd, 19(1), pp. 26–28. doi: 10.1016/j.nmd.2008.09.016.

Malik, P. *et al.* (2010) 'Cell-specific and lamin-dependent targeting of novel transmembrane proteins in the nuclear envelope', *Cellular and Molecular Life Sciences*, 67(8), pp. 1353–1569. doi: 10.1007/s00018-010-0257-2.

Malik, V. *et al.* (2010) 'Aminoglycoside-induced mutation suppression (stop codon readthrough) as a therapeutic strategy for Duchenne muscular dystrophy', *Therapeutic Advances in Neurological Disorders*. SAGE Publications, 3(6), pp. 379–389. doi: 10.1177/1756285610388693.

Malone, C. J. *et al.* (1999) 'UNC-84 localizes to the nuclear envelope and is required for nuclear migration and anchoring during C. elegans development', *Development*, 126(14), pp. 3171–3181. doi: 10.1242/dev.126.14.3171.

Mamchaoui, K. *et al.* (2011) 'Immortalized pathological human myoblasts: Towards a universal tool for the study of neuromuscular disorders', *Skeletal Muscle*, 1:34. doi: 10.1186/2044-5040-1-34.

Manilal, S. *et al.* (1996) 'The Emery-Dreifuss muscular dystrophy protein, emerin, is a nuclear membrane protein', *Human Molecular Genetics*, 5(6), pp. 801–808. doi: 10.1093/hmg/5.6.801.

Manilal, S. *et al.* (1998) 'Mutations in Emery-Dreifuss muscular dystrophy and their effects on emerin protein expression.', *Human molecular genetics*, 7(5), pp. 855–864.

doi: 10.1093/hmg/7.5.855.

Manilal, S. *et al.* (1999) 'Distribution of emerin and lamins in the heart and implications for Emery-Dreifuss muscular dystrophy', *Human molecular genetics*. Hum Mol Genet, 8(2), pp. 353–359. doi: 10.1093/HMG/8.2.353.

Manilal, S. *et al.* (2004) 'A lamin A/C beta-strand containing the site of lipodystrophy mutations is a major surface epitope for a new panel of monoclonal antibodies', *Biochimica et Biophysica Acta - General Subjects*, 1671(1–3). doi: 10.1016/j.bbagen.2004.01.008.

Manilal, S., Nguyen, T. M. and Morris, G. E. (1998) 'Colocalization of emerin and lamins in interphase nuclei and changes during mitosis.', *Biochemical and biophysical research communications*, 249(3), pp. 643–647. doi: 10.1006/bbrc.1998.9209.

Manju, K., Muralikrishna, B. and Parnaik, V. K. (2006) 'Expression of disease-causing lamin A mutants impairs the formation of DNA repair foci', *Journal of Cell Science*, 119(13), pp. 2704–2714. doi: 10.1242/jcs.03009.

Mann, M. *et al.* (2013) 'The Coming Age of Complete, Accurate, and Ubiquitous Proteomes', *Molecular Cell*. Elsevier, 49(4), pp. 583–590. doi: 10.1016/j.molcel.2013.01.029.

Mansharamani, M. and Wilson, K. (2005) 'Direct binding of nuclear membrane protein MAN1 to emerin in vitro and two modes of binding to barrier-to-autointegration factor', *The Journal of biological chemistry*. J Biol Chem, 280(14), pp. 13863–13870. doi: 10.1074/JBC.M413020200.

Markiewicz, E. *et al.* (2002) 'Lamin A/C binding protein LAP2alpha is required for

nuclear anchorage of retinoblastoma protein', *Molecular biology of the cell*. Mol Biol Cell, 13(12), pp. 4401–4413. doi: 10.1091/MBC.E02-07-0450.

Martin, P. T. and Freeze, H. H. (2003) 'Glycobiology of neuromuscular disorders', *Glycobiology*. Oxford Academic, 13(8), pp. 67R-75R. doi: 10.1093/GLYCOB/CWG077.

Masica, D. L. and Karchin, R. (2011) 'Correlation of Somatic Mutation and Expression Identifies Genes Important in Human Glioblastoma Progression and Survival', *Cancer research*. NIH Public Access, 71(13), p. 4561. doi: 10.1158/0008-5472.CAN-11-0180.

Massagué, J. *et al.* (1986) 'Type β Transforming Growth Factor is an Inhibitor of Myogenic Differentiation', *Proceedings of the National Academy of Sciences of the United States of America*, 83(21), pp. 8206–8210. doi: 10.1073/pnas.83.21.8206.

Massenet, J. *et al.* (2021) 'Epigenetic regulation of satellite cell fate during skeletal muscle regeneration', *Skeletal Muscle*. BioMed Central, 11(1), pp. 1–16. doi: 10.1186/S13395-020-00259-W.

Matsumoto, A. *et al.* (2015) 'Global loss of a nuclear lamina component, lamin A/C, and LINC complex components SUN1, SUN2, and nesprin-2 in breast cancer', *Cancer Medicine*. John Wiley & Sons, Ltd, 4(10), pp. 1547–1557. doi: 10.1002/CAM4.495.

Mattioli, E. *et al.* (2011) 'Prelamin A-mediated recruitment of SUN1 to the nuclear envelope directs nuclear positioning in human muscle', *Cell Death & Differentiation*, 18(8), pp. 1305–1315. doi: 10.1038/cdd.2010.183.

Mattioli, E. *et al.* (2018) 'Samp1 Mislocalization in Emery-Dreifuss Muscular Dystrophy.', *Cells*. Multidisciplinary Digital Publishing Institute (MDPI), 7(10), pp. 8206–8210. doi: 10.3390/cells7100170.

McColgan, P. and Tabrizi, S. J. (2018) 'Huntington's disease: a clinical review', *European Journal of Neurology*, 25(1), pp. 24–34. doi: 10.1111/ene.13413.

McDonald, C. M. *et al.* (2017) 'Ataluren in patients with nonsense mutation Duchenne muscular dystrophy (ACT DMD): a multicentre, randomised, double-blind, placebo-controlled, phase 3 trial', *The Lancet*. Elsevier, 390(10101), pp. 1489–1498. doi: 10.1016/S0140-6736(17)31611-2.

Meinke, P. *et al.* (2014) 'Muscular Dystrophy-Associated SUN1 and SUN2 Variants Disrupt Nuclear-Cytoskeletal Connections and Myonuclear Organization', *PLoS Genetics*, 10(9), p. e1004605. doi: 10.1371/journal.pgen.1004605.

Méjat, A. *et al.* (2003) 'Synapse-Specific Gene Expression at the Neuromuscular Junction', *Annals of the New York Academy of Sciences*, 998(1), pp. 53–65. doi: 10.1196/annals.1254.008.

Méjat, A. *et al.* (2009) 'Lamin A/C-mediated neuromuscular junction defects in Emery-Dreifuss muscular dystrophy.', *The Journal of Cell Biology*. Rockefeller University Press, 184(1), pp. 31–44. doi: 10.1083/jcb.200811035.

Melcer, S., Gruenbaum, Y. and Krohne, G. (2007) 'Invertebrate lamins', *Experimental Cell Research*. Academic Press Inc., pp. 2157–2166. doi: 10.1016/j.yexcr.2007.03.004.

Menalled, L. B. *et al.* (2010) 'Comprehensive behavioral testing in the R6/2 mouse model of Huntington's disease shows no benefit from CoQ10 or minocycline', *PLoS ONE*, 5(3), p. e9793. doi: 10.1371/journal.pone.0009793.

Mendell, J. R. *et al.* (2017) 'Single-dose gene-replacement therapy for spinal muscular atrophy', *New England Journal of Medicine*. Massachussetts Medical Society, 377(18),

pp. 1713–1722. doi: 10.1056/NEJMoa1706198.

Mercuri, E. *et al.* (2002) 'Congenital muscular dystrophies', *Seminars in Pediatric Neurology*. W.B. Saunders, 9(2), pp. 120–131. doi: 10.1053/spen.2002.33802.

Mercuri, E. *et al.* (2004) 'Extreme variability of phenotype in patients with an identical missense mutation in the lamin A/C gene: from congenital onset with severe phenotype to milder classic Emery-Dreifuss variant.', *Archives of neurology*, 61(5), pp. 690–694. doi: 10.1001/archneur.61.5.690.

Mercuri, E. *et al.* (2005) 'Extreme variability of skeletal and cardiac muscle involvement in patients with mutations in exon 11 of the lamin A/C gene.', *Muscle & nerve*, 31(5), pp. 602–609. doi: 10.1002/mus.20293.

Mercuri, E. *et al.* (2018) 'Nusinersen versus sham control in later-onset spinal muscular atrophy', *New England Journal of Medicine*. Massachussetts Medical Society, 378(7), pp. 625–635. doi: 10.1056/NEJMoa1710504.

Mievis, S. *et al.* (2007) 'Lack of minocycline efficiency in genetic models of Huntington's disease', *NeuroMolecular Medicine*, 9(1), pp. 47–54. doi: 10.1385/NMM:9:1:47.

Møller, D. V. *et al.* (2009) 'The role of Lamin A/C mutations in Danish patients with idiopathic dilated cardiomyopathy.', *European journal of heart failure*, 11(11), pp. 1031–1035. doi: 10.1093/eurjhf/hfp134.

Montes de Oca, R. *et al.* (2009) 'Barrier-to-autointegration factor proteome reveals chromatin-regulatory partners', *PLoS ONE*, 4(9), p. e7050. doi: 10.1371/journal.pone.0007050.

Morales, P. E., Bucarey, J. L. and Espinosa, A. (2017) 'Muscle lipid metabolism: Role of lipid droplets and perilipins', *Journal of Diabetes Research*. doi: 10.1155/2017/1789395.

Morgan, J. E. *et al.* (2018) 'Necroptosis mediates myofibre death in dystrophin-deficient mice', *Nature Communications*, 9(1), p. 3655. doi: 10.1038/s41467-018-06057-9.

Morham, S. G. *et al.* (1996) 'Targeted disruption of the mouse topoisomerase I gene by camptothecin selection', *Molecular and Cellular Biology*, 16(12), pp. 6804–6809. doi: 10.1128/mcb.16.12.6804.

Morton, L. M. *et al.* (2009) 'Risk of non-Hodgkin lymphoma associated with germline variation in genes that regulate the cell cycle, apoptosis, and lymphocyte development', *Cancer Epidemiology Biomarkers and Prevention*, 18(4), pp. 1259–1270. doi: 10.1158/1055-9965.EPI-08-1037.

Motohashi, N. *et al.* (2013) 'Regulation of IRS1/Akt insulin signaling by microRNA-128a during myogenesis', *Journal of Cell Science*. The Company of Biologists, 126(12), pp. 2678–2691. doi: 10.1242/JCS.119966/263393/AM/REGULATION-OF-IRS1-AKT-INSULIN-SIGNALING-BY.

Mounkes, L. C. *et al.* (2003) 'A progeroid syndrome in mice is caused by defects in A-type lamins', *Nature*, 423(6937), pp. 298–301. doi: 10.1038/nature01631.

Mounkes, L. C. *et al.* (2005) 'Expression of an LMNA-N195K variant of A-type lamins results in cardiac conduction defects and death in mice.', *Human molecular genetics*, 14(15), pp. 2167–2180. doi: 10.1093/hmg/ddi221.

Muchir, A. *et al.* (2000) 'Identification of mutations in the gene encoding lamins A/C in autosomal dominant limb girdle muscular dystrophy with atrioventricular conduction disturbances (LGMD1B).', *Human molecular genetics*, 9(9), pp. 1453–1459. doi: 10.1093/hmg/9.9.1453.

Muchir, A., van Engelen, B. G., *et al.* (2003) 'Nuclear envelope alterations in fibroblasts from LGMD1B patients carrying nonsense Y259X heterozygous or homozygous mutation in lamin A/C gene.', *Experimental cell research*, 291(2), pp. 352–362. doi: 10.1016/j.yexcr.2003.07.002.

Muchir, A., Van Engelen, B. G., *et al.* (2003) 'Nuclear envelope alterations in fibroblasts from LGMD1B patients carrying nonsense Y259X heterozygous or homozygous mutation in lamin A/C gene', *Experimental Cell Research*. Academic Press, 291(2), pp. 352–362. doi: 10.1016/J.YEXCR.2003.07.002.

Muchir, A. *et al.* (2004) 'Nuclear envelope alterations in fibroblasts from patients with muscular dystrophy, cardiomyopathy, and partial lipodystrophy carrying lamin A/C gene mutations.', *Muscle & nerve*, 30(4), pp. 444–450. doi: 10.1002/mus.20122.

Muchir, A. *et al.* (2007) 'Activation of MAPK pathways links LMNA mutations to cardiomyopathy in Emery-Dreifuss muscular dystrophy.', *The Journal of clinical investigation*, 117(5), pp. 1282–1293. doi: 10.1172/JCI29042.

Muchir, A. *et al.* (2009) 'Inhibition of extracellular signal-regulated kinase signaling to prevent cardiomyopathy caused by mutation in the gene encoding A-type lamins.', *Human molecular genetics*, 18(2), pp. 241–247. doi: 10.1093/hmg/ddn343.

Muchir, A., Wu, W., *et al.* (2012) 'Abnormal p38α mitogen-activated protein kinase

signaling in dilated cardiomyopathy caused by lamin A/C gene mutation', *Human molecular genetics*. Hum Mol Genet, 21(19), pp. 4325–4333. doi: 10.1093/HMG/DDS265.

Muchir, A., Reilly, S. A., *et al.* (2012) 'Treatment with selumetinib preserves cardiac function and improves survival in cardiomyopathy caused by mutation in the lamin A/C gene.', *Cardiovascular research*, 93(2), pp. 311–319. doi: 10.1093/cvr/cvr301.

Muchir, A., Wu, W. and Worman, H. J. (2009) 'Reduced expression of A-type lamins and emerin activates extracellular signal-regulated kinase in cultured cells', *Biochimica et Biophysica Acta (BBA) - Molecular Basis of Disease*, 1792(1), pp. 75–81. doi: 10.1016/j.bbadis.2008.10.012.

Muntoni, F. *et al.* (2006) 'Disease severity in dominant Emery Dreifuss is increased by mutations in both emerin and desmin proteins.', *Brain: A Journal of Neurology*, 129(5), pp. 1260–1268. doi: 10.1093/brain/awl062.

Mutesa, L. *et al.* (2007) 'Hutchinson-Gilford progeria syndrome: clinical and molecular analysis in an African patient', *Revue medicale de Liege*, 62(3), pp. 155–158.

Mziaut, H. *et al.* (2001) 'Induction of Stearoyl CoA Desaturase Is Associated with High-Level Induction of Emerin RNA', *Biochemical and Biophysical Research Communications*. Academic Press, 282(4), pp. 910–915. doi: 10.1006/BBRC.2001.4658.

Nagano, A. and Arahata, K. (2000) 'Nuclear envelope proteins and associated diseases.', *Current Opinion in Neurology*, 13(5), pp. 533–539. doi: 10.1097/00019052-200010000-00005.

Naldrett, M. J. *et al.* (2005) 'Concentration and Desalting of Peptide and Protein

Samples with a Newly Developed C18 Membrane in a Microspin Column Format', *Journal of Biomolecular Techniques*. The Association of Biomolecular Resource Facilities, 16(4), p. 423.

Nayak, L., Bhattacharyya, N. P. and De, R. K. (2016) 'Wnt signal transduction pathways: Modules, development and evolution', *BMC Systems Biology*, 10, p. 44. doi: 10.1186/s12918-016-0299-7.

Nelson, M. (2000) 'Rehabilitation concerns in myopathies', *Physical medicine and rehabilitation*, 2, pp. 1009–1045.

Nghiem, P. P. *et al.* (2017) 'Changes in Muscle Metabolism are Associated with Phenotypic Variability in Golden Retriever Muscular Dystrophy', *The Yale Journal of Biology and Medicine*. Yale Journal of Biology and Medicine, 90(3), p. 351.

Nicolas, H. A., Akimenko, M.-A. and Tesson, F. (2019) 'Cellular and Animal Models of Striated Muscle Laminopathies', *Cells*. MDPI AG, 8(4), p. 291. doi: 10.3390/cells8040291.

Nikolova-Krstevski, V. *et al.* (2011) 'Nesprin-1 and actin contribute to nuclear and cytoskeletal defects in lamin A/C-deficient cardiomyopathy.', *Journal of molecular and cellular cardiology*, 50(3), pp. 479–486. doi: 10.1016/j.yjmcc.2010.12.001.

Nikolova, V. *et al.* (2004) 'Defects in nuclear structure and function promote dilated cardiomyopathy in lamin A/C-deficient mice.', *The Journal of clinical investigation*, 113(3), pp. 357–369. doi: 10.1172/JCI19448.

Oerlemans, M. I. F. J. *et al.* (2012) 'Inhibition of RIP1-dependent necrosis prevents adverse cardiac remodeling after myocardial ischemia-reperfusion in vivo', *Basic*

Research in Cardiology, 107(4), p. 207. doi: 10.1007/s00395-012-0270-8.

Onopiuk, M. *et al.* (2009) 'Mutation in dystrophin-encoding gene affects energy metabolism in mouse myoblasts', *Biochemical and Biophysical Research Communications*. Academic Press, 386(3), pp. 463–466. doi: 10.1016/J.BBRC.2009.06.053.

Orzáez, M. *et al.* (2014) 'Apaf-1 inhibitors protect from unwanted cell death in In vivo models of kidney ischemia and chemotherapy induced ototoxicity', *PLoS ONE*, 9(10), p. e110979. doi: 10.1371/journal.pone.0110979.

Osmanagic-Myers, S. and Foisner, R. (2019) 'The structural and gene expression hypotheses in laminopathic diseases - Not so different after all', *Molecular Biology of the Cell*. American Society for Cell Biology, 30(15), pp. 1786–1790. doi: 10.1091/mbc.E18-10-0672.

Ostlund, C. *et al.* (2001) 'Properties of lamin A mutants found in Emery-Dreifuss muscular dystrophy, cardiomyopathy and Dunnigan-type partial lipodystrophy.', *Journal of cell science*, 114(Pt 24), pp. 4435–4445. doi: 10.1242/jcs.114.24.4435.

Ouzzani, M. *et al.* (2016) 'Rayyan—a web and mobile app for systematic reviews', *Systematic Reviews*. BioMed Central Ltd., 5(1), p. 210. doi: 10.1186/S13643-016-0384-4.

Owens, D. J. *et al.* (2020) 'Lamin-Related Congenital Muscular Dystrophy Alters Mechanical Signaling and Skeletal Muscle Growth.', *International journal of molecular sciences*, 22(1), p. 306. doi: 10.3390/ijms22010306.

Ozaki, T. *et al.* (1994) 'Complex formation between lamin A and the retinoblastoma

gene product: identification of the domain on lamin A required for its interaction.', *Oncogene*, 9(9), pp. 2649–2653.

Özyilmaz, B. *et al.* (2019) 'Impact of next-generation sequencing panels in the evaluation of limb-girdle muscular dystrophies', *Annals of human genetics*. Ann Hum Genet, 83(5), pp. 331–347. doi: 10.1111/AHG.12319.

Padiath, Q. S. *et al.* (2006) 'Lamin B1 duplications cause autosomal dominant leukodystrophy.', *Nature genetics*, 38(10), pp. 1114–1123. doi: 10.1038/ng1872.

Pan, C. *et al.* (2009) 'Comparative proteomic phenotyping of cell lines and primary cells to assess preservation of cell type-specific functions', *Molecular and Cellular Proteomics*. American Society for Biochemistry and Molecular Biology, 8(3), pp. 443–450. doi: 10.1074/mcp.M800258-MCP200.

Paoni, N. F. *et al.* (2003) 'Time course of skeletal muscle repair and gene expression following acute hind limb ischemia in mice', *Physiological Genomics*. American Physiological Society, 11, pp. 263–272. doi: 10.1152/physiolgenomics.00110.2002.

Parent, J. J., Towbin, J. A. and Jefferies, J. L. (2015) 'Left ventricular noncompaction in a family with lamin A/C gene mutation.', *Texas Heart Institute journal*, 42(1), pp. 73–76. doi: 10.14503/THIJ-13-3843.

Park, C. H. *et al.* (2005) 'Quercetin, a potent inhibitor against β-catenin/Tcf signaling in SW480 colon cancer cells', *Biochemical and Biophysical Research Communications*. Academic Press, 328(1), pp. 227–234. doi: 10.1016/J.BBRC.2004.12.151.

Park, Y.-E. *et al.* (2009) 'Nuclear changes in skeletal muscle extend to satellite cells in autosomal dominant Emery-Dreifuss muscular dystrophy/limb-girdle muscular

dystrophy 1B.', *Neuromuscular disorders*, 19(1), pp. 29–36. doi: 10.1016/j.nmd.2008.09.018.

Parnaik, V. K. (2008) 'Role of Nuclear Lamins in Nuclear Organization, Cellular Signaling, and Inherited Diseases', *International Review of Cell and Molecular Biology*, 266, pp. 157–206. doi: 10.1016/S1937-6448(07)66004-3.

Pasotti, M. *et al.* (2008) 'Long-term outcome and risk stratification in dilated cardiolaminopathies.', *Journal of the American College of Cardiology*, 52(15), pp. 1250–1260. doi: 10.1016/j.jacc.2008.06.044.

Paulech, J., Solis, N. and Cordwell, S. J. (2013) 'Characterization of reaction conditions providing rapid and specific cysteine alkylation for peptide-based mass spectrometry', *Biochimica et Biophysica Acta (BBA) - Proteins and Proteomics*. Elsevier, 1834(1), pp. 372–379. doi: 10.1016/J.BBAPAP.2012.08.002.

Pendás, A. M. *et al.* (2002) 'Defective prelamin A processing and muscular and adipocyte alterations in Zmpste24 metalloproteinase–deficient mice', *Nature Genetics*. Nature Publishing Group, 31(1), pp. 94–99. doi: 10.1038/ng871.

Perovanovic, J. *et al.* (2016) 'Laminopathies disrupt epigenomic developmental programs and cell fate.', *Science translational medicine*. NIH Public Access, 8(335), p. 335ra58. doi: 10.1126/scitranslmed.aad4991.

Perrot, A. *et al.* (2009) 'Identification of mutational hot spots in LMNA encoding lamin A/C in patients with familial dilated cardiomyopathy.', *Basic research in cardiology*, 104(1), pp. 90–99. doi: 10.1007/s00395-008-0748-6.

Pette, D. and Staron, R. (1990) 'Cellular and molecular diversities of mammalian

skeletal muscle fibers', *Reviews of Physiology, Biochemistry and Pharmacology*, 116, pp. 1–76. doi: 10.1007/3540528806_3.

Pfaffl, M. W. (2001) 'A new mathematical model for relative quantification in real-time RT–PCR', *Nucleic Acids Research*. Oxford Academic, 29(9), pp. e45–e45. doi: 10.1093/NAR/29.9.E45.

Pfizer (2022) *Pfizer to Discontinue Development Program for PF-07265803 for LMNA-Related Dilated Cardiomyopathy*. Available at: https://www.pfizer.com/news/announcements/pfizer-discontinue-development-program-pf-07265803-lmna-related-dilated (Accessed: 23 August 2023).

Picotti, P. and Aebersold, R. (2012) 'Selected reaction monitoring-based proteomics: workflows, potential, pitfalls and future directions', *Nature methods*. Nat Methods, 9(6), pp. 555–566. doi: 10.1038/NMETH.2015.

Pieczenik, S. R. and Neustadt, J. (2007) 'Mitochondrial dysfunction and molecular pathways of disease', *Experimental and Molecular Pathology*, 83(1), pp. 84–92. doi: 10.1016/j.yexmp.2006.09.008.

Plantié, E. *et al.* (2015) 'Model organisms in the fight against muscular dystrophy: Lessons from Drosophila and zebrafish', *Molecules*. MDPI AG, pp. 6237–6253. doi: 10.3390/molecules20046237.

Polesskaya, A., Seale, P. and Rudnicki, M. A. (2003) 'Wnt Signaling Induces the Myogenic Specification of Resident CD45+ Adult Stem Cells during Muscle Regeneration', *Cell*, 113(7), pp. 841–852. doi: 10.1016/S0092-8674(03)00437-9.

Politano, L. *et al.* (2003) 'Gentamicin administration in Duchenne patients with

premature stop codon. Preliminary results', *Official journal of the Mediterranean Society of Myology*, 22(1), pp. 15–21.

Ponchel, F. *et al.* (2003) 'Real-time PCR based on SYBR-Green I fluorescence: An alternative to the TaqMan assay for a relative quantification of gene rearrangements, gene amplifications and micro gene deletions', *BMC Biotechnology*. BioMed Central, 3(1), pp. 1–13. doi: 10.1186/1472-6750-3-18/FIGURES/6.

Potter, N. *et al.* (2008) 'Genomic deletions correlate with underexpression of novel candidate genes at six loci in pediatric pilocytic astrocytoma', *Neoplasia*, 10(8), pp. 757–727. doi: 10.1593/neo.07914.

Prabhakar, B. S. *et al.* (1990) 'Cell surface expression of the 70-kD component of Ku, a DNA-binding nuclear autoantigen', *Journal of Clinical Investigation*, 86(4), pp. 1303–1305. doi: 10.1172/JCI114838.

Prasad, K. M. R. *et al.* (2003) 'Evidence that increased 12-lipoxygenase expression impairs pancreatic β cell function and viability', *Biochemical and Biophysical Research Communications*. Academic Press, 308(3), pp. 427–432. doi: 10.1016/S0006-291X(03)01418-9.

Probst, A. V. and Almouzni, G. (2008) 'Pericentric heterochromatin: dynamic organization during early development in mammals', *Differentiation*, 76(1), pp. 15–23. doi: 10.1111/j.1432-0436.2007.00220.x.

Quarta, G. *et al.* (2012) 'Mutations in the Lamin A/C gene mimic arrhythmogenic right ventricular cardiomyopathy.', *European heart journal*, 33(9), pp. 1128–1136. doi: 10.1093/eurheartj/ehr451.

Quattrocelli, M., Salamone, I. M., *et al.* (2017) 'Intermittent Glucocorticoid Dosing Improves Muscle Repair and Function in Mice with Limb-Girdle Muscular Dystrophy', *American Journal of Pathology*, 187(11). doi: 10.1016/j.ajpath.2017.07.017.

Quattrocelli, M., Barefield, D. Y., *et al.* (2017) 'Intermittent glucocorticoid steroid dosing enhances muscle repair without eliciting muscle atrophy', *Journal of Clinical Investigation*, 127(6). doi: 10.1172/JCI91445.

Quijano-Roy, S. *et al.* (2008) 'De novo *LMNA* mutations cause a new form of congenital muscular dystrophy', *Annals of Neurology*. John Wiley and Sons Inc., 64(2), pp. 177–186. doi: 10.1002/ana.21417.

Quinn, L. B. S. *et al.* (2002) 'Overexpression of interleukin-15 induces skeletal muscle hypertrophy in vitro: Implications for treatment of muscle wasting disorders', *Experimental Cell Research*, 280(1), pp. 55–63. doi: 10.1006/excr.2002.5624.

Raffaele Di Barletta, M. *et al.* (2000) 'Different mutations in the LMNA gene cause autosomal dominant and autosomal recessive Emery-Dreifuss muscular dystrophy.', *American journal of human genetics*, 66(4), pp. 1407–1412. doi: 10.1086/302869.

Raharjo, W. H. *et al.* (2001) 'Nuclear envelope defects associated with LMNA mutations cause dilated cardiomyopathy and Emery-Dreifuss muscular dystrophy.', *Journal of cell science*, 114(Pt 24), pp. 4447–4457. doi: 10.1242/jcs.114.24.4447.

Rajendran, V., Purohit, R. and Sethumadhavan, R. (2012) 'In silico investigation of molecular mechanism of laminopathy caused by a point mutation (R482W) in lamin A/C protein', *Amino Acids*, 43(2), pp. 603–615. doi: 10.1007/s00726-011-1108-7.

Rajgor, D. and Shanahan, C. M. (2013) 'Nesprins: from the nuclear envelope and

beyond', *Expert Reviews in Molecular Medicine*. Cambridge University Press, 15, p. e5. doi: 10.1017/erm.2013.6.

Ramdas, S. and Servais, L. (2020) 'New treatments in spinal muscular atrophy: an overview of currently available data', *Expert Opinion on Pharmacotherapy*. Taylor and Francis Ltd, pp. 307–315. doi: 10.1080/14656566.2019.1704732.

Ramirez, R. D. *et al.* (2003) 'Bypass of telomere-dependent replicative senescence (M1) upon overexpression of Cdk4 in normal human epithelial cells', *Oncogene*. Nature Publishing Group, 22(3), pp. 433–444. doi: 10.1038/sj.onc.1206046.

Randles, K. N. *et al.* (2010) 'Nesprins, but not sun proteins, switch isoforms at the nuclear envelope during muscle development', *Developmental Dynamics*, 239(3), pp. 998–1009. doi: 10.1002/dvdy.22229.

Rankin, J. *et al.* (2008) 'Extreme phenotypic diversity and nonpenetrance in families with the LMNA gene mutation R644C.', *American journal of medical genetics. Part A*, 146A(12), pp. 1530–1542. doi: 10.1002/ajmg.a.32331.

Rayavarapu, S. *et al.* (2013) 'Identification of disease specific pathways using in vivo SILAC proteomics in dystrophin deficient mdx mouse', *Molecular and Cellular Proteomics*, 12(5), pp. 1061–1073. doi: 10.1074/mcp.M112.023127.

Refaat, M. M. *et al.* (2019) 'Non-familial cardiomyopathies in Lebanon: exome sequencing results for five idiopathic cases.', *BMC medical genomics*, 12(1), p. 33. doi: 10.1186/s12920-019-0478-7.

Reiter, L. T. *et al.* (2001) 'A systematic analysis of human disease-associated gene sequences in Drosophila melanogaster', *Genome Research*. Cold Spring Harbor

Laboratory Press, 11(6), pp. 1114–1125. doi: 10.1101/gr.169101.

Renault, V. *et al.* (2002) 'Regenerative potential of human skeletal muscle during aging', *Aging cell*, 1(2), pp. 132–139. doi: 10.1046/j.1474-9728.2002.00017.x.

Ricci, G. *et al.* (2022) 'P.147 Deflazacort treatment in LMNA-related congenital muscular dystrophy: an ongoing Italian cohort pilot study', *Neuromuscular Disorders*. Elsevier, 32, p. S108. doi: 10.1016/J.NMD.2022.07.275.

Ridgeway, A. G. *et al.* (2000) 'Wnt Signaling Regulates the Function of MyoD and Myogenin', *The Journal of Biological Chemistry*. JBC Papers in Press, 275, pp. 32398–32405. doi: 10.1074/jbc.M004349200.

Riemer, D., Dodemont, H. and Weber, K. (1993) 'A nuclear lamin of the nematode Caenorhabditis elegans with unusual structural features; cDNA cloning and gene organization', *European Journal of Cell Biology*, 62(2), pp. 214–223.

Riordan, J. D. and Nadeau, J. H. (2017) 'From Peas to Disease: Modifier Genes, Network Resilience, and the Genetics of Health', *American Journal of Human Genetics*. Elsevier, 101(2), p. 177. doi: 10.1016/J.AJHG.2017.06.004.

Ririe, K. M., Rasmussen, R. P. and Wittwer, C. T. (1997) 'Product Differentiation by Analysis of DNA Melting Curves during the Polymerase Chain Reaction', *Analytical Biochemistry*. Academic Press, 245(2), pp. 154–160. doi: 10.1006/ABIO.1996.9916.

Röber, R. A., Weber, K. and Osborn, M. (1989) 'Differential timing of nuclear lamin A/C expression in the various organs of the mouse embryo and the young animal: a developmental study.', *Development (Cambridge, England)*, 105(2), pp. 365–78. doi: 10.1242/dev.105.2.365.

Robinson, A. *et al.* (2013) 'Is LMNB1 a susceptibility gene for neural tube defects in humans?', *Birth Defects Research Part A: Clinical and Molecular Teratology*. John Wiley & Sons, Ltd, 97(6), pp. 398–402. doi: 10.1002/BDRA.23141.

Roghani, A. *et al.* (1994) 'Molecular cloning of a putative vesicular transporter for acetylcholine.', *Proceedings of the National Academy of Sciences*. Proceedings of the National Academy of Sciences, 91(22), pp. 10620–10624. doi: 10.1073/PNAS.91.22.10620.

Roman, W. and Gomes, E. R. (2018) 'Nuclear positioning in skeletal muscle', *Seminars in Cell & Developmental Biology*. Academic Press, 82, pp. 51–56. doi: 10.1016/J.SEMCDB.2017.11.005.

Rose, N. *et al.* (2023) 'Bioengineering a miniaturized in vitro 3D myotube contraction monitoring chip to model muscular dystrophies', *Biomaterials*. Elsevier, 293, p. 121935. doi: 10.1016/J.BIOMATERIALS.2022.121935.

Rouillon, J. *et al.* (2014) 'Proteomics profiling of urine reveals specific titin fragments as biomarkers of Duchenne muscular dystrophy', *Neuromuscular Disorders*, 24(7), pp. 563–573. doi: 10.1016/j.nmd.2014.03.012.

Rudnik-Schöneborn, S. *et al.* (2007) 'Mutations of the LMNA gene can mimic autosomal dominant proximal spinal muscular atrophy.', *Neurogenetics*, 8(2), pp. 137–142. doi: 10.1007/s10048-006-0070-0.

Ruegg, M. A. (2005) 'Organization of synaptic myonuclei by Syne proteins and their role during the formation of the nerve–muscle synapse', *Proceedings of the National Academy of Sciences of the United States of America*. National Academy of Sciences,

102(16), p. 5643. doi: 10.1073/PNAS.0501516102.

Russo, V. and Nigro, G. (2015) 'ICD role in preventing sudden cardiac death in Emery-Dreifuss muscular dystrophy with preserved myocardial function: 2013 ESC Guidelines on Cardiac Pacing and Cardiac Resynchronization Therapy', *Europace*. Narnia, 17(2), pp. 337–337. doi: 10.1093/europace/euu146.

Sabatelli, P. *et al.* (2001) 'Nuclear alterations in autosomal-dominant emery-dreifuss muscular dystrophy', *Muscle and Nerve*, 24(6), pp. 826–829. doi: 10.1002/mus.1076.

Sakaki, M. *et al.* (2001) 'Interaction between emerin and nuclear lamins', *Journal of Biochemistry*, 129(2), pp. 321–327. doi: 10.1093/oxfordjournals.jbchem.a002860.

Sanchis, D. *et al.* (2003) 'Lack of Apaf-1 expression confers resistance to cytochrome c-driven apoptosis in cardiomyocytes', *Cell Death and Differentiation*, 10(9), pp. 977–986. doi: 10.1038/sj.cdd.4401267.

Sancho, M. *et al.* (2011) 'Minocycline inhibits cell death and decreases mutant Huntingtin aggregation by targeting Apaf-1', *Human Molecular Genetics*, 20(18), pp. 3545–3553. doi: 10.1093/hmg/ddr271.

De Sandre-Giovannoli, A. *et al.* (2002) 'Homozygous defects in LMNA, encoding lamin A/C nuclear-envelope proteins, cause autosomal recessive axonal neuropathy in human (Charcot-Marie-Tooth disorder type 2) and mouse.', *American journal of human genetics*, 70(3), pp. 726–736. doi: 10.1086/339274.

De Sandre-Giovannoli, A. *et al.* (2003) 'Lamin A truncation in Hutchinson-Gilford progeria', *Science*. American Association for the Advancement of Science, 300(5628), p. 2055. doi: 10.1126/science.1084125.

Sang, T. K. *et al.* (2005) 'Inactivation of Drosophila Apaf-1 related killer suppresses formation of polyglutamine aggregates and blocks polyglutamine pathogenesis', *Human Molecular Genetics*, 14(3), pp. 357–372. doi: 10.1093/hmg/ddi032.

Sanga, S. *et al.* (2021) 'Whole-exome analyses of congenital muscular dystrophy and congenital myopathy patients from India reveal a wide spectrum of known and novel mutations.', *European journal of neurology*, 28(3), pp. 992–1003. doi: 10.1111/ene.14616.

Sanger, J. W. (1974) 'The use of cytochalasin B to distinguish myoblasts from fibroblasts in cultures of developing chick striated muscle', *Proceedings of the National Academy of Sciences of the United States of America*, 71(9), pp. 3621–3625. doi: 10.1073/pnas.71.9.3621.

Sanna, T. *et al.* (2003) 'Cardiac features of Emery-Dreifuss muscular dystrophy caused by lamin A/C gene mutations.', *European heart journal*, 24(24), pp. 2227–2236. doi: 10.1016/j.ehj.2003.09.020.

Sarbassov, D. D. *et al.* (2006) 'Prolonged rapamycin treatment inhibits mTORC2 assembly and Akt/PKB', *Molecular cell*. Mol Cell, 22(2), pp. 159–168. doi: 10.1016/J.MOLCEL.2006.03.029.

Sasseville, A. M.-J. and Langelier, Y. (1998) 'In vitro interaction of the carboxy-terminal domain of lamin A with actin', *FEBS Letters*. John Wiley & Sons, Ltd, 425(3), pp. 485–489. doi: 10.1016/S0014-5793(98)00294-4.

Sawada, M. *et al.* (2003) 'Ku70 suppresses the apoptotic translocation of bax to mitochondria', *Nature Cell Biology*, 5(4), pp. 320–329. doi: 10.1038/ncb950.

Saxton, R. A. and Sabatini, D. M. (2017) ‘mTOR Signaling in Growth, Metabolism, and Disease’, *Cell*. NIH Public Access, 168(6), p. 960. doi: 10.1016/J.CELL.2017.02.004.

Sayers, E. W. *et al.* (2022) ‘Database resources of the national center for biotechnology information’, *Nucleic acids research*. Nucleic Acids Res, 50(D1), pp. D20–D26. doi: 10.1093/NAR/GKAB1112.

Scaffidi, P. and Misteli, T. (2005) ‘Reversal of the cellular phenotype in the premature aging disease Hutchinson-Gilford progeria syndrome.’, *Nature medicine*, 11(4), pp. 440–445. doi: 10.1038/nm1204.

Scaffidi, P. and Misteli, T. (2006) ‘Lamin A-dependent nuclear defects in human aging’, *Science*. Science, 312(5776), pp. 1059–1063. doi: 10.1126/SCIENCE.1127168.

Schaeffer, L., de Kerchove d’Exaerde, A. and Changeux, J. P. (2001) ‘Targeting transcription to the neuromuscular synapse.’, *Neuron*, 31(1), pp. 15–22. doi: 10.1016/s0896-6273(01)00353-1.

Scharner, J. *et al.* (2011) ‘Novel LMNA mutations in patients with Emery-Dreifuss muscular dystrophy and functional characterization of four LMNA mutations.’, *Human mutation*, 32(2), pp. 152–167. doi: 10.1002/humu.21361.

Schindler, C., Levy, D. E. and Decker, T. (2007) ‘JAK-STAT signaling: From interferons to cytokines’, *Journal of Biological Chemistry*. Elsevier, 282(28), pp. 20059–20063. doi: 10.1074/jbc.R700016200.

Schirmer, E. C. and Gerace, L. (2004) ‘The Stability of the Nuclear Lamina Polymer Changes with the Composition of Lamin Subtypes According to Their Individual Binding Strengths’, *Journal of Biological Chemistry*. Elsevier, 279(41), pp. 42811–42817. doi:

10.1074/JBC.M407705200.

Schirmer, E. C. and Gerace, L. (2005) 'The nuclear membrane proteome: extending the envelope', *Trends in Biochemical Sciences*. Elsevier Current Trends, 30(10), pp. 551–558. doi: 10.1016/J.TIBS.2005.08.003.

Schneider, S. M. *et al.* (2018) 'Glucose Metabolism as a Pre-clinical Biomarker for the Golden Retriever Model of Duchenne Muscular Dystrophy', *Molecular Imaging and Biology*. Springer New York LLC, 20(5), pp. 780–788. doi: 10.1007/S11307-018-1174-2/FIGURES/5.

Schubert, O. T. *et al.* (2017) 'Quantitative proteomics: Challenges and opportunities in basic and applied research', *Nature Protocols*. Nature Publishing Group, pp. 1289–1294. doi: 10.1038/nprot.2017.040.

Schulze, S. R. *et al.* (2009) 'A Comparative Study of Drosophila and Human A-Type Lamins', *PLoS ONE*, 4(10), p. 7564. doi: 10.1371/journal.pone.0007564.

Sechi, S. and Chait, B. T. (1998) 'Modification of cysteine residues by alkylation. A tool in peptide mapping and protein identification', *Analytical chemistry*. Anal Chem, 70(24), pp. 5150–5158. doi: 10.1021/AC9806005.

Sewry, C. A. *et al.* (2001) 'Skeletal muscle pathology in autosomal dominant Emery-Dreifuss muscular dystrophy with lamin A/C mutations.', *Neuropathology and applied neurobiology*, 27(4), pp. 281–290. doi: 10.1046/j.0305-1846.2001.00323.x.

Shakeri, R., Kheirollahi, A. and Davoodi, J. (2021) 'Contribution of Apaf-1 to the pathogenesis of cancer and neurodegenerative diseases', *Biochimie*, 190, pp. 91–110. doi: 10.1016/j.biochi.2021.07.004.

Shaklai, S. *et al.* (2007) 'Gene silencing at the nuclear periphery', *The FEBS Journal*. John Wiley & Sons, Ltd, 274(6), pp. 1383–1392. doi: 10.1111/J.1742-4658.2007.05697.X.

Sharma, U. *et al.* (2003) 'Skeletal muscle metabolism in Duchenne muscular dystrophy (DMD): an in-vitro proton NMR spectroscopy study', *Magnetic Resonance Imaging*. Elsevier, 21(2), pp. 145–153. doi: 10.1016/S0730-725X(02)00646-X.

Sheffield, J. (2007) 'ImageJ, A Useful Tool for Biological Image Processing and Analysis', *Microscopy and Microanalysis*. Cambridge University Press, 13(S02), pp. 200–201. doi: 10.1017/S1431927607076611.

Shen, X. *et al.* (2003) 'Genome-wide examination of myoblast cell cycle withdrawal during differentiation', *Developmental Dynamics*. John Wiley & Sons, Ltd, 226(1), pp. 128–138. doi: 10.1002/DVDY.10200.

Sherman, B. T. *et al.* (2022) 'DAVID: a web server for functional enrichment analysis and functional annotation of gene lists (2021 update)', *Nucleic acids research*. Nucleic Acids Res, 50(W1), pp. W216–W221. doi: 10.1093/NAR/GKAC194.

Shi, X. *et al.* (2018) 'Zebrafish heart failure models: opportunities and challenges', *Amino Acids*. Springer-Verlag Wien, pp. 787–798. doi: 10.1007/s00726-018-2578-7.

Shi, Y. (2002) 'Mechanisms of caspase activation and inhibition during apoptosis', *Molecular Cell*, 9(3), pp. 459–470. doi: 10.1016/S1097-2765(02)00482-3.

Shoeman, R. L. and Traub, P. (1990) 'The in vitro DNA-binding properties of purified nuclear lamin proteins and vimentin', *Journal of Biological Chemistry*, 265(16), pp. 9055–9061. doi: 10.1016/s0021-9258(19)38810-6.

Shumaker, D. K. *et al.* (2006) 'Mutant nuclear lamin A leads to progressive alterations of epigenetic control in premature aging', *Proceedings of the National Academy of Sciences of the United States of America*, 103(23), pp. 8703–8708. doi: 10.1073/pnas.0602569103.

Shumaker, D. K. *et al.* (2008) 'The highly conserved nuclear lamin Ig-fold binds to PCNA: its role in DNA replication', *Journal of Cell Biology*. The Rockefeller University Press, 181(2), pp. 269–280. doi: 10.1083/JCB.200708155.

Simon, D. N., Zastrow, M. S. and Wilson, K. L. (2010) 'Direct actin binding to A- and B-type lamin tails and actin filament bundling by the lamin A tail', *Nucleus*. Taylor & Francis, 1(3), p. 264. doi: 10.4161/NUCL.1.3.11799.

Sinensky, M. *et al.* (1994) 'The processing pathway of prelamin A', *Journal of Cell Science*. The Company of Biologists, 107(1), pp. 61–67. doi: 10.1242/JCS.107.1.61.

Smith, C. C. T. *et al.* (2007) 'Necrostatin: A potentially novel cardioprotective agent?', *Cardiovascular Drugs and Therapy*, 21(4), pp. 227–233. doi: 10.1007/s10557-007-6035-1.

Smith, D. L. *et al.* (2003) 'Minocycline and doxycycline are not beneficial in a model of Huntington's disease', *Annals of Neurology*, 54(2), pp. 186–196. doi: 10.1002/ana.10614.

Smith, P. K. *et al.* (1985) 'Measurement of protein using bicinchoninic acid', *Analytical Biochemistry*. Academic Press, 150(1), pp. 76–85. doi: 10.1016/0003-2697(85)90442-7.

Solovei, I. *et al.* (2013) 'LBR and lamin A/C sequentially tether peripheral heterochromatin and inversely regulate differentiation.', *Cell*, 152(3), pp. 584–98. doi:

10.1016/j.cell.2013.01.009.

Somech, R. *et al.* (2005) 'Nuclear envelopathies--raising the nuclear veil', *Pediatric research*, 57, pp. 8–15. doi: 10.1203/01.PDR.0000159566.54287.6C.

Song, S., Zhang, Y. and Zhong, N. (2005) 'Laminopathies-one gene, multiple diseases', *ournal of Peking University. Health sciences*, 37(1), pp. 96–99.

Spann, T. P. *et al.* (2002) 'Alteration of nuclear lamin organization inhibits RNA polymerase II-dependent transcription', *Journal of Cell Biology*, 156(4), pp. 603–608. doi: 10.1083/jcb.200112047.

Stack, E. C. *et al.* (2006) 'Combination therapy using minocycline and coenzyme Q10 in R6/2 transgenic Huntington's disease mice', *Biochimica et Biophysica Acta - Molecular Basis of Disease*, 1762(3), pp. 373–380. doi: 10.1016/j.bbadis.2005.11.002.

Stearns, F. W. (2010) 'Anecdotal, Historical and Critical Commentaries on Genetics: One Hundred Years of Pleiotropy: A Retrospective', *Genetics*. Oxford University Press, 186(3), p. 767. doi: 10.1534/GENETICS.110.122549.

Steele-Stallard, H. B. *et al.* (2018) 'Modeling Skeletal Muscle Laminopathies Using Human Induced Pluripotent Stem Cells Carrying Pathogenic LMNA Mutations.', *Frontiers in physiology*, 9, p. 1332. doi: 10.3389/fphys.2018.01332.

Stierlé, V. *et al.* (2003) 'The carboxyl-terminal region common to lamins A and C contains a DNA binding domain.', *Biochemistry*, 42(17), pp. 4819–4828. doi: 10.1021/bi020704g.

Storey, E. C. *et al.* (2020) 'Muscle cell differentiation and development pathway defects in Emery-Dreifuss muscular dystrophy', *Neuromuscular Disorders*. Elsevier,

30(6), pp. 443–456. doi: 10.1016/j.nmd.2020.04.002.

Stougaard, M. *et al.* (2009) 'Single-molecule detection of human topoisomerase I cleavage-ligation activity', *ACS Nano*, 3(1), pp. 223–233. doi: 10.1021/nn800509b.

Strehl, C. *et al.* (2016) 'Defining conditions where long-term glucocorticoid treatment has an acceptably low level of harm to facilitate implementation of existing recommendations: Viewpoints from an EULAR task force', *Annals of the Rheumatic Diseases*. doi: 10.1136/annrheumdis-2015-208916.

Streisinger, G. *et al.* (1966) 'Frameshift Mutations and the Genetic Code', *Cold Spring Harbor Symposia on Quantitative Biology*. Cold Spring Harbor Laboratory Press, 31, pp. 77–84. doi: 10.1101/SQB.1966.031.01.014.

Strober, W. (2015) 'Trypan Blue Exclusion Test of Cell Viability', *Current protocols in immunology*. NIH Public Access, 111(1), p. A3.B.1. doi: 10.1002/0471142735.IMA03BS111.

Stuurman, N., Heins, S. and Aebi, U. (1998) 'Nuclear lamins: Their structure, assembly, and interactions', *Journal of Structural Biology*. Academic Press Inc., 122(1–2), pp. 42–66. doi: 10.1006/JSBI.1998.3987.

Stuurman, N., Sasse, B. and Fisher, P. A. (1996) 'Intermediate Filament Protein Polymerization: Molecular Analysis of Drosophila Nuclear Lamin Head-to-Tail Binding', *Journal of Structural Biology*. Academic Press, 117(1), pp. 1–15. doi: 10.1006/JSBI.1996.0064.

Sullivan, T. *et al.* (1999) 'Loss of A-type lamin expression compromises nuclear envelope integrity leading to muscular dystrophy', *Journal of Cell Biology*. The

Rockefeller University Press, 147(5), pp. 913–919. doi: 10.1083/jcb.147.5.913.

Sumner, C. J. and Crawford, T. O. (2018) 'Two breakthrough gene-targeted treatments for spinal muscular atrophy: challenges remain.', *The Journal of clinical investigation*, 128(8), pp. 3219–3227. doi: 10.1172/JCI121658.

Swailes, N. T. *et al.* (2006) 'Non-muscle myosins 2A and 2B drive changes in cell morphology that occur as myoblasts align and fuse', *Journal of Cell Science*, 119(17), pp. 3561–3570. doi: 10.1242/jcs.03096.

Swash, M. (2007) 'Learning from failed trials in ALS', *Lancet Neurology*. Elsevier, 6(12), pp. 1034–1035. doi: 10.1016/S1474-4422(07)70271-5.

Swift, J. *et al.* (2013) 'Nuclear lamin-A scales with tissue stiffness and enhances matrix-directed differentiation', *Science*. American Association for the Advancement of Science, 341(6149), p. 1240104. doi: 10.1126/science.1240104.

Synofzik, M. *et al.* (2016) 'SYNE1 ataxia is a common recessive ataxia with major non-cerebellar features: a large multi-centre study.', *Brain: A Journal of Neurology*, 139(5), pp. 1378–1393. doi: 10.1093/brain/aww079.

Szklarczyk, D. *et al.* (2021) 'The STRING database in 2021: customizable protein-protein networks, and functional characterization of user-uploaded gene/measurement sets', *Nucleic acids research*. Nucleic Acids Res, 49(D1), pp. D605–D612. doi: 10.1093/NAR/GKAA1074.

Taddei, A. *et al.* (2004) 'The function of nuclear architecture: a genetic approach', *Annual review of genetics*, 38, pp. 305–45. doi: 10.1146/annurev.genet.37.110801.142705.

Taguchi, A. *et al.* (2017) 'Structure-Activity Relationship Study of Leucyl-3-epi-deoxynegamycin for Potent Premature Termination Codon Readthrough', *ACS Medicinal Chemistry Letters*. American Chemical Society, 8(10), pp. 1060–1065. doi: 10.1021/acsmedchemlett.7b00269.

Tan, D. *et al.* (2015) 'Phenotype-Genotype Analysis of Chinese Patients with Early-Onset LMNA-Related Muscular Dystrophy.', *PloS one*, 10(6), p. e0129699. doi: 10.1371/journal.pone.0129699.

Tang, K. *et al.* (2000) 'Identification of 12-Lipoxygenase Interaction with Cellular Proteins by Yeast Two-Hybrid Screening', *Biochemistry*. American Chemical Society, 39(12), pp. 3185–3191. doi: 10.1021/BI992664V.

Tannu, N. S. *et al.* (2004) 'Comparative proteomes of the proliferating C2C12 myoblasts and fully differentiated myotubes reveal the complexity of the skeletal muscle differentiation program', *Molecular and Cellular Proteomics*. Elsevier, 3(11), pp. 1065–1082. doi: 10.1074/mcp.M400020-MCP200.

Tapley, E. C. and Starr, D. A. (2013) 'Connecting the nucleus to the cytoskeleton by SUN-KASH bridges across the nuclear envelope', *Current Opinion in Cell Biology*. Elsevier Ltd, 25(1), pp. 57–62. doi: 10.1016/j.ceb.2012.10.014.

Tesauro, C. *et al.* (2019) 'Topoisomerase i activity and sensitivity to camptothecin in breast cancer-derived cells: A comparative study', *BMC Cancer*, 19(1), p. 1158. doi: 10.1186/s12885-019-6371-0.

Thanisch, K. *et al.* (2017) 'Nuclear envelope localization of LEMD2 is developmentally dynamic and lamin A/C dependent yet insufficient for heterochromatin tethering',

Differentiation, 94, pp. 58–70. doi: 10.1016/j.diff.2016.12.002.

The C. elegans sequencing consortium (1998) 'Genome sequence of the nematode C. elegans: A platform for investigating biology', *Science*. American Association for the Advancement of Science, pp. 2012–2018. doi: 10.1126/science.282.5396.2012.

Thorley, M. *et al.* (2016) 'Skeletal muscle characteristics are preserved in hTERT/cdk4 human myogenic cell lines', *Skeletal Muscle*, 6(1), p. 43. doi: 10.1186/s13395-016-0115-5.

van Tienen, F. H. J. *et al.* (2018) 'Assessment of fibroblast nuclear morphology aids interpretation of LMNA variants', *European Journal of Human Genetics*. Nature Publishing Group, 27(3), pp. 389–399. doi: 10.1038/s41431-018-0294-0.

Timpani, C. A., Hayes, A. and Rybalka, E. (2015) 'Revisiting the dystrophin-ATP connection: How half a century of research still implicates mitochondrial dysfunction in Duchenne Muscular Dystrophy aetiology', *Medical Hypotheses*. Churchill Livingstone, 85(6), pp. 1021–1033. doi: 10.1016/J.MEHY.2015.08.015.

Torvaldson, E., Kochin, V. and Eriksson, J. E. (2015) 'Phosphorylation of lamins determine their structural properties and signaling functions.', *Nucleus*, 6(3), pp. 166–171. doi: 10.1080/19491034.2015.1017167.

Towbin, H., Staehelin, T. and Gordon, J. (1979) 'Electrophoretic transfer of proteins from polyacrylamide gels to nitrocellulose sheets: Procedure and some applications', *Proceedings of the National Academy of Sciences of the United States of America*. National Academy of Sciences, 76(9), pp. 4350–4354. doi: 10.1073/pnas.76.9.4350.

Turgay, Y. *et al.* (2017) 'The molecular architecture of lamins in somatic cells', *Nature*.

Nature Publishing Group, 543(7644), pp. 261–264. doi: 10.1038/nature21382.

Uehara, T. *et al.* (2015) 'The Tumor Suppressor BCL7B Functions in the Wnt Signaling Pathway', *PLoS Genetics*, 11(1), p. e1004921. doi: 10.1371/journal.pgen.1004921.

Ungricht, R. and Kutay, U. (2015) 'Establishment of NE asymmetry-targeting of membrane proteins to the inner nuclear membrane', *Current Opinion in Cell Biology*, pp. 135–141. doi: 10.1016/j.ceb.2015.04.005.

Untergasser, A. *et al.* (2007) 'Primer3Plus, an enhanced web interface to Primer3', *Nucleic acids research*. Nucleic Acids Res, 35(Web Server issue), pp. W71-74. doi: 10.1093/NAR/GKM306.

Vantyghem, M. C. *et al.* (2004) 'Patients with familial partial lipodystrophy of the Dunnigan type due to a LMNA R482W mutation show muscular and cardiac abnormalities.', *The Journal of clinical endocrinology and metabolism*, 89(11), pp. 5337–5346. doi: 10.1210/jc.2003-031658.

Vaughan, O. A. *et al.* (2001) 'Both emerin and lamin C depend on lamin A for localization at the nuclear envelope', *Journal of Cell Science*, 114(14), pp. 2577–2590. doi: 10.1242/jcs.114.14.2577.

Vaziri, H. and Benchimol, S. (1998) 'Reconstitution of telomerase activity in normal human cells leads to elongation of telomeres and extended replicative life span', *Current Biology*. Cell Press, 8(5), pp. 279–282. doi: 10.1016/S0960-9822(98)70109-5.

Vergnes, L. *et al.* (2004) 'Lamin B1 is required for mouse development and nuclear integrity.', *Proceedings of the National Academy of Sciences of the United States of America*, 101(28), pp. 10428–10433. doi: 10.1073/pnas.0401424101.

Vigouroux, C. *et al.* (2001) 'Nuclear envelope disorganization in fibroblasts from lipodystrophic patients with heterozygous R482Q/W mutations in the lamin A/C gene.', *Journal of cell science*, 114(Pt 24), pp. 4459–4468. doi: 10.1242/jcs.114.24.4459.

Vis, J. C. *et al.* (2005) 'Expression pattern of apoptosis-related markers in Huntington's disease', *Acta Neuropathologica*, 109(3), pp. 321–328. doi: 10.1007/s00401-004-0957-5.

Vishnudas, V. K. and Miller, J. B. (2009) 'Ku70 regulates Bax-mediated pathogenesis in laminin-α2-deficient human muscle cells and mouse models of congenital muscular dystrophy', *Human Molecular Genetics*, 18(23), pp. 4467–4477. doi: 10.1093/hmg/ddp399.

Vitkup, D., Sander, C. and Church, G. M. (2003) 'The amino-acid mutational spectrum of human genetic disease', *Genome Biology*. BioMed Central, 4(11), pp. 1–10. doi: 10.1186/gb-2003-4-11-r72.

Vogel, B. *et al.* (2009) 'In-vivo characterization of human dilated cardiomyopathy genes in zebrafish', *Biochemical and Biophysical Research Communications*, 390(3), pp. 516–522. doi: 10.1016/j.bbrc.2009.09.129.

Voit, T. (1998) 'Congenital muscular dystrophies: 1997 update', *Brain and Development*. Elsevier, pp. 65–74. doi: 10.1016/S0387-7604(97)00094-6.

Voit, T. *et al.* (2007) 'C.O.4 Congenital muscular dystrophy with adducted thumbs, mental retardation, cerebellar hypoplasia and cataracts is caused by mutation of Enaptin (Nesprin-1): The third nuclear envelopathy with muscular dystrophy',

Neuromuscular Disorders. Elsevier BV, 17(9–10), pp. 833–834. doi: 10.1016/j.nmd.2007.06.245.

Vytopil, M. *et al.* (2003) 'Mutation analysis of the lamin A/C gene (LMNA) among patients with different cardiomuscular phenotypes.', *Journal of medical genetics*, 40(12), p. e132. doi: 10.1136/jmg.40.12.e132.

Vytopil, M. *et al.* (2004) 'The screening for X-linked Emery-Dreifuss muscular dystrophy amongst young patients with idiopathic heart conduction system disease treated by a pacemaker implant.', *European journal of neurology*, 11(8), pp. 531–534. doi: 10.1111/j.1468-1331.2004.00825.x.

Wang, J. C. (2002) 'Cellular roles of DNA topoisomerases: A molecular perspective', *Nature Reviews Molecular Cell Biology*, 3(6), pp. 430–440. doi: 10.1038/nrm831.

Wang, J. Y. J. (2001) 'DNA damage and apoptosis', *Cell Death & Differentiation*. Nature Publishing Group, 8(11), pp. 1047–1048. doi: 10.1038/sj.cdd.4400938.

Wang, Q. *et al.* (2006) 'Characterization of the structures involved in localization of the SUN proteins to the nuclear envelope and the centrosome', *DNA and Cell Biology*, 25(10), pp. 554–562. doi: 10.1089/dna.2006.25.554.

Wang, Y., Herron, A. J. and Worman, H. J. (2006) 'Pathology and nuclear abnormalities in hearts of transgenic mice expressing M371K lamin A encoded by an LMNA mutation causing Emery-Dreifuss muscular dystrophy.', *Human molecular genetics*, 15(16), pp. 2479–2489. doi: 10.1093/hmg/ddl170.

Wang, Y. Q. *et al.* (2012) 'Necrostatin-1 suppresses autophagy and apoptosis in mice traumatic brain injury model', *Neurochemical Research*, 37(9), pp. 1849–1858. doi:

10.1007/s11064-012-0791-4.

Wei, W. *et al.* (2016) 'The NF-κB-modulated microRNAs miR-195 and miR-497 inhibit myoblast proliferation by targeting Igf1r, Insr and cyclin genes', *Journal of Cell Science*. Company of Biologists Ltd, 129(1), pp. 39–50. doi: 10.1242/jcs.174235.

Welz, P. S. *et al.* (2011) 'FADD prevents RIP3-mediated epithelial cell necrosis and chronic intestinal inflammation', *Nature*, 477(7364), pp. 330–334. doi: 10.1038/nature10273.

Wiesel, N. *et al.* (2008) 'Laminopathic mutations interfere with the assembly, localization, and dynamics of nuclear lamins', *Proceedings of the National Academy of Sciences of the United States of America*. National Academy of Sciences, 105(1), pp. 180–185. doi: 10.1073/pnas.0708974105.

Wilkie, G. S. *et al.* (2011) 'Several novel nuclear envelope transmembrane proteins identified in skeletal muscle have cytoskeletal associations', *Molecular and Cellular Proteomics*, 10(1), p. M110.003129. doi: 10.1074/mcp.M110.003129.

Wilschanski, M. *et al.* (2000) 'A pilot study of the effect of gentamicin on nasal potential difference measurements in cystic fibrosis patients carrying stop mutations', *American journal of respiratory and critical care medicine*. Am J Respir Crit Care Med, 161(3 Pt 1), pp. 860–865. doi: 10.1164/AJRCCM.161.3.9904116.

Wilschanski, M. *et al.* (2009) 'Gentamicin-Induced Correction of CFTR Function in Patients with Cystic Fibrosis and CFTR Stop Mutations', *The New England journal of medicine*. Massachusetts Medical Society, 349(15), pp. 1433–1441. doi: 10.1056/NEJMOA022170.

Winbanks, C. E. *et al.* (2011) 'TGF-β regulates miR-206 and miR-29 to control myogenic differentiation through regulation of HDAC4', *Journal of Biological Chemistry*. Elsevier, 286(16), pp. 13805–13814. doi: 10.1074/jbc.M110.192625.

Wishart, T. M. *et al.* (2014) 'Dysregulation of ubiquitin homeostasis and β-catenin signaling promote spinal muscular atrophy', *Journal of Clinical Investigation*, 124(4). doi: 10.1172/JCI71318.

Wishner, B. C. *et al.* (1975) 'Crystal structure of sickle-cell deoxyhemoglobin at 5 Å resolution', *Journal of Molecular Biology*, 98(1), pp. 179–194. doi: 10.1016/S0022-2836(75)80108-2.

Woo, M. *et al.* (1998) 'Essential contribution of caspase 3/CPPp32 to apoptosis and its associated nuclear changes', *Genes and Development*, pp. 806–819. doi: 10.1101/gad.12.6.806.

Wood, W. B. (1988) *The Nematode Caenorhabditis elegans*. Cold Spring Harbor Laboratory.

Worman, H. J. and Bonne, G. (2007) '"Laminopathies": A wide spectrum of human diseases', *Experimental Cell Research*, 313(10), pp. 2121–2133. doi: 10.1016/j.yexcr.2007.03.028.

Worman, H. J. and Courvalin, J.-C. (2004) 'How do mutations in lamins A and C cause disease?', *J Clin Invest*, 113(3), pp. 349–351. doi: 10.1172/JCI20832.

Wright, W. E. and Shay, J. W. (2002) 'Historical claims and current interpretations of replicative aging.', *Nature biotechnology*, 20(7), pp. 682–8. doi: 10.1038/nbt0702-682.

Wu, H., Xiong, W. C. and Mei, L. (2010) 'To build a synapse: signaling pathways in

neuromuscular junction assembly', *Development (Cambridge, England)*. Company of Biologists, 137(7), p. 1017. doi: 10.1242/DEV.038711.

Wu, J. *et al.* (2010) 'The phosphoCTD-interacting domain of Topoisomerase I', *Biochemical and Biophysical Research Communications*, 397(1), pp. 117–119. doi: 10.1016/j.bbrc.2010.05.081.

Wu, J. *et al.* (2013) 'Mlkl knockout mice demonstrate the indispensable role of Mlkl in necroptosis', *Cell Research*, 23(8), pp. 994–1006. doi: 10.1038/cr.2013.91.

Xu, Y. *et al.* (2021) 'Identification of Potential Driver Genes Based on Multi-Genomic Data in Cervical Cancer', *Frontiers in Genetics*. Frontiers Media S.A., 12, p. 598304. doi: 10.3389/FGENE.2021.598304/FULL.

Yablonka-Reuveni, Z. *et al.* (1988) 'Biochemical and morphological differences between fibroblasts and myoblasts from embryonic chicken skeletal muscle', *Cell and Tissue Research*, 252(2), pp. 339–348. doi: 10.1007/BF00214376.

Yaffe, D. and Saxel, O. (1977) 'Serial passaging and differentiation of myogenic cells isolated from dystrophic mouse muscle', *Nature*. Nature, 270(5639), pp. 725–727. doi: 10.1038/270725a0.

Yakovlev, A. G. *et al.* (2001) 'Differential expression of apoptotic protease-activating factor-1 and caspase-3 genes and susceptibility to apoptosis during brain development and after traumatic brain injury', *Journal of Neuroscience*, 21(19), pp. 7439–7446. doi: 10.1523/jneurosci.21-19-07439.2001.

Yamazaki, M., Esumi, E. and Nakano, I. (2005) 'Is motoneuronal cell death in amyotrophic lateral sclerosis apoptosis?', *Neuropathology*, 25(4), pp. 381–387. doi:

10.1111/j.1440-1789.2005.00648.x.

Yang, D. *et al.* (2010) 'Expression of Huntington's disease protein results in apoptotic neurons in the brains of cloned transgenic pigs', *Human Molecular Genetics*, 19(20), pp. 3983–3994. doi: 10.1093/hmg/ddq313.

Yang, S. *et al.* (2017) 'Nec-1 alleviates cognitive impairment with reduction of Aβ and tau abnormalities in APP / PS 1 mice', *EMBO Molecular Medicine*, 9(1), pp. 61–77. doi: 10.15252/emmm.201606566.

Yang, S. H. *et al.* (2011) 'Are B-type lamins essential in all mammalian cells?', *Nucleus*. Taylor & Francis, 2(6), p. 562. doi: 10.4161/NUCL.2.6.18085.

Yang, X. *et al.* (2001) 'Patterning of muscle acetylcholine receptor gene expression in the absence of motor innervation', *Neuron*. Neuron, 30(2), pp. 399–410. doi: 10.1016/S0896-6273(01)00287-2.

Ben Yaou, R. *et al.* (2007) 'Multitissular involvement in a family with LMNA and EMD mutations: Role of digenic mechanism?', *Neurology*, 68(22), pp. 1883–1894. doi: 10.1212/01.wnl.0000263138.57257.6a.

Yap, C. C. and Winckler, B. (2009) 'Vesicular Sorting to Axons and Dendrites', *Encyclopedia of Neuroscience*. Academic Press, pp. 115–120. doi: 10.1016/B978-008045046-9.00743-9.

Yates, C. M. and Sternberg, M. J. E. (2013) 'The effects of non-synonymous single nucleotide polymorphisms (nsSNPs) on protein-protein interactions', *Journal of Molecular Biology*, pp. 3949–3963. doi: 10.1016/j.jmb.2013.07.012.

Yates, J. R. and Washburn, M. P. (2013) 'Quantitative proteomics', *Analytical*

chemistry. Anal Chem, 85(19), p. 8881. doi: 10.1021/AC402745W.

Ye, K. (2005) 'Nucleophosmin/B23, a multifunctional protein that can regulate apoptosis', *Cancer Biology and Therapy*, 4(9), pp. 918–923. doi: 10.4161/cbt.4.9.2072.

Ye, Q. and Worman, H. J. (1995) 'Protein-Protein Interactions between Human Nuclear Lamins Expressed in Yeast', *Experimental Cell Research*. Academic Press, 219(1), pp. 292–298. doi: 10.1006/EXCR.1995.1230.

Yu, Z. *et al.* (2021) 'Necroptosis: A Novel Pathway in Neuroinflammation', *Frontiers in Pharmacology*, 12, p. 701564. doi: 10.3389/fphar.2021.701564.

Yue, P., Li, Z. and Moult, J. (2005) 'Loss of protein structure stability as a major causative factor in monogenic disease', *Journal of Molecular Biology*, 353(2), pp. 459–473. doi: 10.1016/j.jmb.2005.08.020.

Zani, V. J. *et al.* (1996) 'Molecular cloning of complex chromosomal translocation t(8;14;12)(q24.1;q32.3;q24.1) in a Burkitt lymphoma cell line defines a new gene (BCL7A) with homology to caldesmon', *Blood*, 87(8), pp. 3124–3134. doi: 10.1182/blood.v87.8.3124.bloodjournal8783124.

Zastrow, M. S., Vlcek, S. and Wilson, K. L. (2004) 'Proteins that bind A-type lamins: integrating isolated clues.', *Journal of cell science*, 117(Pt 7), pp. 979–987. doi: 10.1242/jcs.01102.

Zhang, D. W. *et al.* (2009) 'RIP3, an energy metabolism regulator that switches TNF-induced cell death from apoptosis to necrosis', *Science*, 325(5938), pp. 332–336. doi: 10.1126/science.1172308.

Zhang, Q. *et al.* (2007a) 'Nesprin-1 and -2 are involved in the pathogenesis of Emery–

Dreifuss muscular dystrophy and are critical for nuclear envelope integrity', *Human molecular genetics*, 16(23), pp. 2816–2833. doi: 10.1093/hmg/ddm238.

Zhang, Q. *et al.* (2007b) 'Nesprin-1 and -2 are involved in the pathogenesis of Emery Dreifuss muscular dystrophy and are critical for nuclear envelope integrity.', *Human molecular genetics*, 16(23), pp. 2816–2833. Available at: http://search.ebscohost.com/login.aspx?direct=true&db=cmedm&AN=17761684&site=ehost-live&scope=site&authtype=ip,shib&custid=s5040751.

Zhang, Q. *et al.* (2019) 'Mechanical stabilization of the glandular acinus by linker of nucleoskeleton and cytoskeleton complex', *Current biology : CB*. NIH Public Access, 29(17), p. 2839.e4. doi: 10.1016/J.CUB.2019.07.021.

Zhang, S. *et al.* (2019) 'RIP1 kinase inhibitor halts the progression of an immune-induced demyelination disease at the stage of monocyte elevation', *Proceedings of the National Academy of Sciences of the United States of America*, 116(12), pp. 5675–5680. doi: 10.1073/pnas.1819917116.

Zhang, X. *et al.* (2007) 'Syne-1 and Syne-2 play crucial roles in myonuclear anchorage and motor neuron innervation.', *Development (Cambridge, England)*, 134(5), pp. 901–8. doi: 10.1242/dev.02783.

Zhang, X. *et al.* (2009) 'SUN1/2 and Syne/Nesprin-1/2 complexes connect centrosome to the nucleus during neurogenesis and neuronal migration in mice', *Neuron*. Neuron, 64(2), pp. 173–187. doi: 10.1016/J.NEURON.2009.08.018.

Zhang, X. *et al.* (2011) 'Akt, FoxO and regulation of apoptosis', *Biochimica et biophysica acta*. Biochim Biophys Acta, 1813(11), pp. 1978–1986. doi:

10.1016/J.BBAMCR.2011.03.010.

Zhang, Y. *et al.* (2013) 'Protein Analysis by Shotgun/Bottom-up Proteomics', *Chemical reviews*. NIH Public Access, 113(4), p. 2394. doi: 10.1021/CR3003533.

Zhou, C. *et al.* (2017) 'Novel nesprin-1 mutations associated with dilated cardiomyopathy cause nuclear envelope disruption and defects in myogenesis', *Human molecular genetics*, 26(12), pp. 2258–2276. doi: 10.1093/hmg/ddx116.

Zhu, C. H. *et al.* (2007) 'Cellular senescence in human myoblasts is overcome by human telomerase reverse transcriptase and cyclin-dependent kinase 4: Consequences in aging muscle and therapeutic strategies for muscular dystrophies', *Aging Cell*, 6(4), pp. 515–523. doi: 10.1111/j.1474-9726.2007.00306.x.

Zhu, S. *et al.* (2002) 'Minocycline inhibits cytochrome c release and delays progression of amyotrophic lateral sclerosis in mice', *Nature*, 417(6884), pp. 74–78. doi: 10.1038/417074a.

Ziat, E. *et al.* (2016) 'FHL1B Interacts with Lamin A/C and Emerin at the Nuclear Lamina and is Misregulated in Emery-Dreifuss Muscular Dystrophy', *Journal of Neuromuscular Diseases*. IOS Press, 3(4), pp. 497–510. doi: 10.3233/JND-160169.

Ziat, E. and Bertrand, A. T. (2015) 'FHL1 protein isoforms in Emery-Dreifuss muscular dystrophy', *Orphanet Journal of Rare Diseases*. BioMed Central, 10(Suppl 2), p. O18. doi: 10.1186/1750-1172-10-S2-O18.

Ziskind-Conhaim, L. and Bennett, J. I. (1982) 'The effects of electrical inactivity and denervation on the distribution of acetylcholine receptors in developing rat muscle', *Developmental Biology*. Academic Press, 90(1), pp. 185–197. doi: 10.1016/0012-

1606(82)90224-X.